

AD 679593

AFFDL-TR-68-85

**INVESTIGATION OF THE EFFECTS OF GUSTS
ON V/STOL CRAFT IN TRANSITION
AND HOVER**

GRANT B. SKELTON

Honeywell, Inc.

TECHNICAL REPORT AFFDL-TR-68-85

OCTOBER 1968

AD 679593
DEC 24 1968

This document has been approved for public
release and sale; its distribution is unlimited.

AIR FORCE FLIGHT DYNAMICS LABORATORY
AIR FORCE SYSTEMS COMMAND
WRIGHT-PATTERSON AIR FORCE BASE, OHIO

**INVESTIGATION OF THE EFFECTS OF GUSTS
ON V/STOL CRAFT IN TRANSITION
AND HOVER**

GRANT B. SKELTON

This document has been approved for public
release and sale; its distribution is unlimited.

FOREWORD

This report was prepared by Honeywell Inc. for the Air Force Flight Dynamics Laboratory, Directorate of Laboratories, Air Force Systems Command, United States Air Force, Wright-Patterson Air Force Base, Ohio. The study was conducted under United States Air Force Contract No. F33615-67-C-1563, "Investigation of the Effects of Gusts on V/STOL Craft in Transition and Hover". The work was administered under the direction of the Air Force Flight Dynamics Laboratory; Mr. Evard Flinn was the Technical Monitor.

The research reported was conducted by the Research Department of the Systems and Research Division of Honeywell Inc. Dr. G. B. Skelton was the principal investigator, Mr. C. Stone prepared the V/STOL model employed, and Messrs. T. W. Toivanen, J. Arneson, and T. Johnson prepared and conducted the nonlinear investigations. Technical consultation was provided by Prof. John Dutton of Pennsylvania State University and Prof. Bernard Etkin of the University of Toronto.

The reporting period was April, 1967 to March, 1968. The report was first submitted in April, 1968. The contractor's report number is Honeywell ADG Report 12060-FR1.

The investigators in this study would like to thank Mr. W. B. Davis of the Ryan Aeronautical Company for his assistance in preparing the XV-5A model, and Prof. H. A. Panofsky of Pennsylvania State University and Drs. W. Vaughan and J. Scoggins of the National Aeronautics and Space Administration, George C. Marshall Space Flight Center, for their help in the gust model preparation.

The investigators would especially like to thank Prof. Dutton for his extensive help with the gust models and Prof. Etkin for his many constructive suggestions for conducting the gust model investigations and the linear and nonlinear vehicle analyses. Their suggestions greatly influenced and enriched the course and content of the program.

Finally, the investigators would like to thank Mr. Flinn for his enthusiastic support, for his assistance in obtaining gust covariance data, and for arranging for the greatly appreciated consulting services of Professors Dutton and Etkin.

This technical report was reviewed and is approved.



C. B. Westbrook
Chief, Control Criteria Branch
Flight Control Division
Air Force Flight Dynamics Laboratory

ABSTRACT

The concern in the work reported is the development of statistical models for the gust environment in the earth's boundary layer for use in determining the gust response characteristics of V/STOL aircraft. A general gust model based upon published gust data was developed, and analyses of V/STOL responses with that model were conducted to determine the gust descriptors significant to V/STOL performance. An interim gust model embodying the significant descriptors was then developed for use in V/STOL gust analyses. Suggestions for meteorological experiments to measure the significant descriptors are made. The significant gust descriptors determined from the analyses are the diagonal terms of the gust covariance tensor, gust probability distributions, mean wind probability distributions, and the dependencies of these statistics on thermal stability, surface roughness, and altitude. Less critical descriptors include the off-diagonal components in the gust covariance tensor and the space-time interplay in that tensor. The significant gusts seen by the aircraft are head-on and vertical gusts on the wings; head-on and vertical gust shears across the wings; head-on, side, and vertical gusts on the tail; and head-on and side gusts on the fuselage. Mean airspeed and sideslip angle are important parameters in V/STOL gust responses. The wing-to-tail transport delay of the gusts in forward flight also has a significant effect. V/STOL gust responses at low airspeeds are generally small due to the low dynamic pressures, and the responses are decidedly nonlinear except at low gust amplitudes.

TABLE OF CONTENTS

SECTION		PAGE
I	INTRODUCTION	1
II	WIND MODEL: KNOWN WIND PHYSICS	7
	A. Stability	7
	1. Hydrostatic Stability	7
	2. Dynamic Stability	8
	B. Winds and Gusts	11
	C. Derivations from the Navier-Stokes Equations	13
	1. General	13
	2. Energy	16
	3. Friction Velocity	16
	4. Covariance Differential Equation	17
	5. Velocity Divergence	18
	6. Stationarity and Horizontal Homogeneity	19
	7. Isotropy	19
	8. Isotropic Cross Correlations	22
	D. Richardson Numbers	25
	E. Wind Profiles	26
	F. Energy Spectra	29
	G. The Taylor Hypothesis	31
	H. Turbulence Scales	33
	1. General	33
	2. Turbulence Levels	35
	J. Available Covariance Data	38
	K. Available Gust Probability Densities	38
	L. Gaps	38
III	INTERIM GUST MODEL	41
	A. Premises	41
	B. Assumptions	43
	1. Richardson Number	43
	2. Wind Profile	43
	3. Nominal Gust Intensities	46
	4. Distance Metric	47
	5. Probabilities	50
	C. Approximations	51
	1. Shear Spectra	51
	2. Integration	53
	3. Irrational Spectra	54
	D. The Gust Model	56
	1. Force and Moment Approximation	57
	2. Cross Correlations of Orthogonal Gusts	61
	3. Cross Correlations of Parallel Gusts	65
	4. Angle Dependence	67

TABLE OF CONTENTS (cont'd)

SECTION		PAGE
	5. Spectral Form	79
	6. Final Filter Form	70
	E. Summary	75
IV	TOLCAT REQUIREMENTS	81
	A. Premises and Long-Time Averages	81
	1. First TOLCAT Experiment	82
	2. Second TOLCAT Experiment	82
	B. Gust Measurements	83
	1. Third TOLCAT Experiment	84
	2. Fourth TOLCAT Experiment	85
	3. Fifth TOLCAT Experiment	85
	4. Sixth TOLCAT Experiment	85
	5. Seventh TOLCAT Experiment	86
	6. Eighth TOLCAT Experiment	86
	7. Ninth TOLCAT Experiment	86
	8. Data Reduction	87
V	LINEAR ANALYSES	89
	A. Gust Models	91
	B. Linear Analysis Results	95
	1. Flight Conditions	95
	2. Dominant Poles	99
	3. Correlation Length	100
	4. Wing Shear	101
	5. Frozen Gust Field Hypothesis	110
	6. Spectral Shape	113
	7. Magnitude Dependence	113
	8. Cross Correlations	116
	9. Heading Angle	116
	C. Computer Program	119
	1. Perturbation Equation Coefficients	119
	2. Covariance Calculation	121
VI	NONLINEAR ANALYSIS	125
	A. Simulation Details	126
	B. Statistical Test Data	129
	1. Airspeed and Sideslip Tests	131
	2. Correlation Length Tests	131
	3. Shear Effects	131
	4. Cross Correlation Tests	136
	5. Gust Penetration Tests	141
	6. Intensity	141

TABLE OF CONTENTS (cont'd)

SECTION	PAGE
C. Linearity	158
1. Inconsequential Nonlinearities	161
2. σ_g/V_{as} Ratio	162
3. $\sigma_{\alpha}^g/(\alpha_S-\alpha_T)$ Ratios	181
4. $\sigma_r/\sigma_r(\omega_n)$ Ratios	182
D. Other Simulation Topics	185
1. Controller Design	185
2. Reingestion	186
3. Normalization	188
4. Fan Dependence on Dynamic Pressure Changes	190
REFERENCES	191
APPENDIX I - A DYNAMIC MODEL OF THE RYAN XV-5A AIRCRAFT	197
APPENDIX II - HYBRID SIMULATION	223

LIST OF ILLUSTRATIONS

FIGURE		PAGE
1	Schematic Spectrum of Wind Speed Near the Ground Estimated From a Study of Van der Hoven (1957)	12
2	Cross Correlation Geometry	22
3	Universal Function ψ	26
4	Probability Distribution of Mean Wind Speed at 100 Meters Altitude	45
5	Definition of Angles	68
6	Gust Sources	76
7	Gust Combination at Zero Sideslip	77
8	Gust Combination at 180-Degree Sideslip	78
9	Gust Combination at ± 90 -Degree Sideslip	79
10	Flight Conditions	96
11	Translation Rate Response Standard Deviations versus Correlation Length	102
12	Angular Rate Response Standard Deviations versus Correlation Length	103
13	Angular Response Standard Deviations versus Correlation Length	104
14	Control Response Standard Deviations versus Correlation Length	105
15	Translation Rate Response Standard Deviations versus Correlation Length	106
16	Angular Rate Response Standard Deviations versus Correlation Length	107
17	Angular Response Standard Deviations versus Correlation Length	108

LIST OF ILLUSTRATIONS (cont'd)

FIGURE		PAGE
18	Total and Aerodynamic Forces versus Gust Intensity Hybrid Tests -- 112-ft/sec Airspeed	148
19	Total and Aerodynamic Moments versus Gust Intensity Hybrid Tests -- 112-ft/sec Airspeed	149
20	Hybrid and Linear Attitude Rates versus Gust Intensity -- 112-ft/sec Airspeed	150
21	Total and Aerodynamic Forces versus Gust Intensity Hybrid Tests -- 22-ft/sec Airspeed	151
22	Total and Aerodynamic Moments versus Gust Intensity Hybrid Tests -- 22-ft/sec Airspeed	152
23	Hybrid and Linear Attitude Rates versus Gust Intensity -- 22-ft/sec Airspeed	153
24	Total and Aerodynamic Forces versus Gust Intensity Hybrid Tests -- Hover	154
25	Total and Aerodynamic Moments versus Gust Intensity Hybrid Tests -- Hover	155
26	Hybrid Attitude Rates versus Gust Intensity -- Hover	156
27	Vertical Gust Probability Density (ft/sec)	167
28	Total Rolling Moment Probability Density -- 120-ft/sec Airspeed (ft-lbs)	168
29	Roll Rate Probability Density -- 120-ft/sec Airspeed (deg/sec)	169
30	Aerodynamic Lift Force Probability Density -- 20-ft/sec Airspeed, Low Gust Amplitude (lbs)	170
31	Aerodynamic Side Force Probability Density -- 20-ft/sec Airspeed, Low Gust Amplitude (lbs)	171
32	Aerodynamic Pitching Moment Probability Density -- 20-ft/sec Airspeed, Large Gust Amplitude (ft-lbs)	172
33	Pitch Rate Probability Density -- 20-ft/sec Airspeed, Moderate Gust Amplitude (deg/sec)	173

LIST OF ILLUSTRATIONS (cont'd)

FIGURE		PAGE
34	Pitch Rate Probability Density -- 20-ft/sec Airspeed, Large Gust Amplitude (deg/sec)	174
35	Roll Rate Probability Density -- 20-ft/sec Airspeed, Large Gust Amplitude (deg/sec)	175
36	Total Side Force Probability Density -- Hover (lbs)	176
37	Total Yawing Moment Probability Density -- Hover (ft-lbs)	177
38	Aerodynamic Yawing Moment Probability Density -- Hover (ft-lbs)	178
39	Pitch Rate Probability Density -- Hover (deg/sec)	179
40	Force Schematic	184
41	Pitch, Roll and Yaw Attitude Controllers	225

LIST OF TABLES

TABLE		PAGE
I	XV-5 Trim Settings	97
II	XV-5 Response Standard Deviations, Airspeed and Sideslip Angle Dependence	98
III	XV-5 Response Standard Deviations, Tests of Shear Effects	109
IV	XV-5 Response Standard Deviations, Test of Taylor Hypothesis	112
V	XV-5 Response Standard Deviations, β Dependence	114
VI	XV-5 Response Standard Deviations, α Sensitivity - Per Unit	115
VII	XV-5 Response Standard Deviations, Tests of Cross Correlations	117
VIII	XV-5 Response Standard Deviations, Test of Heading Angle	118
IX	Notation	130
X	Nonlinear XV-5 Response Standard Deviations, Tests of Airspeeds	132
XI	Nonlinear XV-5 Response Standard Deviations, Test of Correlation Length.	133
XII	Nonlinear XV-5 Response Standard Deviations, Test of Correlation Length	134
XIII	Nonlinear XV-5 Response Standard Deviations, Tests of Gust Shears Across the Wings	135
XIV	Nonlinear XV-5 Response Standard Deviations, Test of Gust Cross Correlations	137
XV	Nonlinear XV-5 Response Standard Deviations, Test of Gust Cross Correlations	138
XVI	Nonlinear XV-5 Response Standard Deviations, Test of Gust Cross Correlations	139

LIST OF TABLES (cont'd)

TABLE		PAGE
XVII	Nonlinear XV-5 Response Standard Deviations, Test of Cross Correlation with Reduced Side Gust	140
XVIII	Nonlinear XV-5 Response Standard Deviations, Tests of Gust Penetration	142
XIX	Nonlinear XV-5 Response Standard Deviations, Tests of Gust Penetration	143
XX	Nonlinear XV-5 Response Standard Deviations, Tests of Gust Intensity	144
XXI	Nonlinear XV-5 Response Standard Deviations, Tests of Gust Intensity	145
XXII	Nonlinear XV-5 Response Standard Deviations, Tests of Gust Intensity	146

NOMENCLATURE

The employment of both meteorological and aerodynamic notations in this report has in several cases required a double use of symbols. In all cases the particular definition implied is clear from its context. Aircraft notations used only in the final sections of the report and in the appendixes are listed when they are first employed.

b	wing span
c	gust filter bandwidth
\bar{c}	wing chord
C_p	specific heat of air at constant pressure
C_v	specific heat of air at constant volume
d	wing-to-tail distance
E	expectation operator
\mathcal{E}	gust energy density
$f(r, t)$	isotropic correlation of gusts parallel to path
$F(z)$	force on air parcel at altitude z
\mathcal{F}	force
g	gravitational constant
$g(r, t)$	isotropic correlation of gusts orthogonal to path
H	heat
K	wave number (radians/meter)
L	characteristic length (correlation length)
\mathcal{L}	rolling moment
p	air pressure
\underline{r}	$(r_1 r_2 r_3)' =$ distance vector

NOMENCLATURE (Continued)

r	$(r_1^2 + r_2^2 + r_3^2)^{1/2}$ = distance metric
R	gas constant for air
$R(\mathbf{r}, t)$	gust covariance tensor
R_f	flux Richardson number
R_i	gradient Richardson number
T	temperature
\underline{U}	mean wind vector
U	mean wind amplitude
\underline{u}	wind vector
\underline{u}'	gust vector
u^*	friction velocity
u, v, w	downwind, crosswind, vertical gust components
u_1, u_2, u_3	head-on, side, vertical gust components on aircraft
u_{1L}, u_{2L}, u_{3L}	gust components at left wing tip
u_{1R}, u_{2R}, u_{3R}	gust components at right wing tip
u_{1T}, u_{2T}, u_{3T}	gust components at tail
u_{1w}, u_{2w}, u_{3w}	gust components on fuselage
u_y, w_y	horizontal shear of u, w gusts in y direction
V	aircraft ground speed
V_{as}	aircraft airspeed
x, y, z	aircraft body axes
z_0	roughness length
z	altitude

NOMENCLATURE (Concluded)

α_i	gust cross correlation parameters
β	sideslip angle
β_i	gust spectral fit parameters
γ	lapse rate
θ	potential temperature of air
ν	viscosity of air
ρ	air density
σ	standard deviation
ψ_h	heading angle
ψ_a	azimuth angle

SECTION I INTRODUCTION

Winds and wind gusts can severely degrade the flight performance of an aircraft. To be able to predict the severity of wind effects in aircraft and aircraft-system design, it is necessary that mathematical models of the wind environment be developed. Before physically realistic models can be developed, in turn, it is necessary to gather a great quantity of the statistical wind data which will define the models' properties. This is an overall objective of the Air Force ALLCAT program, ALL standing for all altitudes and CAT for critical air turbulence.

The present study was directed towards one phase of that effort, the TOLCAT program, whose objective is to define the wind field at takeoff and landing altitudes. These altitudes (300 feet and below) are called the planetary boundary layer in the meteorological literature, as the wind environment there is strongly affected by the shear of the wind field produced by the roughness of earth's surface. Winds at these altitudes affect the takeoff and landing of all aircraft, and they affect a significant portion of the flight envelopes of V/STOL aircraft.

The wind field at low altitudes is particularly significant to V/STOL aircraft as gusts there can fundamentally limit a V/STOL's mission capabilities. At worst, gusts can cause a fatal upset, and at best they will move a V/STOL about in the air. The possibility of upset influences the aerodynamic design of a V/STOL and the size and placement of its force and moment producers. A weight penalty must be paid if excess force and moment capabilities are required for flight in turbulent air. Gust-induced motions further reduce the abilities of a V/STOL to meet such mission requirements as hovering, flying in close formation, and landing softly in a small space, and the possibility of encountering gusts severe enough to produce upset limits the set of meteorological conditions in which a V/STOL can be safely flown. Possessing an accurate model of the gust field at low altitudes is thus important in V/STOL design, as gusts may both fundamentally influence the configuration of a V/STOL aircraft and reduce its overall utility.

The present study had two objectives. The first and main objective was identification of the wind field descriptors that significantly affect V/STOL performance so that these descriptors could be experimentally defined in the TOLCAT program. The second objective was development of an interim gust model embodying those descriptors for use in aircraft gust analyses until the TOLCAT experiments are completed. The study had three phases, generation of candidate gust models, linear and nonlinear gust analyses of a typical V/STOL aircraft to determine the significant parameters in those models, and finally simplification of the gust models to a model containing the significant parameters and listing of TOLCAT measurement requirements.

The Ryan XV-5 V/STOL was selected as the study vehicle for the second phase analyses because of the very complete mathematical model of the vehicle that Ryan had developed.

A somewhat unusual format has been chosen for presenting the results of the study in this report and in this introduction. The report is addressed both to TOLCAT meteorologists who require only a superficial knowledge of the details of aircraft gust analyses, and to aircraft analysts who must be familiar with meteorological notions and nomenclature to be able to evaluate the significance of results obtained with the interim gust model. To accommodate both types of readers, gust model and vehicle analysis results are discussed in separate parts of the report, the gust discussions are in part written in an introductory manner, and the approximations made in generating the interim model are discussed in detail. The format for the report and the main results it contains are as follows.

Section II presents the results of a literature survey conducted to determine the known descriptors of the gust field in the earth's boundary layer. This section is written in an introductory manner to introduce thermal stability, gradient Richardson number, nonisotropy, gust covariance tensor, and the other concepts necessary to understanding the interim gust model to readers unfamiliar with the notions and terminology of meteorology.

To summarize the results presented in that section, a great many things are known about winds and wind gusts and very good models of some gust physics have been developed. In particular, the shear of the mean wind near the surface is well modeled, many probability distributions of the mean wind are available, and the time and space distributions of gust energy are fairly well known. Some of the gust physics critical to V/STOL performance have never been measured or modeled, however. Perhaps the most critical of these is the dependence of the gust covariance tensor on azimuth, elevation, time, and distance. The conclusion reached is that too little is known today to generate a realistic gust model.

The interim model developed is presented in Section III. Generating this model required making a great many assumptions and approximations. Some of the assumptions are supported by existing data, but others are almost completely arbitrary. The weakest assumption made was to hypothesize a particular form for the distance metric. The approximations made were based on a strong desire that the various gust spectra seen by the aircraft be expressible as proper rational fractions; this particular spectral form is much more amenable to gust simulation and aircraft gust analyses than irrational spectra would be. Finally, the gust model was constructed to include the gust descriptors which the linear and nonlinear analyses showed were important.

The model on the whole will produce realistic force and moment magnitudes, but it is expected that it will differ in many details from the model that will be developed from the TOLCAT data.

Section IV lists a sequence of TOLCAT experiments which would measure the important gust descriptors. This is the last section dealing with gusts, and meteorologists not interested in detailed aircraft gust analyses need read no further. The experiments measure probability densities and the distance-metric statistics required to define the gust covariance tensor, and they also test several of the fundamental hypotheses upon which gust theory is built.

It is not intended that the format of the listed experiments be followed in the TOLCAT program, or even that the exact measurements suggested be made. The purpose of expressing the TOLCAT requirements as an experiment list was to isolate the different types of gust data desired for aircraft analyses, and any measurements which would produce data equivalent to that information will suffice.

Sections V and VI present the results of the linear and nonlinear analyses upon which the interim model and the list of TOLCAT requirements are based. These results are:

- Mean airspeed and mean sideslip angle are critical parameters in defining V/STOL gust response magnitudes.
- Mean heading angle is important to the extent that it defines the relative intensities of the head-on and side gusts seen by the aircraft.
- Gust spectral form and gust intensities are critical in defining V/STOL response magnitudes. As the spectral form are dependent upon azimuth of the flight path, sideslip angle, altitude, mean wind speed, and Richardson number, all of these parameters are important gust descriptors.
- Cross correlations of orthogonal gust components are not important if the maximum correlation-coefficient magnitudes are less than 0.3. It is believed from what data exist and from engineering intuition that this is the case. If TOLCAT can verify this, then for aircraft analysis purposes there is little need to measure the off-diagonal components of the gust covariance tensor.
- The shears of head-on and vertical gusts across the wings of a V/STOL produce significant roll and yaw moments, especially at lower altitudes, and these shears must be included with head-on, side, and vertical gusts in the gust model.
- The hypothesis of a gust field frozen in time moving downwind with the mean wind speed is acceptable to quite low airspeeds. An estimate based upon the little distance-metric data available places the lowest airspeed at which the frozen gust hypothesis is acceptable at one-third of the mean wind speed.

- The gust penetration effect where, in forward flight, the gusts encountered by the wing are encountered by the tail d/V_{as} seconds later (where d/V_{as} is the wing-to-tail distance divided by the mean airspeed), significantly affects V/STOL gust responses, and this effect must be included in the gust model.
- A reasonably configured V/STOL aircraft is not very gust sensitive at low airspeeds. By reasonable configuration it is meant that the V/STOL does not have unusually large aerodynamic surfaces, unusual thrust sensitivity to dynamic pressure changes, or marginal excess thrust capability. This conclusion specifically applies to low airspeeds, and it is not true at airspeeds where the total aerodynamic lift is more than about one-half the aircraft weight.
- The principal nonlinearities affecting V/STOL performance in gusts are parabolic velocity products in aerodynamic force terms and aerodynamic force saturations (stall). Inertial velocity product terms and gravity dependence on angle cosines can be ignored. There is no strong evidence that instantaneous changes in Kussner lag time constants and wing-to-tail transport delays are important except when the ratio of gust amplitudes to mean airspeed is quite large. Thruster nonlinearities can be important, depending upon the particular thruster configuration, but these nonlinearities can in part be eliminated by passing thruster command signals through inverse nonlinearities.
- Stall-induced pitchup is the most dramatic nonlinear effect. This effect is, of course, fatal at low altitudes. Therefore, it is essential that gust probability densities be measured as accurately as possible so that the likelihoods of stall and upset can be precisely ascertained.

Section V also contains descriptions of the gust model employed in the linear analyses, the method used to calculate perturbation coefficients, and the method used to calculate response covariances. The latter is of general interest as it is a faster method than residue evaluation.

Section VI contains a description of the simulation problems which constrained the content and quantity of nonlinear data collected, explanations of the nonlinear effects as evidenced in the responses, an attempt to determine the gust amplitudes where linearity is reasonable, and an explanation of the controller design method employed.

The Ryan XV-5 model employed in the studies is presented in Appendix I. Ryan's original model was quite complete, but it was necessary to extend their aerodynamic force terms to include local airspeed reversals. Approximations to Kussner and Wagner lags were added, and the fan dynamics were slightly simplified.

To summarize the study, the generation of a stochastic gust model is not an easy task, both because of a lack of critical data and because of a need to approximate gust physics with reasonable mathematical expressions. The TOLCAT experiments suggested should supply the missing data, but the analyst generating a gust model from that data will have a far more difficult task than was the generation of the interim model as he will not have the freedom of assumption that existed in this study. Even with this freedom, with sufficient study time, and with the aid of aerodynamicists and meteorologists, generation of the interim model was not easy, as it was necessary to guess physics, generate approximations, and evaluate the consequences of assumptions made. The gust model generated is not mathematically self consistent, one of many desirable properties given up in favor of computational simplifications.

The aircraft analyst wishing to use the interim gust model will find it far more complex than high-altitude models and far more complex than he would like it to be. It would not be surprising if aircraft analysts protested the complexity of the model and appealed for generation of a simpler one. To this it must be replied that all of the simplifications made in the interim model generation were made to simplify the analyst's task, and further, all of the elements remaining in the model were shown analytically and by simulation experiment to be important gust parameters.

To the aircraft analyst looking for a simple gust model, it is suggested that only upwind or downwind flight at zero average sideslip be considered, that neutral stability and a single roughness be assumed, and that as few as possible altitudes and mean wind speeds be considered. Also, the faster and the higher the aircraft flies, the simpler the gust model can be.

Analysts employing linearity are reminded that linearity was shown valid in the tests in this study only at low gust-amplitude-to-airspeed ratios where stall was very unlikely. Linearity was very good at deducing trends, but it was very bad at deducing likelihoods.

SECTION II

WIND MODEL: KNOWN WIND PHYSICS¹

A literature survey was conducted to determine published wind data and published notations on the physics of wind behavior. The data and notions found are discussed in this section.

As mentioned in the introduction, a second purpose of this section is to introduce the vocabulary and physics fundamentals of wind behavior to the reader unfamiliar with meteorology. The format chosen to accomplish this is to present the individual physics topics in an order determined by the desire to treat them almost wholly in terms of material already presented, with a minimum of new vocabulary being introduced in each topic discussion. The presentation will thus appear somewhat disorganized, as some of the earlier topics apparently bear little relation to each other. The reader is asked to bear with this; the various threads are eventually tied together.

A. STABILITY

The first topic of interest is hydrostatic and dynamic thermal stability.

1. Hydrostatic Stability

Consider a unit mass of air at an altitude z_1 . The vertical force on this mass is

$$F(z_1) = -g - \frac{1}{\rho} \frac{\partial p}{\partial z}$$

where g is gravity, ρ is air density, and p is pressure. Let R be the gas content and T be temperature. Then

$$p/\rho = RT$$

Assuming the density of the air parcel is the same as the surrounding air, assumed constant,

¹The writer would like to thank Professors John Dutton and Hans Panofsky of Pennsylvania State University and Drs. William Vaughan and James Scoggins of the National Aeronautics and Space Administration, George C. Marshall Space Flight Center, for illuminating discussions of the material presented in this section. The writer would also like to thank Professor Bernard Etkin of the University of Toronto for suggesting several of the referenced publications.

$$\begin{aligned}\frac{\partial p}{\partial z} &= \rho R \frac{\partial T}{\partial z} \\ &= -\rho R \gamma\end{aligned}$$

where

$$\gamma = -\frac{\partial T}{\partial z}$$

is the "lapse rate" of the air. Substituting this into the above,

$$\begin{aligned}F(z_1) &= -g + \frac{1}{\rho} \rho R \gamma \\ &= R(\gamma - g/R)\end{aligned}$$

The parcel will rise of its own accord if

$$F(z_1) > 0$$

or

$$\gamma > g/R$$

If the lapse rate γ is greater than g/R , hotter air from below will rise and will be added to the colder air above; this will raise the temperature of the air above, reduce the lapse rate γ , and reduce the forces on rising parcels of air. Hydrostatic instabilities thus tend to disappear, and air on the average will be in hydrostatic equilibrium.

2. Dynamic Stability

Actually, air will rise at a lower lapse rate than g/R . Suppose that the entire air mass is in hydrostatic equilibrium, and a parcel of air has by one means or another been displaced from an altitude z_1 to $z_1 + dz$ without heat being added to it by conduction or radiation. Then

$$\begin{aligned}\Delta H &= \text{heat added} = 0 \\ &= C_v \Delta T + \int p d\left(\frac{1}{\rho}\right) - \int F(z) dz\end{aligned}$$

where

C_v = specific heat at constant volume

$C_v \Delta T$ = increase in internal energy

$$\int p d(1/\rho) = \text{work done expanding}$$

$$\int F(z) dz = \text{change in potential energy due to altitude increase}$$

Differentiating with respect to altitude,

$$\begin{aligned}\frac{\partial H}{\partial z} &= 0 \\ &= C_v \frac{\partial T}{\partial z} + p \frac{d(1/\rho)}{dz} - F(z)\end{aligned}$$

Using the above equation for $F(z)$ and

$$R = C_p - C_v$$

where C_p is the specific heat at constant pressure, then

$$\begin{aligned}0 &= C_v \frac{\partial T}{\partial z} + p \frac{d(1/\rho)}{dz} + g + \frac{1}{\rho} \frac{\partial p}{\partial z} \\ &= C_v \frac{dT}{dz} + g + \frac{\partial}{\partial z} (p/\rho) \\ &= C_v \frac{\partial T}{\partial z} + g + \frac{\partial}{\partial z} (RT) \\ &= (R+C_v) \frac{\partial T}{\partial z} + g \\ &= C_p \frac{\partial T}{\partial z} + g\end{aligned}$$

so the lapse rate of the rising parcel is

$$\begin{aligned}\gamma_d &= \frac{-\partial T}{\partial z} \\ &= g/C_p\end{aligned}$$

Let T_d , ρ_d , γ_d refer to the temperature, density, and lapse rate of the displaced parcel, and T , ρ , γ refer to the surrounding air. At $z_1 + dz$ the force $F(z_1 + dz)$ on the displaced parcel is

$$\begin{aligned}
F(z_1 + dz) &= -g - \frac{1}{\rho_d} \frac{\partial p}{\partial z} \\
&= -g - \frac{RT_d}{p} \frac{\partial p}{\partial z} \\
&= -g - R(T_d - T) \frac{1}{p} \frac{\partial p}{\partial z} - RT \frac{1}{p} \frac{\partial p}{\partial z}
\end{aligned}$$

At $z_1 + dz$

$$T_d = T(z_1) - \gamma_d dz$$

$$T = T(z_1) - \gamma dz$$

so that

$$F(z_1 + dz) = -g - RT \frac{1}{p} \frac{\partial p}{\partial z} + dz R(\gamma_d - \gamma) \frac{1}{p} \frac{\partial p}{\partial z}$$

Assuming the surrounding air is in hydrostatic equilibrium,

$$F(z_1 + dz) \Big|_{\text{surroundings}} = 0 = -g - \frac{RT}{p} \frac{\partial p}{\partial z}$$

then the net force on the displaced parcel is

$$F(z_1 + dz) = dz R(\gamma_d - \gamma) \frac{1}{p} \frac{\partial p}{\partial z}$$

With the pressure gradient negative (from the assumption of hydrostatic equilibrium),

$$\frac{\partial p}{\partial z} < 0$$

the displaced parcel will continue to rise [$F(z_1 + dz) > 0$] if

$$\gamma > \gamma_d$$

The conditions $\left\{ \begin{array}{l} \gamma > \gamma_d \\ \gamma = \gamma_d \\ \gamma < \gamma_d \end{array} \right\}$ are called unstable, neutral, and stable air respectively.

Define for the surrounding air the potential temperature θ , by

$$\frac{1}{\theta} \frac{d\theta}{dz} = \frac{1}{T} \frac{\partial T}{\partial z} - \frac{R}{C_p} \frac{1}{p} \frac{\partial p}{\partial z}$$

so that

$$T/\theta = \text{const } p^{R/C_p}$$

It is common practice to choose the constant in this equation so that $\theta = T$ at the altitude where p is 1000 millibars. With this definition the net force is

$$\begin{aligned} F(z_1+dz) &= -dz \frac{R}{p} \frac{\partial p}{\partial z} (\gamma - g/C_p) \\ &= dz \left[g R/C_p \frac{1}{p} \frac{\partial p}{\partial z} - \frac{R}{\rho RT} \frac{\partial p}{\partial z} \gamma \right] \\ &= dz g \left[R/C_p \frac{1}{p} \frac{\partial p}{\partial z} - \frac{1}{T} \frac{\partial T}{\partial z} \right] \\ &= - \left(dz \frac{g}{\theta} \frac{d\theta}{dz} \right) \end{aligned}$$

so $\frac{g}{\theta} \frac{d\theta}{dz}$ is a measure of the restoring force (spring constant) on the displaced parcel. This term appears in the Richardson number discussed below.

To summarize, if the lapse rate γ satisfies $\gamma > g/R$, hot air from below will rise of its own accord, warming the air above and lowering γ towards stability. If the air mass is nearly in hydrostatic equilibrium, a parcel of air displaced by any mechanical process will continue to rise if $\gamma > g/C_p$, also warming the air above so that following parcels will not have as strong a tendency to rise.

The number $-g/\theta \frac{\partial \theta}{\partial z}$ is a direct measure of the bouyant force on the rising parcel.

Air must on the average be in hydrostatic equilibrium. In turbulent air the mixing of hotter and colder air parcels will tend to produce that equilibrium locally. If $\gamma > g/C_p$, a motion of an air parcel which displaces other air parcels via local pressure gradients will induce motion of the newly displaced parcels. Thus if $\gamma > g/C_p$, the air has a tendency towards turbulence.

B. WINDS AND GUSTS

Figure 1 (from reference 1) is a plot of the power spectrum of the response of an anemometer (which measures wind speed) fixed with respect to the earth.

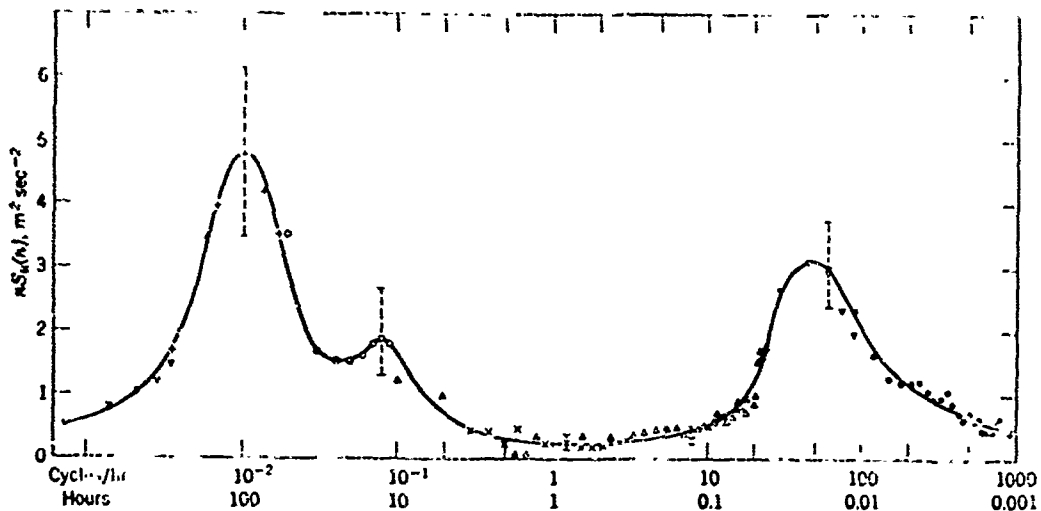


Figure 1. Schematic Spectrum of Wind Speed Near the Ground Estimated From a Study of Van der Hoven (1957)

It is seen that measured winds contain high-frequency energy, peaking about 70 cycles-per-hour (cph), and low-frequency energy, peaking about 0.01 cph, and that there is a wide frequency region near 1 cph where there is little wind energy.

The curve justifies dividing the wind into a slowly-time-varying, mean-wind component and a rapidly-time-varying gust component. Let \underline{u} be the three vectors of wind components at a point (forward, sideways, and up), and let \underline{U} be the time average

$$\underline{U} = \frac{1}{2T} \int_{-T}^T \underline{u} dt$$

where T is of the order of 1/2 hour. Let \underline{u}' be the difference

$$\underline{u}' = \underline{u} - \underline{U}$$

From the above spectra plot, \underline{U} will consist almost entirely of winds with frequency components near 0.01 cph, and \underline{u}' of winds with frequency components near 70 cph. \underline{U} and \underline{u}' are defined to be the mean wind and gust components of \underline{u} , respectively.

C. DERIVATIONS FROM THE NAVIER-STOKES EQUATIONS

1. General

Most of the useful information obtained on gust physics has been obtained from equations derived from the Navier-Stokes equations. Let \underline{u} be the velocity of a unit volume of air at a point and ρ be its density. Let r_1, r_2, r_3 be distances measured in the downwind, crosswind, and vertical directions (that is, r_1 is in the direction of the mean wind \underline{U} , assumed horizontal, and r_2 and r_3 are assigned by the right-hand rule, with r_3 vertical). $F = ma$ for a unit volume of air is then

$$\begin{aligned}\frac{d}{dt}(\rho \underline{u}) &= \frac{\partial}{\partial t}(\rho \underline{u}) + \underline{u} (\nabla \cdot \rho \underline{u}) \\ &= -\nabla p + \nu \rho \nabla^2 \underline{u} - \rho g \delta_{i3}\end{aligned}$$

where ∇ is the divergence operator $\nabla = \left(\frac{\partial}{\partial r_1} \quad \frac{\partial}{\partial r_2} \quad \frac{\partial}{\partial r_3} \right)$, the dot (\cdot) indicates a vector product, ν is the coefficient of viscosity, and δ_{ij} is the Kronecker delta ($\delta_{ij} = 1$ if $i = j$, 0 if $i \neq j$) used to indicate that the gravity term produces only a vertical force.

Letting

$$\underline{u} = \underline{U} + \underline{u}'$$

where \underline{U} is the mean wind (the bar under U has been dropped as U is a scalar in the r_1 direction in this coordinate system), the above equation can be manipulated by taking time averages of all terms to obtain a \underline{U} equation, then subtracting these terms to obtain a \underline{u}' gust equation. Lumley does this in reference 2 as follows: $\rho, T,$ and p are written as deviations from nominal values ρ_0, T_0, p_0 .

$$\rho = \rho_0 + \rho'$$

$$T = T_0 + T'$$

$$p = p_0 + p'$$

where ρ_0, T_0, p_0 satisfy

$$\rho_0 R T_0 = p_0$$

$$\frac{\partial p_0}{\partial z} = -\rho_0 g$$

$$\frac{\partial T_0}{\partial z} = -g/C_p$$

It is then assumed that the density deviation ρ' is not a function of the local pressure deviation p' , producing the gas law

$$(\rho_0 + \rho') R(T_0 + T') = p_0$$

or, to a first approximation,

$$\frac{\rho'}{\rho_0} = -\frac{T'}{T_0}$$

The z force term in the Navier-Stokes equations then becomes

$$\begin{aligned} -\frac{1}{\rho} \frac{\partial p}{\partial z} - g &= -\frac{1}{\rho_0 + \rho'} \frac{\partial(p_0 + p')}{\partial z} - g \\ &\approx -\frac{1}{\rho_0} \frac{\partial p_0}{\partial z} - g - \frac{1}{\rho_0} \frac{\partial p'}{\partial z} + \frac{\rho'}{\rho_0} \frac{\partial p_0}{\partial z} \\ &= -\frac{1}{\rho_0} \frac{\partial p'}{\partial z} + g \frac{T'}{T_0} \end{aligned}$$

The terms ρ' , T' , and p' are then written as sums of time average values and deviations,

$$\rho' = \overline{\rho'} + \rho''$$

$$T' = \overline{T'} + T''$$

$$p' = \overline{p'} + p''$$

where the overbar (—) indicates a time average. The above potential temperature (θ) is then introduced and similarly divided into a time average value and a deviation,

$$\theta = \overline{\theta} + \theta''$$

and it is argued that the deviations θ'' and T'' are approximately equal,

$$g \frac{T''}{T_0} \approx g \frac{\theta''}{T_0}$$

Returning to the original Navier-Stokes equations, Lumley first ignores the density variation terms,

$$\left(\frac{\partial \rho'}{\partial t}, \nabla \rho' \right)$$

as being negligible compared to the velocity variation terms

$$\left(\frac{\partial \underline{u}'}{\partial t}, \nabla \cdot \underline{u}' \right)$$

The only density variation term retained is the z force term $g \frac{T'}{T_0}$, as this

term is critical as far as thermal stability. Subtracting the time-averaged terms from the Navier-Stokes equations and dropping the double prime superscripts from p'' and θ'' , Lumley finally obtains for the components,

$$\underline{u}' = \begin{bmatrix} u \\ v \\ w \end{bmatrix} = \begin{bmatrix} \text{downwind gusts} \\ \text{crosswind gusts} \\ \text{vertical gusts} \end{bmatrix}$$

the equations

$$\begin{aligned} \frac{\partial u}{\partial t} + \frac{\partial U}{\partial r_3} w + \frac{\partial u}{\partial r_1} U + (\underline{u}' \cdot \nabla u) - \overline{\underline{u}' \cdot \nabla u} \\ = - \frac{1}{\rho_0} \frac{\partial p}{\partial r_1} + \nu \nabla^2 u \end{aligned}$$

$$\begin{aligned} \frac{\partial v}{\partial t} + \frac{\partial v}{\partial r_1} U + (\underline{u}' \cdot \nabla v) - \overline{\underline{u}' \cdot \nabla v} \\ = - \frac{1}{\rho_0} \frac{\partial p}{\partial r_2} + \nu \nabla^2 v \end{aligned}$$

$$\begin{aligned} \frac{\partial w}{\partial t} + \frac{\partial w}{\partial r_1} U + (\underline{u}' \cdot \nabla w) - \overline{\underline{u}' \cdot \nabla w} \\ = - \frac{1}{\rho_0} \frac{\partial p}{\partial r_3} + \nu \nabla^2 w + \frac{g}{T_0} \theta \end{aligned}$$

2. Energy

The gust energy \mathcal{E} of a volume of air of unit mass is defined to be the sum of velocity products

$$\mathcal{E} = \frac{1}{2} (u^2 + v^2 + w^2)$$

Multiplying the above equations on the left by u , v , w respectively, taking the time average of both sides, and adding the equations, there results the average energy equation

$$\begin{aligned} \frac{d\bar{\mathcal{E}}}{dt} &= \frac{d}{dt} \frac{1}{2} \overline{(u^2 + v^2 + w^2)} \\ &= u \frac{\partial \bar{u}}{\partial t} + v \frac{\partial \bar{v}}{\partial t} + w \frac{\partial \bar{w}}{\partial t} + (\bar{U} + \bar{u}') \cdot \nabla \bar{\mathcal{E}} \\ &= \frac{\partial \bar{U}}{\partial r_3} \bar{u} \bar{w} - \frac{1}{\rho_0} \overline{u' \cdot \nabla^2 u'} + \frac{g}{T_0} \bar{\theta} \bar{w} \end{aligned}$$

Here $\frac{\partial \bar{U}}{\partial r_3} \bar{u} \bar{w}$ is the rate of extraction of gust energy from the mean wind via vertical shear, $\frac{1}{\rho} \overline{u' \cdot \nabla p}$ is the rate of work done moving against pressure gradients, $\overline{u' \cdot \nabla^2 u'}$ is the rate of energy lost to viscosity, and $\frac{g}{T_0} \bar{\theta} \bar{w}$ is the rate of vertical transport of heat energy. The two terms $\frac{\partial \bar{U}}{\partial r_3} \bar{u} \bar{w}$ and $\frac{g}{T_0} \bar{\theta} \bar{w}$ are commonly called mechanical and heat energy production terms respectively. The pressure gradient term $\frac{1}{\rho_0} \overline{u' \cdot \nabla p}$ does nothing more than distribute this energy among the gust components, while the viscous term dissipates the gust energy (as heat).

3. Friction Velocity

The correlation $\bar{u} \bar{w}$ in the energy equation is experimentally negative, implying an association of down gusts with downwind gusts and up gusts with gusts in the $-U$ direction.

The friction velocity u^* is defined to be

$$u^* = (-\overline{uw})^{1/2}$$

so u^* is a direct measure of the downwind, up-gust cross correlation.

4. Covariance Differential Equation

The equation of greatest interest for aircraft gust analyses is that for the covariances of gust components. Let \underline{r}_0, t_0 and \underline{r}_1, t_1 denote two points in time and space, and $u' = (u_1, u_2, u_3)$ be the gust components at a point.

Define $R(\underline{r}_0, \underline{r}_1, t_0, t_1)$ to be the matrix of gust covariances:

$$\begin{aligned} R(\underline{r}_0, \underline{r}_1, t_0, t_1) &= E \{ [u'(\underline{r}_0, t_0)] [u'(\underline{r}_1, t_1)] \} \\ &= [E \{ u_i(\underline{r}_0, t_0) u_j(\underline{r}_1, t_1) \}] \end{aligned}$$

That is, the ij^{th} component of R is the covariance of the i^{th} gust component at \underline{r}_0, t_0 with the j^{th} component at \underline{r}_1, t_1 . (E is the expectation operator, indicating an ensemble average. \overline{E} does not indicate a time average, a time average being denoted by an overbar.)

The derivative of R with respect to the time displacement $t_1 - t_0$ between the two points $\underline{r}_0, \underline{r}_1$ is

$$\begin{aligned} \frac{\partial R}{\partial(t_1 - t_0)} &= -E \left\{ \left[\frac{\partial u'}{\partial t_0}(\underline{r}_0, t_0) \right] [u'(\underline{r}_1, t_1)] \right\} \\ &\quad + E \left\{ [u'(\underline{r}_0, t_0)] \left[\frac{\partial u'}{\partial t_1}(\underline{r}_1, t_1) \right] \right\} \end{aligned}$$

Multiplying the above gust-component equations at \underline{r}_0, t_0 by the gust components at \underline{r}_1, t_1 , doing the same at \underline{r}_1, t_1 and \underline{r}_0, t_0 , taking expectations, and taking the differences between the resulting terms, there results the component equation

$$\begin{aligned} \frac{\partial R_{ij}}{\partial(t_1 - t_0)} &= \sum_K \frac{\partial}{\partial r_K} (\overline{u_i u_K u_j} - \overline{u_i u_K} \overline{u_j}) + \frac{1}{\rho} \left(\overline{\frac{\partial p}{\partial r_i} u_j} - \overline{\frac{\partial p}{\partial r_j} u_i} \right) \\ &\quad + 2v \nabla^2 R_{ij} \\ &\quad + \frac{g}{T_0} U_i \theta' \delta_{j3} + \frac{g}{T_0} \theta U_j' \delta_{i3} \end{aligned}$$

where the primed variables are evaluated at \underline{r}_1, t_1 and the unprimed variables at \underline{r}_0, t_0 .

It is noted that R in this equation is a product of two velocities, but its time and space dependence depend on space derivatives of a triple-velocity product ($u_i u_K u_j'$). Looking back at the Navier-Stokes equations, the velocities there depend upon a velocity product. In general, the time and space dependence of any product of n velocities will depend upon space derivatives of products of $n + 1$ velocities. It is this fact that makes solving for R impossible. To calculate R , or any product of n velocities for that matter, one would have to calculate a countable infinity of higher order velocity products at the same time. No one has found a way to write an equation for any such product that contains only products of that order or lower.

Attempts to close this infinity of velocity products by assuming the higher order products to be functions of the lower order products have been made, but the solutions obtained have proved incapable of useful generalization.²

5. Velocity Divergence

Density variation terms $\frac{\partial \rho}{\partial t}, \nabla \rho$ were dropped in deriving the above gust equations as being negligible when compared with velocity variation terms. This is equivalent to assuming that, for the purposes of those equations, air is an incompressible fluid. Since the integral

$$\int \rho u' \cdot ds$$

over a closed surface s is the net mass increase of the enclosed volume per unit time, which must be zero, it follows that the velocity divergence is zero

$$\nabla \cdot u' = 0$$

Multiplying this by the velocity at a remote point and taking an ensemble average, it follows that the divergence of the covariance matrix is zero,

$$\nabla \cdot R = 0$$

(i. e., the divergence of the row or column vectors of R is zero). The gust covariance sensor must then satisfy this equation as well as the time decay equation above.

²The closures have been made by introducing "Austausch coefficients," which process the writer has not been able to follow. The above conclusion is based on the absence of discussions of general solutions obtained in this manner in the literature.

6. Stationarity and Horizontal Homogeneity

From the power spectra presented above, for time intervals of an hour or so it appears reasonable to assume that the gust covariances are going to depend on the time displacement between the two points $t_1 - t_0$, but not on either of the points t_0 or t_1 . This has been experimentally verified. It is therefore reasonable to drop the t_0 dependence from R and write

$$R(\underline{r}_0, t_0, \underline{r}_1, t_1) = R(\underline{r}_0, \underline{r}_1, t_1 - t_0)$$

This, of course, is equivalent to assuming that the gust random processes are wide-sense stationary in time.

Assuming the terrain below to be homogeneous, it is also reasonable to assume that R will be dependent on the vector displacement between the two points $\underline{r}_1 - \underline{r}_0$ and on the altitude of one of the points, but independent of the horizontal position of either of the points. Let z be the altitude of the left-hand point in R. R can then be written

$$R(\underline{r}_0, \underline{r}_1, t_1 - t_0) = R(z, \underline{r}_1 - \underline{r}_0, t_1 - t_0)$$

Horizontal homogeneity is then equivalent to assuming wide-sense stationarity with regard to distance variations in the horizontal plane.

These two assumptions reduce the independent arguments of R from eight to five.

7. Isotropy

Isotropy is an assumption that the gust covariance tensor R is independent of translations, rotations, and reflections of the $r = (r_1, r_2, r_3)$ coordinate axes. The gusts at higher altitudes are normally assumed isotropic.

The translation independence is the same as assuming that the gusts are both horizontally and vertically homogeneous. This eliminates the altitude dependence above so that R can be written

$$R(\underline{r}_0, t_0, \underline{r}_1, t) = R(\underline{r}_1 - \underline{r}_0, t_1 - t_0)$$

Taking the vector $\underline{r}_1 - \underline{r}_0$ to lie in the r_1 direction, rotation of the r_2, r_3 coordinate axes 180 degrees about r_1 produces the equalities

$$E\{u_1(0,0)u_2(r_1,t)\} = -E\{u_1(0,0)u_2(r_1,t)\} = 0$$

$$E\{u_1(0,0)u_3(r_1,t)\} = -E\{u_1(0,0)u_3(r_1,t)\} = 0$$

and rotation by 90 degrees about r_1 produces

$$E\{u_2(0,0)u_2(r_1,t)\} = E\{u_3(0,0)u_3(r_1,t)\} = g(r_1,t)$$

Reflection of the r_2 axis across the r_1, r_3 plane produces

$$E\{u_2(0,0)u_3(r_1,t)\} = -E\{u_2(0,0)u_3(r_1,t)\} = 0$$

Hence for $\underline{r}_1 - \underline{r}_0$ in the r_1 direction, R if isotropic must take the form

$$R(r_1, r_2, r_3, t) \Big|_{r_2 = r_3 = 0} = \begin{bmatrix} f(r_1, t) & 0 & 0 \\ 0 & g(r_1, t) & 0 \\ 0 & 0 & g(r_1, t) \end{bmatrix}$$

Let r be the distance metric

$$r = (r_1^2 + r_2^2 + r_3^2)^{1/2}$$

Since R must be independent of rotations of the coordinate system, the covariances of gusts at any two points separated by r must be

$$R(\underline{r}, t) = \begin{bmatrix} f(r, t) & 0 & 0 \\ 0 & g(r, t) & 0 \\ 0 & 0 & g(r, t) \end{bmatrix}$$

where $R = [R_{ij}]$, u_1 is the gust component parallel to r , and u_2 and u_3 are gust components orthogonal to u_1 and to each other.

Given a coordinate system r_1, r_2, r_3 and two points separated by r , the gust components in the original coordinate system can be obtained from those parallel and orthogonal to r (defined above) by vector transformation. Without going through the trigonometry, the direction cosines in this transformation are $r_1/r, r_2/r, r_3/r$, and R can be written

$$R(\underline{r}, t) = \left[\frac{f(r, t) - g(r, t)}{r^2} \right] [\underline{r} \underline{r}'] + g(r, t) \cdot I$$

where I is the 3 x 3 identity matrix.

The application of $\nabla \cdot R = 0$ to the first column of R yields

$$\begin{aligned} \sum_{i=1}^3 \frac{\partial R_{ij}}{\partial r_i} &= 0 \\ &= \frac{2r_1}{r^2} [f-g] + \frac{\partial r}{\partial r_1} \left[(f'-g') \frac{r_1^2}{r^2} + (f-g) \left(\frac{-2r_1^2}{r^3} \right) + g' \right] \\ &\quad + \frac{r_1}{r^2} [f-g] + \frac{\partial r}{\partial r_2} \left[(f'-g') \frac{r_1 r_2}{r^2} + (f-g) \left(\frac{-2r_1 r_2}{r^3} \right) \right] \end{aligned}$$

where the prime (') superscript indicates a partial derivative with respect to r. With $\partial r / \partial r_i = r_i / r$, this reduces to

$$0 = \frac{4r_1}{r^2} [f-g] + \frac{r_1}{r} [f'-g'] - \frac{2r_1}{r^2} [f-g] + \frac{r_1}{r} g'$$

whence

$$g(r, t) = f(r, t) + \frac{1}{2} r \frac{\partial f(r, t)}{\partial r}$$

so that only one function of two variables, $f(r, t)$, need be specified to define the covariance tensor $R(r, t)$ completely. The choice

$$f(r, 0) = \exp[-|r|/L]$$

yields

$$g(r, 0) = 1 - \frac{1}{2} \frac{|r|}{L} \exp[-|r|/L]$$

for example, and the choice

$$f(r, 0) = \exp[-r^2/L^2]$$

yields

$$g(r, 0) = [1 - r^2/L^2] \exp[-r^2/L^2]$$

As discussed below, the first correlation function above is commonly employed as a fit to experimental gust correlations, but it contains an anomaly not present in the second correlation.

8. Isotropic Cross Correlations

Consider the paths r and r_1 through the atmosphere indicated in Figure 2.

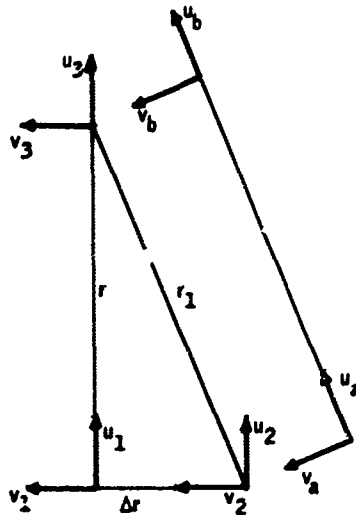


Figure 2. Cross Correlation Geometry

It is clear that since u_1, u_3 are parallel to each other and to r , and v_1, v_3 are parallel to each other and orthogonal to r , then, from the isotropic tensor,

$$E\{u_1 u_3\} = f(r)$$

$$E\{v_1 v_3\} = g(r)$$

$$E\{v_1 u_3\} = E\{v_3 u_1\} = 0,$$

so the orthogonal gust pairs $u_1 v_3$ and $u_3 v_1$ are uncorrelated for all r . For an aircraft flying along path r the head-on gusts (u) and the side gusts (v) will be uncorrelated.

It does not follow that the shear of the head-on gusts (u) across the path r (spanwise shear across the wing) and the side gusts v are uncorrelated. It can easily be proved that they are correlated. Consider the path r_1 . Here u_a, u_b are parallel to each other and to r_1 , while v_a, v_b are parallel to each other and orthogonal to r_1 . With

$$\begin{bmatrix} u_2 \\ v_2 \end{bmatrix} = \begin{bmatrix} \frac{r}{r_1} & \frac{-\Delta r}{r_1} \\ \frac{\Delta r}{r_1} & \frac{r}{r_1} \end{bmatrix} \begin{bmatrix} u_a \\ v_a \end{bmatrix} \quad \begin{bmatrix} u_3 \\ v_3 \end{bmatrix} = \begin{bmatrix} \frac{r}{r_1} & \frac{-\Delta r}{r_1} \\ \frac{\Delta r}{r_1} & \frac{r}{r_1} \end{bmatrix} \begin{bmatrix} u_b \\ v_b \end{bmatrix}$$

then

$$\begin{aligned} E \begin{bmatrix} u_2 \\ v_2 \end{bmatrix} [u_3 v_3] &= \begin{bmatrix} \frac{r}{r_1} & \frac{-\Delta r}{r_1} \\ \frac{\Delta r}{r_1} & \frac{r}{r_1} \end{bmatrix} E \begin{bmatrix} u_a \\ v_a \end{bmatrix} [u_b v_b] \begin{bmatrix} \frac{r}{r_1} & \frac{\Delta r}{r_1} \\ \frac{-\Delta r}{r_1} & \frac{r}{r_1} \end{bmatrix} \\ &= \begin{bmatrix} \frac{r}{r_1} & \frac{-\Delta r}{r_1} \\ \frac{\Delta r}{r_1} & \frac{r}{r_1} \end{bmatrix} \begin{bmatrix} f(r_1) & 0 \\ 0 & g(r_1) \end{bmatrix} \begin{bmatrix} \frac{r}{r_1} & \frac{\Delta r}{r_1} \\ \frac{-\Delta r}{r_1} & \frac{r}{r_1} \end{bmatrix} \\ &= \begin{bmatrix} \frac{f(r_1)r^2 + g(r_1)\Delta r^2}{r_1^2} & (f(r_1) - g(r_1)) \frac{r\Delta r}{r_1} \\ (f(r_1) - g(r_1)) \frac{r\Delta r}{r_1} & \frac{(f(r_1) - \Delta r^2 + g(r_1)r^2)}{r_1^2} \end{bmatrix} \end{aligned}$$

Therefore

$$E\{u_2 v_3\} = (f(r_1) - g(r_1)) \frac{r\Delta r}{r_1}$$

Defining the across-path shear u_y of u as

$$u_y = \lim_{\Delta r \rightarrow 0} \frac{u_2 - u_1}{\Delta r}$$

the cross correlation of u_y and v_3 is

$$\begin{aligned} E\{u_y v_3\} &= \lim_{\Delta r \rightarrow 0} \left[\frac{E_2\{u_2 v_3\} - E\{u_1 v_3\}}{\Delta r} \right] \\ &= \lim_{\Delta r \rightarrow 0} \left[\frac{(f(r_1) - g(r_1)) \frac{r \Delta r}{2}}{r_1 \Delta r} \right] \\ &= \lim_{\Delta r \rightarrow 0} \left[(f(r_1) - g(r_1)) \frac{r}{r_1} \right] \\ &= \frac{f(r) - g(r)}{r} \end{aligned}$$

From the above formula relating f and g ,

$$E\{u_y v_3\} = \frac{f(r) - g(r)}{r} = 1/2 \frac{\partial f(r)}{\partial r}$$

This cannot be zero unless $f(r)$ is a constant, which is impossible.

The choice of a correlation function

$$f(r) = e^{-|r/L|}$$

produces the cross correlation

$$E\{u_y v_3\} = \frac{1}{2L} e^{-|r/L|}$$

while the choice

$$f(r) = e^{-(r/L)^2}$$

produces the cross correlation

$$E\{u_y v_3\} = \frac{r}{L^2} e^{-(r/L)^2}$$

Clearly u_y and v_3 are uncorrelated at a point ($r = 0$) if the correlation $f(r)$ has a zero derivative there.

Using the same derivation as the above, it can be shown for isotropic turbulence that the vertical gust shear across the path w_y is uncorrelated with u , v , w ,

$$E\{w_y u_3\} = E\{w_y v_3\} = E\{w_y w_3\} = 0$$

and in addition that

$$E\{u_y u_3\} = E\{v_y v_3\} = E\{w_y u_y\} = E\{w_y v_y\} = 0$$

where v_y is the side-gust shear across the path. The only other nonzero correlation of interest in aircraft gust analyses is that of side-gust shear to head-on gusts,

$$E\{v_y u_3\} = -\frac{1}{2} \frac{\partial f(r)}{\partial r}$$

These shears are of interest because they produce rolling and yawing moments on an airplane via differential lift and drag on the two wings.

D. RICHARDSON NUMBERS

From the above energy equation the ratio of rates of energy lost by buoyancy to energy introduced mechanically through the mean wind shear is defined to be the flux Richardson number R_f ,

$$R_f = \frac{\frac{-g}{T} \overline{\theta w}}{\frac{-\partial U}{\partial r_3} \overline{uw}}$$

If $R_f > 1$, energy is lost faster than it is introduced through the mean wind shear, and the total turbulent energy will decay. This does not imply an absence of turbulence -- turbulence can be introduced by forcing air around obstacles, etc.; $R_f > 1$ implies only that what turbulent energy there is will eventually decay away.

The flux Richardson number is seldom used in practice, as measurement of $\frac{g}{T_0} \theta w$ involves elaborate measurement and calculation. The gradient Richardson number, R_i , which is easily measured, is used instead. R_i is a dimensionless number relating the bouyant force $\frac{g}{\theta} \frac{\partial \theta}{\partial z}$, derived above, to the shear $\frac{\partial U}{\partial r_3}$ which produces the mechanical energy,

$$R_i = \frac{\frac{g}{\theta} \frac{\partial \theta}{\partial z}}{\left(\frac{\partial U}{\partial r_3}\right)^2}$$

This number then expresses the same physical 'notions' as the flux Richardson number as it is a ratio of bouyancy and mechanical effects. From the above stability discussion, the air is unstable if $R_i < 0$, and for R_i positive and large the air is stable. For R_i positive and small the tendency of the shear term to introduce instability and turbulence can be larger than the ability of the $\frac{g}{\theta} \frac{\partial \theta}{\partial z}$ term to "damp" this tendency, and the air can be unstable.

Linearized theory indicates that the air will be unstable and turbulent if $R_i < 0$, stable if $R_i > 1/4$, and possibly unstable if $0 < R_i < 1/4$ (reference 3).³

E. WIND PROFILES

The vertical shear of the mean wind as it passes over a rough surface (the earth) must intuitively increase with increasing mean wind speed and with increasing surface roughness and decrease with distance from the rough surface (altitude). It must also be a function of thermal stability, as instability implies pumping bouyant energy into both the gust and mean-motion energies.

In his book (reference 2) Panofsky has been able to fit the velocity profiles for all thermal stability conditions with a single function, valid for the lowest few meters of the atmosphere,

$$U(z) = \frac{u^*}{K} [\ln(z/z_0) - \Psi]$$

³Pointed out to the writer by Professor Dutton

where z_0 is the "roughness length" of the surface, K is the Von Karman constant, equal to 0.4, and Ψ contains the effect of thermal instability. In using this equation one must choose a reference altitude z_1 , the velocity $V(z_1)$ there, a roughness length z_0 , and the Richardson number R_i at that altitude. z_0 varies from 0.03 meter for smooth surfaces to 5 meters for very rough surfaces. A characteristic length L' is then computed from R_i via [taken from section 3.5 of reference 2]

$$z_1/L' = R_i(1-18R_i)^{-1/4} \text{ for } R_i < 0$$

$$z_1/L' = R_i[1+7R_i]^{-1} \text{ for } 0 < R_i < 0.1$$

Ψ is then found from Figure 3.3 of reference 2, presented here as Figure 3. The above equation is then solved for friction velocity u^* ,

$$u^* = KU(z_1) [\ln(z_1/z_0) - \Psi(z_1/L')]^{-1}$$

u^* and L' are then assumed constant with altitude. $V(z)$ at $z \neq z_1$ is then found by solving first for $\Psi(z/L')$ and then using the first profile equation above.

Note that L' is infinity for neutrally stable air (where $R_i = 0$), in which case

$$U(z) = \frac{u^*}{K} \ln(z/z_0)$$

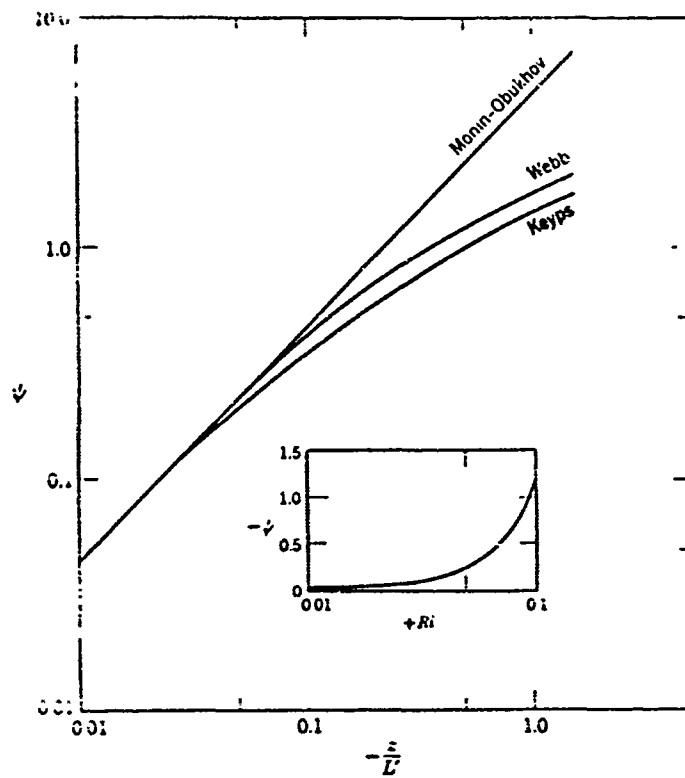
$$\frac{\partial U(z)}{\partial z} = \frac{u^*}{Kz}$$

$$\frac{U(z) - U(z_1)}{U(z_1)} = \frac{u^*}{KU(z_1)} \ln(z/z_1)$$

$$\exp \frac{U(z) - U(z_1)}{U(z_1)} = (z/z_1) \frac{u^*}{KU(z_1)}$$

For $U(z) - U(z_1)$ small, this is approximately

$$\begin{aligned} \exp \frac{U(z) - U(z_1)}{U(z_1)} &\approx \frac{U(z)}{U(z_1)} \\ &= (z/z_1)^p \end{aligned}$$



Universal function, ψ , for the integrated wind profile. Main graph for unstable stratification; insert, for stable conditions. For $|z/L$, or $|Ri| \leq 0.01$, $\psi = 4.5 z/L = 4.5 Ri$. (According to Panofsky, 1963.)

Figure 3. Universal Function ψ

where

$$p = \frac{u^*}{KU}(z_1)$$

This latter form of wind profile is widely reported, and was used by Scoggins, et al, in NASA TMX-53328 to generate typical wind profiles for missile work.

Typical roughness lengths z_0 are 0.03 meter for an open airport, 0.5 m for a forest, and 0.66 m to 5 m for a city.⁴ A few trial calculations with these lengths shows the above formula to be sensitive to z_0 for z_1/z_0 small, but insensitive to z_0 for z_1/z_0 large. In the latter case, the difference between $U(z)/U(z_1)$ and $\exp[(U(z) - U(z_1))/U(z_1)]$ for z/z_0 large is quite small.

Professor Panofsky suggested using the exponent formula

$$\frac{U(z)}{U(z_1)} = (z/z_1)^p$$

with $p = 0.12$ for smooth terrain to $p = 0.38$ for rough terrain, $p = 0.25$ being a reasonable figure for slightly unstable conditions and moderate terrain. While this formula will not produce accurate velocities at small z , near the ground, it is reasonable at higher altitudes.

F. ENERGY SPECTRA⁵

The energy density \mathcal{E} whose time rate was derived above is a scalar function of position and time. Holding time fixed, one can take its fourier transform with respect to distance along any straight line. Doing this successively in the downwind, crosswind, and vertical directions, one obtains a three-dimensional transform $\mathcal{E}(K_1, K_2, K_3)$, where K_1, K_2, K_3 are the wave numbers (frequencies, in radians per meter) in the three directions. Integrating over a spherical surface of constant wave number K ,

$$K^2 = K_1^2 + K_2^2 + K_3^2$$

⁴Related by Professor Panofsky in a letter to the writer from Professor Dutton dated 11 July 1967.

⁵From Batchelor, reference 1.

produces

$$\mathcal{E}(K) = \iiint \mathcal{E}(K_1, K_2, K_3) \underline{dK}$$

$$K = K_1^2 + K_2^2 + K_3^2$$

where $\mathcal{E}(K)$ is the wave number density of \mathcal{E} . That is,

$$\mathcal{E} = \int \mathcal{E}(K) dK$$

so $\mathcal{E}(K)$ is a space power-spectra.

Doing this, Batchelor and Lumley [reference 2] argue that energy is introduced at low wave numbers (over long distances) by the

$$\frac{\partial U}{\partial r_3} (u^*)^2 \text{ and } \frac{g}{T_0} \overline{\theta w}$$

production terms, in the r_1, r_3 directions. It is then distributed uniformly among the gust components by the ∇p pressure gradient term, and dissipated at short wavelengths by the viscosity term. The energy is transferred from the low-wave-number, energy-production region to the high-wave-number, dissipation region of the spectra by the mechanism of the triple velocity products in the $\frac{\partial R}{\partial t}$ equation derived above. These nonlinear products add spectral frequencies, just as

$$\cos^2 K = \frac{1}{2} (1 + \cos 2K)$$

does in conventional nonlinear analyses, accounting for the energy transfer phenomenon.

(If it were not for this effect, the energy equations would be linear and would undoubtedly have been solved long ago. The above nonlinear argument of frequency summing to push energy to higher wave numbers seems tenuous. It is not. Nonlinearities always introduce energies at new frequencies, and one need know only that a triple velocity product appears in the covariance tensor equation to know that this effect is present. Further, energy is introduced at low wave numbers and dissipated at high wave numbers; the nonlinearities must produce a net transfer of energy up the wave-number scale as there are no other mechanisms present to produce this phenomenon.)

The transfer of energy among the gust components via the pressure gradient term in the energy equation implies that the gust spectra at high wave numbers should be isotropic. This has been observed experimentally. From

isotropy considerations it follows that the cross-gust spectra (between gust components) should be zero at high wave numbers along any path through the gust field.

Elderkin's data [reference 4] has this property.

Further examination of $\mathcal{E}(K)$ reveals a wave number region, the inertial subrange, where energy is neither produced nor dissipated. From dimensional arguments over such a region $\mathcal{E}(K)$ must possess the shape

$$\mathcal{E}(K) = a \epsilon^{2/3} K^{-5/3}$$

where a is a universal constant and ϵ is the rate of dissipation of energy.

Almost all experimental data exhibit this inertial subrange. In fact, the $K^{-5/3}$ law experimentally holds to lower wave numbers than the lower limit of the inertial subrange. The reason for this has not been explained.

G. THE TAYLOR HYPOTHESIS

Returning to the gust covariance tensor R , under assumptions of time stationarity and horizontal homogeneity R can be expressed as a function of the altitude z of one of the points, the vector displacement $\underline{r} = (r_1, r_2, r_3)$ between the points, and the time displacement t between the points,

$$\begin{aligned} R(\underline{r}_0, t_0, \underline{r}_0 + \underline{r}, t_0 + t) &= R(z, \underline{r}, t) \\ &= R(z, r_1, r_2, r_3, t) \end{aligned}$$

Since the friction velocity u^* is a function of stability, as shown in the wind profile discussion above, the Richardson number R_i should also be included as an argument in R ,

$$R = R(R_i, z, r_1, r_2, r_3, t)$$

The Taylor hypothesis is an assumption made about the downwind correlations $R(R_i, z, r_1, 0, 0, t)$. It states that the space rate of decay of covariances in the downwind direction equals the time rate of decay of the covariances at a point, normalized by the mean wind speed. That is

$$R(R_i, z, 0, 0, 0, t) = R(R_i, z, U(z) t, 0, 0, 0)$$

This hypothesis permits experimental collection of spatial covariances from anemometers mounted at a point.

This hypothesis is often construed to imply a frozen gust field, frozen in time and space with respect to a coordinate system moving downwind with the mean wind,

$$\underline{u}'(r_1, r_2, r_3, t) = \underline{u}'(r_1 - Ut, r_2, r_3, 0)$$

as this produces the above covariance relation. However, in general, any distance metric $r(r_1, U, t)$

$$R(R_i, z, r_1, 0, 0, t) = R(R_i, z, r, 0, 0, 0)$$

with the two properties

$$r(r_1, U, 0) = r_1$$

$$r(0, U, t) = Ut$$

will satisfy the Taylor Hypothesis.

Figure 5.22 in reference 2 is a plot from measured data of constant r lines (equivalent to constant R lines, called isopleths) on an r_1, t surface. The constant r lines are approximately ellipses, at least for r small, satisfying

$$\begin{aligned} r &= \left[\frac{99(r_1 - Ut)^2 + (r_1 + Ut)^2}{100} \right]^{1/2} \\ &= \left[(r_1 - 0.98Ut)^2 + 0.0394(Ut)^2 \right]^{1/2} \end{aligned}$$

The frozen field hypothesis that

$$r = r_1 - Ut$$

is thus almost correct.

The space-time relation is actually not as simple as the above formula indicates. Batchelor calculates in reference 1 that $R(R_i, \underline{r}, t)$ must asymptotically approach

$$R_{ij}(R_i, \underline{r}, t) = \frac{\text{CONST}}{(t)^{5/2}} \left[a_{ij} - \frac{c_{ij} \underline{r}' \underline{r}}{4vt} \right] \exp[-r^2/8vt]$$

as t advances to infinity, which does not concur with the Taylor hypothesis. Further, from energy considerations, large eddys tend to persist so that $R(R_i, z, \underline{r}, t)$ should be nearly independent of t for r large, t small. Inertia effects tend to push energy from low to high wave numbers (large to small eddys), pressure forces tend to distribute the energy uniformly among gust components, and the larger wave number eddys are fairly rapidly damped by viscosity. Thus one would expect that, even with the Taylor hypothesis, the distance metric should be something like

$$r = \{ [r_1 - f(r_1) Ut]^2 + [1 - f(r_1)^2] (Ut)^2 \}^{1/2}$$

where $f(r_1)$ increases rapidly for r_1 small, but is nearly constant for large r_1 . For example,

$$f(r_1) = 0.98 [1 - \exp(-r_1)]$$

has this property.

H. TURBULENCE SCALES

1. General

The integral scale of an autocorrelation function is defined to be the integral over a path \underline{r}

$$L = \frac{\int_0^{\infty} R_{ii}(R_i, z, \underline{r}, 0) d\underline{r}}{R_{ii}(R_i, z, 0, 0)}$$

L is then the normalized area under an autocorrelation curve. As such, it has little significance.

However, if an analytical form for the autocorrelation R is assumed, L has a great deal of significance. If one assumes an exponential autocorrelation,

$$R_{ii}(R_i, z, \underline{r}, 0) = \sigma^2 \exp[-|\underline{r}|/L^*]$$

then $L = L^*$, so that $1/L$ is the "bandwidth" of the corresponding gust spectra, or the location of the peak on a plot of

$$K \int_{-\infty}^{\infty} e^{jKr} R_{ii}(R_i, z, r, 0) dr$$

versus K . $1/L$ measures the space rate of decay of the autocorrelations, and, via the Taylor hypothesis, U/L measures its time rate of decay. Both of the latter are, of course, important parameters in V/STOL gust analyses.

The integral scale L then can be read from the peak of a spectral plot if a form for the spectra is assumed. Therein lies the difficulty. There is a great deal of spread in the spectral data, and the data are band-limited. Thus one can choose a great many autocorrelation forms which would fit the spectral data as well as they can be fit. For example, many choices of (σ^2, L^*, a) can be made such that a spectra form

$$\sigma^2(KL^*) \frac{a(KL^*)^2 + 1}{[(KL^*)^2 + 1]^2}$$

will fit a given set of spectral data. L^* here determines the space and decay rates of the corresponding autocorrelations, yet the peak of these curves occurs at

$$K_{\text{peak}} = \frac{1}{L} = \frac{1}{L^*} \frac{3(1-a) + \sqrt{9(1-a)^2 + 4a}}{2a}$$

Therefore, the space decay rate $1/L^*$ cannot be read from the peak spectra point without assuming the constant a ; L^* thus depends on the form of the spectra assumed.

This is not the only problem with L . Elderkin's data indicates that the peak frequencies for the various gust component spectra in the downwind direction are different. Whether this implies that the space and time decay rates of the various correlations are different as well is not known.

The scale-length situation is considerably more complex than the above curve-fitting argument indicates. Panofsky indicates in section 5.7 of reference 2 that ten-to-one variations in L have been observed for different conditions of thermal stability. Further, the scale of the downwind gust component in the downwind direction has been observed to be considerably longer than its scale in the cross-wind direction in stable air, indicating some sort of eddy stretching in the downwind direction. This stretching can be seen in Figure 5.22 of reference 3. In unstable air the u , v scales are more nearly independent of the azimuth of the correlation path chosen.

The experimental spectra plotted in Figure 5.3 of reference 2 indicate that the horizontal scales increase linearly with altitude,

$$L = \text{const. } z$$

Elderkin's data supports this linear dependence.

No information was found on the effect of wind speed on turbulence scales. (The Taylor hypothesis associates space and time scales at a given wind speed, but does not imply that they are independent of speed.) Elderkin's data, for relatively low wind speeds, indicates that the scales are independent of wind speed. Whether this is true in very strong winds is not known.

2. Turbulence Levels

Panofsky stated in a conversation with the writer that all of the data he had seen indicated that the standard deviation of vertical gusts σ_w and the friction velocity u^* were in nearly constant ratio for all stability conditions,

$$\sigma_w / u^* \approx 1.3$$

There is no theory explaining this constant.

Elderkin's data for the various gust components gives

$$\sigma_u / \sigma_v / \sigma_w \approx 2.8 / 2 / 1.3$$

while Håkūner and Martin (reference 5) give

$$\sigma_u / \sigma_v / \sigma_w \approx 1 / 1.16 / 0.75$$

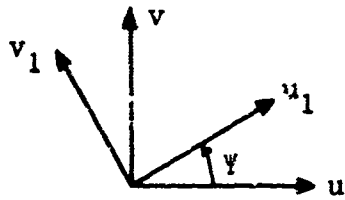
Norman Bowne of the Travelers Research Center stated in a letter to the writer that he had found the ratios

$$\sigma_u / \sigma_v / \sigma_w \approx 1 / 0.8 / 0.42$$

These standard deviations were calculated from finite-length time histories. They can be regarded then as measuring the area under a power spectral curve that has been truncated at both low and high wave numbers. Elderkin's energy density plots (and everyone else's) have not converged to zero at the low-wave-number cutoff, and it is thus entirely possible that there is a significant amount of energy in the wave-number range below the cutoff. Thus, the reported standard deviations may well be sensitive to record length.

The fact that σ_u and σ_v are different implies that the gust field is not horizontally isotropic (i. e., isotropic with regard to the r_1 , r_2 coordinates).

Isotropy requires that the cross correlation of orthogonal, horizontal gust components be zero along every horizontal path. Elderkin's data indicates a zero correlation of downwind and crosswind gust components in the downwind direction. However, for a path at an angle ψ with respect to the downwind direction, the down-path and cross-path gusts u , v are



$$\begin{bmatrix} u_1 \\ v_1 \end{bmatrix} = \begin{bmatrix} \cos \psi & \sin \psi \\ -\sin \psi & \cos \psi \end{bmatrix} \begin{bmatrix} u \\ v \end{bmatrix}$$

so that

$$\begin{bmatrix} \overline{u_1 u_1} & \overline{u_1 v_1} \\ \overline{u_1 v_1} & \overline{v_1 v_1} \end{bmatrix} = \begin{bmatrix} \sigma_u^2 \cos^2 \psi + \sigma_v^2 \sin^2 \psi & (\sigma_v^2 - \sigma_u^2) \cos \psi \sin \psi \\ (\sigma_v^2 - \sigma_u^2) \cos \psi \sin \psi & \sigma_u^2 \sin^2 \psi + \sigma_v^2 \cos^2 \psi \end{bmatrix}$$

The cross correlation $(\sigma_v^2 - \sigma_u^2) \cos \psi \sin \psi$ is nonzero for $\sigma_v^2 \neq \sigma_u^2$.

I. AVAILABLE PROFILE DATA

The wind profile formula

$$V(z) = \frac{u^*}{K} [\ln(z/z_0) + \Psi(R_i)]$$

relates five parameters, z , $V(z)$, z_0 , u^* , R_i . The shear formula

$$\frac{\partial V(z)}{\partial z} = \frac{u^*}{K} \left[\frac{1}{z} + \frac{\partial \Psi(R_i)}{\partial R_i} \frac{\partial R_i}{\partial z} \right]$$

relates z , $\frac{\partial V(z)}{\partial z}$, u^* , R_i , so the two equations together relate six parameters, four of which are independent.

Dr. Scoggins of NASA-MSFC presents data in reference 6 on the probability distribution of $V(z)$ at $z = 9.1$ meters for Cape Kennedy, and he stated in a conversation with the writer that the roughness length there was about 2 meters. Using his data leaves one variable to be specified, either $\frac{\partial V}{\partial z}$, u^* , or R_i . Therefore, one must arbitrarily specify one of these to generate a wind profile of a given likelihood for Cape Kennedy.

No joint statistics of $V(z)$, $\frac{\partial V(z)}{\partial z}$, or of the other parameters which can be used to define them, were found in the literature search.

Norman Bowne gave the writer a probability curve for V at 152 feet for Millstone, Connecticut, but neither z_0 nor R_1 , u^* or $\frac{\partial V}{\partial z}$ was specified.

It is interesting that Scoggins wind-speed distributions plot as nearly straight lines on normal graph paper, indicating that the wind speed is approximately Gaussian. Bowne's data, however, do not plot as a straight line. Wind speed cannot be Gaussian as it is non-negative (it is the magnitude of the vector wind velocity). Assuming that the east-west and north-south wind-velocity components are Gaussian, independent, of zero mean, and of equal standard deviation, the probability distribution of the mean wind speed is

$$\text{Prob}\{U < \alpha\} = 1 - e^{-1/2 \left(\frac{\alpha}{\sigma}\right)^2}$$

the average mean wind is

$$\text{average } U = \sigma \frac{\pi}{2}$$

and the 0.5 likelihood mean wind is

$$U_{(0.5)} = 1.178\sigma$$

This probability function does not plot as a straight line on normal graph paper, and it does not fit Scoggins' or Bowne's data.

The non-Gaussianity of the mean wind speed can be regarded as no more than a curiosity. The fact that Bowne's data at 152 feet does not plot as a straight line on normal graph paper when Scoggins' 9.1-meter data does, however, poses a problem. Because they are different, it is reasonable to assume that the probability distribution of the mean wind speed as a function of altitude depends both on the standard deviation $\sigma(z)$ as a function of altitude, and on altitude explicitly. Rather, it would be unreasonable to assume that the probability distribution at one altitude could be extrapolated to another altitude merely by replacing one normalization constant, $\sigma(z)$. Therefore, wind-speed probability distributions must be experimentally determined at all altitudes of interest.

J. AVAILABLE COVARIANCE DATA

Almost every meteorological paper with the words "wind spectra" in its title has a power spectrum (autocorrelation) of the vertical or downwind gust component in the downwind direction. All that have been found are similar in form to Elderkin's data.

Elderkin's data were the only data found that measured spectra of all gust components and their cospectra.

The only data found in other than the downwind direction are those referred by Panofsky in section 5.7 of his book and in a recent Japanese paper on on-shore winds (reference 7).

No discussions of gust shears, shear correlations, or shear spectra were found in the literature.

No discussions of approximate solutions to the covariance differential equation were found in the literature.

K. AVAILABLE GUST PROBABILITY DENSITIES

The only gust probability densities found were those in reference 7. In the words of the author, "They were not Gaussian in more cases than we had expected". The data there are reasonably bell shaped, however, and Gaussianity may well be a reasonable approximation for some purposes.

L. GAPS

The above fairly well summarizes that which was extracted from the meteorological literature as pertaining to gust model generation. It is apparent that there are many gaps that will have to be filled if a respectable gust model is to be generated. In particular:

- Gust intensities depend upon the friction velocity u^* , which in turn depends upon thermal stability, roughness, and the mean wind. Statistical data on only the latter are available.
- The gust covariance tensor must satisfy a complex differential equation and a divergence equation. Boundary conditions in the form of downwind covariances are available, but generation of a tensor satisfying the equations and boundary conditions is an extremely formidable task. It has never been done. Further, the gust tensor is not completely defined (mathematically) by the above equations and boundary conditions. Covariance data along vertical and crosswind paths are required.

- The implications of thermal stability on the covariance tensor are neither modeled nor understood.
- Integral scales, correlation lengths, and spectral peak points are not clearly related unless a form for the covariance tensor is assumed. The spread of data is sufficient in any experimental spectra plot to preclude defining the form of the correlation functions, so these scales cannot be precisely stated. That they be precisely determined is important to the extent that they define the space and time decay rates of the correlation functions.
- The effects of altitude on probability distributions of mean winds and wind shears are not known, and one cannot today deduce a probability distribution for friction velocity (which defines gust intensities, hence gust severity).
- To the writer's knowledge, the form of spectra and cospectra in other than the downwind direction and their dependence upon stability, wind speed, and wind shear are not known.
- The writer was unable to ascertain whether the models above should be considered valid for high-wind-speed and/or high-turbulence-intensity conditions. These conditions represent very low probability events (they seldom occur), and therefore it is improbable that many such events were included in the validations of the models which exist. For example, non-linear viscosity effects in high turbulence may well affect the upper limit of the inertial subrange. Therefore, extrapolation of the existing models to such conditions may be incorrect. This issue exists in all statistical verifications of physics theories. In many problems the physics theories are sufficiently strong to justify such extrapolations, but the above theories were generated to fit existing data and there is little reason to suppose that extrapolations will be accurate.

It is necessary to conclude that generation of a realistic gust model given today's data is impossible. Too little is known about the gust covariance tensor to claim that any model generated is realistic. The only gust model situations one can be comfortable about today are those very close to situations where data has been collected, e. g., a gust model for an airplane nearly hovering with respect to the ground, and a gust model for an airplane flying sufficiently fast that only the inertial subrange of the gust spectra is of consequence.

SECTION III INTERIM GUST MODEL

The interim gust model generated in the study is presented in this section. It is intended that this model be used for V/STOL gust analyses until more complete gust data becomes available through the TOLCAT study.

As discussed in Section II, too little is known of the gust covariance tensor and the space-time interdependence in that tensor in other than the downward direction to claim realism for any model generated. The model presented is faithful within the constraints of computational realities and what is known about winds, however, and it can be used with the confidence that it contains the essence of reality.

The model presented here differs in a number of details from that described in the interim report on the contract, Honeywell Report 12060-IR1. First, because this model is to be used as an interim model, nominal values were selected for the various parameters left free in the earlier model.

Linear analyses showed that spectral form, gust intensity, and gust shear across the wings were important, but possible cross correlations of the various orthogonal gust components were of little consequence. Nonlinear analyses showed that gust penetration effects and nonlinear aerodynamic and engine effects will affect responses. These analyses are described in Sections V and VI of this report. The model was changed to better present the intensity, shear, spectral form, and penetration effects, and it was simplified by dropping the cross correlations of orthogonal gust components (penetration effects were not included in the previous model at all).

The discussion of the model generated is divided into five parts. The premises on which the model is based are presented in the first part, and most of the assumptions made in its generation are presented in the second. The approximation of irrational spectra and the extrapolation of the spectra to high frequencies are discussed in the third subsection; it is felt that these issues are critical to use of the model in future V/STOL analyses, and as such deserve the attention of a separate subsection. The final assumption of a gust tensor form and details of approximating the cross correlations in that tensor are presented in the fourth subsection. The final subsection is a short summary on the validity of the assumptions and approximations made.

A. PREMISES

The model generated is based on the following premises.

- To avoid having to vary the gust model along a flight trajectory, the V/STOL aircraft is assumed to fly in a (nearly) straight, horizontal line at a (nearly) uniform ground speed. As a consequence, scale lengths, intensities, and forms assigned to the various turbulence correlations can be assumed constant in an analysis of a single flight condition. The gust model employed in analyzing a flight condition can thus be time-stationary.
- Gusts are normally described in earth-fixed downwind, crosswind, and vertical coordinates, while gust force and moment equations are written in terms of gusts defined in vehicle body coordinates. This implies including a complex, time-varying coordinate transformation in the gust model. To avoid having to consider instantaneous body orientation, it is assumed that the deviations of the body axes from their nominal (zero gust, steady flight) values are sufficiently small that the gust components defined in instantaneous body coordinates can be satisfactorily approximated by replacing them one-one with the gust components defined in the body coordinates of the same vehicle in a zero gust environment. This assumption is made in virtually all aircraft gust analyses, and it is regarded as reasonable.
- The gust model generated should agree with published wind data and published notions of the physics of wind behavior to the extent that these data and notions will significantly affect V/STOL performance. For example, the gust model should resemble Elderkin's spectra, and wind profiles should resemble Panofsky's formulae, but inclusion of Batchelor's infinite-time covariance asymptote in the model is not warranted by the model's intended use. This premise is employed in the generation of almost all engineering models.
- The model should be as computationally simple as possible. In particular, it should, if possible, employ rational spectra. For example, approximation of the inertial subrange with a K^{-2} rather than a $K^{-5/3}$ asymptote will not appreciably affect V/STOL performance analyses, and it greatly simplifies those analyses. Rational spectra problems can be treated with finite-order differential equations, determinant evaluations of residues, etc., while irrational spectra problems require partial differential equations and point-by-point spectral integrations. The attendant mathematical and computational difficulties are not warranted by the intended use of the model.

B. ASSUMPTIONS

To generate a wind model it is necessary to assume some of the statistics missing in the data available today. In some cases these assumptions are uncomfortably arbitrary, but in others they are reasonable as replacing them at a later date with measured data will not significantly affect conclusions based upon them. The assumptions made and the writers' opinions of their arbitrariness and importance follow.

1. Richardson Number

The Richardson number will be assumed to be negative and negligibly small. This condition corresponds to instability with strong winds overhead, the two conditions which produce the greatest turbulence. Presumably this choice describes low-likelihood (high-amplitude) winds at all altitudes, so with it one can extrapolate the low-likelihood portion of wind probability distributions at one altitude to the low-likelihood distributions at another via Panofsky's wind profile formula. Also, correlation lengths in unstable air are nearly independent of the azimuth of the line connecting the two points whose gusts are averaged, while this is not true in stable air, so this assumption simplifies the task of specifying a gust covariance tensor.

This assumption is acceptable if one is interested in high-amplitude winds and gusts, which is the case here.

2. Wind Profile⁶

The wind speeds at very high altitudes are presumably independent of the roughness of the surface beneath. It is reasonable, therefore, to extrapolate downwards (rather than upwards) from high-altitude wind speeds to low-altitude speeds, the particular extrapolation formula employed depending upon roughness length and Richardson number. Since the latter has already been assumed, it remains to choose the formula and the probability distribution of winds at high altitudes.

- (a) Roughness length will be assumed to vary from 0.03 m to 5 m.
- (b) The probability distribution of wind speeds at 9.1 m altitude with a roughness length of 0.03 m will be assumed to be that obtained by drawing a straight line on normal graph paper between 4 m/s at 0.5 likelihood and 12 m/s at 0.01 likelihood. This closely approximates Scoggin's data for Cape Kennedy reported in NASA TM X-53328.

⁶These assumptions have been changed from those reported in the third monthly progress report, Honeywell Report 12060-PR3, at the suggestion of Dr. Panofsky.

The wind probability distribution at an altitude z equal or less than 100 m over a surface of 0.03 m roughness length will be assumed to be the above distribution extrapolated by Panofsky's formula

$$U(z) = U(9.1) (z/9.1)^{0.12}$$

That is, the probability that $U(z) < \alpha$ given $z_0 = 0.03$ m will be assumed to be equal to the probability that $U(9.1) < \alpha \cdot (9.1/z)^{0.12}$ given $z_0 = 0.03$ m. In equation form, this is

$$\text{Prob}\{U(z) < \alpha | z_0 = 0.03 \text{ m}\} = \text{Prob}\{U(9.1) < \alpha \cdot (9.1/z)^{0.12} | z_0 = 0.03 \text{ m}\}$$

This extrapolates Scoggin's probability distribution to all altitudes equal or less than 100 m, for surfaces of roughness length 0.03 m.

The wind probability distribution at 100 m altitude will be assumed to be the same everywhere in the world, independent of the roughness length of the surface beneath. This assumes that 100 m is sufficiently high that the winds there are not significantly affected by the roughness of the surface below. The resulting probability distribution is shown in Figure 4.

The wind probability distributions at all altitudes below 100 m and all roughness lengths will be assumed to be the above 100 m distribution extrapolated downwards by the formula

$$U(z) = U(100) (z/100)^{p(z_0)}$$

where $p(z_0)$ is a constant dependent upon the roughness length z_0 . That is,

$$\text{Prob}\{U(z) < \alpha | z_0\} = \text{Prob}\{U(100) < \alpha \cdot (100/z)^{p(z_0)}\}$$

$p(z_0)$ will be assumed to lie within the range

$$p(0.03) = 0.12 \leq p(z_0) \leq 0.38 = p(5)$$

which corresponds to Panofsky's numbers. Generating a formula which will define $p(z_0)$, in the lowest few meters of the atmosphere in near-neutral air

$$U(z) = \frac{u^*}{K} \ln(z/z_0)$$

so that, from the expansion of $\exp[(U(z) - U(z_1))/U(z_1)]$ in Section II,

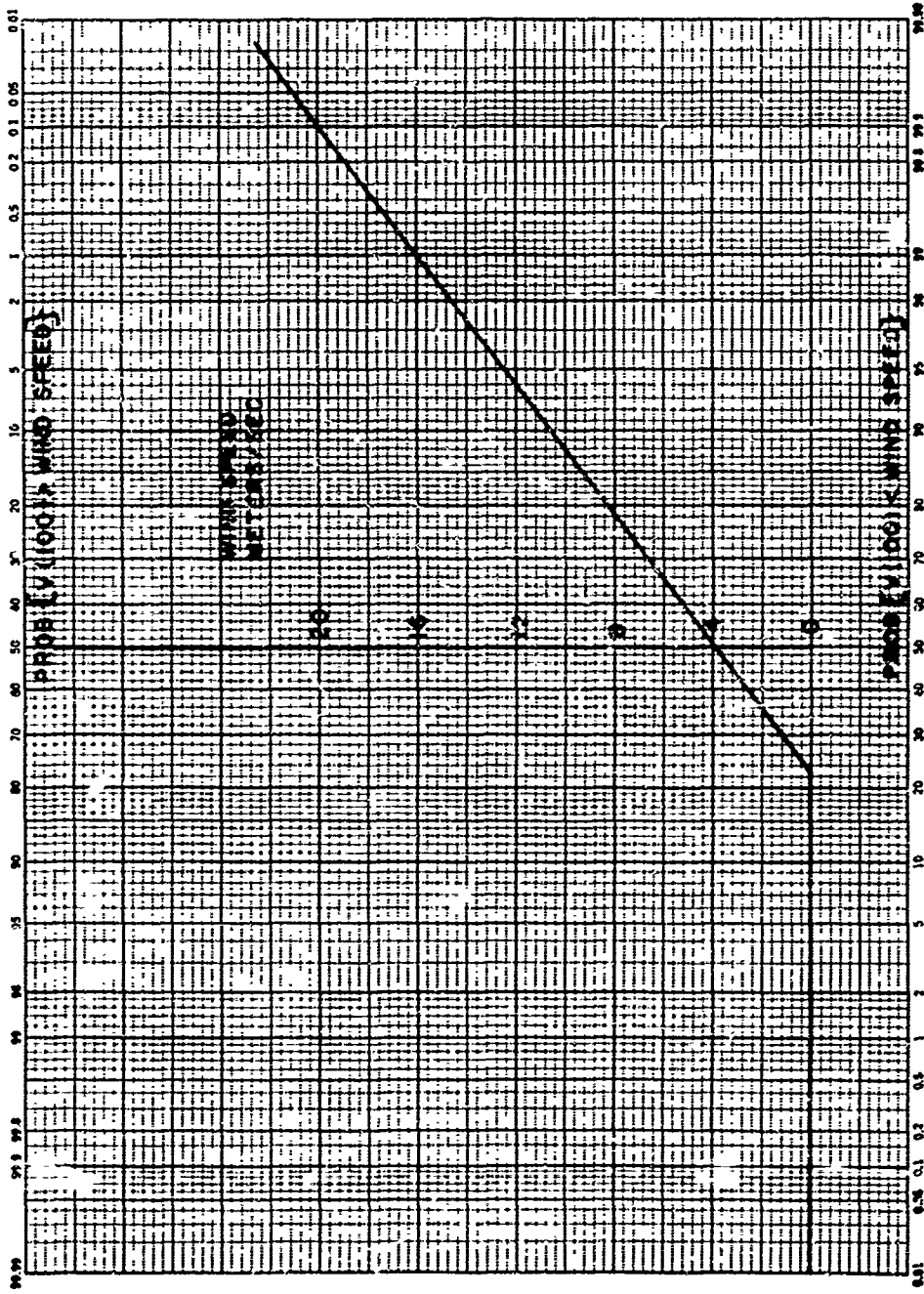


Figure 4. Probability Distribution of Mean Wind Speed at 100 Meters Altitude

$$p = \frac{u^*}{KU(z)} = \frac{1}{4 \ln(z/z_0)}$$

p thus apparently depends on the reciprocal of the logarithm of the roughness length. Choosing a formula

$$p = \frac{a}{b - 4 \ln z_0}$$

$p = 0.12$ for $z_0 = 0.03$ m and $p = 0.38$ for $z_0 = 5$ m produces the constants $a = 0.9$, $b = 4$, so that

$$p(z_0) = \frac{0.9}{4 - 4 \ln z_0}$$

The wind profiles $U(z)$ given $U(z_1)$ at an altitude z_1 and the roughness length z_0 will be assumed to be

$$U(z) = U(z_1)(z/z_1)^{p(z_0)}$$

This assigns the shear

$$\frac{dU(z)}{dz} = \frac{p(z_0)}{z} U(z)$$

to the wind $U(z)$.

These assumptions define the winds and wind shears at all altitudes below 100 m as functions of roughness length z_0 and the likelihood associated with the wind at any altitude. The assumptions are undoubtedly poor approximations to the wind profiles and wind probability distributions which actually exist as they very much oversimplify the real world. However, the values they produce for winds and wind shears are probably within a factor of two or so of what experimental data will produce, except for extremely low-likelihood winds, as the shear formulas are not overly sensitive to their coefficients at higher altitudes. They contain the essence of reality, at least, and are acceptable on that basis until more data are made available.

3. Nominal Gust Intensities

As mentioned in Section II, there is minor disagreement in the literature on the ratios of the standard deviations of gust components σ_u , σ_v , σ_w , and the friction velocity u^* . There is no need to take a firm position on these ratios at this time, as they will certainly be measured in the TOLCAT study.

For the purposes of an interim V/STOL gust model, it is proper to pick nominal values for the $\sigma_u/\sigma_v/\sigma_w/u^*$ ratios that agree with available data.

Since $p(z_0) = u^*/KU(z)$, the friction velocity

$$u^* (z_0, z) = 0.4 p(z_0) U(z)$$

defined by the above profile assumptions will be adopted as a nominal value. The nominal ratios of gust standard deviations will be chosen to be

$$\sigma_u/\sigma_v/\sigma_w/u^* = 2.8/2/1.3/1$$

and the nominal cross correlations $E\{uv\}$, $E\{vw\}$ will be chosen everywhere zero, both assumptions agreeing with Elderkin's data.

With $(u^*)^2$ the negative of $E\{uw\}$, this produces the expectations

$$E \left\{ \begin{array}{l} [u] \\ [v] \\ [w] \end{array} \begin{array}{l} [uvw] \end{array} \right\} = R(z, \underline{0}, 0)$$

$$= (0.4 p(z_0) U(z))^2 \begin{bmatrix} 7.8 & 0 & -1 \\ 0 & 4 & 0 \\ -1 & 0 & 1.7 \end{bmatrix}$$

4. Distance Metric

This assumption is tenuous. Let r_1, r_2, r_3 be the downwind distance, crosswind distance, vertical distances respectively between two points and t be the time displacement between measurements of gusts at the two points. Let z be the altitude of one of the points (r_3 is assumed small, so that the altitude of either point may be used), and let $U(z)$ be the mean wind in the r_1 direction. Let λ_z, λ_t be the constants

$$\lambda_t = 0.98$$

$$\lambda_z = 1$$

and let r , the equivalent distance between the two points, be

$$r = [(r_1 - \lambda_t U(z)t)^2 + r_2^2 + r_3^2 + (1 - \lambda_t^2)(U(z)t)^2]^{1/2} / \lambda_z z$$

The intention in defining this distance measure is to write the components of the gust covariance tensor $R_{ij}(z, r, t)$ as functions only of r and the angles between the vector $r = (r_1, r_2, r_3)$ and the r_1, r_2, r_3 coordinate axes,

$$R_{ij}(z, \underline{r}, t) = f_{ij}(r, \Psi_1, \Psi_2, \Psi_3)$$

where

$$\cos \Psi_K = r_K / (r_1^2 + r_2^2 + r_3^2)^{1/2}$$

Writing the R_{ij} as functions only of distance r and the angles Ψ_1, Ψ_2, Ψ_3 , and defining d in the above manner implies several assumptions:

- (a) For $t = 0$, r is a conventional vector sum normalized by the scale length $L_z = \lambda_z z$. Since the distances r_1, r_2, r_3 enter r in the same manner, this model assigns the same scale L_z to all azimuth angles Ψ . Since a single r is used for all R_{ij} , every term in the gust tensor has the same scale length L_z . This assumes then that "eddy dimensions" are the same in all horizontal directions, which agrees with Panofsky's scale-length result in unstable air and the choice of a small, negative Richardson number.
- (b) The scale form $L_z = \lambda_z z$ assumes that scale length is a linear function of altitude, agreeing with similarity theory. The value $\lambda_z = 1$ is reasonably close to the spectral peaks in Elderkin's data and the correlation lengths described by Panofsky in reference 2 as occurring at different azimuths in stable air.
- (c) For $r_1 = r_2 = r_3 = 0$, $r = U(z)t = \lambda_z z$, agreeing with the Taylor hypothesis. Hence, the above assumes the Taylor hypothesis is true for distance measured along every horizontal trajectory. Transport of the gust field, however, is limited to the downwind direction only (there is not a three-dimensional diffusion).
- (d) The elliptical dependence of r on downwind distance and t agrees with Panofsky's data, mentioned above, and the value $\lambda_t = 0.98$ is exactly his figure. However, Panofsky's data is for small r_1, t only (0 to 75 meters); the above extends this relation to all r_1, r_2, r_3, t .

The assumption that the distance metric can be expressed in this form is justified in the downwind direction by Panofsky's ellipses for r_1 small. Extending these ellipses to r_1 large is reasonable if R_{ij} is assumed sufficiently small for large distances and/or times that 100 percent errors in magnitude there are of little consequence as far as $V/STOL$ analyses. Physics intuition says that all of the R_{ij} will almost converge to zero within two or three L_z distances, so the ellipses can probably be safely extended.

Extending this distance measure to all azimuth angles is justified only by convenience. There are no data on which to base an assumed distance-time interaction in other than near downwind directions. Assuming the same distance measure in all directions is an arbitrary assumption.

The convenience it purchases, of course, is that for an airplane flying horizontally at a velocity V whose angles with the r_1, r_2, r_3 axes are ψ_a , $90 - \psi_a$, 0 , r can be written as a function of Vt , z , $U(z)$, and ψ_a only. With

$$r_1 = Vt \cos \psi_a$$

$$r_2 = Vt \sin \psi_a$$

$$r_3 = 0$$

r is

$$r = |t| (V^2 + U(z)^2 - 2\lambda_T U(z)V \cos \psi_a)^{1/2} / \lambda_z z$$

For hover with respect to the ground

$$r = \frac{|U(z)t|}{\lambda_z z}$$

for hover with respect to the wind

$$r = \frac{|U(z)t|}{\lambda_z z} (2 - 2\lambda_T)^{1/2}$$

and for high-speed flight $V \gg U(z)$,

$$r = \frac{|Vt|}{\lambda_z z}$$

in all cases r is a constant times the elapsed time between encountering two points in the r_1, r_2, r_3, t space.

A result of the linear analyses, discussed in Section V, is that, assuming Panofsky's $\lambda_t = 0.98$ is approximately correct, one can safely take the last high-speed form for r ,

$$r = \frac{|Vt|}{\lambda_z z}$$

at airspeeds V_{as} greater than one third the mean wind speed

$$V_{as} = (V^2 + U(z)^2 - 2U(z)V \cos \psi_a)^{1/2}$$

$$> \frac{U(z)}{3}$$

At lower airspeeds the more general form

$$r = \left| t \right| (V^2 + U(z)^2 - 2\lambda_T U(z)V \cos \psi)^{1/2} / \lambda_z z$$

must be adopted. The error introduced by incorrectly employing the high-air-speed approximation at low airspeeds is that it produces gust spectra of too low bandwidth; at hover with respect to the wind it produces zero gusts (constant winds).

5. Probabilities

Specification of the gust tensor $R(z, \underline{r}, t)$ alone does not define the gust random processes, and it of itself is useful only for computing V/STOL response covariances, for whatever purposes they might be used. To define the gust random processes it is necessary to specify the joint probability densities of every finite collection of gust components.

The simplest assumption that can be made is that the gust random processes are completely defined by the gust covariance tensor. If the V/STOL is assumed to respond linearly to the gusts, its responses will be Gaussian as well. Gaussianity is thus a most convenient assumption.

A Gaussianity assumption implies a difficult-to-accept physics hypothesis, however. Two Gaussian random variables which are uncorrelated are statistically independent, and two Gaussian random processes which are everywhere uncorrelated are everywhere statistically independent. From Elderkin's data, the cross correlations of crosswind gusts with both vertical and downwind gusts at a point are zero, $E\{vw\} = E\{vu\} = 0$. Further, despite the scatter in his vw , vu cospectra, the magnitudes are sufficiently small to warrant assuming that crosswind gusts at a point are not correlated with vertical or downwind gusts anywhere in the downwind direction. The v random process must then be statistically independent of the u , w random processes if Gaussianity is assumed. Statistical independence, however, is a mathematical assumption equivalent to a physics assumption that the physical mechanism producing crosswind gusts operate independently of those producing vertical and downwind gusts. Given the Navier-Stokes equations, this is difficult to accept.

An implication of the Navier-Stokes equation was that the high-frequency (short-wavelength) portions of the gust spectra is isotropic. It was proved above that in isotropic turbulence the shears of downwind gusts in the crosswind direction are correlated with crosswind gusts. Therefore there must exist physical mechanisms connecting the downwind and crosswind gusts. The fact that cross correlations of orthogonal gust components in isotropic

turbulence are zero implies only that positive and negative correlations are equally likely. One would expect the absolute magnitudes of crosswind and downwind gust components at remote points to be correlated.

Whether or not this is the case cannot be deduced from Elderkin's data, as his spectra are of component velocities and not component magnitudes. The statistical independence of v from u and w can easily be checked experimentally in the TOLCAT program, however. If they are statistically independent, the expected values of all products of powers of component velocities at all remote points will equal the product of the expected values of those powers,

$$E\{u^n v^m\} = E\{u^n\} E\{v^m\}$$

$$E\{w^n v^m\} = E\{w^n\} E\{v^m\}$$

for all real numbers m, n . Choosing $m = n = 2$ and running an experiment should settle the issue.

The gusts will be assumed Gaussian in this model, an assumption for convenience.

C. APPROXIMATIONS

The final assumption that must be made is to assume forms for the functions $R_{ij}(z, \underline{r}, t) = f_{ij}(r, v_1, v_2, v_3)$. Before making these assumptions, it is well to consider the consequences of the extrapolations and approximations that will have to be made because of a lack of high-frequency gust data and the desire to have a computationally simple representation for gust forces and moments.

1. Shear Spectra

As mentioned above, experimental gust spectra can be satisfactorily fit over the range of available data frequencies with any number of spectral forms. Perhaps the simplest correlation form possible which provides a reasonable

fit is the exponential $e^{-\left|\frac{x}{L}\right|}$, where x is the displacement between the points in question. Press, Meadows, Steiner, et al, at NASA Langley chose this form as a fit to downwind spectra. Assuming isotropy, this led them to the vertical gust autocorrelation form

$$E\{u(x_0) u(x_0 + x)\} = \sigma^2 e^{-\left|\frac{x}{L}\right|} \left(1 - \frac{1}{2} \left|\frac{x}{L}\right|\right)$$

or, in spectral form,

$$\frac{\sigma^2 L}{2\pi} \frac{3(KL)^2 + 1}{(KL)^2 + 1)^2}$$

With any stationary gust autocorrelation, the autocorrelation of the corresponding gust shears along the direction of the line connecting the two points is

$$\begin{aligned}
 E \left\{ \frac{\partial u(x_0)}{\partial x_0} \frac{\partial u(x_0 + x)}{\partial (x_0 + x)} \right\} &= \frac{\partial}{\partial x} E \left\{ \frac{\partial u(x_0)}{\partial x_0} u(x_0 + x) \right\} \\
 &= \frac{\partial}{\partial x} E \left\{ \frac{\partial u(x_0 - x)}{\partial x_0} u(x_0) \right\} \\
 &= \frac{-\partial^2}{\partial x^2} E \{ u(x_0 - x) u(x_0) \} \\
 &= \frac{-\partial^2}{\partial x^2} E \{ u(x_0) u(x_0 + x) \}
 \end{aligned}$$

Applying this to the above form,

$$\begin{aligned}
 & - \frac{\partial^2}{\partial x^2} \left[\sigma^2 e^{-\left| \frac{x}{L} \right|} \left(1 - \frac{1}{2} \left| \frac{x}{L} \right| \right) \right] \\
 &= - \frac{\partial}{\partial x} \left[\frac{\sigma^2}{2L} e^{-\left| \frac{x}{L} \right|} \left(\frac{x}{L} - \frac{3x}{|x|} \right) \right] \\
 &= \frac{\sigma^2}{2L^2} e^{-\left| \frac{x}{L} \right|} \left[-4 + \frac{|x|}{L} \right] + \frac{3\sigma^2}{L} \delta(x)
 \end{aligned}$$

where $\delta(x)$ is the Dirac delta function. Since $\delta(x)$ is the autocorrelation of white noise, the above exponential autocorrelation produces a wind shear $\partial u / \partial x$ that contains white noise. Physically, of course, this is nonsense.

The presence of white noise in the shear is not due to a poor fit to the spectral data, but rather to extrapolating that fit to higher frequencies than the range of available data. A gust spectrum of the form

$$\frac{\sigma^2 L}{2\pi} \frac{3(KL)^2 + 1}{(KL)^2 + 1} \cdot \frac{1}{(KS)^2 + 1}$$

where $S \ll L$, would fit the data as well and not produce a gust shear containing white noise.

An airplane will respond to wind shears since shears imply asymmetrical gust forces on the wing, tail, and fuselage. Normally one is concerned with analyses of airplane attitudes, attitude rates, and translation rates. The double integrations of Kussner lags (lift-buildup) and rigid body force-to-response-rate wash out the white noise. That is, while the white-noise-input to gust-shear transfer function is n/n (as many poles as zeros), the gust-shear to airplane-response transfer functions are always at least $(m-2)/m$ (two less zeros than poles), so integrals of response spectra will always be finite (no responses will contain white noise). It would seem that the white-noise-shear is not a problem.

It is a problem, however. Suppose that the airplane responds measurably to wave numbers out to $K \leq 1/L_a$ and gust data is available over a range of wave numbers $1/L_1 \leq K \leq 1/L_2$, where $1/L_2 < 1/L_a$. Then calculated airplane responses will be sensitive to the gust spectra extrapolation above $1/L_2$.

This is the situation today in calculating fatigue lifetimes and likelihoods of too-large stresses in missile and conventional aircraft flight. The "bandwidth" of the vehicle response transfer functions for stress and stress-rate are defined by the high-frequency dynamics assumed in the Kussner approximation, which are not well known, particularly at large angles of attack, and these frequencies are higher than those of the available gust data. This situation could well be true for V/STOL acceleration responses, particularly if one were looking at such responses at the accelerations of a gun or camera platform.

2. Integration

The shear problem is further complicated by integrating the wind over the wings and fuselage. Total forces are area integrals of local force densities. If b and d are the wingspan and fuselage length respectively, it is clear that first-order force and moment effects will depend on b and d only, the wind being essentially constant over the vehicle. "Shear" forces and moments will depend on the b/L , d/L ratios, larger correlation lengths L producing smaller effects. For example, if the autocorrelation of vertical gusts across the span b is assumed to be $\exp[-|x|/L]$, and the force per unit span per unit gust is assumed constant across the span, the mean square lift force is

$$\begin{aligned} E\{\dot{z}^2\} &= \text{CONST} [2L^2] [e^{-b/L} - (1-b/L)] \\ &= \text{CONST} [b^2] \left[1 - \frac{1}{3} \left(\frac{b}{L}\right) + \dots \right] \end{aligned}$$

and the mean square rolling moment is

$$\begin{aligned} E\{x^2\} &= \text{CONST} [2L^4] \left[1 - \left(\frac{b}{2L}\right)^2 + \frac{2}{3} \left(\frac{b}{2L}\right)^3 - \left(1 + \frac{b}{2L}\right)^2 e^{-b/L} \right] \\ &= \text{CONST} [b^4] \left[\frac{1}{60} \frac{b}{L} + \dots \right] \end{aligned}$$

the dots . . . indicating terms of order $(b/L)^2$ and higher.⁷

The above shear-white-noise problem comes about by approximating the first and second order effects by expanding the incident wind in a Taylor's series about the vehicle c.g. (that is, differentiating the wind). Where this expansion is used to calculate mean square values of acceleration rates and stress rates (for use in the Rice level-crossing formula to get estimates of likelihoods of large accelerations, large stresses, and fatigue damage), one is forced either to ignore the white noise or to truncate the calculations, as the white noise-to-response transfer functions are m/m (as many zeros as poles) and higher. The truncation is commonly employed, and is usually implemented either by truncating power spectra integrations or by adding enough lags to wind spectra or Kussner dynamics to assure convergence of spectral integrations and/or covariance differential equations.

Choosing a truncation frequency or a break frequency for the added lags is not a problem in most mean-square value calculations as "shear" effects are usually significantly smaller than first-order, "constant wind" forces and moments, and a large enough percentage of the response energy is contained in the rigid body frequency region that variation of the truncation frequency causes little change in the mean-square values. Successive derivatives of these responses, however, are more and more sensitive to truncation frequencies, and second-order effects are proportionately more important as the b/L d/L ratios decrease. For a V/STOL, where L is very small at low altitudes, the latter is a cause for concern.

The necessity of considering shear effects introduces a computational problem as well as the above truncation problem.

3. Irrational Spectra

It was a premise that the gust model generated be computationally as simple as possible. The simplest and most desirable model would employ rational gust spectra, as rational spectra permit the computational simplicities of expressing gust problems in terms of finite-order, lumped-parameter differential equations.

Suppose an aircraft is flying horizontally in a straight line with zero sideslip, and suppose that the autocorrelation of the vertical gust component at a point on the wing is $\exp[-|x|/L]$, where x is distance along the flight path. With $x = V_{as}t$, airspeed times time, the gust spectrum seen by the aircraft is

$$\frac{2L/V_{as}}{\left(\frac{L}{V_{as}}S\right)^2 + 1}$$

a proper rational fraction.

⁷ The α on the left side of this equation is rolling moment.

Let y be distance across the wing. Assuming the gusts are isotropic, the cross correlation of vertical gusts at y_1 and y_2 at t seconds displacement is

$$\exp \left[- \left(\frac{(V_{as} t)^2 + (y_1 - y_2)^2}{L^2} \right)^{1/2} \right]$$

The cospectrum

$$\int_{-\infty}^{\infty} e^{-j\omega t} \exp \left[- \left(\frac{(V_{as} t)^2 + (y_1 - y_2)^2}{L^2} \right)^{1/2} \right] dt$$

is, unfortunately, irrational.

The cospectra of orthogonal gust components at remote points on the vehicle will similarly be irrational. Further, since forces and moments are area integrals of local force and moment densities, the auto and cospectra of all force and moments will be irrational.

The writer was unable to find a form for the gust covariance tensor that would produce rational gust cospectra and rational force and moment spectra and cospectra. It is doubted that any such form exists.

The escape from irrational autospectra and cospectra is to approximate them with rational spectra. Such approximations pose no conceptual or theoretical difficulties as experimental spectra can be approximated to any desired accuracy over any chosen (finite) wavelength region.

However in the present case the only gust spectra known are autospectra and cospectra obtained from anemometers mounted at a point, and extrapolating these to downwind space spectra requires assumption of a distance metric. There are no cospectra of parallel gust components along any parallel paths available for approximating wing shear spectra, there are no cospectra of orthogonal gust components along parallel paths on which to base cross correlation approximations, and there are no spectra in other than the downwind direction on which azimuth dependence approximations can be based. In short, there are no cospectra available on which to base rational approximations.

Thus any rational spectra chosen for the interim model will be approximations to assumptions based upon very sparse data, an uncomfortable modeling situation. The best that can be done in this situation is to assume simple, intuitively reasonable spectra and to ascertain when assessments of vehicle performance are overly dependent upon weak assumptions. In particular, all rapid-response calculations will be suspect, as the high-frequency portions of the gust spectra and Kussner dynamics are not well known. Also all low-altitude calculations where correlation lengths are one-half a wing span or less will be suspect, as correlations of parallel gusts will not be uniformly large, as they are at longer correlation lengths, but will take intermediate, difficult-to-approximate values.

D. THE GUST MODEL

It remains to choose forms for the terms in the gust covariance tensor and to develop approximations to shear effects.

The following model is considered reasonable as far as the forces and moments it will generate, and it is computationally simple.

Let u , v , w be downwind, crosswind, and vertical gusts, and r_1 , r_2 , r_3 be distances in those directions. Let $U(z)$ be the mean wind, in the r_1 direction, and let ψ_h be the angle between the vehicle fuselage and $U(z)$. Let $\underline{u} = (u_1, u_2, u_3)$ be the vector of head-on gusts, side gusts, and vertical gusts seen by the vehicle, so that

$$\begin{bmatrix} u_1 \\ u_2 \\ u_3 \end{bmatrix} = \begin{bmatrix} \cos(\psi_h) & \sin(\psi_h) & 0 \\ -\sin(\psi_h) & \cos(\psi_h) & 0 \\ 0 & 0 & 1 \end{bmatrix} \begin{bmatrix} u \\ v \\ w \end{bmatrix}$$

Let x , y , z be distances along the fuselage, out the wing, and vertical measured in vehicle body coordinates.

1. Force and Moment Approximation

It is assumed that the gusts and gust shears which produce significant forces and moments on the vehicle are:

- The average head-on and vertical gusts on the wing, on the fuselage, and on the tail
- The average side gusts on the fuselage and on the tail
- The spanwise shear of head-on and vertical gusts across the wing

The vertical shears of side and head-on gust components are ignored as they are significant only if the vehicle tail is very large and extends both below and above the vehicle centerline. The spanwise shear of side gusts and vertical shear of vertical gusts produce no forces or moments. The moments due to head-on, side, and vertical gust shears along the fuselage are ignored as being second-order in comparison to the moments produced by gusts on the tail.

The effects of the shear forces and moments can be closely approximated by introducing eight gust sources on the wings, at the wing root, and at the tail. Let

- u_{1L} = head-on gust halfway out left wing
- u_{1R} = head-on gust halfway out right wing
- u_{1T} = head-on gust at tail
- u_{2w} = side gust at center of fuselage, halfway between wing tips
- u_{2T} = side gust at tail
- u_{3L} = vertical gust halfway out left wing
- u_{3R} = vertical gust halfway out right wing
- u_{3T} = vertical gust at tail

Let the "average" gust over the left wing be constant and consist of u_{1L} , u_{2w} , u_{3L} . Let the "average" gust over the right wing, fuselage, and tail be constant and consist of u_{1R} , u_{2w} , u_{3R} for the right wing, $(u_{1R} + u_{1L})/2$, u_{2w} , $(u_{3R} + u_{3L})/2$ for the fuselage, and u_{1T} , u_{2T} , u_{3T} for the tail.

Assuming that the winds hitting the aircraft can be described as above ignores completely the shear of side gusts along the fuselage and up the tail and the shear of head-on and vertical gusts along the fuselage. The moments introduced by the vertical shear at the tail are definitely second-order compared to those due to side gusts on the tail (unless the tail extends well below the vehicle centerline, in which case the rolling moment due to side gusts will be small). The fuselage shear forces and moments (there are forces as the fuselage is not symmetric fore and aft of its geometric center) are definitely secondorder compared to those due to the average gusts on the wing and tail, as the fuselage, though large, is an inefficient aerodynamic body.

The above model approximates the spanwise shear of vertical and head-on gusts across the wing with the differences of constant gusts on each wing. To show how good an approximation this is, consider small gust velocities and let the lift per-unit-span due to a vertical gust u_3 be

$$\frac{\partial \mathcal{L}}{\partial y} = \text{CONST} \cdot u_3(y)$$

where y is distance measured from the centerline out the wing. The total rolling moment due to vertical gusts is then

$$\mathcal{L} = \int_{-b/2}^{b/2} \text{CONST} \cdot u_3(y) y dy$$

where b is the wingspan. The above approximation gives

$$\mathcal{L}_a = \text{CONSTANT} \cdot (u_{3R} - u_{3L}) \cdot \frac{b}{2} \cdot \frac{b}{4}$$

($b/2$ is the half span, $b/4$ the moment arm). The actual mean square rolling moment is

$$E\{\mathcal{L}^2\} = (\text{CONST})^2 \cdot \int_{-b/2}^{b/2} \int_{-b/2}^{b/2} y_1 y_2 E\{u_3(y_1) u_3(y_2)\} dy_1 dy_2$$

Using the exponential autocorrelation

$$E\{u_3(y_1) u_3(y_2)\} = \sigma_2^2 e^{-\left| \frac{y_1 - y_2}{L} \right|}$$

this gives after integration

$$E\{\mathcal{L}^2\} = \text{CONST}^2 \cdot b^4 2L^4 \left(1 - \frac{1}{4} \left(\frac{b}{L}\right)^2 + \frac{1}{12} \left(\frac{b}{L}\right)^2 - e^{-\frac{b}{L}} \left(1 + \frac{b}{2L}\right)^2 \right)$$

After expansion in b/L this reduces to

$$E\{z^2\} = \text{CONST}^2 \cdot b^4 \frac{1}{60} \frac{b}{L} \sum_{n=5}^{\infty} \frac{n^2 - 5n + 1}{4} (-1)^{n+1} \frac{b}{L}^{n-5} \frac{5!}{n!}$$

$$= \text{CONST}^2 \cdot b^4 \frac{1}{60} \frac{b}{L} \cdot \phi(b/L)$$

The sum $\phi(b/L)$ is tabulated below as a function of b/L :

$\phi(b/L)$ Correction ⁸			
b/L	$\phi(b/L)$	b/L	$\phi(b/L)$
0.001	0.9996	1	0.6729
0.01	0.9958	1.5	0.5591
0.02	0.9917	2	0.4706
0.05	0.9794	3	0.3400
0.1	0.9594	5	0.1949
0.15	0.9398	7	0.1238
0.2	0.9208	10	0.07127
0.3	0.8841		
0.5	0.8160		
0.7	0.7544		

The approximate expression gives the mean square rolling moment

$$E\{z_a^2\} = \text{CONST} \cdot \frac{b^4}{64} E\{(u_{3R} - u_{3L})^2\}$$

$$= \text{CONST} \cdot \frac{b^4}{64} 2\sigma_3^2 (1 - e^{-b/2L})$$

The ratio of the two is

⁸This table was generated by taking 1000 term sums

$$\phi(b/L) = \sum_{n=5}^{1005} \frac{n^2 - 5n + 1}{4} (-1)^{n+1} \frac{b}{L}^{n-5} \frac{5!}{n!}$$

$$\frac{E\{x^2\}}{E\{x_a^2\}} = \frac{\frac{1}{60} \frac{b}{L} \phi \frac{b}{L}}{\frac{1}{32}(1-e^{-b/2L})}$$

$$= \frac{32}{60} \frac{b}{L} \phi \left(\frac{b}{L}\right) / \left(1 - e^{-\frac{b}{2L}}\right)$$

This ratio takes the values:

for $b/L = 0.01,$	$E\{x^2\} / E\{x_a^2\} =$	1.06
0.1		1.09
1		0.91
10		0.385

Thus the approximation is quite accurate at long correlation lengths (higher altitudes), and is only 10 percent in error at correlation lengths corresponding to a wingspan. It produces 2.6 times too large mean square rolling moments due to shear at correlation lengths 1/10 of the wingspan. Such low correlation lengths occur only at very low altitudes.

The same theory with only the constant changed applies to yaw moment due to differential drag on the wings due to vertical gusts, and to roll and yaw moments due to head-on gusts.

It is common practice in gust analyses to ignore the roll and yaw moments produced by the shears of head-on and vertical gusts across the wing. They should not be ignored. The lift-per-unit-span on the wing due to vertical gusts is

$$\frac{\partial \mathcal{F}}{\partial y} = \frac{1}{2} \rho c_{L_\alpha} \bar{c} V_{as} \int_{-b/2}^{b/2} y u_3(y) dy$$

which leads to the mean square rolling moment

$$E\{x^2\} = \left(\frac{1}{2} \rho c_{L_\alpha} \bar{c} V_{as}\right)^2 b^4 \sigma_3^2 \cdot \frac{1}{60} \frac{b}{L} \phi(b/L)$$

On an ordinary airplane the tail area is about one-fifth the wing area, and the tail moment arm is about one-sixth the wingspan. This produces the side force due to side gusts on the tail

$$\mathcal{F} = \frac{1}{2} \rho c_{L_\alpha} \frac{\bar{c} b}{5} V_{as} u_{2T}$$

and the mean square rolling moment

$$E\{x_t^2\} = \left(\frac{1}{2} \rho c_{L_\alpha} \frac{\bar{c} b}{5} V_{as} \frac{b}{6}\right)^2 \sigma_2^2$$

The ratio of shear to tail mean square moments is

$$\frac{E\{x^2\}}{E\{x_t^2\}} = \frac{\sigma_3^2 \frac{1}{60} \frac{b}{L} \phi(b/L)}{\frac{1}{900} \sigma_2^2}$$

$$= 15 \left(\frac{\sigma_3}{\sigma_2} \right) \frac{b}{L} \phi(b/L) .$$

With the nominal gust standard deviations above

$$\sigma_3/\sigma_2 = \frac{1.3}{2}$$

so that for $b/L = 1$,

$$\frac{E\{x^2\}}{E\{x_t^2\}} = 15 \left(\frac{1.3}{2} \right)^2 0.6729$$

$$= 4.3$$

For $b/L = 1/10$ this reduces to

$$\frac{E\{x^2\}}{E\{x_t^2\}} = 15 \left(\frac{1.3}{2} \right)^2 \frac{0.9594}{10}$$

$$= 0.605$$

In neither case is the shear contribution negligibly small.)

The advantage the above shear model has over a Taylor's series expansion of the wind at c.g. is that it does not require differentiation of the wind. White noise difficulties are thus precluded. The advantage that it has over integration of the shears over the wing is simplicity, for which less than a 10 percent price in the accuracy of mean-square moments is paid.

2. Cross Correlations of Orthogonal Gusts

The generation of the gust model is considerably simplified by the apparently small cross correlations between the head-on, side, and vertical gust components and the head-on and vertical gust shears across the wing. These cross correlations are important only when they are large in magnitude and, simultaneously, the contributions of the correlated inputs to a response of interest are nearly equal.

For example, let r be a response, u and w be disturbing inputs, σ denote a standard deviation, and ρ_{uw} be the uw correlation coefficient. The standard deviation of r is then (from linear theory),

$$\sigma_r = \left(\left(\sigma_u \frac{\partial \sigma_r}{\partial \sigma_u} \right)^2 + \left(\sigma_w \frac{\partial \sigma_r}{\partial \sigma_w} \right)^2 + 2\rho_{uw} \left(\sigma_u \frac{\partial \sigma_r}{\partial \sigma_u} \right) \left(\sigma_w \frac{\partial \sigma_r}{\partial \sigma_w} \right) \right)^{1/2}$$

where $\frac{\partial \sigma_r}{\partial \sigma_u}$ and $\frac{\partial \sigma_r}{\partial \sigma_w}$ are positive constants obtained from linear analyses.

Letting

$$a = \sigma_u \frac{\partial \sigma_r}{\partial \sigma_u}, \quad b = \sigma_w \frac{\partial \sigma_r}{\partial \sigma_w}, \quad \text{then}$$

$$\sigma_r = (a^2 + b^2 + 2\rho_{uw}ab)$$

With $-1 \leq \rho_{uw} \leq +1$, the ratio of maximum to minimum values that σ_r can take is

$$\frac{\sigma_r \text{ max}}{\sigma_r \text{ min}} = \left(\frac{a^2 + b^2 + 2ab}{a^2 + b^2 - 2ab} \right)^{1/2} = \left| \frac{a+b}{a-b} \right|$$

which ratio is distinctly different from unity only when $a \approx b$.

The cross correlation of vertical and head-on gusts seen by the aircraft is $-0.275 \leq \rho \leq +0.275$, the sign and magnitude depending upon the azimuth and heading angles. The maximum that the σ_r ratio can take for these gusts is $a = b$, where

$$\frac{\sigma_r \text{ max}}{\sigma_r \text{ min}} = \left(\frac{2.550}{1.450} \right)^{1/2} = 1.32$$

a 32 percent difference. The maximum difference between σ_r and the σ_{r_0} obtained assuming zero cross correlation is

$$\frac{\sigma_r \text{ max} - \sigma_{r_0}}{\sigma_{r_0}} = \left(\frac{2.550}{2} \right)^{1/2} - 1 = 0.132$$

a 13 percent difference at most. This is not large enough to be a concern.

Horizontal gusts measured in a coordinate system at an angle γ_a to the down-wind direction are also correlated because of nonisotropy. Letting u_1^* , u_2^* be horizontal gusts parallel and orthogonal to the flight path,

$$\begin{bmatrix} u_1^* \\ u_2^* \end{bmatrix} = \begin{bmatrix} \cos \Psi_a & \sin \Psi_a \\ -\sin \Psi_a & \cos \Psi_a \end{bmatrix} \begin{bmatrix} u \\ v \end{bmatrix}$$

then

$$E \left\{ \begin{bmatrix} u_1^{*2} & u_1^* u_2^* \\ u_1^* u_2^* & u_2^{*2} \end{bmatrix} \right\} = \begin{bmatrix} \cos \Psi_a & \sin \Psi_a \\ -\sin \Psi_a & \cos \Psi_a \end{bmatrix} \begin{bmatrix} \sigma_u^2 & 0 \\ 0 & \sigma_v^2 \end{bmatrix} \begin{bmatrix} \cos \Psi_a & -\sin \Psi_a \\ \sin \Psi_a & \cos \Psi_a \end{bmatrix}$$

$$= \begin{bmatrix} \sigma_u^2 \cos^2 \Psi_a + \sigma_v^2 \sin^2 \Psi_a & (\sigma_v^2 - \sigma_u^2) \cos \Psi_a \sin \Psi_a \\ (\sigma_v^2 - \sigma_u^2) \cos \Psi_a \sin \Psi_a & \sigma_u^2 \sin^2 \Psi_a + \sigma_v^2 \cos^2 \Psi_a \end{bmatrix}$$

The u_1^*, u_2^* correlation coefficient is

$$\rho_{u_1^* u_2^*} = \frac{(\sigma_v^2 - \sigma_u^2) \cos \Psi_a \sin \Psi_a}{\sqrt{(\sigma_u^2 \cos^2 \Psi_a + \sigma_v^2 \sin^2 \Psi_a)(\sigma_u^2 \sin^2 \Psi_a + \sigma_v^2 \cos^2 \Psi_a)}}$$

The maximum magnitude of $\rho_{u_1^* u_2^*}$ occurs at $\Psi_a = 45^\circ + n\pi$, where

$$\max_{\Psi_a} \left| \rho_{u_1^* u_2^*} \right| = \frac{|\sigma_v^2 - \sigma_u^2|}{\sigma_u^2 + \sigma_v^2}$$

With $\sigma_u^2 = 7.8$, $\sigma_v^2 = 4$, this produces a correlation coefficient

$$\max_{\Psi_a} \left| \rho_{u_1^* u_2^*} \right| = \frac{7.8 - 4}{7.8 + 4} = 0.322$$

Ignoring this correlation produces an error of at most

$$\sqrt{\frac{2.644}{2}} - 1 = 0.15$$

or 15 percent.

The only other known non-zero cross correlation is that of the shear of head-on gusts across the wing to side gusts on the tail. The magnitude of this correlation is not known. Assuming isotropy and a correlation form

$$E\{u_1 u_1\} = \sigma^2 e^{-(r/L)^2}$$

then the shear intensity is

$$E\left\{\frac{\partial u_1}{\partial y} \frac{\partial u_1}{\partial y}\right\} = -\frac{\partial}{\partial r^2} \sigma^2 e^{-(r/L)^2} \Big|_{r=0}$$

$$= \frac{2\sigma^2}{L^2}$$

while the shear-tail cross correlation is

$$E\left\{\frac{\partial u_1}{\partial y} u_2\right\} = -\frac{1}{2} \frac{\partial}{\partial r} \sigma^2 e^{-(r/L)^2} \Big|_{r=d}$$

$$= \sigma^2 \frac{d}{L^2} e^{-(d/L)^2} \quad \begin{array}{l} r = d \\ = \text{wing-to-tail distance} \end{array}$$

The correlation coefficient between shear and side gusts on the tail is then

$$\rho = \frac{\sigma^2 d/L^2 e^{-(d/L)^2}}{\sigma \cdot \sqrt{\frac{2\sigma^2}{L^2}}}$$

$$= \frac{1}{\sqrt{2}} \frac{d}{L} e^{-(d/L)^2}$$

The maximum of this correlation coefficient occurs at

$$\frac{\partial \rho}{\partial (d/L)} = 0 = \frac{1}{\sqrt{2}} e^{-(d/L)^2} [1 - 2(d/L)]$$

or $d/L = 1/2$,

where

$$\rho = \frac{1}{2\sqrt{2}} e^{-1/4}$$

$$= 0.276$$

From the above analysis, assuming this cross correlation is zero will produce at most at 13 percent error in a response standard deviation.

All of the various gust cross correlations will be assumed zero in the gust model. Unless the cross correlations measured in TOLCAT are much larger than the measured 0.275 vertical, downwind correlation coefficient, and the 0.276 shear, side gust correlation coefficient derived above, the errors introduced into linear analyses results by assuming them zero will be negligible.

As far as the effects of zero cross correlations on nonlinear analysis results, as discussed in Section VI the nonlinearities themselves (parabolic dependence of forces and moments on local airspeed, stall, and thruster dependence on control inputs and dynamic pressure) so dominate response characteristics when the gust inputs are large that they wash out dependence on fine detail in the gust model.

Assuming zero cross correlations is then justified by linear theory, by the little correlation data available, by a "reasonable" calculation of the shear-side gust correlation, and by the nonlinear data generated in this study. Undeniably, assuming zero cross correlations is also a most convenient assumption for generating a gust model. The reason it is convenient is described in the angle dependence discussion below.

3. Cross Correlations of Parallel Gusts

The cross correlations of parallel gusts, for example the head-on gusts at the wing and tail, are not large at all but very small correlation lengths. Their cospectra are also irrational, as discussed above. Further, in forward flight the gusts at the tail are very nearly the average of the wing gusts (the fuselage gusts) delayed by d/V_{as} seconds, the wing-to-tail distance divided by airspeed, so the cross correlations of the wing and tail gusts at zero time displacement will be smaller than the same cross correlations at d/V_{as} time displacement. The cross correlation coefficients in general will be sufficiently large that setting them equal to unity would not introduce serious errors in total lift, drag, and side force calculations. Roll, pitch, and yaw moments however are dependent on the differences between the wing gusts, the differences between the wing and tail gusts, and the tail gust themselves, and having reasonable estimates of the cross correlations is therefore important.

The gust cospectra must be assumed, as no cospectra of parallel gusts along parallel paths have been measured. The assumed cospectra should produce realistic moment magnitudes, but with no data one cannot determine whether assumed, realistic cospectra are worst-case, best-case, or typical; approximations in general are usually classified in this manner to aid the designer in interpreting analyses results. In the present case the best that can be done is to assume cospectra that will produce realistic magnitudes.

The particular cospectra assumed depend upon whether the line connecting the correlated point gusts is parallel or orthogonal to the flight path, and whether or not the gust components themselves are parallel or orthogonal to the line connecting them or the flight path. The former determines whether gust penetration need be considered, and the latter is important because of spectral dependence on choice of coordinates. Models for the various cases are presented below. All of the models approximate the cospectra in the following manner.

Consider vertical gusts at remote points on the vehicle. Assume the cross correlation of vertical gusts displaced by r feet and t seconds is $\sigma^2 g(r, t)$, where $g(0, 0) = 1$. For gust pairs where the line connecting the gusts is orthogonal to the flight path at $t = 0$, the cross correlation of the gusts as time

advances is $\sigma^2 g(\sqrt{d^2 + (V_{as} t)^2}, t)$ where d is the displacement of the gusts at $t = 0$ (the distance between the gusts is $\sqrt{d^2 + (V_{as} t)^2}$, where V_{as} is airspeed).

For gust pairs where the line connecting the gusts is parallel to the flight path, the gust cross correlation as time advances is $\sigma^2 g(|d - V_{as} t|, t)$. Both of these correlations will produce irrational cospectra if the autocorrelation $\sigma^2 g(V_{as} t, t)$ is rational.

The first cross correlation can be approximated by

$$\sigma^2 g(\sqrt{d^2 + (V_{as} t)^2}, t) \approx \sigma^2 g(V_{as} t, t) \cdot g(d, 0)$$

as constant times the autocorrelation. This produces a rational cospectra, and it is a good approximation except for the time interval $0 < t < 2d/V_{as}$, where the approximation can decrease faster than the actual cross correlation (depending upon the form $g(r, t)$ assumed). It will at worst produce slightly larger moments than those in nature, and it meets the realism criterion.

The $\sigma^2 g(|d - V_{as} t|, t)$ cross correlation is more difficult to approximate as, unlike the above cross correlation, its maximum does not occur at $t = 0$ except at zero airspeed. This cross correlation contains a time delay or gust penetration effect as well as the space and time decays, and any approximation employed should retain these features. The simplest approximation which does this is

$$\begin{aligned} \sigma^2 g(|d - V_{as} t|, t) \approx & \sigma^2 g(0, d/V_{as}) \cdot g(V_{as}(t - d/V_{as}), 0) \\ & + \sigma^2 (1 - g(0, d/V_{as})) \cdot g(d, 0) \cdot g(V_{as} t, t) \end{aligned}$$

The correlation $g(V_{as}(t - d/V_{as}), 0)$ embodies the delay line, while the second term preserves the space and time dependence of the cross correlation at very large delay times d/V_{as} , where the time correlation of the gust at a point $g(0, d/V_{as})$ has decayed to a small value.

These two approximations appear in all of the cross correlations below. In addition, the dependence of correlation form on whether or not the gusts are parallel to the line connecting them is partially taken into account as follows. Let the correlation of gusts parallel to the line connecting them be $\sigma^2 f(r, t)$, and the correlation of gusts orthogonal to the line connecting them be $\sigma^2 g(r, t)$. If the gusts are parallel or orthogonal to the line connecting them for all time, the forms $\sigma^2 f(r, t)$ and $\sigma^2 g(r, t)$ are used respectively exactly as $\sigma^2 g(r, t)$ is used in the above discussions. For gusts which are orthogonal to the line connecting them at $t = 0$, but which become parallel to that line as time increases, the actual correlation is

$$\sigma^2 g(r, t) \cos^2 \psi + \sigma^2 f(r, t) \sin^2 \psi$$

where

$$r = d^2 + (V_{as} t)^2 \text{ and } \psi = \tan^{-1}(V_{as} t/d)$$

This is approximated in the model by

$$\sigma^2 g(r, t) \cos^2 \psi + \sigma^2 f(r, t) \sin^2 \psi \approx \sigma^2 g(d, 0) \cdot f(V_{as} t, t)$$

which produces a simple, rational cospectrum. The errors introduced by this approximation are not serious, and the resulting moment magnitudes will be realistic.

4. Angle Dependence

As shown in Figure 5, let

- ψ_h = heading angle = angle between fuselage and downwind direction
- ψ_a = azimuth angle = angle between flight path and downwind direction
- β = sideslip angle = angle between fuselage and airspeed vector

The sideslip angle β and the airspeed V_{as} define the aerodynamics of the aircraft. Their only direct effect on the gust field as seen by the aircraft, however, is the dependence of the gust penetration delay on β . At $\beta = 0$ degrees the gusts at the tail are those at the wing roots delayed by d/V_{as} seconds, the wing-to-tail distance divided by the airspeed t . At $\beta = 90$ degrees the gusts on the left wing are those on the right wing delayed by $b/2V_{as}$ ($b/2$ is the half span), and at $\beta = 180$ degrees the wing root gusts are the tail gusts delayed by d/V_{as} . As discussed in Section VI, the effects of these delays are not negligible and must be taken into account in defining the gust field as seen by the aircraft.

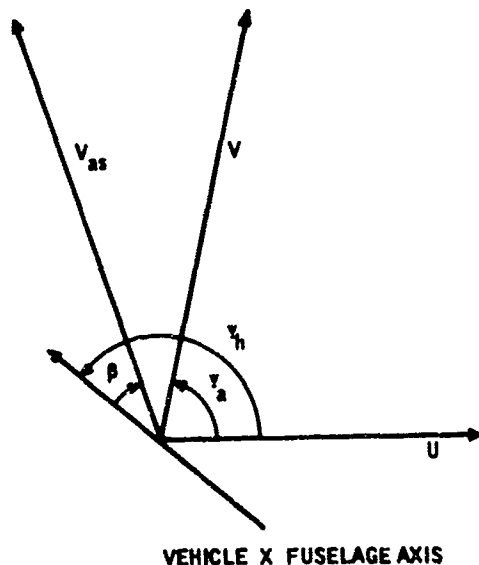


Figure 5. Definition of Angles

The heading angle ψ_h determines the transformation of downwind and crosswind gusts to head-on and side gusts. Letting u_1, u_2, u_3 be head-on, side, and vertical gusts and u, v, w be downwind, crosswind, and vertical gusts, then

$$\begin{bmatrix} u_1 \\ u_2 \\ u_3 \end{bmatrix} = \begin{bmatrix} \cos \psi_h & \sin \psi_h & 0 \\ -\sin \psi_h & \cos \psi_h & 0 \\ 0 & 0 & 1 \end{bmatrix} \begin{bmatrix} u \\ v \\ w \end{bmatrix}$$

where right-hand rule coordinate systems have been chosen for u_1, u_2, u_3 and u, v, w (the choice of coordinates determined the signs in the transformations). ψ_h thus defines the head-on, side, and vertical gust intensities.

The azimuth angle ψ_a and ground speed V together define the distance metric used in the gust covariance tensor,

$$r = |t| (V^2 + U(z)^2 - 2\lambda_t V \cos \psi_a)^{1/2} / \lambda_z z$$

This dependence was discussed above.

Azimuth angle also affects the spectra and cospectra of the downwind, crosswind, and vertical gust components as seen by the aircraft. In isotropic turbulence and undoubtedly in the earth's boundary layer as well, the spectrum of a gust component parallel to a path as measured along that path is different

than the measured spectrum of the same gust measured along a path orthogonal to the gust component direction; Ψ_a determines the mixes of downwind, crosswind gusts parallel and orthogonal to the flight path. This dependence is easily accounted for in isotropic turbulence, but it has never been measured or even estimated in the earth's boundary layer.

The azimuth angle Ψ_a and the heading angle Ψ_h together define the cross correlations (cospectra) of the head-on, side, and vertical gust components and the head-on and vertical gust shears across the wing. Without azimuth dependence data, choosing the various gust cospectra is guesswork. It is in fact very difficult guesswork, as it is hard to assign azimuth dependencies that are mathematically self consistent. Fortunately, as discussed above, these cospectra are of no consequence if the correlation coefficients are small and/or if the contributions of the correlated inputs to responses of interest are of distinctly different magnitudes.

Ignoring the correlations, then, the only angle dependencies which must be taken into account are the distance metric dependence, the penetration effect, the intensity dependence on heading, and the spectrum dependence on whether gust components are parallel or orthogonal to the flight path. Of these only the penetration, sideslip angle relation causes any difficulty; the problem here is that the portion of the wing directly in line with the tail (and therefore affected by the time delay) is a function of sideslip angle. Accounting for this continuity adds a great deal of algebraic complexity to the gust model. One must first calculate the distance metric r between the two wings and every point on the flight path of the tail, a function of azimuth angle, sideslip angle, airspeed and ground speed, wing-to-tail distance, and the wing quarter-span distance. The time displacements and correlations between the two wings and tail must then be calculated for each wing, for both vertical and head-on gusts. Both forms of the correlation functions and the time delays are functions of azimuth and sideslip angles. One must then calculate the cross correlations of the wing gusts with the tail gusts at these displacements using approximations of the above type, and then add independent gust inputs to the tail (for $|\beta| < 90$ degrees, to the wings for $|\beta| > 90$ degrees) to bring the gust intensities up to their proper magnitudes. This produces eight gust sources and three tapped delay lines, two of the delay lines being tapped twice for the gusts on the two wings. From a trial calculation it will be seen that these calculations are exceedingly complex. The intended use of the gust model does not warrant this complexity.

For simplicity in generating the gusts as seen by the aircraft it will be assumed that the aircraft flies at one of four sideslip angles, $\beta = 0, \pm 90$ degrees, and 180 degrees. In the first case the tail gusts will be generated in part by the delaying the wing gusts, and in the 180 degree case the wing gusts will be generated in part from the tail gusts. At 90 degrees the head-on and vertical gust shears will be generated with delays.

5. Spectral Form

The simplest form that can be assumed for the autocorrelation of gusts parallel to the flight path is the exponential

$$f(r, 0) = \sigma^2 e^{-|r/L|}$$

The gusts orthogonal to the flight path will have a different autocorrelation (no matter what flight path). For isotropic turbulence the cross-path spectra are $g = f + 1/2 rf'$, which produces with the above form

$$g(r, 0) = \sigma^2 e^{-|r/L|} (1 - 1/2|r/L|).$$

As discussed previously, many different spectral forms can be fit to the measured spectral data. It is shown by example in Section V that the differences in response standard deviations produced by the above two forms can be as much as 30 percent; presumably larger changes would be produced by other attempts at spectral fits.

Spectral fits are thus important, and exactly what good choices for the spectra are has not been settled. For simplicity it will be assumed in the gust model that the above forms hold, that the spectra of gusts parallel to the flight path are of the form

$$\int_{-\infty}^{\infty} e^{-sr} \sigma^2 e^{-|r/L|} dr = \frac{2L}{-L^2 s^2 + 1} = \frac{\sqrt{2L}}{-Ls+1} \cdot \frac{\sqrt{2L}}{Ls+1}$$

and those orthogonal to the flight path are

$$\begin{aligned} \int_{-\infty}^{\infty} e^{-sr} \sigma^2 e^{-|r/L|} (1 - \frac{1}{2}|r/L|) dr &= L \frac{3L^2 s^2 + 1}{(-L^2 s^2 + 1)^2} \\ &= \sqrt{L} \left(\frac{\sqrt{3Ls+1}}{(Ls+1)^2} \right) \left(\sqrt{L} \frac{-\sqrt{3Ls+1}}{(-Ls+1)^2} \right) \end{aligned}$$

6. Final Filter Form

Putting these assumptions together, the intensities of the head-on, side, and vertical gusts seen by the aircraft are

$$\sigma_{u_1} = \sqrt{E\{u_1^2\}} = (7.8 \cos^2 \psi_h + 4 \sin^2 \psi_h)^{1/2}$$

$$\sigma_{u_2} = \sqrt{E\{u_2^2\}} = (7.8 \sin^2 \psi_h + 4 \cos^2 \psi_h)^{1/2}$$

$$\sigma_{u_3} = \sqrt{E\{u_3^2\}} = 1.7$$

The distance metric r measured along the flight path is

$$r = c |i|$$

where

$$c = [V^2 + U(z)^2 - 2\lambda_t U(z)V \cos \psi_a]^{1/2} / \lambda_z z$$

For nominal values choose $\lambda_t = 0.98$, agreeing with Panofsky's figure, and $\lambda_z = 1$, the median of the available figures.

The spectra of gusts parallel and orthogonal to the flight path are then of the form

$$\frac{2c}{-s^2 c^2 + 1} : \text{parallel}$$

$$\frac{c(-3s^2 c^2 + 1)}{(-s^2 c^2 + 1)^2} : \text{orthogonal}$$

The angle between the fuselage axis and the flight path in the moving gust field is β , the sideslip angle, so the spectra of head-on, side, and vertical gusts seen by the aircraft are the above spectra transformed through β . This gives

$$\phi_{u_1 u_1}(s) = \sigma_{u_1}^2 \left(\frac{2c}{-s^2 c^2 + 1} \cos^2(\beta) + \frac{c(-3s^2 c^2 + 1)}{(-s^2 c^2 + 1)^2} \sin^2(\beta) \right)$$

$$\phi_{u_2 u_2}(s) = \sigma_{u_2}^2 \left(\frac{2c}{-s^2 c^2 + 1} \sin^2(\beta) + \frac{c(-3s^2 c^2 + 1)}{(-s^2 c^2 + 1)^2} \cos^2(\beta) \right)$$

$$\phi_{u_3 u_3}(s) = \sigma_{u_3}^2 \frac{c(-3s^2 c^2 + 1)}{(-s^2 c^2 + 1)^2}$$

The first two reduce to

$$\varphi_{u_1 u_1}(s) = \frac{\varphi_{u_1}^2 c(-2 + \sin^2(\beta)) s^2 c^2 + 1 + \cos^2(\beta)}{(-s^2 c^2 + 1)^2}$$

$$\varphi_{u_2 u_2}(s) = \frac{\varphi_{u_2}^2 c(-2 + \cos^2(\beta)) s^2 c^2 + 1 + \sin^2(\beta)}{(-s^2 c^2 + 1)^2}$$

By assumption we have set the cospectra equal to zero,

$$\varphi_{u_1 u_2}(s) = \varphi_{u_1 u_3}(s) = \varphi_{u_2 u_3}(s) = 0$$

At zero sideslip the correlation coefficients of head-on and vertical gusts halfway out each wing are (because both are orthogonal to the line connecting them)

$$\rho_{u_{1L} u_{1R}} = e^{-\frac{b}{2L} \left(1 - \frac{b}{4L}\right)} = g\left(\frac{b}{2}, 0\right)$$

$$\rho_{u_{3L} u_{3R}} = e^{-\frac{b}{2L} \left(1 - \frac{b}{4L}\right)} = g\left(\frac{b}{2}, 0\right)$$

where $b/2$ is the half span distance and L is the correlation length $L = \lambda_z$.

The gusts $\frac{u_{1L} + u_{1R}}{2}, u_{2w}, \frac{u_{3L} + u_{3R}}{2}$ at the fuselage between the wings will be

delayed by d/V_{as} seconds before reaching the tail, where d is the wing-to-tail distance and V_{as} is airspeed. The correlation coefficients of these gusts after being delayed by d/V_{as} are

$$\rho_{u_{1w} u_{1T}} = e^{-\frac{c'd}{V_{as}}} = f(0, d/V_{as})$$

$$\rho_{u_{2w}u_{2T}} = e^{-\frac{c'd}{V_{as}}} \left(1 - \frac{c'd}{2V_{as}} \right) = g(0, d/V_{as})$$

$$\rho_{u_{3w}u_{3T}} = e^{-\frac{c'd}{V_{as}}} \left(1 - \frac{c'd}{2V_{as}} \right) = g(0, d/V_{as})$$

where

$$u_{1w} = \frac{u_{1L} + u_{1R}}{2}, \quad u_{3w} = \frac{u_{3L} + u_{3R}}{2}, \quad \text{and } u_{1T}, u_{2T}, \text{ and } u_{3T} \text{ here}$$

are those portions of the tail gusts contributed by the delayed wing gusts, and

$$c' = U(z)(2 - 2\lambda_t \cos \psi_a)^{1/2} / \lambda_z z$$

the above c with V set equal to $U(z)$. The spatial correlations of the wing and tail gusts at zero time displacements are

$$\rho_{u_{1w}u_{1T}} = e^{-d/L} = f(d, 0)$$

$$\rho_{u_{2w}u_{2T}} = e^{-d/L(1-d/2L)} = g(d, 0)$$

$$\rho_{u_{3w}u_{3T}} = e^{-d/L(1-d/2L)} = g(d, 0)$$

At 180 degrees sideslip the wing gusts u_{1w} , u_{2w} , u_{3w} are the tail gusts delayed by d/V_{as} seconds, and the above correlation coefficients hold. Because the tail gusts define the average wing gusts u_{1w} , u_{3w} , it will be convenient to generate u_{1L} , u_{1R} , u_{3L} , u_{3R} by generating

$$u_{1w}, \quad \frac{u_{1R} - u_{1L}}{2}, \quad u_{3w}, \quad \frac{u_{3R} - u_{3L}}{2}$$

and adding, rather than generate u_{1L} , u_{1R} , u_{3L} , u_{3R} directly.

In sideways flight a wing is an inefficient lifting surface, and the moments induced by gust propagation along a wing can be assumed negligible. However, existing V/STOL aircraft have fans, jets, and rotors located on the wings, and the moments produced by the airspeed differences seen by these thrusters may well be significant. The propagation of gusts along the wing must therefore be taken into account. In the following it is assumed that the thrusters are located at the wing tips; for thrusters located within the wing, the half-span $b/2$ in the formulae below and in Figure 9 should be replaced by the distance between the thrusters.

At ± 90 degrees sideslip the correlated coefficients of u_{1w} , u_{2w} , u_{3w} and u_{1T} , u_{2T} , u_{3T} are

$$\rho_{u_{1w}u_{1T}} = e^{-\frac{d}{L}} = f(d, 0)$$

$$\rho_{u_{2w}u_{2T}} = e^{-\frac{d}{L} \left(1 - \frac{d}{2L}\right)} = g(d, 0)$$

$$\rho_{u_{3w}u_{3T}} = e^{-\frac{d}{L} \left(1 - \frac{d}{2L}\right)} = g(d, 0)$$

The delay time across the half span is $b/2V_{as}$, in which time the across-wing correlation coefficients decay to

$$\rho_{u_{1L}u_{1R}} = e^{-\frac{c'b}{2V_{as}} \left(1 - \frac{c'b}{4V_{as}}\right)}$$

$$\rho_{u_{3L}u_{3R}} = e^{-\frac{c'b}{2V_{as}} \left(1 - \frac{c'b}{4V_{as}}\right)}$$

The spatial cross correlations at zero time displacement are

$$\rho_{u_{1L}u_{1R}} = e^{-b/2L(1 - b/4L)} = g(b/2, 0)$$

$$\rho_{u_{3L}u_{3R}} = e^{-b/2L(1 - b/4L)} = g(b/2, 0)$$

Because at the different sideslip angles the independent gust inputs are added at different places and the various correlation coefficients change, it is

convenient to generate first eight statistically independent signals (u_{1a}, u_{1b}, u_{1c}), (u_{2a}, u_{2b}), (u_{3a}, u_{3b}, u_{3c}) that have the spectra of (u_1), (u_2), (u_3) respectively. Filters which do this are shown in Figure 6.

The combination of the outputs of these filters to generate the various delayed gusts are shown in Figures 7, 8 and 9. In each figure the constants at the bottom of the figure have been introduced to account for the various correlation coefficients.

This completely defines the gusts as seen by the aircraft.

E. SUMMARY

It was necessary to make a great many assumptions to generate a gust model.

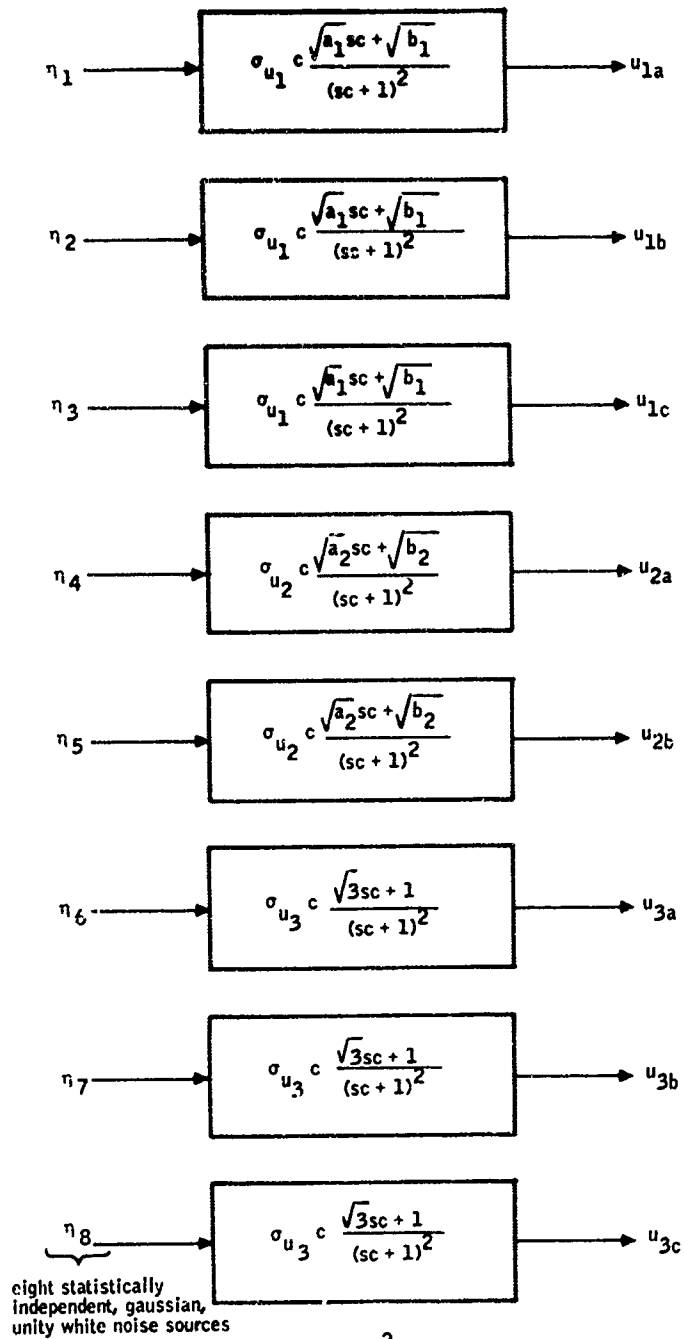
Assumptions of wind profile characteristics were made to define the mean wind, mean wind shear, and nominal gust covariances at a point in time and space. The assumptions are reasonably justified by existing data, with the exception of an assumed mean wind probability distribution. Constructing a more elaborate profile model would not produce essentially different numbers. The probability assumption is justified only by convenience and the 9.1-meter data from Cape Kennedy.

Gaussian probability densities were arbitrarily assumed for the gusts.

Average winds and wind shears were approximated by sums and differences of gusts halfway out the wings and at the tail. This assumption is reasonable for correlation lengths larger than the vehicle dimensions, but it produces up to 1.6 times too large shear moments at very low altitudes where the correlation length is 1/10 the wingspan.

The gust covariance tensor is based upon extending a distance metric supported by a single set of data to all azimuth angles. All cross correlations of orthogonal gust components were set equal to zero for simplicity, an assumption supported by calculations showing that the resulting response standard deviations could at most be 15 percent in error. The cospectra of parallel gusts at remote points were assumed to be constants times their autospectra, in reasonable agreement with available covariance data. The spectral forms of the various gust components were chosen to display the effects of the angles between the gust components and the flight path on the spectra in the same manner as if the gusts were isotropic. The gust intensities were obtained by transforming downwind and crosswind intensities through the heading angle.

This model has been contrived to reasonably present the gust descriptors which the linear and nonlinear analyses showed were important. These descriptors are spectral form, gust intensity, gust shear across the wings, and gust penetration.



$$a_1 = 2 + \sin^2(\theta)$$

$$b_1 = 1 + \cos^2(\theta)$$

$$a_2 = 2 + \cos^2(\theta)$$

$$b_2 = 1 + \sin^2(\theta)$$

Figure 6. Gust Sources

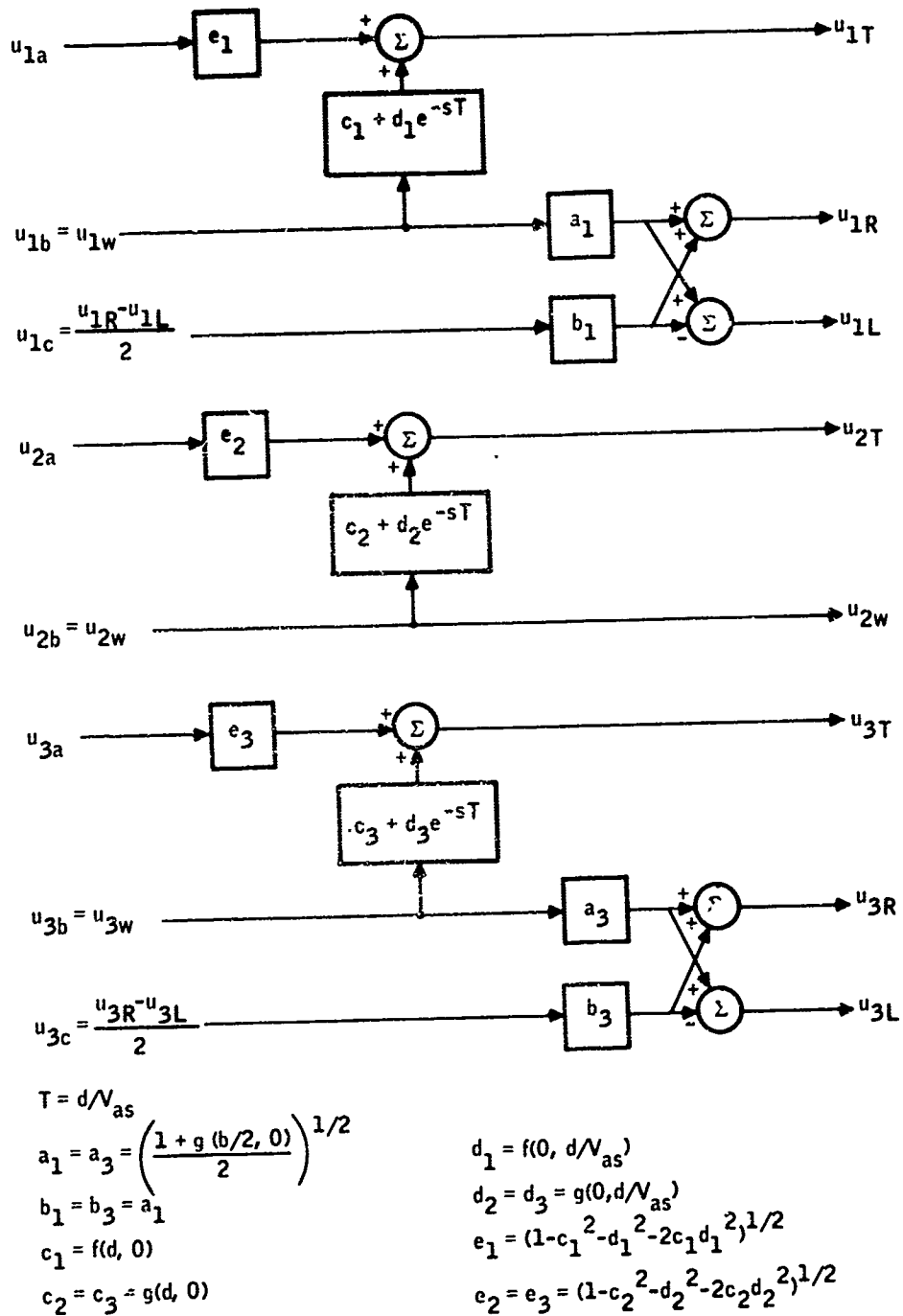


Figure 7. Gust Combination at Zero Sideslip

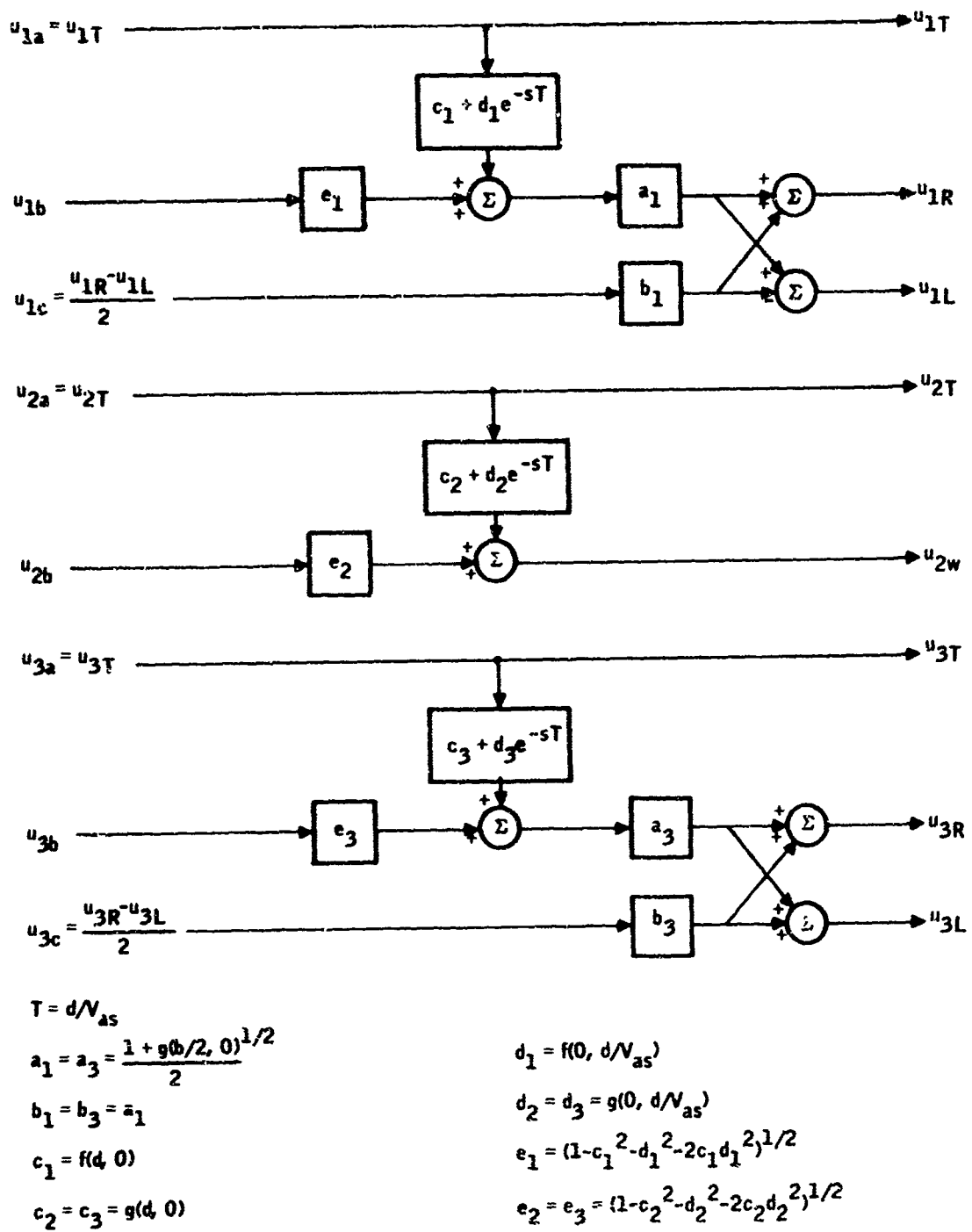


Figure 8. Gust Combination at 180-degree Sideslip

SECTION IV TOLCAT REQUIREMENTS

The twin goals of this study were development of an interim gust model and specification of the TOLCAT gust measurements required to generate a better model. The interim model developed was described in Section III. The gust measurements required of the TOLCAT program are presented in this section.

It should be stated at the outset that collecting enough data in TOLCAT to completely define a statistical gust model is impossible. A complete model would require measuring all finite-order joint probability densities of all gust components at all spatial and time displacements as functions of mean wind, mean wind shear, thermal stability, altitude, and surface roughness, and this much data cannot be generated in a five-year experiment. Even this description assumes that gust statistics are defined by three long-time-average descriptors plus altitude and roughness, and proving experimentally that no more descriptors are required would require collecting a great deal of very accurate data. In order to limit TOLCAT to manageable proportions, it is necessary to assume some of the physical relations, limit spectral bandwidths to those visible in aircraft responses, and measure only essential data.

The discussion of TOLCAT requirements which follows is divided into two parts. The first part deals with the premises under which the TOLCAT experiments will be run and the long-time-average experiments required. These subjects are treated together as the major premise of gust modeling should be verified in a long-time-average experiment. The second subsection discusses the gust measurements themselves.

A. PREMISES AND LONG-TIME AVERAGES

The major premises upon which all gust models are based are that:

- The winds consist of slowly and rapidly time-varying components and there is a clear demarcation between the two in that there is a frequency range between them that possesses little wind energy,
- The statistics of the rapidly varying portion of the winds are defined entirely by descriptors of the slowly varying portion.

The first premise defines mean winds and gusts as the slowly and rapidly varying portions of the winds. The second premise is defensible, providing the first is true, by deriving Navier-Stokes equations for the mean wind and subtracting the resulting terms from the original equations to obtain gust equations.

Everything thus depends upon separation of gusts and mean winds. That there is a separation is evidenced by the data in Figure 1.9 of reference 2 (reproduced here as Figure 2) to defend the separation. However, this premise is so essential that it should be verified again in TOLCAT.

1. First TOLCAT Experiment

Measure the gust spectra at a point over a very long time (to very low frequencies) and show that there is a clear demarcation between gusts and mean winds.

A third premise is that the long-time-average descriptors required to define gust statistics consist of:

- Mean wind, friction velocity, and gradient Richardson number at a known altitude over a surface of known roughness, with no other descriptors being required.

That no more descriptors are required is always true in a statistical sense as one can write conditional gust statistics conditioned by any number of variables; what is meant is that no other long-time descriptor adds any more useful information as far as describing gusts. This premise is based upon the absence of discussion of any other descriptor in the gust literature, perhaps a weak justification.

Other descriptors equivalent to these, derivable from them, or from which they can be derived (such as temperature gradient and the vertical shear of the mean wind) would serve gust description purposes as well as the above. Any other long-time descriptors found in TOLCAT to better or more directly define gust statistics should be added to the above list.

Mean wind, friction velocity, gradient Richardson number, and altitude are inter-related with mean wind shear and surface roughness by Panofsky's profile formulae presented in Section II. Since TOLCAT will presumably use five or so test sites, surface roughness probably will not be continuously variable, and it will be necessary to use a profile formula to extrapolate data from one roughness length to another. However, the gust experiments require a vertical arrangement of wind sensors (on a tower) so there is no need to assume a profile formula in TOLCAT.

2. Second TOLCAT Experiment

Measure the joint probability density of mean wind amplitude, friction velocity, and gradient Richardson number as a function of altitude.

These probabilities should be conditioned by information normally available to a V/STOL pilot, such as time of day, temperature, presence of nearby storms, fetch, and the angular difference between the mean winds high up and those on the

ground; the pilot's being able to predict the kinds of gusts he will see when landing will make that landing safer. This information also would be useful for determining the causes of observed mean winds, friction velocities, and thermal stabilities.

It is emphasized that this experiment is a means to two ends, defining the mean winds and defining the gust environment. While it is not intended that it be a wind profile experiment, it should be one to the extent that profiles define mean winds and gusts at altitudes other than that at which a V/STOL currently flies. A V/STOL will respond to a mean wind shear when landing, after all. But the goal is definition of the mean wind and gusts; profile formulae are a means to that end, but they are not the goal itself.

The fourth premise is the gust frequencies to which an aircraft will respond. The dominant closed-loop poles of most aircraft lie between 2 and 4 rad/sec, but B52 flexure modes have been measured in flight at 60 rad/sec. Wings produce forces at V_{ag}/\bar{c} rad/sec; airspeeds V_{ag} can run from zero for a V/STOL to 1000 ft/sec for a terrain following fighter, and wing chords \bar{c} run from 6 feet for a small aircraft to 150 feet for the SST, so V_{ag}/\bar{c} can go as high as 100 rad/sec. Wingspans run typically from 30 to 180 feet, and wing-to-tail distances from 10 to 90 feet.

The gust time-spectra bandwidth to which aircraft will respond then run from 1/10 rad/sec to 100 rad/sec. The corresponding wavelengths are 6 feet, a wing chord, out to 1000 ft/sec divided by 1/10 rad/sec, or 10,000 feet. These are very large dynamic ranges. To narrow them one must focus on a particular type of aircraft.

For a typical V/STOL it is reasonable to assume airspeeds from hover to 200 ft/sec in the boundary layer, 7- to 12-foot chords, and 1/10 to 30 rad/sec time frequencies. The corresponding wavelengths are 7 feet to 2000 feet.

In general, however, the wider the wavelength and time-frequency bandwidths of the gust data, the better -- especially with regard to the wavelengths⁹.

B. GUST MEASUREMENTS

The gust measurements are chosen to define the gust spectra, magnitudes, and probability densities as functions of mean wind amplitude, friction velocity, and gradient Richardson number.

The first experiment described will define the gust magnitudes and probability densities.

⁹ It is thought that a wing will not respond significantly to wavelengths less than a wing chord. However, the National Aeronautics and Space Administration has constructed a wind tunnel at Langley Field, Virginia, capable of measuring these responses, and wavelength data should be available before TOLCAT is completed. If that data shows smaller wavelength dependence, reducing the 6-foot minimum wavelength in TOLCAT will be desirable.

1. Third TOLCAT Experiment

Measure the individual probability densities of downwind, crosswind, and vertical gust components conditioned by mean wind amplitude, friction velocity, gradient Richardson number, altitude, and roughness length.

The rms magnitudes defined by the densities are of course important to determining rms $V/STOL$ responses, but they also can be determined from spectral measurements. The interest here is the occasion of a violent gust that will upset the $V/STOL$. The probabilities should therefore be measured out to as low likelihoods as possible.

This experiment is considerably simpler than measuring all joint gust densities at remote points and times. The thoughts behind these measurements are that the densities plus spectral calculations should suffice for estimating the likelihood of upset, and it will be possible to simulate the resulting gust model on a computer for gust response tests. The joint densities would be only slightly more descriptive, especially if cross correlations are small, and they, of course, require a great deal more data collection. Measuring the gust densities to very low likelihoods is most desirable, as it is difficult to recover from upset at low altitudes and moderate airspeeds, and the likelihoods will determine the likelihood of crashing.

Gust spectra are known to be dependent upon mean wind amplitude, friction velocity, Richardson number, altitude, and azimuth of the measurement path (angle between the path and the downwind direction). The mean wind determines the downwind transport of the gust field, and friction velocity in part defines gust magnitudes. Altitude in part determines correlation length, and correlation length for crosswind paths is known to be Richardson-number-dependent. Azimuth also affects spectral shape, as (from isotropic turbulence) it is known that the spectra of gusts orthogonal and parallel to a path differ. The spectra tests should define all of these interdependencies.

All of the above refer individually to downwind, crosswind, and vertical gusts along a path. Also of concern are cross correlations of these gusts and cross correlations of gusts along parallel paths. The latter define the intensity of head-on and vertical gust shears across the wing and the correlation of these shears with side gusts at the tail of a $V/STOL$. Other than the correlation's determination of shear magnitudes, they are unimportant if less than 0.3 in magnitude, a considerable simplification.

All of the spectral measurements can be made from a line of fixed towers plus a 90-foot "T" arrangement of anemometers. The first spectra experiment is designed to define distance metrics.

2. Fourth TOLCAT Experiment

Choose a horizontal line such that the (azimuth) angle between the mean wind and the line will vary from zero to 90 degrees, at least, throughout the course of the experiments. Arrange towers (and possibly arms on the towers) along this line so that sensors can be placed at logarithmically increasing distances from each other, starting with sensors at 3-foot displacement and with five sensors per decade (i. e., 1, 1.5, 2.5, 4, 7, 10, 15, 25, ... meters from each other)¹⁰.

Fix three anemometers on each tower, all at the same altitude, such that the anemometers measure horizontal gust components parallel to the tower line and orthogonal to the tower line, and vertical gust components. Measure the correlation coefficients of parallel gust components on the towers (vertical with vertical, parallel to the tower line with parallel to the tower line, orthogonal to the tower line with orthogonal to the tower line) at all time displacements between the correlated pairs where the correlation coefficients are 0.5 or greater in magnitude. Plot the results for each gust component as lines of constant correlation coefficient (isopleths) on a distance, time plane.

Richardson number, mean wind magnitude, azimuth, and friction velocity should be measured for each of these experiments and recorded on the plots for that experiment.

The experiment should be repeated at other Richardson numbers, friction velocities, mean wind magnitudes, azimuth angles, and altitudes.

This will define the distance metric, "correlation length", and spectral form dependence on Richardson number, friction velocity, mean wind magnitude, azimuth, and altitude.

3. Fifth TOLCAT Experiment

Measure rms gust intensities simultaneously with the above experiment, on one tower, thus defining their dependence on the same independent variables.

4. Sixth TOLCAT Experiment

On all zero-azimuth tests obtain time series autocorrelations of the responses of sensors on one tower, and compare these with the spatial correlation coefficients at the different towers at zero time displacements. The space correlations should differ from the time series correlations only in that the distance abscissa in the former is $U(z)$ times the time abscissa in the latter, where $U(z)$ is the mean wind speed. This will verify the Taylor hypothesis.

¹⁰ These sensors need not be arranged at the stated distances from a single fixed point, nor do the same distance ratios within a decade have to be obtained exactly. With a little cleverness, the number of sensors can be less than the total number of distance increments. For example, with towers at zero, 10, 12, and 16 meters from a point, one can obtain 2, 4, 6, 10, 12 and 16-meter increments.

None of the above experiments measure cross correlations of orthogonal gust components, though not because there is no intent to measure them. With cross correlations of orthogonal gust components one examines the data as they are obtained, because if they are small they will be of little import in V/STOL gust analyses. It is suspected that they are small, but they may not be.

5. Seventh TOLCAT Experiment

Repeat the fourth experiment above, but for orthogonal gust components. If the correlation coefficients are all small, repeat this experiment only under markedly different conditions of Richardson number, etc., to ensure that they stay small. If they are large, however, measure them all every time the fourth experiment is run.

This experiment requires about the same data reduction time as the fourth experiment, and it requires no more equipment or data recording. If the computation time proves to be a small portion of the budget, one may as well run these experiments along with experiment four. (It is suspected that data reduction will be the least of the expenses involved.) This experiment should also be run for three sensors on one tower.

6. Eighth TOLCAT Experiment

While the data from the seventh experiment is still in the computer, compute also the average values of the squares of the velocity products of the orthogonal gusts, whether the correlation coefficients are small or not. Compare these averages with the expected values of the same products calculated assuming Gaussianess.

If the two sets of numbers are very different, there is a magnitude interdependence in the orthogonal gust components that is lost in the averaging of positive and negative values in computing correlation coefficients. Knowing the probability densities from experiment 3 and the spectra and cospectra from the fourth, fifth, and seventh experiments, one can include this magnitude dependence in the gust model by introducing multipliers into the model filter inputs. If the two sets of numbers are very similar, there is no magnitude dependence and the issue can be dropped.

All of the above experiments are to be run with sensors arranged in a single line. With the addition of a right-angle leg to this line, measurements of gust shear across the wings of an airplane and the correlation of those shears with other gusts on the airplane can also be made.

7. Ninth TOLCAT Experiment

Select pairs of sensors on the tower line 15, 20, 30, 45, 60, 75, and 90 feet apart. On the orthogonal bisectors of the lines connecting them place sensor

triplets 1/3, 2/3, and 1 times the distance between the point pairs, measured from the point of intersection of the two lines. (This can be done with a T-shaped horizontal frame where the three sensor triplets can be moved about, or with any other arrangement that is convenient.)

Measure the magnitudes of the differences between parallel gusts on the two arms of the T (the differences will give a more accurate shear magnitude measurement than can be calculated from the correlation coefficients produced by the fourth experiment). Find also the correlation coefficients of these differences with each other at zero time displacement, and with the three gusts at each point on the stem of the T at zero to 3-second displacements.

Repeat this experiment every time experiment 7 is repeated. As with 7, there is no need to obtain other than verification data for the correlation coefficients which are small. Unlike experiment 7, however, the cross correlation of the difference of horizontal gusts orthogonal to the tower line and gusts on the stem of the T parallel to the tower line may well be large, especially at correlation lengths of the order of the length of the stem.

There is no need to measure any autospectra as these can be calculated from the data from experiment 4. If any of the above correlation coefficients is large, however, calculation of cospectra will be worthwhile.

8. Data Reduction

It is an axiom of physics that few functional relations are found experimentally for which the investigators were not searching in designing the experiments. In the above experiments the existence of functional relations between gust statistics and Richardson number, friction velocity, mean wind magnitude, altitude, and azimuth were assumed, but not specified. Reduction of the gust data to a form convenient for aircraft analyses implies searching for and trying to define these functional relations, for with them one can reduce many "special case" gust models to a few fairly general and convenient models.

The convenient forms for the gust probability densities and rms magnitudes when employed in aircraft analyses are just as they are generated by the above experiments. The convenient forms for the correlation coefficient data of experiments 4, 7, and 9, however, are spectra and cospectra as seen by the aircraft, rather than isopleths on distance-time planes. Converting the isopleths to cospectra requires changing the space dimension to airspeed times time; that is, picking the angle of a line emanating from the origin on the distance-time isopleth planes. This can be done once if the isopleths are concentric, geometrically similar, closed curves, as the correlations measured along any line then are of a single functional form depending upon a single function of the line angle and time. This is the first functional form sought.

The second functional forms sought are connections between cospectra of orthogonal gusts along a path and the autospectra of those gusts. Hopefully the cospectra are proportional to the products of the square roots of the autospectra; this would greatly simplify model making.

The third functional forms sought are simple, exponential cosine approximations to the autocorrelations. These can be calculated with mean-square-error fit subroutines, either in terms of the correlations or the autospectra. If good fits are found with simple functions, well and good. If not, functions which fit two-decade wide portions of the spectra should be generated. The designer doing the gust analysis can then pick the function suited to his purpose.

The fourth functional forms sought are relations between the spectral forms and azimuth, and between the spectral forms and altitude. Finding a single azimuth dependence valid for all mean winds, intensities, altitudes, and Richardson numbers would be a useful simplification. Finding that spectral bandwidths (or correlation lengths) depend simply on altitude, Richardson number, and azimuth would be a useful simplification. Finding these will require looking at a great many isopleths, but the simplifications are worth the trouble.

Of course, eliminating dependences of any of the statistical gust data on any of the independent variables or on combinations of those variables will simplify the gust field description. It is asked here that funds be set aside to search for such functional relations. The thought behind asking for functional relations is that the gust model is going to be complex, and its utility in V/STOL gust analyses will be inverse to its complexity. In addition, finding such relations would provide useful vehicles for insights into satisfactory, approximate solutions of the Navier-Stokes equations, which will be of interest to everyone in fluids in the world.

This concludes the discussion of TOLCAT requirements.

SECTION V LINEAR ANALYSES

The linear analyses performed under the contract consisted of solving covariance differential equations to obtain the sensitivity of V/STOL responses to vehicle and gust model parameters. The vehicle parameters investigated were mean airspeed, mean sideslip angle, and mean heading angle. The gust model parameters investigated were spectral form, gust intensities, correlation length, cross correlations, shear intensities, and the frozen-field hypothesis.

The major results of the linear analyses may be summarized as follows:

- (a) Mean airspeed and mean sideslip angle are critical parameters in defining V/STOL response magnitudes.
- (b) Mean heading angle is important to the extent that it defines the relative intensities of the head-on and side gusts seen by the aircraft.
- (c) Gust spectral form, correlation length, and gust intensities are critical in defining V/STOL response magnitudes.
- (d) The shears of head-on and vertical gusts across the wings produce significant roll and yaw moments, especially at lower correlation lengths, and these shears must be included in the gust model.
- (e) Cross correlations of the various gust components are not critical when small.
- (f) The frozen-field hypothesis is an acceptable approximation to the time-varying gust field at airspeeds greater than $1/3$ the mean wind amplitude.¹¹

The nonlinear analyses described in Section VI supported conclusions (a), (c), (d), (e) [(b) and (f) were not tested in the nonlinear analyses]. They also contributed three results which should be taken into account in evaluating the above six.

- (g) The wing-to-tail transport delay in forward flight is important in determining vehicle responses (these delays were not tested in the linear analyses).
- (h) XV-5 V/STOL nonlinearities of importance are stall angles-of-attack, parabolic velocity products at low airspeeds, and nonlinear fan dependence on gust velocities and control inputs.

¹¹Note "airspeeds", not "ground velocities". The former is the magnitude of vector sum of the latter with the mean wind velocity.

- (i) The upper bound on the range of gust magnitudes where linearity is an acceptable hypothesis depends both on the ratio of gust intensity to mean airspeed (σ/V_{as}) and on the nearness of the mean angle of attack plus the standard deviation of angle-of-attack to stall angle-of-attack. The XV-5 has a pitchup problem near 120 ft/sec forward airspeed due to the wing fans. Relatively small gusts there will stall the tail and cause the airplane to pitch up violently. Trim could not always be recovered. Therefore it is incorrect to base assessments of linearity on σ/V_{as} ratios alone.

All of the results above are based upon analyses of the Ryan XV-5 V/STOL, a fan-in-wing aircraft with relatively large wings and a relatively large tail located approximately half the vehicle length from the wings. Result (e) on cross correlations applies to all aircraft configurations, but the other eight results are configuration-dependent.

All nine results carry over with modifications to fixed-wing aircraft with relatively large tails. The importance of heading angle and sideslip angle increase with increasing wing-lift/weight ratio, and the importance of spectral form will increase with increasing wing efficiency. The significance of gust shears across the wings increases with increasing span and decreasing roll and yaw moments of inertia. The 1/3 figure concluded for the airspeed/mean-wind amplitude ratio will increase as the vehicle response bandwidth and size increase. The wing-to-tail transport delay becomes less important as the center of pressure on the wings is moved aft (as on the F4 fighter), tail size is reduced, or the pitch response bandwidth decreases. The importance of stall, especially stall-induced upset, will vary with vehicle force and weight distributions and with trim requirements; the XV-5, with its near-stall tail trim, is thought to be particularly stall sensitive.

Tilt-wing V/STOL aircraft are another matter, as with the wings tilted, the wings may be continuously in stall. On the XV-5 the wings and tail contributed the significant forces and moments, but side gust effects on the XV-5's rather tall fuselage were not negligible. One would expect the forces and moments on a tilt-wing aircraft with wings tilted to be relatively smaller than on the XV-5, but the magnitudes of the forces and moments could vary significantly with wing chord and span, the difference between wing and tail angles, and the fuselage configuration. Without data, it is not reasonable to carry XV-5 conclusions over to such aircraft.

The effects of gusts on the thrusts produced by rotors, jets, and fans were not examined in this study, and no conclusions can be drawn. The XV-5 wing fans were noticeably affected by gusts, and the effects were dependent on fan parameters, but the force and moment changes produced were in general much smaller than those produced by the aerodynamic surfaces. The importance of gust-induced thrust variations will vary among aircraft and, for an aircraft, with airspeed, interference effects, and thrust parameters, and each V/STOL configuration will have to be treated separately.

The only conclusions one can draw about helicopters or other vehicles with large rotors and large rotor downwash from the present study are that gust intensities and airspeed will be significant parameters. No data were generated which would permit further conclusions.

Returning to the XV-5 results, the discussion of linear analyses in this section is divided into three parts. The gust models employed in the analyses are discussed in the first part; these models differ from the model presented in the previous section in that parameter values were variable, non-zero cross correlations were considered, and gust penetration effects were not included. The linear analysis results obtained are presented second. Several details of the computer program used to obtain the XV-5 response standard deviations are discussed in the final subsection; this program will be documented in a separate report.

A. GUST MODELS

The gust models employed in the linear analyses were those described in the interim report, Honeywell Report 12060-IR1. The following model description summarizes what was presented there.

The mean square amplitudes of the downwind (u), crosswind (v), and vertical (w) gust amplitudes were assumed to be

$$E \begin{pmatrix} u^2 & uv & uw \\ uv & v^2 & vw \\ uw & vw & w^2 \end{pmatrix} = (u^*)^2 \begin{bmatrix} 7.8\alpha_1 & \alpha_4 & -1 \\ \alpha_4 & 4\alpha_2 & \alpha_5 \\ -1 & \alpha_5 & 1.7\alpha_3 \end{bmatrix}$$

where u^* is the friction velocity and $\alpha_1, \alpha_2, \alpha_3, \alpha_4, \alpha_5$ were free parameters. Variation of $\alpha_1, \alpha_2, \alpha_3$ varied the downwind, crosswind, and vertical gust amplitudes respectively. Variation of α_4, α_5 varied the cross correlations of side gusts to downwind and vertical gusts. Variation of the friction velocity u^* varied all amplitudes uniformly, and the $u_1 u_3$ cross correlation (-1 in the above) could be varied by increasing the α 's and decreasing u^* . The nominal values assumed for the intensity parameters were $\alpha_1 = \alpha_2 = \alpha_3 = 1, \alpha_4 = \alpha_5 = 0$.

Letting ψ_h be the angle between the downwind direction and the fuselage, the

$$\begin{bmatrix} \text{head-on} \\ \text{side} \\ \text{vertical} \end{bmatrix} \text{ gusts } \begin{bmatrix} u_1 \\ u_2 \\ u_3 \end{bmatrix} \text{ are}$$

$$\begin{bmatrix} u_1 \\ u_2 \\ u_3 \end{bmatrix} = \begin{bmatrix} \cos \psi_h & \sin \psi_h & 0 \\ -\sin \psi_h & \cos \psi_h & 0 \\ 0 & 0 & 1 \end{bmatrix} \begin{bmatrix} u \\ v \\ w \end{bmatrix}$$

At any time instant the autocorrelation of any gust component u_i along the flight path was assumed to be

$$E\{u_i(x_1) u_i(x_1 + x)\} = E\{u_i^2\} e^{-\frac{|x|}{L}} \left(1 - \beta_i \frac{|x|}{L}\right)$$

where x is distance along the flight path and L is the correlation length. L was varied from 3 to 1,500 feet. The nominal value chose for L for each flight condition was 1.5 second times the vehicle mean airspeed,

$$L = 1.5V_{as}$$

Letting U be the mean wind amplitude, V be the mean vehicle ground speed, and ψ_a be the angle between the flight path and the downwind direction, the vehicle airspeed V_{as} is

$$V_{as} = (U^2 + V^2 - 2UV \cos \psi_a)^{1/2}$$

The distance metric assumed was

$$r = [(r_1 - \lambda_t Ut)^2 + r_2^2 + r_3^2 + (1 - \lambda_t^2)(Ut)^2]^{1/2} / L$$

where r_1 , r_2 , r_3 are distances in the downwind, crosswind, and vertical directions. With

$$r_1 = Vt \cos \psi_a$$

$$r_2 = Vt \sin \psi_a$$

$$r_3 = 0$$

then

$$\begin{aligned} r &= |t| (U^2 + V^2 - 2\lambda_t UV \cos \psi_a)^{1/2} / L \\ &= \frac{V_{as} |t|}{L} \left(1 + 2(1 - \lambda_t) \frac{UV}{V_{as}^2} \cos \psi_a\right)^{1/2} \end{aligned}$$

Defining a new constant λ_c equal to

$$\lambda_c = \left(1 + 2(1-\lambda_t) \frac{UV}{V_{as}^2} \cos \Psi_a \right)^{1/2}$$

the autocorrelation of the u_i gust components as seen by the aircraft was

$$E\{u_i(t_1)u_i(t_1+t)\} = E\{u_i^2\} e^{-\frac{V_{as}\lambda_c |t|}{L}} \left(1 - \beta_i \frac{V_{as}\lambda_c |t|}{L} \right)$$

The corresponding power spectrum is

$$\begin{aligned} \phi_{u_i u_i}(\omega) &= \int_{-\infty}^{\infty} e^{-j\omega t} E\{u_i(t_1)u_i(t_1+t)\} dt \\ &= 2c \frac{\omega^2(1+\beta_i) + c^2(1-\beta_i)}{(\omega^2 + c^2)^2} \end{aligned}$$

where

$$c = \frac{V_{as}\lambda_c}{L}$$

The three-dimensional gust field on the XV-5 was generated by downwind, crosswind, and head-on gusts at the two wing tips and the tail (these were moved inboard in the model presented in Section III to better approximate shear effects). The cross correlation of parallel gust components displaced by a distance x (the wing tip-to-wing tip or wing tip-to-tail distance) was approximated by the autocorrelation of that gust component times the distance weight

$$e^{-\frac{|x|}{L}} \left(1 - \beta_i \frac{|x|}{L} \right)$$

The cross correlation of orthogonal gust components at a point (say at a wing tip) was approximated by the inverse

$$E\{u_i(t_1)u_j(t_1+t)\} = E\{u_i u_j\} \cdot \frac{1}{2\pi} \int_{-j\infty}^{+j\infty} e^{st} 2c \frac{(s\sqrt{1+\beta_i} + c\sqrt{1-\beta_i})(-s\sqrt{1+\beta_j} + c\sqrt{1-\beta_j})}{(-s^2 + c^2)^2}$$

and the cross correlation of orthogonal gust components at remote points was approximated by the above times the weight

$$e^{-\frac{|x|}{L}} \left(1 - \frac{\beta_i + \beta_j}{2} \frac{|x|}{L} \right)$$

The gust model is thus defined by the three intensity parameters $u^{*2}\alpha_1$, $u^{*2}\alpha_2$, $u^{*2}\alpha_3$, the three cross-correlation parameters $u^{*2}\alpha_4$, $u^{*2}\alpha_5$, $-u^{*2}$, the three spectral fit parameters β_1 , β_2 , β_3 , the correlation length L , and the filter time constant

$$c = \frac{V_{as} \lambda_c}{L} \text{ sec}^{-1}$$

The nominal gust model used for the calculations was

$$y_h = \beta = \text{sideslip angle}$$

$$y_a = 0$$

$$u^* = \alpha_1 = \alpha_2 = \alpha_3 = 1$$

$$\alpha_4 = \alpha_5 = \beta_1 = \beta_2 = \beta_3 = 0$$

$$\lambda_c = 1$$

$$c = 2/3$$

$$L = 3/2 V_{as}$$

The parameters were varied from their nominal values to determine the various parameter sensitivities.

This model differs from that presented in Section III in that it includes cross correlations, and free intensity and spectral fit parameters, but it excludes gust penetration. Note that in the nominal model the vehicle is flying downwind.

In accordance with common practice, in what follows the vehicle equations of motion are written in a coordinate system moving downwind with the mean wind. Translation velocity is airspeed in these coordinates, and the mean wind vector itself will not appear in any of the results. The magnitude of the mean wind therefore need not be specified in specifying the gust model; heading angle, however, must be specified as it determines the relative gust component intensities seen by the aircraft.

B. LINEAR ANALYSIS RESULTS

The results of the linear analyses are discussed in this subsection. The data presented support the conclusions listed at the beginning of the section.

A slight change of notation has been made in this section to avoid a duplication of symbols. The symbols u , v , w are commonly used by aerodynamicists as x , y , z body axes components of instantaneous vehicle velocity, and by the meteorologists as the downwind, crosswind, and vertical components of gust velocity. To avoid confusion the subscript "g" for "gust" has been added to the latter.

1. Flight Conditions

The flight conditions considered are shown in Figure 10. Trim settings for these conditions (obtained from the SDS 9300 hybrid simulation) are given in Table I. The angle indicated is the mean sideslip angle (angle between the fuselage and the airspeed vector), and u , v , w are the average airspeed components in fuselage coordinates. The trim values presented produce nearly zero angular rates p , q , r and nearly zero altitude rate dh/dt . The control surfaces (ailerons, elevator, and rudder) were not used and are zero for all flight conditions.

The response standard deviations produced by the linear covariance calculations for these flight conditions are presented in Table II. In all of these calculations, the downwind direction was assumed parallel to the fuselage. The nominal gust model above was employed with the correlation length L chosen so that the gust spectral bandwidth would remain about $2/3$. The calculations are for a unit friction velocity u^* , so the tabulated figures may be regarded as per-unit- u^* responses.

It is evident from the five zero-sideslip flight conditions that increasing airspeed increases the gust sensitivity. Comparing the zero and 90-degree cases, linear perturbation analyses indicate very little pitch plane response in sideways flight. Comparing the zero and 180-degree cases, the XV-5 is slightly less sensitive to gusts in rearward flight than forward flight.

**FLIGHT CONDITIONS
FOR EACH POINT**

ORDINATE = FORWARD VELOCITY
 ABCISSA = SIDEWAYS VELOCITY
 $(\text{ORDINATE}^2 + \text{ABCISSA}^2)^{1/2} = \text{AIRSPEED}$
 $\frac{\text{ABCISSA}}{\text{AIRSPEED}} = \sin(\text{SIDESLIP ANGLE})$

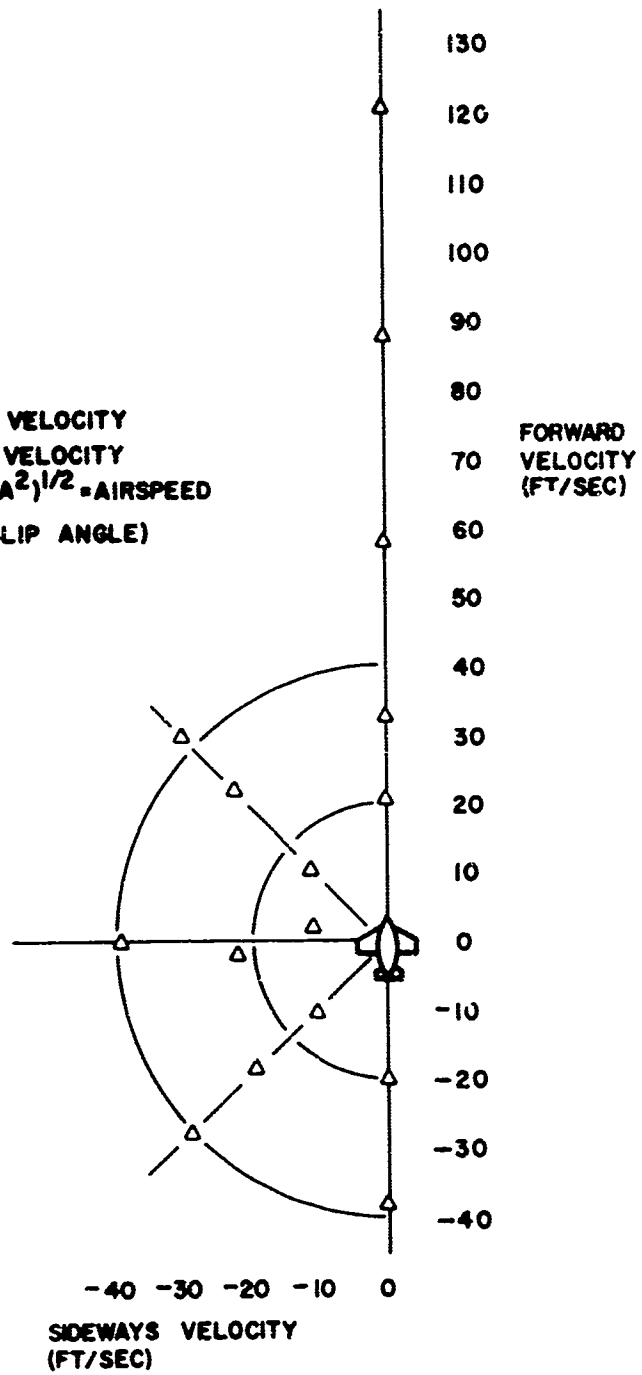


Figure 10. Flight Conditions

Table I. XV-5 Trim Settings*

Flight Condition	u (ft/sec)	v (ft/sec)	w (ft/sec)	ϕ (deg)	θ (deg)	δ_{AR} (deg)	δ_{SL} (deg)	δ_{VR} (deg)	δ_{VL} (deg)	100 KNf	$\frac{P_F}{250}$ ^{2/3}	I_t (deg)
Forward Flight												
1	20.80	0.00	0.00	0.000	0.000	24.70	24.70	2.50	2.50	20.40	88.17	20.00
2	33.00	0.00	1.86	0.000	-0.280	19.80	19.80	6.00	6.00	7.30	88.17	20.00
3	58.10	0.00	1.00	0.000	-0.690	10.00	10.00	14.00	14.00	-14.70	88.17	20.00
4	88.33	0.00	-5.44	0.000	-3.320	7.80	7.80	24.00	24.00	-25.10	89.77	20.00
5	120.80	0.00	11.70	0.000	-5.730	7.80	7.80	39.60	39.60	-9.70	89.77	20.00
45-deg Sideslip Flight												
1	10.78	-11.28	0.28	1.150	0.057	25.03	27.00	0.42	1.19	29.10	88.17	20.00
2	22.12	-22.60	1.94	-4.760	-0.173	15.70	23.90	1.19	4.86	21.20	88.17	20.00
3	30.20	30.40	4.55	8.780	0.530	4.90	21.40	2.00	9.13	15.50	88.17	20.00
90-deg Sideslip Flight												
1	2.30	-10.40	0.47	-0.573	0.000	26.60	27.80	-0.22	0.19	32.10	88.17	20.00
2	1.69	-21.80	0.28	-2.980	0.110	24.03	27.60	-1.28	1.84	31.50	88.17	20.00
3	0.78	-39.60	7.16	-9.980	-2.173	16.01	27.50	-4.31	5.97	29.00	88.17	20.00
135-deg Sideslip Flight												
1	-10.60	-10.10	-0.72	-0.920	0.754	26.59	27.64	-0.38	0.56	32.70	88.17	20.00
2	-18.70	-19.70	-1.67	-3.560	1.610	24.30	27.30	-2.00	1.97	32.80	88.17	20.00
3	-27.20	-29.20	-5.70	-7.900	3.160	18.40	25.30	-4.10	4.10	30.90	88.17	20.00
180-deg Sideslip Flight												
1	-19.20	0.00	-0.94	0.000	2.180	27.50	27.50	0.15**	0.15**	33.70	88.17	20.00
2	-37.20	0.00	-3.00	0.000	5.730	25.50	25.50	0.15**	0.15**	35.20	88.17	20.00

*These trim values were obtained from the SDS 9300 simulation. Trim is defined as zero attitude rates and zero altitude rate.

**Actual trim values are 0.00, not 0.15. The latter are used to generate perturbation models as there is a discontinuity in the drag due to the stagger at zero vector.

Table II. XV-5 Response Standard Deviations, Airspeed and Sideslip Angle Dependence (downwind direction along fuselage for all cases)

Airspeed (ft/sec)	Correlation Length (meters)	Mean Responses $\frac{u}{v/w}$ (ft/sec)	u (ft/sec)	v (ft/sec)	w (ft/sec)	p (deg/sec)	q (deg/sec)	r (deg/sec)	θ (deg)	ϕ (deg)	ψ (deg)
0-deg Sideslip Flight											
20.8	10	20.8/0/0	1.28	0.56	0.47	0.072	0.15	0.29	0.085	0.18	0.44
33	16	33/0/1.86	1.48	0.82	0.57	0.20	0.22	0.38	0.20	0.24	0.55
58	29	58/0/1.0	1.26	1.05	0.76	0.19	0.20	0.47	0.16	0.19	0.63
88	44	88/0/-5.44	1.62	1.31	1.07	0.34	0.11	0.57	0.24	0.11	0.70
121	60	120.8/0/-11.7	1.57	1.60	1.37	0.48	0.13	0.68	0.34	0.15	0.80
-45-deg Sideslip Flight											
15.6	8	10.78/-11.28/-0.28	1.01	0.69	0.37	0.13	0.064	0.25	0.11	0.10	0.38
32	15	22.1/-22.6/-1.94	1.31	0.97	0.53	0.31	0.137	0.47	0.21	0.17	0.63
43	21	30.2/-30.4/-4.55	1.46	1.10	0.59	0.33	0.153	0.59	0.20	0.17	0.74
-90-deg Sideslip Flight											
11	5	2.3/-10.4/-0.47	0.42	0.55	0.22	0.095	0.0069	0.214	0.069	0.016	0.30
22	11	-1.69/-21.8/0.28	0.62	0.63	0.47	0.23	0.011	0.72	0.17	0.016	1.10
40	20	0.78/-39.6/-7.6	1.23	1.06	0.47	0.33	0.021	0.61	0.18	0.019	0.82
-135-deg Sideslip Flight											
14.8	7	-10.6/-10.1/-0.72	0.79	0.62	0.36	0.12	0.029	0.25	0.09	0.032	0.37
27	12	-18.2/-19.7/-1.7	1.02	0.85	0.49	0.22	0.052	0.47	0.14	0.053	0.66
40	20	-27.2/-29.2/-5.7	1.28	1.13	0.66	0.35	0.075	0.68	0.21	0.078	0.95
-180-deg Sideslip Flight											
19.3	10	-19.2/0/-0.94	0.96	0.53	0.50	0.069	0.053	0.22	0.066	0.058	0.35
37.5	19	-37.2/0/-3.0	1.24	0.79	0.70	0.094	0.103	0.36	0.080	0.103	0.57

N

The only conclusions to be drawn from these figures are:

- Increasing airspeed increases gust sensitivity and airspeed is thus an important parameter.
- Sideslip angle is an important parameter.
- Linear perturbation analyses are not trustworthy at small forward velocities (\bar{u} of the order of 1 ft/sec), for two reasons. The Kussner lag time constants on the wing are the mean chord over \bar{u} , and for \bar{u} small these time constants are very large and the wing is a very low-bandwidth low-pass filter. Secondly, the magnitudes of the lift and drag forces are proportional to the airspeed products u^2 , uw , and when linearized about \bar{u} these produce too small gust sensitivities $2\bar{u} \Delta u$, $\bar{u} \Delta w$ (the gust sensitivities are exactly zero for exactly 90 degrees sideslip).

No linear covariance calculations were made at or near hover ($\bar{u} = \bar{v} = \bar{w} = 0$) for these reasons.

2. Dominant Poles

At low airspeeds the aerodynamic rate feedbacks are very small, and the closed-loop dynamics (dominant poles) of the XV-5 are defined almost entirely by the vehicle inertias, fan-louver dynamics, and control gains. The control system employed in this study controls attitudes and attitude rates, but not translation velocities. Ignoring aerodynamic terms, transfer functions of attitude-rate responses to any input δ are (closed-loop)

$$q/\delta(s) = \frac{\partial \dot{q}}{\partial \delta} \frac{s(s+10)}{(s+1.14)(s^2+8.86s+75.2)}$$

$$p/\delta(s) = \frac{s(s+10) \left[(s^3+10s^2+14.1s+14.1) \frac{\partial \dot{p}}{\partial \delta} + (18.8s+18.8) \frac{\partial \dot{r}}{\partial \delta} \right]}{(s^2+1.5s+2)(s^2+8.5s+70)(s+8.36)(s+1.6)}$$

$$r/\delta(s) = \frac{s(s+10) \left[(s^3+10s^2+84.6s+113) \frac{\partial \dot{r}}{\partial \delta} - (5.6s+7.46) \frac{\partial \dot{p}}{\partial \delta} \right]}{(s^2+1.5s+2)(s^2+8.5s+70)(s+8.36)(s+1.6)}$$

The dominant poles of the responses to nose fan door, differential stagger, and differential vector commands are

$$q/K_{Nf_c}(s) = \frac{0.198 s}{s+1.14}$$

$$p/\beta_{s_c}(s) = \frac{0.0123 s}{s+1.6} \quad p/\beta_{v_c}(s) = \frac{0.0109 s^3}{(s+1.6)(s^2+1.5s+2)}$$

$$r/\beta_{s_c}(s) = \frac{0.00108 s^3}{(s+1.6)(s^2+1.5s+2)} \quad r/\beta_{v_c}(s) = \frac{-0.064 s}{s^2+1.5s+2}$$

These transfer functions are valid for airspeeds less than, say, 50 ft/sec.

The translation rate transfer functions at the 20.8 ft/sec forward airspeed. flight condition are

$$u/\delta(s) \approx \frac{\frac{\partial u}{\partial \delta}}{s+0.098}$$

$$v/\delta(s) \approx \frac{\frac{\partial v}{\partial \delta}}{s+0.055}$$

$$w/\delta(s) \approx \frac{\frac{\partial w}{\partial \delta}}{s+0.0625}$$

(the poles here are the stability derivatives $\partial \dot{u}/\partial u$, $\partial \dot{v}/\partial v$, $\partial \dot{w}/\partial w$).

Thus at low airspeeds one expects peak attitude and attitude rate responses at correlation lengths L in the neighborhood of half the airspeed (where the gust spectral bandwidth $c = \frac{V}{L} \approx 2$). One further expects very slow translation responses which monotonically increase with increasing L (decreasing c). These were observed in the correlation length tests below.

3. Correlation Length

The effects of increasing the correlation length L on XV-5 responses are twofold. Increasing L decreases the spectral bandwidth c of the incident gusts with the effect noted above. Increasing L also decreases the shears of head-on and vertical gusts across the wing, decreasing then the shear contributions to roll and yaw moments.

The effects of increasing L on the 20.8 and 120.8 forward airspeed flight conditions are displayed in Figures 11 through 17. The correlation length points used to generate these curves were $L = 1, 2, 5, 10, 20, 50, 100, 200, 500$ meters; smooth curves were drawn through the standard deviations obtained at these points.

The curves behave as one would expect. In the low-speed case, the attitude rate responses peak near 5 meters, or a gust bandwidth of $c = 20.8/15 \approx 1.3$. The attitude responses peak around 15 meters, or $c \approx 0.4$. The translation responses are monotone, and the control inputs peak with peaking attitude and attitude rate.

In the high-speed case the aerodynamic feedbacks are significant. These feedbacks add damping to all responses and therefore will cause the responses to peak at higher c values (lower correlation lengths) than the $c \approx 2$ of the lower airspeeds. The fact that the attitude and attitude rate peaks occur at approximately the same correlation lengths as for low airspeeds is not considered significant.

It is evident from these curves that the gust spectral bandwidth $c = \frac{V \lambda_c}{L}$ is an important parameter.

4. Wing Shear

As mentioned above, increasing L both decreases the spectral bandwidth and decreases the shears of head-on and vertical gusts across the wing. The effects of these shears on roll are commonly ignored in aircraft analyses. They should not be.

To test the magnitude of the shear contribution to roll, both the correlation length L and the constant λ_c were increased by a factor of 10 from their nominal values. This decreased the shears while maintaining the gust spectral bandwidth $c = \frac{V \lambda_c}{L}$. The results are shown in Table III. The greater than 1/3 reduction in the roll and yaw rate standard deviations imply that shear cannot be ignored.

These data are based on obtaining the shear magnitudes by differencing the wing-tip gusts

$$\frac{\partial u_g}{\partial y} \approx \frac{u_g(b/2) - u_g(-b/2)}{b}$$

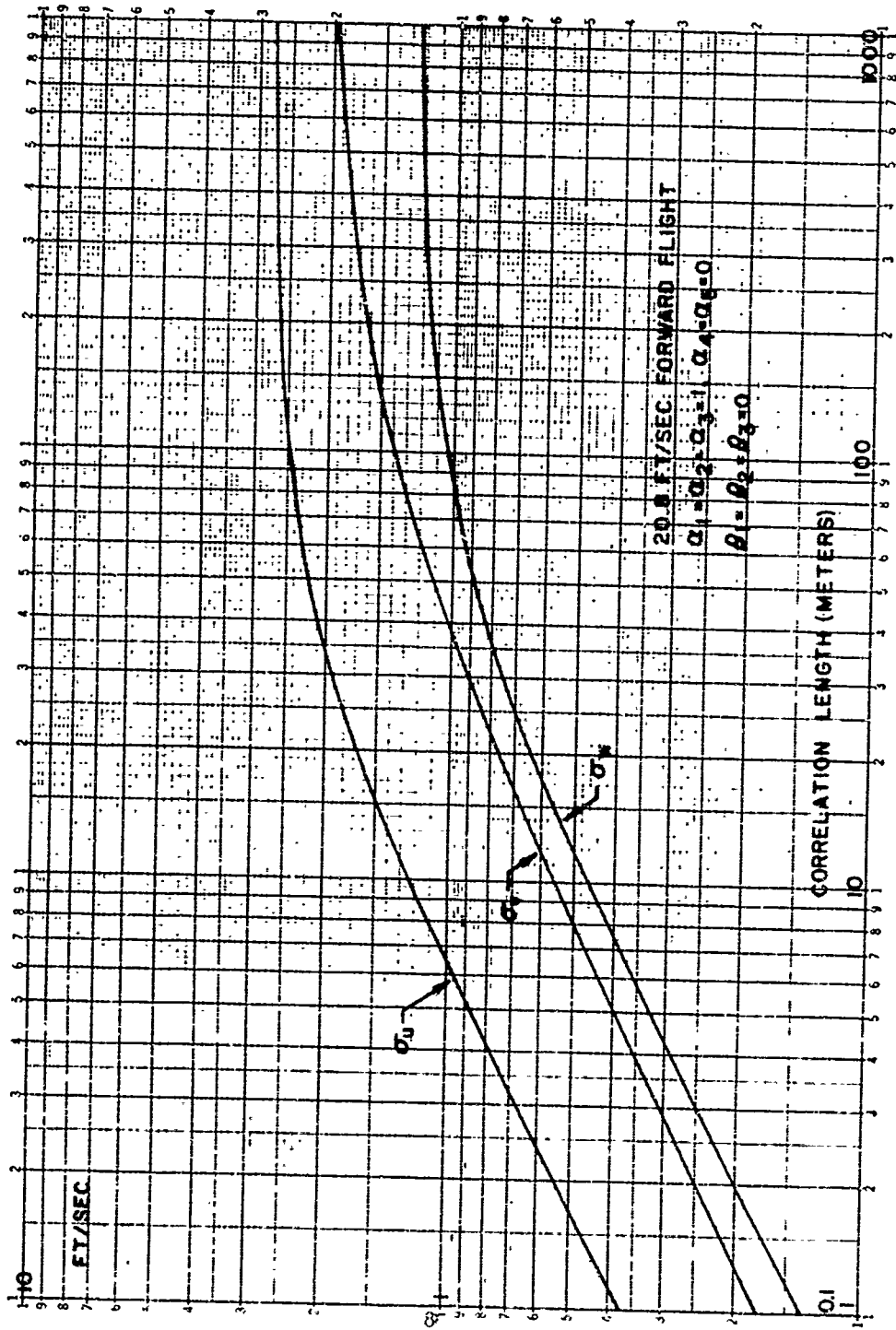


Figure 11. Translation Rate Response Standard Deviations versus Correlation Length

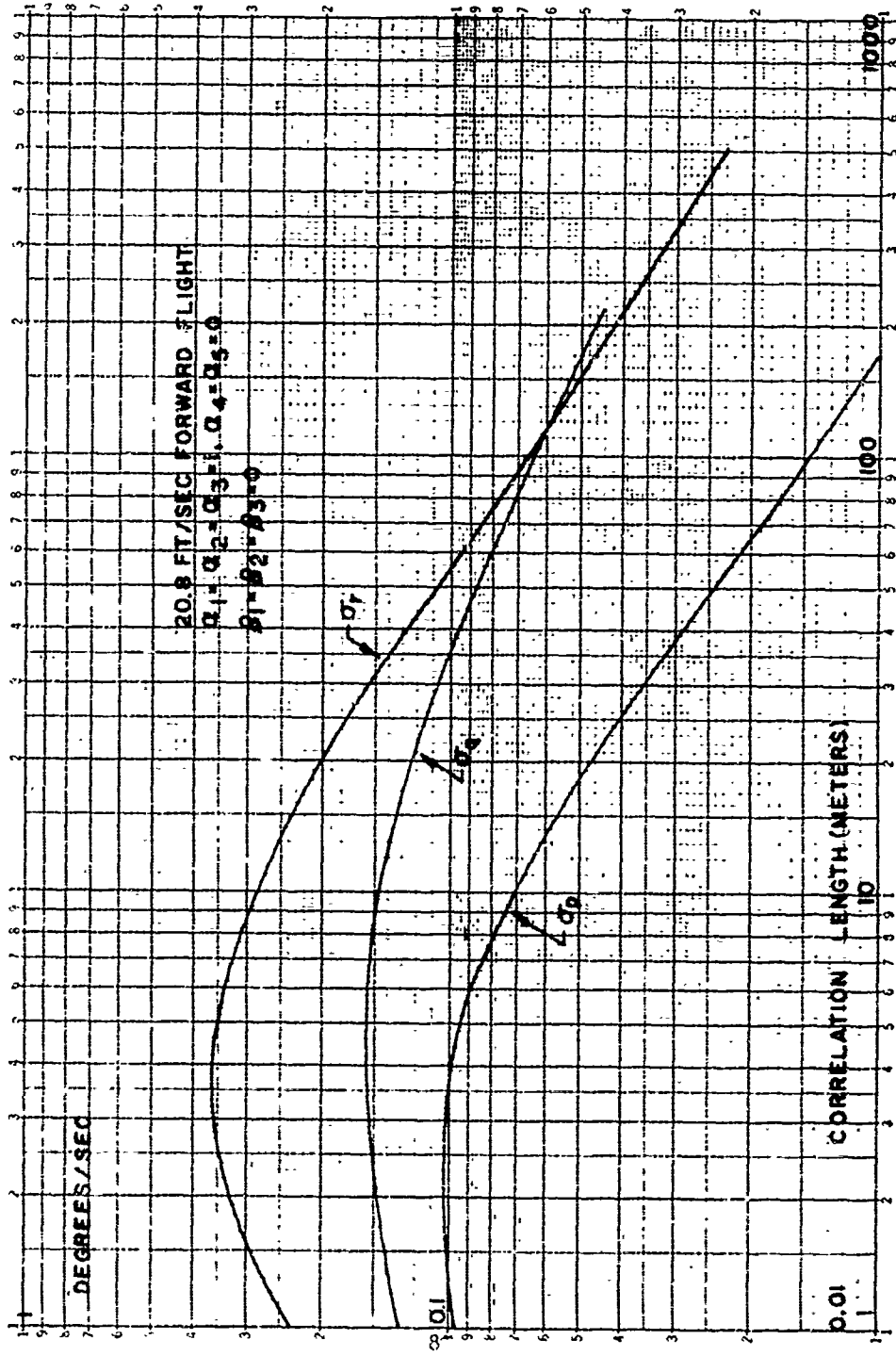


Figure 12. Angular Rate Response Standard Deviations versus Correlation Length

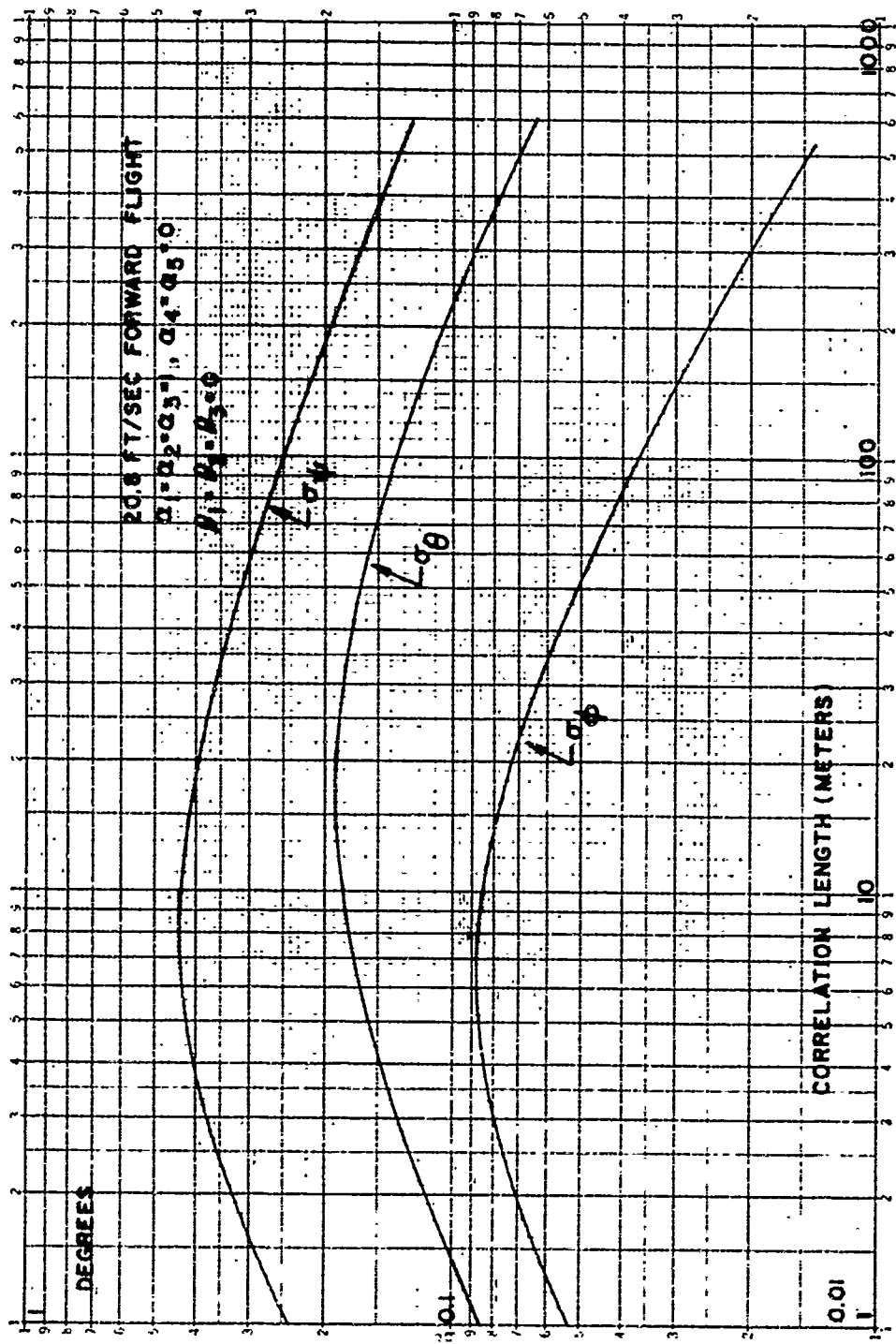


Figure 13. Angular Response Standard Deviations versus Correlation Length

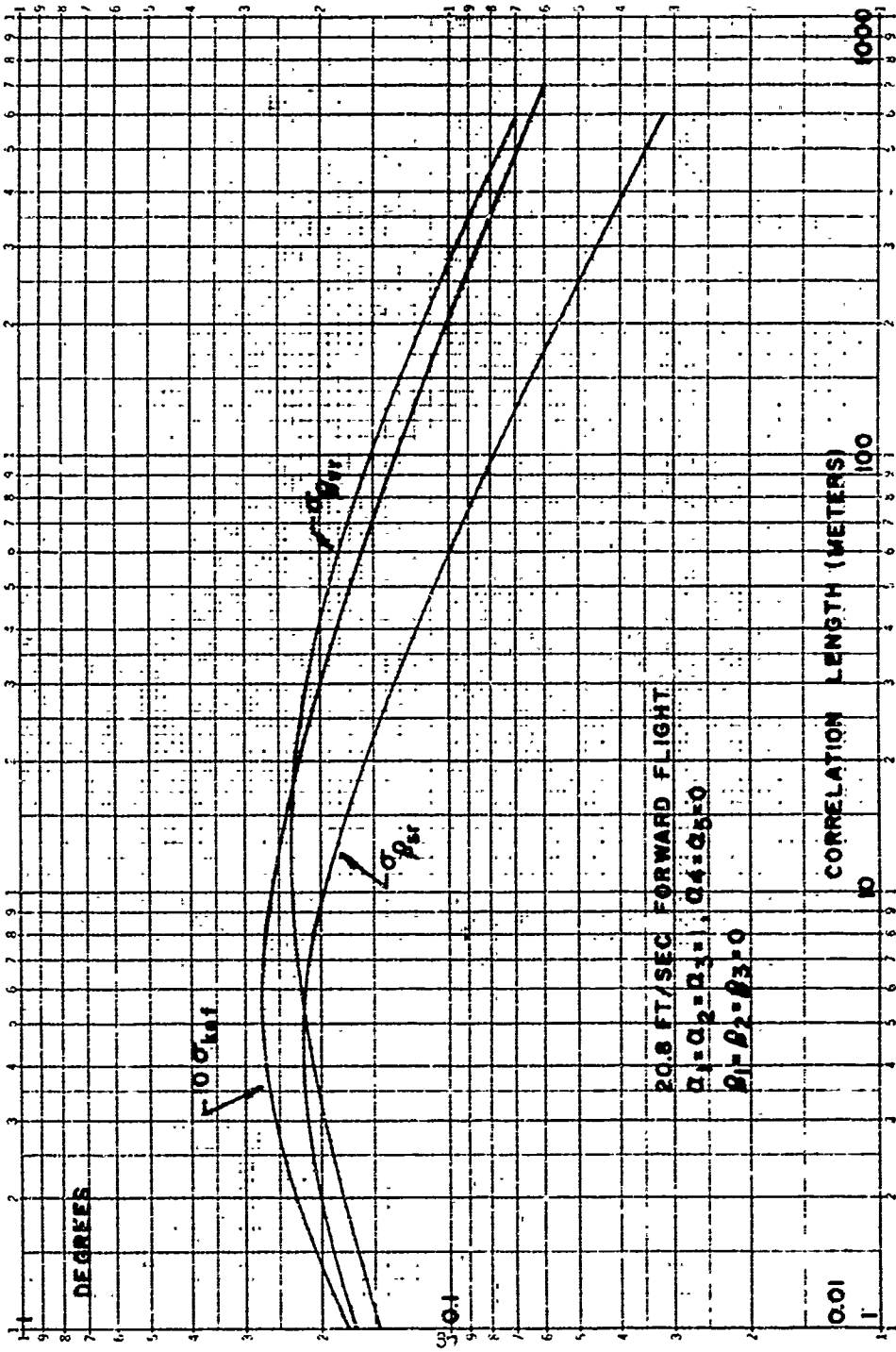


Figure 14. Control Response Standard Deviations versus Correlation Length

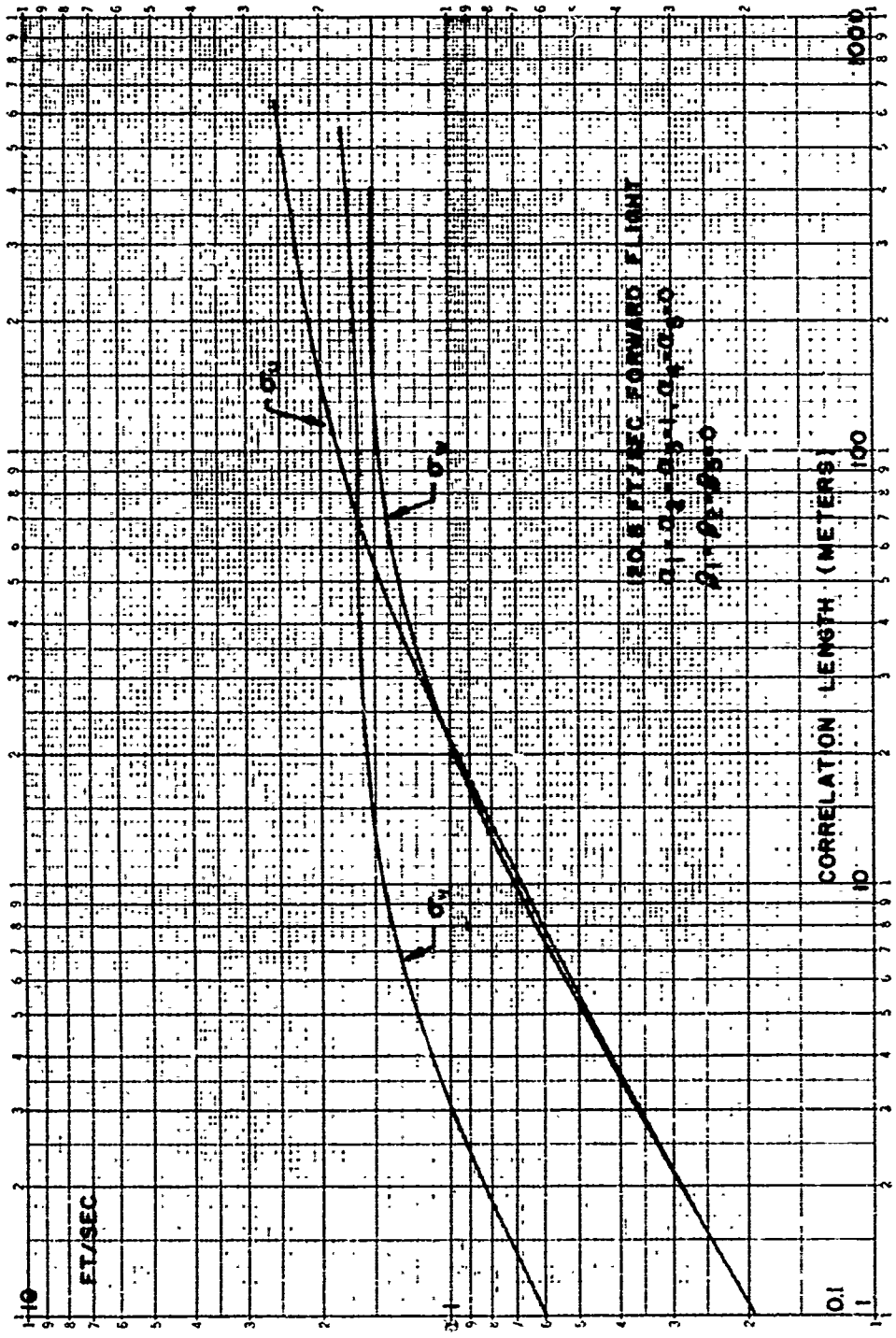


Figure 15. Translation Rate Response Standard Deviations versus Correlation Length

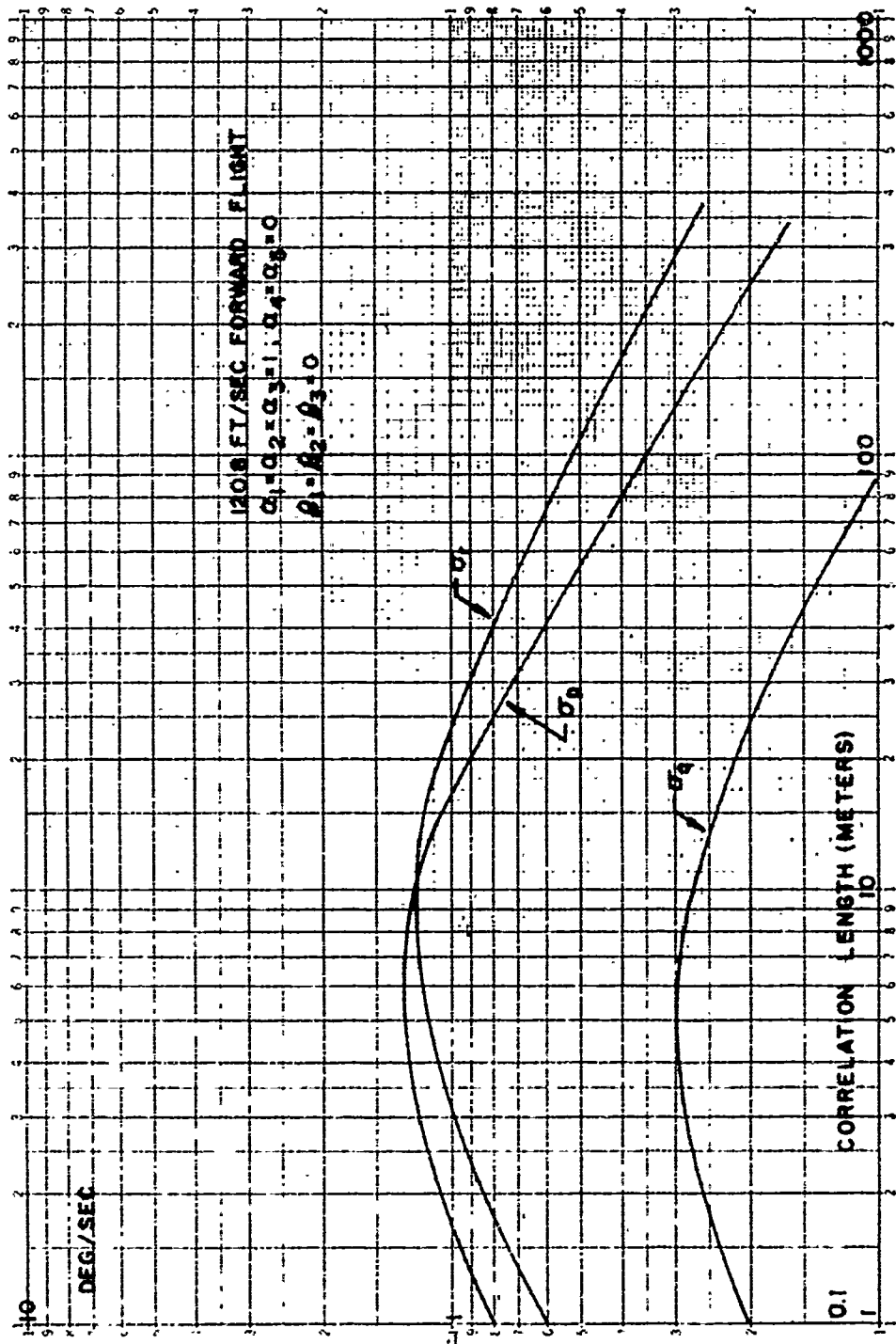


Figure 16. Angular Rate Response Standard Deviations versus Correlation Length

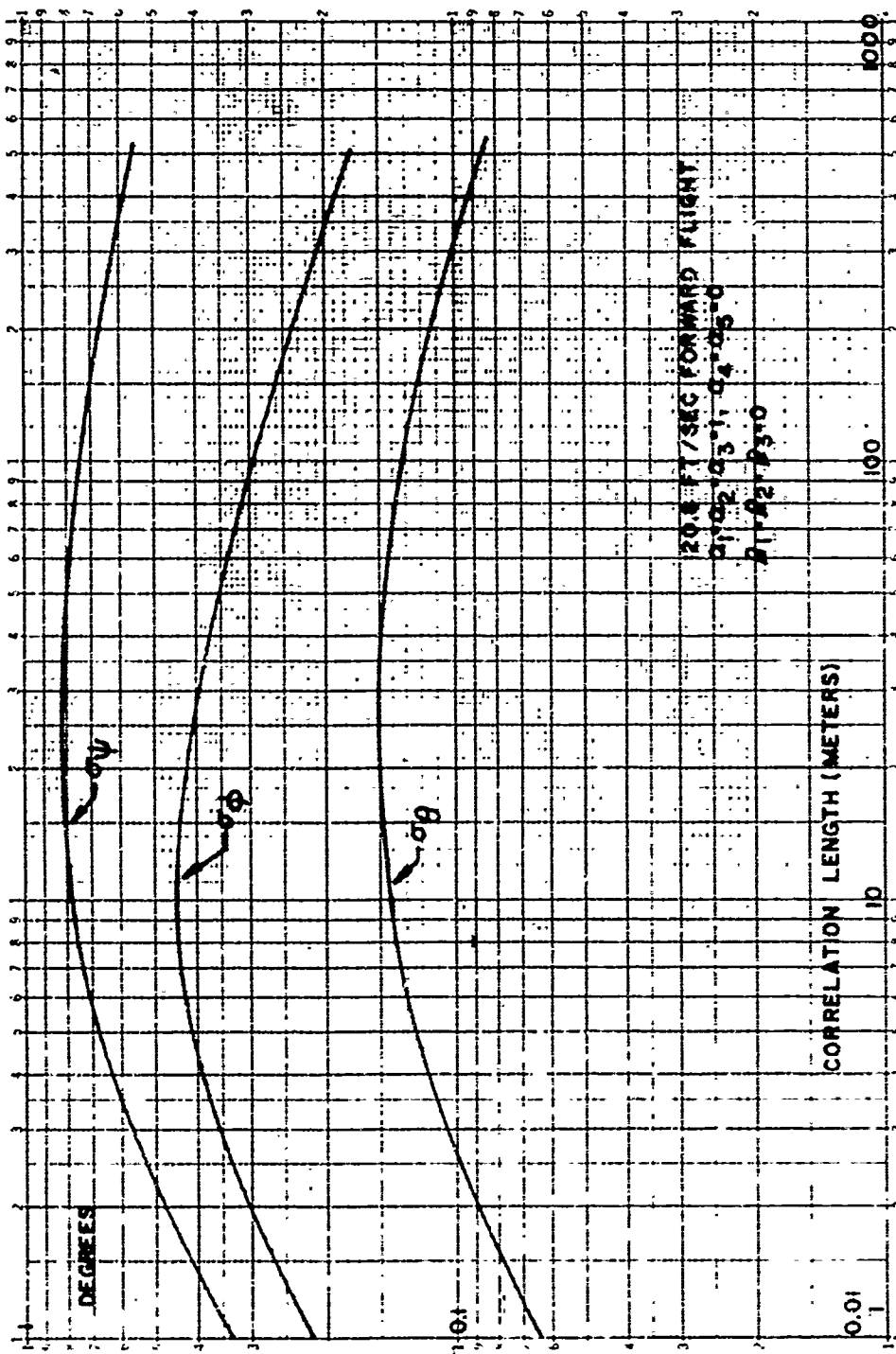


Figure 17. Angular Response Standard Deviations versus Correlation Length

Table III. XV-5 Response Standard Deviations, Tests of Shear Effects

$\sigma_{u_1} = \sigma_{u_g} = 2.79 \text{ ft/sec}, \sigma_{u_2} = \sigma_v = 2.50 \text{ ft/sec}; \sigma_{u_3} = \sigma_w = 1.3 \text{ ft/sec}; \rho_{uv} = 0; \rho_{uw} = -0.275$												
Case	u (ft/sec)	v (ft/sec)	w (ft/sec)	p (deg/sec)	q (deg/sec)	r (deg/sec)	ϕ (deg)	θ (deg)	ψ (deg)	β_{SR} (deg)	β_{VR} (deg)	K-Nf
Low airspeed $\bar{u} = 20.8 \text{ ft/sec}, v = 0, w = 0; \text{correlation length} = 10 \text{ meters}$												
Case (1)	1.28	0.558	0.472	0.720	0.148	0.288	0.854	0.184	0.444	0.200	0.263	0.0234
Case (2)	1.49	0.608	0.559	0.407	0.165	0.167	0.361	0.205	0.237	0.092	0.142	0.0260
Case (1) Wing-tip to wing-tip correlation coefficient = 0.368, wing-tip to tail = 0.434												
Case (2) Wing-tip to wing-tip correlation coefficient = 0.905, wing-tip to tail = 0.920												
High airspeed $\bar{u} = 120.8 \text{ ft/sec}, v = 0, w = -11.7 \text{ ft/sec}; \text{correlation length} = 60 \text{ meters}$												
Case (3)	1.58	1.60	1.37	0.482	0.128	0.677	0.337	0.147	0.800	0.952	0.517	0.0189
Case (4)	1.62	1.49	1.43	0.371	0.104	0.477	0.198	0.107	0.522	0.652	0.382	0.0144
Case (3) Wing-tip to wing-tip correlation coefficient = 0.846, wing-tip to tail = 0.870												
Case (4) Wing-tip to wing-tip correlation coefficient = 0.983, wing-tip to tail = 0.986												

where b is the wingspan, and then assuming that the gusts on each wing are constant over the wings and equal to the gusts at the fuselage center line plus or minus the shear times a one-fifth span moment arm,

$$u_g \pm \frac{1}{5} b \frac{\partial u_g}{\partial y}$$

This is a larger separation and a smaller moment arm than are suggested for the interim gust model in Section III. The standard deviations of the roll and yaw moments produced by this shear approximation are 1.5 and 9.5 percent larger than those that would be produced by the interim gust model in Section III at the 20.8-ft/sec and 120.8ft/sec flight conditions respectively. Shear conclusions based on the above data are therefore valid.

The spectra of shears of head-on and vertical gusts across the wing may well be different than that of side gusts on the tail. If this is so, one can always find an airspeed that will emphasize the shear response over that of the side gusts. Even if the spectra are different, then, the conclusion that the shear terms cannot be ignored still holds.

5. Frozen Gust Field Hypothesis

The hypothesis of a gust field frozen in space moving with the mean wind leads one to a gust spectral bandwidth of

$$c = \frac{V_{as}}{L} \text{ sec}^{-1}$$

while including the possibility of a slowly varying gust field produces

$$c = \frac{V_{as}}{L} \lambda_c$$

where

$$\lambda_c = \left(1 + 2(1-\lambda_t) \frac{UV}{V_{as}^2} \cos \gamma_a \right)^{1/2}$$

Having λ_c less than 1 then increases the spectral bandwidth without producing a corresponding correlation length change.

where b is the wingspan, and then assuming that the gusts on each wing are constant over the wings and equal to the gusts at the fuselage center line plus or minus the shear times a one-fifth span moment arm,

$$u_g \pm \frac{1}{5} b \frac{\partial u_g}{\partial y}$$

This is a larger separation and a smaller moment arm than are suggested for the interim gust model in Section III. The standard deviations of the roll and yaw moments produced by this shear approximation are 1.5 and 9.5 percent larger than those that would be produced by the interim gust model in Section III at the 20.8-ft/sec and 120.8ft/sec flight conditions respectively. Shear conclusions based on the above data are therefore valid.

The spectra of shears of head-on and vertical gusts across the wing may well be different than that of side gusts on the tail. If this is so, one can always find an airspeed that will emphasize the shear response over that of the side gusts. Even if the spectra are different, then, the conclusion that the shear terms cannot be ignored still holds.

5. Frozen Gust Field Hypothesis

The hypothesis of a gust field frozen in space moving with the mean wind leads one to a gust spectral bandwidth of

$$c = \frac{V_{as}}{L} \text{ sec}^{-1}$$

while including the possibility of a slowly varying gust field produces

$$c = \frac{V_{as}}{L} \lambda_c$$

where

$$\lambda_c = \left(1 + 2(1-\lambda_t) \frac{UV}{V_{as}^2} \cos \psi_a \right)^{1/2}$$

Having λ_c less than 1 then increases the spectral bandwidth without producing a corresponding correlation length change.

Table IV. XV-5 Response Standard Deviations, Test of Taylor Hypothesis*
 (20.8-ft/sec flight, zero average sideslip, downwind)

c, λ_z	u	v	w	p	q	r	ϕ	ρ	ψ	β_{sR}	β_{vR}	K_{NR}
$c = 0.32, \lambda_z = 10$	0.25	0.28	0.27	-0.11	-0.18	-0.17	0.07	0	0.10	0	0.03	-0.07
$c = 0.32, \lambda_z = 20$	0.35	0.33	0.39	-0.25	-0.15	-0.31	-0.15	0.05	-0.10	-0.25	-0.15	-0.02
Difference	0.10	0.05	0.12	-0.14	0.03	-0.14	-0.22	0.05	0.20	-0.25	-0.18	0.05
$c_{\text{nominal}} = \frac{V_{sR}}{\lambda_z} = \frac{20.8}{10 \times \frac{39.36}{12}} = 0.64$												

*Tabulated data are fractional changes from nominal values obtained when c and λ_z are varied as indicated.

6. Spectral Shape

The power spectra of the incident gusts derived above is

$$\varphi_{u_i u_i}(\omega) = 2c \frac{\omega^2 (1 + \beta_i) + c (1 - \beta_i)}{(\omega^2 + c^2)^2}$$

Increasing β shifts the input energy to higher frequencies, an effect analogous to decreasing L .

The effects of changing β_i on the 20.8-ft/sec forward-flight flight condition are shown in Table V.

All of the trends in the table are predictable from the graphs of correlation length effects. Note that changing β_1 from 0 to 0.5 changes the u standard deviation by 30 percent.

Spectral shape is therefore important, and because it is, the angle between the fuselage axis and the flight path is important.

7. Magnitude Dependence

The dependence of the various responses on the head-on, side, and vertical gust components was tested by individually quadrupling the gust intensities $\alpha_1, \alpha_2, \alpha_3$ (that is, doubling the standard deviations of the head-on, side, and vertical gusts, respectively). The results are shown in Table VI.

The fourth row of figures for each flight condition is one minus the sum of the first three. Since the nominal gust model was employed ($\alpha_4 = \alpha_5 = 0$), this row expresses the effect of increasing the u - w cross correlation from -1 to -4 (the effects of quadrupling $\alpha_1, \alpha_2, \alpha_3$ and the u - w cross correlation all at once should double the response standard deviations).

From examination of figures, the x and y drags are determined almost solely by the head-on and side gusts respectively. Lift depends on both head-on and vertical gusts (the common practice of considering vertical gusts only in the longitudinal axis is thus invalid at low airspeeds). The dependence of p and r on the head-on gust is due both to the wing shear and the tail, while their dependence on vertical gusts is due entirely to the wing shear. The increasing dependence of q and θ on vertical gusts with increasing airspeed is thought to be due to the increasing lift/drag ratio on the tail plus the increasing wing moment.

From the 1-sum rows, the effect of changing the cross correlation of head-on and vertical gusts is larger at high airspeeds than at low airspeeds. Doubling this coefficient produces at most a 30 percent change in the w standard deviations.

Table V. XV-5 Response Standard Deviations, β Dependence
(20.8-ft/sec forward flight, downwind, 10-meter
correlation length)

β Values*	U (ft/sec)	V (ft/sec)	W (ft/sec)	P (deg/sec)	Q (deg/sec)	R (deg/sec)	δ (deg)	ϵ (deg)	ψ (deg)	β_{eR} (deg)	β_{vR} (deg)	K_{NR}
$\beta_2 = \beta_3 = 0$ $\beta_1 = -1$	1.27	0.53	0.46	0.94	0.12	0.22	0.62	0.22	0.38	0.16	0.22	0.025
	1.56	0.56	0.48	0.87	0.14	0.21	0.61	0.20	0.43	0.19	0.24	0.024
	1.27	0.56	0.47	0.72	0.15	0.29	0.85	0.16	0.44	0.20	0.26	0.023
	0.5	0.55	0.45	0.78	0.16	0.33	0.87	0.17	0.45	0.21	0.23	0.023
$\beta_1 = \beta_3 = 0$ $\beta_2 = -1$	1.27	0.52	0.47	0.63	0.15	0.25	0.82	0.16	0.43	0.18	0.25	0.023
	1.27	0.69	0.47	0.67	0.15	0.27	0.84	0.18	0.44	0.19	0.26	0.023
	1.27	0.86	0.47	0.72	0.15	0.29	0.88	0.18	0.44	0.20	0.26	0.023
	0.5	0.43	0.47	0.77	0.15	0.31	0.87	0.16	0.44	0.21	0.27	0.023
$\beta_1 = \beta_2 = 0$ $\beta_3 = -1$	1.27	0.53	0.66	0.59	0.14	0.29	0.69	0.19	0.44	0.16	0.20	0.023
	1.27	0.56	0.58	0.64	0.15	0.29	0.82	0.18	0.44	0.19	0.26	0.023
	1.27	0.56	0.47	0.72	0.15	0.29	0.85	0.18	0.44	0.20	0.26	0.023
	0.5	0.55	0.37	0.81	0.15	0.28	0.86	0.19	0.44	0.21	0.26	0.024
1	1.27	0.58	0.25	0.87	0.16	0.29	0.85	0.19	0.22	0.26	0.024	

* β_1 : head-on gusts

β_2 : side gusts

β_3 : vertical gusts

Increasing β shifts the input gust energy to higher frequencies

$$S_{uu}(s) = 2c \frac{-s^2(1+c) + g(1-\beta)}{(-s^2+c)^2}$$

Table VI. XV-5 Response Standard Deviations, α Sensitivity -- per unit*

α Values**	u	v	w	p	q	r	ϕ	θ	ψ	β_{eR}	β_{vR}	K_{Nf}
20.8-ft./sec forward flight, 10-meter correlation length, downwind flight												
α_1	0.99	0.13	0.31	0.34	0.86	0.49	0.60	0.84	0.52	0.55	0.51	0.85
α_2	0	0.71	0	0.22	0	0.35	0.10	0	0.32	0.13	0.33	0
α_3	0	0.09	0.83	0.38	0.02	0	0.41	0.05	0	0.40	0	0.05
1-sum	0.01	0.07	0.06	0.08	0.12	0.16	-0.11	0.13	0.16	-0.06	0.16	0.12
120.8-ft./sec forward flight, 60-meter correlation length, downwind flight												
α_1	0.99	0.05	0.31	0.10	0.58	0.08	0.04	0.53	0.10	0.07	0.10	0.55
α_2	0	0.87	0	0.58	0	0.79	0.56	0	0.77	0.58	0.78	0
α_3	0	0.01	0.38	0.10	0.26	0.02	0.19	0.25	0.01	0.15	0.01	0.26
1-sum	0.01	0.07	0.31	0.22	0.16	0.11	0.21	0.22	0.12	0.20	0.19	0.19

*Tabulated data are fractional changes in response standard deviations obtained when the α_j are individually quadrupled.

** α_1 : head-on gust intensity

α_2 : side gust intensity

α_3 : vertical gust intensity

8. Cross Correlations

Data showing the effects of varying the uw and uv correlation coefficients are given in Table VII. Again, the consequences of large variations are observable, but whether or not they are large enough to justify measuring cospectra is debatable.

The uv correlation coefficient has zero effect in forward flight as the pitch and lateral axes are uncoupled. At 45- and 90-degree sideslips its dominant effects are on p and r , both because of the u shear across the wing and the uv product in the tail side force.

The uw cross correlation has little effect except in roll in forward flight. The changes produced here do not completely correspond to those predicted by the 1-sum rows of the α sensitivity tests, though the trends which are different are in responses which change little. The differences are attributed to the inaccuracy of approximating a slope with a large difference

$$\frac{\partial \sigma}{\partial \alpha} \approx \frac{\sigma(2\alpha) - \sigma(\alpha)}{\alpha}$$

The main conclusion to be drawn from this table is that cross correlations are not important to response standard deviations when the cross correlations are small.

9. Heading Angle

Sideslip angle was defined above to be the angle between the fuselage and the airspeed vector. A second angle of interest in gust analysis is the angle between the fuselage and the downwind (mean wind) direction (see Figure 5). This heading angle determines the cross correlation of head-on and vertical gusts and the relative intensities of head-on and side gusts.

The effects of varying this angle from zero to 180 degrees in the 20.8-ft/sec airspeed, forward flight condition (zero sideslip) are shown in Table VIII. Again, the data in this table are about what one would expect.

The u and v response standard deviations are proportional to the head-on and side gust intensities, as expected from the α sensitivity tests. The minima of w , q , and θ responses at 90 degrees are due to the minima of head-on gust velocity there. The difference in the 0 and 180-degree values of the u , w , q , θ standard deviations are due to the effective reversal of the cross correlation of head-on and vertical gusts. In the 180-degree case, an up gust infers a tail-to-nose head-on gust, while in the 0-degree case, it infers a nose-to-tail head-on gust. The small differences in these values indicate the relative independence of the pitch axis responses of the head-on - vertical gust cross correlation.

Table VIII. XV-5 Response Standard Deviations. Test of Heading Angle

Angle (deg)	u (ft/sec)	v (ft/sec)	w (ft/sec)	P (deg/sec)	q (deg/sec)	r (deg/sec)	$\dot{\phi}$ (deg)	θ (deg)	ψ (deg)	β_{SR} (deg)	β_{VR} (deg)	K_{NF}
0	1.28	0.56	0.47	0.072	0.15	0.29	0.085	0.16	0.44	0.20	0.26	0.023
45	1.11	0.65	0.46	0.073	0.13	0.30	0.085	0.16	0.45	0.20	0.27	0.030
90	0.91	0.73	0.45	0.081	0.10	0.31	0.080	0.13	0.46	0.21	0.28	0.018
135	1.10	0.67	0.40	0.085	0.12	0.30	0.102	0.15	0.46	0.24	0.27	0.019
180	1.27	0.59	0.52	0.086	0.14	0.29	0.109	0.17	0.45	0.25	0.27	0.022

$$\begin{bmatrix} u_g \\ v_g \\ w_g \end{bmatrix} = \begin{bmatrix} \text{head-on} \\ \dots \\ \text{vertical} \end{bmatrix}$$

$$\text{guste} = \begin{bmatrix} \cos & \sin & 0 \\ -\sin & \cos & 0 \\ 0 & 0 & 1 \end{bmatrix} \begin{bmatrix} u_1 \\ u_2 \\ u_3 \end{bmatrix}$$

$\sigma_{u_1} / \sigma_{u_2} / \sigma_{u_3} = 2.79 / 2.10 / 1.3, \rho_{11} u_2 = \rho_{13} u_2 = \rho_{23} u_2 = 0, \rho_{11} u_2 = -0.275$

20.8-ft/sec forward flight
 10 meter correlation length

The r , ψ yaw responses and the p , ϕ roll responses depend both upon the side gusts at the tail and the shear of head-on and vertical gusts across the wing. In the 0-degree case, an up-gust shear infers a head-on gust shear producing a moment of the opposite sign, while in the 180-degree case the two shear moments add.

Again, the cross correlation effects are small because the cross correlations are small.

C. COMPUTER PROGRAM

The computer program used to calculate the XV-5 response standard deviations are discussed in detail in Honeywell Report 12060-FR2. Of interest here are the methods used to calculate the coefficients of the linearized equations of motion and the response covariances. The coefficients were calculated by finite differences rather than by partial differentiation. The covariance program is of interest because it is the fastest method known for computing mean square values.

1. Perturbation Equation Coefficients

The coefficients of the linearized equations of motion for a nonlinear system are normally computed by partial differentiation. For example, given a response rate \dot{x} as a nonlinear function $f(\)$ of x and an input u

$$\dot{x} = f(x, u)$$

and given equilibrium values x_0 , u_0 for x , u , for which $\dot{x} = 0$

$$0 = f(x_0, u_0)$$

the coefficients of the linearized perturbation equation for x

$$\frac{d}{dt} (x-x_0) = a(x-x_0) + b(u-u_0)$$

are normally obtained by partial differentiation

$$a = \left. \frac{\partial f(x, u)}{\partial x} \right|_{\substack{x = x_0 \\ u = u_0}}$$

$$b = \left. \frac{\partial f(x, u)}{\partial u} \right|_{\substack{x = x_0 \\ u = u_0}}$$

Partial differentiation is a fine way to obtain these coefficients when the nonlinearities in the equations of motion are simple. The XV-5 equations of motion and the XV-5 fan equations employed in the study are presented in Appendix I. These equations are not simple. The aerodynamic terms in the equations and the gravity and inertial product terms are reasonably straightforward and can be differentiated with some labor. A computer program calculating these derivatives was written early in the study. The fan equations however require iteration, the slopes of the various fan curves are difficult to read in the Ryan data, and accurate determination of the fan differential forces and moments due to velocity changes and vector and stagger angle changes is difficult and hazardous.

The schedule of the study was such that the SDS 9300 program calculating forces and moments for the nonlinear simulation was written and debugged before the linear analyses were begun. Rather than add fan derivatives to the already written aerodynamic coefficient subroutine and then have to debug that program, it was convenient to obtain the perturbation coefficients by differencing the outputs of the SDS 9300 force and moment program.

Trim (equilibrium) values of the various velocities, attitudes, and control inputs were obtained from the SDS 9300 simulation for 16 flight conditions. These values are equivalent to x_0 , u_0 in the above example. The partial derivatives were then approximated by differencing the forces, moments, and states of the Wagner filters obtained when the various inputs were increased and decreased by a small amount. In terms of the above example, this was equivalent to

$$\left. \frac{\partial f}{\partial x} \right|_{\substack{x = x_0 \\ u = u_0}} \approx \frac{f(x_0 + \epsilon, u_0) - f(x_0 - \epsilon, u_0)}{2\epsilon}$$

$$\left. \frac{\partial f}{\partial u} \right|_{\substack{x = x_0 \\ u = u_0}} \approx \frac{f(x_0, u_0 + \epsilon) - f(x_0, u_0 - \epsilon)}{2\epsilon}$$

ϵ equal to 0.1 (degrees, deg/sec, ft/sec depending upon the input) was used for all derivative calculations.

2. Covariance Calculation

There are many methods available for calculating the mean square values of the responses of a time-invariant linear system to stationary noise. For simple systems mean square values can be evaluated with algebraic formulae. For high-order systems the most popular method is the two-sided Laplace transform and the residue theorem.

The method used in the study solves a covariance differential equation. By test, the method is faster than residue calculation, and it is the fastest solution method known to the writer.

In using the method gusts are described as the outputs of linear filters driven by a vector of white noise processes η

$$E\{\eta(t)\eta(\tau)'\} = N\delta(t-\tau),$$

where the prime (superscript) indicates a vector or matrix transpose and δ is the Dirac delta function. The linearized perturbation equations for the vehicle plus the wind filters are then written in the vector differential equation form

$$\dot{x} = Fx + G\eta$$

$$r = Hx$$

where x is the state vector and r is the vector of responses whose mean square values are to be computed; x in the XV-5 case is 41st order.

Solving the equations

$$x(t) = e^{Ft}[x(0) + \int_0^t e^{-F\tau} G\eta(\tau) d\tau]$$

$$\begin{aligned} x(t)x(t)' &= e^{Ft} x(0)x(0)' e^{Ft'} \\ &+ e^{Ft} x(0) \int_0^t \eta(\tau)' G' e^{-F\tau'} d\tau e^{Ft'} \\ &+ e^{Ft} \int_0^t e^{-F\tau} G\eta(\tau) d\tau x(0)' e^{Ft'} \\ &+ e^{Ft} \int_0^t \int_0^t e^{-Ft_1} G\eta(t_1) \eta(\tau)' G' e^{F\tau'} d\tau dt_1 e^{Ft'} \end{aligned}$$

With $\eta(t)$ white noise

$$E\{\eta(t)x(0)'\} = 0 \text{ for } t \geq 0$$

so that

$$E\{x(t)x(t)'\} = e^{Ft} E\{x(0)x(0)'\} e^{Ft'} + e^{Ft} \int_0^t \int_0^t e^{-Ft_1} G E\{\eta(t_1)\eta(\tau)'\} G' e^{F\tau'} d\tau dt_1 e^{Ft'}$$

Substituting

$$E\{\eta(t_1)\eta(\tau)'\} = N\delta(t_1 - \tau)$$

this reduces to

$$E\{x(t)x(t)'\} = e^{Ft} [E\{x(0)x(0)'\} + \int_0^t e^{-F\tau} GNG' e^{-F\tau'} d\tau] e^{Ft'}$$

Letting

$$X(t) = E\{x(t)x(t)'\}$$

and differentiating with respect to t produces the covariance differential equation

$$\dot{X}(t) = FX(t) + X(t)F' + GNG'$$

The mean square values of the components of r are the diagonal terms of the matrix

$$\begin{aligned} E\{r(t)r(t)'\} &= E\{Hx(t)x(t)'H'\} \\ &= HE\{x(t)x(t)'\}H' \\ &= HX(t)H' \end{aligned}$$

In the stationary problem X is constant (\dot{X} is zero), so the equation

$$\dot{X}(t) = FX(t) + X(t)F' + GNG'$$

must be solved until it converges. The formal solution is

$$X(t) = e^{Ft} [X(0) + \int_0^t e^{-F\tau} GNG' e^{-F\tau'} d\tau] e^{Ft'}$$

The following method of solution was developed by Mr. Gunter Stein of Honeywell to calculate Lyapunov functions for a stochastic convergence algorithm employed in the AFFDL study "Application of Self-Organizing Techniques to Multi-Parameter Control Problems". Mr. Stein observed that with zero initial conditions

$$X(0) = 0$$

$$X(t) = e^{Ft} \left[\int_0^t e^{-F\tau} GNG' e^{-F\tau'} d\tau \right] e^{Ft'}$$

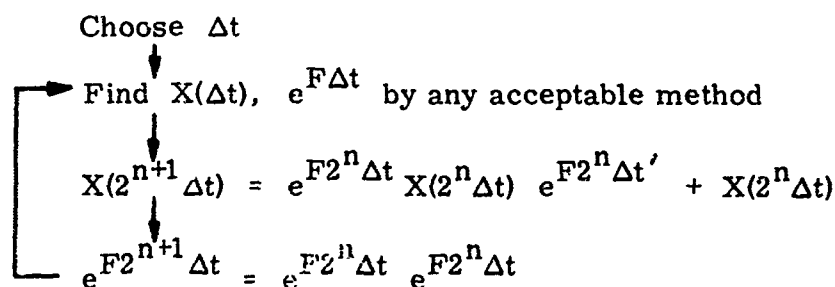
X at 2t could be written

$$X(2t) = e^{F(2t-t)} X(t) e^{F(2t-t)'} + \int_t^{2t} e^{F(2t-\tau)} GNG' e^{F(2t-\tau)'} d\tau$$

$$= e^{Ft} X(t) e^{Ft'} + e^{Ft} \int_0^t e^{-F\tau} GNG' e^{-F\tau'} d\tau e^{Ft'}$$

$$= e^{Ft} X(t) e^{Ft'} + X(t)$$

This led him to the subroutine:



The subroutine then doubles the calculation interval each iteration. Running twice as long in real time requires one more iteration, eight times as long requires three more iterations, etc. The subroutine is thus very fast. In the XV-5 example x was 41st order, and X (since it is symmetric) is $41 \times 42/2 = 861$ st order. Starting with $\Delta t = 1/100$ times one over the magnitude of the largest diagonal term in F ($\Delta t \approx 0.001$ seconds), the above routine reached convergence in 17 iterations and required about 2.5 minutes on the Honeywell 1800 computer.

The above routine is currently in use on the AFFDL "LAMS" study. By test there, it is almost twice as fast as the fastest residue method known to the writer.

The subroutine is sensitive to truncation errors, which accumulate, so it can be used as a starting subroutine when very accurate values are required. Since the interest in the present study is in response changes of the order of 10 percent, it was used alone in this study. Its use is recommended to other investigators.

SECTION VI NONLINEAR ANALYSIS

The nonlinear analyses performed in the study consisted of a sequence of investigations run on a nonlinear, hybrid (analog-digital) simulation of the XV-5 V/STOL. The investigations were:

- Tests of the validity of the force and moment equations generated for the XV-5
- Design of a three-axis XV-5 controller
- Determination of trim values for control inputs and XV-5 responses at various flight conditions for use as equilibrium values in defining the perturbation models
- Tests of XV-5 fan sensitivity to dynamic pressure
- Statistical tests of XV-5 response sensitivity to changes of various vehicle and gust model parameters

The goals of these investigations were to prepare for and then validate the linear analyses and, in addition, to test nonlinearity and gust-penetration effects not accounted for in the linear analyses.

Statistical tests of vehicle airspeed and sideslip angle and gust-model correlation length, shear, and cross correlation effects were run as cross checks of the linear analyses results; the experimental standard deviations produced with small gust inputs were found to be in reasonable agreement with those calculated by the linear covariance program. The tests of gust penetration and gust intensity effects showed that both were important parameters in determining the gust responses of the XV-5.

In addition to the above, it was concluded from the nonlinear gust-intensity tests that a V/STOL at low airspeeds can withstand a severe gust environment. The ride will be rough, but the vehicle will translate slowly enough to be flyable if reasonable excess thrust capability is provided.¹²

¹²The XV-5 had enough thrust capability as no thrust saturation problems were seen at low airspeeds. Stating exactly how much excess thrust is enough with any other thruster configuration would be begging the question; one of the purposes of developing a gust model is to have the capability of investigating this issue.

However, the ability of a V/STOL to withstand gusts at higher airspeeds is strongly dependent on the thrusters employed and the V/STOL's aerodynamic configuration. The airflow over the wings into the XV-5 wing fans produced a large pitchup moment at higher airspeeds that had to be counterbalanced with a near-stall tail trim. Fairly small up-gusts would stall the tail and induce violent pitchups. V/STOL thruster configurations not requiring near-stall trims will be less sensitive to gusts at higher airspeeds than the XV-5 is. However, the XV-5 is reasonably aerodynamically clean and has relatively small aerodynamic surfaces; a V/STOL with larger aerodynamic surfaces will be more gust sensitive, and one with lower lift/drag ratios will have different kinds of stall problems (for example, aircraft where thrusters are fixed to movable wings).

The discussion of the nonlinear analyses below is divided into four parts. Several details of the hybrid simulation which limited the statistical data collected are presented in the first part. The statistical data obtained, the collection of which was the main goal of the nonlinear analyses, are presented in the second. The third discussion addresses the question of assessing the magnitudes of gust inputs for which linear analyses will produce approximately correct results. The final subsection consists of discussions of the other uses made of the XV-5 simulation.

A. SIMULATION DETAILS

The hybrid computer tests of XV-5 gust responses required expenditure of more time and money than the rest of the study items put together. Equipment limitations, a major equipment problem, and a major debugging problem combined to limit the quantity and content of the hybrid data collected. As these limitations affect interpretations of the data presented below, it is appropriate that they be discussed first.

The simulation consisted of nonlinear force and moment equations and aerodynamic lags for the XV-5 programmed on the SDS 9300 computer located at Honeywell's Aeronautical Division simulation facility, plus gust models and XV-5 inertial dynamics synthesized on connected Pace analog computers. Special SDS 9300 subroutines were prepared that sampled the inputs, outputs, and internal variables of the force and moment program and computed experimental means, standard deviations, and probability densities.

The major equipment problem encountered was an SDS 9300 card reader that would skip cards, skip parts of cards, read parts of two cards as one, add zeros to cards, and so on. This problem was solved by replacing the card reader, but it cost this study two months lost time at the time when the programs were being debugged.

The major debugging problem was a combination of noise pickup on poorly grounded leads and improper amplitude scaling. During most of the tests the gust shear inputs to the XV-5 were set to zero (for reasons described below); the zeroing was accomplished by grounding the analog-to-digital (A/D) shear inputs on the Pace computer on which the gust model was synthesized. This computer was connected by 30 feet of cable to the SDS 9300 computer. It turned out that the Pace ground connections were floating, the shear inputs were not zero but hundreds of millivolts of noise pickup, and the scaling of shear inputs was such that the resulting forces and moments produced by the noise shears were of the same order of magnitude as those produced by the other variables. This problem was corrected by repairing the grounding and changing the noise scaling.

The shear-noise problem manifested itself as a too-large response problem at higher vehicle airspeeds. The problem was detected when the high-air-speed tests were completed two months from the end of the contract. It took one month of detective work to find and prove that shear-noise was the cause. The noise provided many false clues in that the magnitude errors were airspeed-dependent, different in the three axes, and repeatable, and the noise was finally located after many more likely causes were eliminated.

Determination of noise as the cause necessitated repeating all of the statistical response measurements made previously.¹³ This was done in the last month of the study. The response magnitudes obtained in these last tests were in reasonable agreement with those predicted by the linear analyses, with two exceptions. The pitch attitude responses were universally smaller than linear analyses predicted and were smaller than the values obtained in the previous (noisy) tests, and the pitch rate responses at high airspeeds were still too large (though not as large as in the noisy tests).

The only possible cause of the attitude error was loss of the pitch signal in the cabling or A/D link between the Pace analog computer and the SDS 9300. The cables and link were checked and found fully operative by technicians assigned to the simulation facility. Therefore either the pitch data is correct or the technicians made an error. A lack of time prevented determining which was the case.

The pitch rates ran 0.22 deg/sec to 0.26 deg/sec when they should have been 0.13 deg/sec; 0.04 deg/sec of the difference was due to nonlinear wing and wing fan asymmetry, proved by tests with side gusts only, and 0.01 of it is attributable to dependence of dynamic pressure on vertical and side gusts. The cause of the remaining difference was never located.

¹³The hybrid data presented here were obtained in the final tests. The data presented in the last study progress report, Honeywell Report 12060-PR 11, all contained the noise and are all in error.

The attitude error does not affect the validity of the data to any extent. The linear analyses predicted pitch attitude standard deviations of the order of 0.15 degrees. The only terms in the force and moment equations affected by pitch attitude are the $mg \sin \theta$, $mg \cos \theta \sin \phi$, $mg \cos \theta \cos \phi$ gravity contributions to x, y, z forces. With these small standard deviations the $\cos \theta$ terms don't vary at all, and the standard deviation of the x gravity force is about 25 pounds, small compared to the 180-pound measured standard deviation of the x force.

The pitch rate error at high airspeeds affects the pitch and vertical velocity results. The latter agree with the linear analyses results, further clouding the problem. In all tests the pitch rate and vertical velocity trends at functions of parameter changes agreed with the trends predicted by the linear analyses. The data in general can safely be assumed reasonably correct, with the exception of pitch attitude in all tests and pitch rate at high airspeeds.

The equipment limitations which limited the data content were the availability of only three noise sources for simulation, as opposed to the eight required by the complete gust model, and the inability of the SDS 9300 to read or write tapes on line. The first limitation forced setting some of the gusts to zero and equating other gusts. In the intensity, correlation length, and cross correlation tests the gusts on the two wings and those on the tail were made equal ($u_L = u_R = u_T$, $v_w = v_T$, $w_L = w_R = w_T$). In the gust penetration tests the wing gusts were made equal ($u_L = u_R$, $w_L = w_R$), and the tail gusts were made equal to those on the wing delayed by $22/u$ seconds [wing-to-tail distance/x component of instantaneous airplane velocity relative to the mean wind]. In the shear tests the wing gusts were made equal and opposite ($u_L = -u_R$, $w_L = -w_R$), the head-on and vertical gusts on the tail were set to zero ($u_T = w_T = 0$), and the fuselage and tail side gusts were made equal ($v_T = v_w$). The equating of the various gusts is indicated in the data tables by appropriate equal signs.

The SDS 9300 can read or write tapes serially with computation, but not at the same time. Using the tapes would require either stopping the simulation or increasing the sampling interval (55 milliseconds in most tests) beyond a reasonable limit. Further, the external (not connected to the SDS 9300) tapes available for the simulation were not of the highest quality and could not be operated remotely; given the complexity of the simulation, it was decided that using them would cause more problems than they could cure.

The inability to use tapes affected the simulation in two ways. The rms outputs of the noise sources used drifted; it was found that vehicle response standard deviations were reasonably converged after two minutes of data collection, and increasing the collection time to six minutes did not reduce the little scatter in them. Not having tapes prevented using exactly the same noise traces for all runs, so the drift had to be accepted.

Not having tapes meant that all of the statistical data had to be stored in the SDS 9300 memory. This did not affect the acquisition of mean and standard deviation data, which operations required little memory, but it did limit the probability density data. In the latter case 6000 data words could be stored; in a two-minute run with data recording every 55 milliseconds, this limited the number of variables that could be recorded to three $\left(\frac{110 \text{ sec}}{55 \text{ milliseconds}} = \frac{6000}{3} \right)$. Since from 18 to 35 variables were recorded, six or more runs were required for a test of a particular gust/vehicle parameter. Including printout and setup time, each test ran from one to two hours.

As the tests all had to be repeated in a relatively short time, it was necessary to limit the collection of probability data to only a portion of the total tests.

The only other limitation in the data is that the vehicle x, y, and z velocity data are not reliable at low airspeeds. These responses (u, v, w) varied too slowly for reliable statistical measurement in a reasonable run time.

B. STATISTICAL TEST DATA

The statistical data obtained from the nonlinear hybrid tests are presented in this subsection. These data describe airspeed, sideslip angle, correlation length, cross correlation, shear, intensity, and gust penetration effects.

The same notation is employed in all of the data tables. Rather than repeat units and titles in every table, the notation is presented separately in Table IX.

The nominal gust model used for all hybrid tests was basically the same as that employed in the linear analyses. Downwind, crosswind, and vertical gust spectra were set to $\sigma^2 2c / (-c^2 s^2 + 1)$, the ratio of standard deviations was 2.8/2/1.3, and the correlation coefficient of downwind and vertical gusts was $\rho_{uw} = 0.275$. As discussed above, only three gust sources were used, and drift in the rms outputs of these sources prevented obtaining the 2.8/2/1.3 standard deviations exactly. The gust filter time constant c was set to 3/2 seconds in the nominal gust mode³, giving a correlation length of

$$\begin{aligned} L &= \lambda_z z = c V_{as} \\ &= 3/2 V_{as} \\ &\left(= 1/2 V_{as} \text{ for } V_{as} \text{ in ft/sec, } L \text{ in meters} \right), \end{aligned}$$

Table IX. Notation

Symbol	Definition
F_x, F_y, F_z	= total x, y, z forces, lbs
L, M, N	= total roll, pitch, yaw moments, ft-lbs
$F_{x_A}, F_{y_A}, F_{z_A}$	= aerodynamic x, y, z forces, lbs ^a
L_A, M_A, N_A	= aerodynamic roll, pitch yaw moments, ft-lbs ^a
u, v, w	= aircraft x, y, z velocities relative to mean wind, ft/sec ^b
p, q, r	= roll, pitch, yaw rates (body axes), deg/sec
θ, ϕ	= pitch, roll attitudes, rad ^c
α, β	= angle-of-attack, sideslip angle, rad ^d
Q	= average dynamic pressure, lb/ft ²
u_g, v_g, w_g	= average head-on, side, vertical gusts at wing $\left(u_g = \frac{u_L + u_R}{2}, \text{ etc.} \right)$ ft/sec
u_T, v_T, w_T	= head-on, side, vertical gusts at tail, ft/sec
u_y, w_y	= head-on, vertical gust shears across wing, rad/sec ^e
β_{sL}, β_{vL}	= left fan stagger, vector angles, deg
K_{Nf}	= nose fan door position (unitless)

^aThe aerodynamic forces and moments are the forces and moments generated by ordinary aerodynamics plus the lift, drag, and moment induced by fan airflow over the top front of the wings and the efflux under the wings to the rear.

^bThese data are not reliable at low airspeeds.

^cThe θ data is suspect.

^dThese are vertical and side components of airspeed respectively over the airspeed magnitude, rather than the arc sine of these ratios.

^e $u_y = \frac{u_L - u_R}{b}, w_y = \frac{w_L - w_R}{b}$, where b is the wing span and u_L, u_R, w_L, w_R are wing tip gusts.

where V_{ue} is the vehicle airspeed. The average heading angle was zero for all tests so that head-on, side, and vertical gusts could be replaced one-one with downwind, crosswind, and vertical gusts.

1. Airspeed and Sideslip Tests

The effects of airspeed and sideslip on the XV-5 response standard deviations are shown in the data for seven flight conditions presented in Table X. These data show the same trends as exhibited by the linear responses, Table II. Increasing airspeed increases the roll and yaw rate responses monotonically, and the pitch rate response increases then takes a dip around 80 ft/sec, then increases again. Comparing the 57- and 34-ft/sec data with the 43-ft/sec, 45-degree sideslip data, sideslip increases the roll and yaw rate responses and decreases the pitch rate response.

It is clear that airspeed and sideslip angle are important parameters to vehicle gust responses.

2. Correlation Length Tests

Correlation length data corresponding to the linear data in Figures 11 through 17 are given in Tables XI and XII. Note that in the tabulated data the gust intensities vary a great deal. The power spectra of the outputs of the three white noise sources were not flat and were not the same.

The u , v , w aircraft velocities increase with increasing correlation length, agreeing with the linear results. The yaw rate response peaks between 30 and 6 meter correlation lengths for the high-air-speed case and near 10 meters for the low-speed case, again agreeing with the linear results. The pitch and roll rate responses increase monotonically with decreasing correlation length, contradicting the linear results. However, the peaks in the linear results are very broad, and the small errors at 1 and 6 meters can be accounted for by statistical sampling errors and the non-uniformity of the noise sources.

Clearly correlation length is an important parameter.

3. Shear Effects

The contributions of head-on and vertical gust shears across the wing to roll and yaw are shown in the low- and high-air-speed data in Table XIII. As evidenced by the roll and yaw rate response data, the shear effects are not simple. At high airspeeds, both augment both roll and yaw, but they partially buck each other. At low airspeeds, the head-on gust shear

Table X. Nonlinear XV-5 Response Standard Deviations, Test of Airspeeds
(All tests at zero average heading)

Average Airspeed (ft/sec)	106	82	57	34	15	0	43
Average Sideslip (deg)	0	0	0	0	0	0	45
Correlation Length (meters)	53	41	28	17	9	c=1.5 sec	21
F _x	190	178	170	133	113	25	133
F _y	574	329	189	91	49	13	226
F _z	379	221	119	82	61	16	140
L	226	147	81	41	25	20	309
M	363	127	207	236	136	51	157
N	658	394	261	129	78	70	350
F _{xA}	159	148	141	115	89	16	95
F _{yA}	145	114	85	56	37	9	129
F _{zA}	307	216	155	86	51	9	70
L _A	205	141	95	61	39	21	341
M _A	221	172	298	385	364	57	259
N _A	391	305	222	151	98	17	214
u	1.65	1.22	1.55	0.92	1.24	0.76	0.97
v	1.57	1.45	1.01	0.75	0.48	0.51	1.32
w	1.59	1.08	0.99	0.75	0.46	1.15	1.02
p	0.68	0.41	0.22	0.14	0.04	0.05	0.65
q	0.22	0.075	0.14	0.20	0.13	0.04	0.12
r	0.85	0.58	0.43	0.25	0.17	0.04	0.59
θ	0.00026	0.00026	0.00026	0.00026	0.00026	0.00034	0.00037
φ	0.0044	0.0028	0.0013	0.0009	0.00034	0.00076	0.0039
α	0.013	0.017	0.024	0.041	0.085	0.30	0.048
β	0.015	0.020	0.031	0.058	0.105	0.59	0.033
Q	0.68	0.50	0.34	0.20	0.14	0.02	0.211
u _g	2.98	2.72	2.87	2.60	3.11	2.82	2.35
v _g	2.13	2.29	2.05	2.15	2.13	1.89	2.05
w _g	1.44	1.32	1.54	1.46	1.35	1.29	1.25
u _T	= u _g						
v _T	= v _g						
w _T	= w _g						
u _y	0	0	0	0	0	0	0
w _y	0	0	0	0	0	0	0
β _{sL}	1.05	0.63	0.33	0.25	0.095	0.08	0.93
β _{vL}	0.50	0.40	0.29	0.19	0.13	0.04	0.40
K _{Nf}	0.025	0.009	0.016	0.024	0.020	0.003	0.015

Table XI. Nonlinear XV-5 Response Standard Deviations, Test of Correlation Length (20-ft/sec flight downwind, zero average sideslip)

Correlation Length (meters)	100	50	10	5	1
F_x	68	115	113	103	90
F_y	26	32	51	48	41
F_z	59	76	58	56	49
L	12	14	21	34	43
M	47	59	111	143	256
N	27	36	67	76	80
F_{xA}	50	88	84	75	62
F_{yA}	22	27	38	37	36
F_{zA}	63	70	61	52	35
L_A	25	31	41	39	30
M_A	236	354	361	300	193
N_A	64	78	101	90	67
u	3.0	3.4	0.98	0.81	0.37
v	1.0	1.5	0.60	0.53	0.26
w	3.2	2.4	1.4	0.56	0.30
p	0.044	0.044	0.059	0.080	0.094
q	0.064	0.078	0.128	0.140	0.160
r	0.070	0.086	0.167	0.152	0.130
θ	0.00035	0.00036	0.00038	0.00036	0.00036
ϕ	0.00067	0.00072	0.00072	0.00075	0.00071
ψ	0.083	0.098	0.082	0.078	0.074
β	0.058	0.074	0.103	0.107	0.140
Q	0.074	0.13	0.13	0.13	0.14
u_g	3.37	4.14	2.73	2.68	2.82
v_g	1.53	2.01	2.16	2.19	2.12
w_g	1.95	1.66	1.48	1.37	1.39
u_T	= u_g				
v_T	= v_g				
w_T	= w_g				
u_y	0	0	0	0	0
w_y	0	0	0	0	0
β_{sL}	0.053	0.052	0.086	0.113	0.126
β_{vL}	0.086	0.102	0.140	0.120	0.099
K_{NI}	0.012	0.018	0.019	0.017	0.014

Table XII. Nonlinear XV-5 Response Standard Deviations, Test of Correlation Length (110-ft/sec flight downwind, zero average sideslip)

Correlation Length (meters)	600	300	60	30	6
F_x	85	101	158	209	180
F_y	169	262	519	650	613
F_z	132	187	321	425	433
L	68	106	218	295	474
M	115	162	397	504	862
N	190	285	634	853	980
F_{xA}	76	91	138	182	152
F_{yA}	69	82	142	181	212
F_{zA}	113	159	251	321	291
L_A	126	136	190	221	237
M_A	112	142	183	245	216
N_A	208	230	378	487	595
u	3.2	1.4	0.97	1.17	0.54
v	1.9	1.6	1.4	1.5	1.0
w	2.5	1.8	1.4	1.3	0.66
p	0.20	0.31	0.65	0.86	1.11
q	0.086	0.11	0.24	0.32	0.45
r	0.26	0.40	0.79	0.99	0.95
θ	0.00038	0.00036	0.00038	0.00040	0.00040
ϕ	0.0023	0.0026	0.0041	0.0050	0.0049
α	0.0065	0.0086	0.012	0.015	0.014
β	0.0069	0.0082	0.014	0.018	0.022
Q	0.30	0.36	0.50	0.77	0.74
u_g	3.43	1.89	2.39	3.06	2.84
v_g	2.32	2.00	1.84	2.17	2.15
w_g	2.34	1.66	1.57	1.51	1.50
u_T	= u_g				
v_T	= v_g				
w_T	= w_g				
u_y	0	0	0	0	0
w_y	0	0	0	0	0
β_{uL}	0.36	0.49	0.97	1.28	1.52
β_{vL}	0.26	0.30	0.46	0.56	0.50
K_{NI}	0.011	0.014	0.024	0.031	0.035

Table XIII. Nonlinear XV-5 Response Standard Deviations, Tests of Gust Shears Across the Wings (All tests at zero average sideslip, zero average heading angle)

Airspeed (ft/sec) Correlation Length (meters) Gusts Included	108 54				20 10			
	$v+u_y+w_y$	v only	$v+u_y$	$v+w_y$	$v+u_y+w_y$	v only	$v+u_y$	$v+w_y$
F_x	25	13	18	17	9	7	7	8
F_y	534	471	585	551	35	52	49	58
F_z	31	25	25	28	10	8	8	10
L	238	208	252	224	38	21	23	49
M	33	30	37	33	31	31	30	30
N	626	568	695	658	112	72	107	58
F_{xA}	16	8	11	5	2	1	1	2
F_{yA}	141	130	148	149	40	38	34	47
F_{zA}	16	10	12	10	7	5	6	6
L_A	314	176	272	259	82	41	48	77
M_A	31	18	22	15	14	12	14	12
N_A	394	348	397	406	134	100	130	101
u	0.22	0.11	0.15	0.07	0.06	0.06	0.06	0.06
v	1.66	1.25	1.51	1.68	0.96	0.47	0.88	0.91
w	0.17	0.09	0.12	0.06	0.18	0.14	0.16	0.16
p	0.67	0.59	0.73	0.68	0.101	0.063	0.070	0.113
q	0.04	0.04	0.04	0.04	0.04	0.04	0.04	0.04
r	0.82	0.71	0.88	0.83	0.24	0.18	0.24	0.14
θ	0.00036	0.00036	0.00035	0.00035	0.00036	0.00037	0.00036	0.00036
ϕ	0.0045	0.0037	0.0045	0.0051	0.0014	0.00073	0.0010	0.0013
α	0.0015	0.0008	0.0010	0.0006	0.0009	0.0008	0.0074	0.0078
β	0.014	0.013	0.015	0.015	0.098	0.101	0.091	0.112
Q	0.11	0.034	0.10	0.034	0.037	0.0078	0.028	0.025
u_g	0	0	0	0	0	0	0	0
v_g	2.0	1.79	1.91	2.24	2.17	2.18	2.05	2.52
w_g	0	0	0	0	0	0	0	0
u_T	0	0	0	0	0	0	0	0
v_T	$= v_g$	$= v_g$	$= v_g$	$= v_g$	$= v_g$	$= v_g$	$= v_g$	$= v_g$
w_T	0	0	0	0	0	0	0	0
u_y	0.0511	0	0.0586	0	0.105	0	0.0935	0
w_y	0.0227	0	0	0.0255	0.0485	0	0	0.0503
β_{sL}	1.03	0.89	1.09	1.08	0.20	0.09	0.14	0.20
β_{vL}	0.53	0.42	0.53	0.50	0.20	0.14	0.19	0.13
K_{Nt}	0.003	0.002	0.002	0.002	0.01	0.01	0.01	0.01

augments the yawing moment much more than does the vertical gust shear, but their roles are interchanged with regard to the rolling moment. The 0.14-deg/sec yaw rate figure for side gusts plus vertical gust shear must be a bad datum as it theoretically cannot be less than the 0.18-deg/sec yaw rate produced by side gusts only, as the shears here are not correlated with each other or with the side gusts. The 0.101/0.063 ratio of roll rate responses with and without shears at the low airspeed is sufficient for arguing the necessity of including shears in the interim gust model.

These data predict the more limited linear shear data presented in Table III. Shears are clearly not ignorable.

4. Cross Correlation Tests

The importance of cross correlations of gust components was tested by comparing the responses obtained with ± 1 correlation coefficients with those with zero cross correlation. The results of tests at 20- and 108-ft/sec airspeed, downwind flight conditions are presented in Tables XIV and XV, and the results at a 43-ft/sec, 45-degree sideslip, zero heading flight condition in Table XVI.

It was proved above that, to the extent that a vehicle is linear, cross correlations are critical if and only if they are large in magnitude and, simultaneously, the responses due to the correlated inputs are of approximately equal magnitudes. Both of these conditions must be present for gust cross correlations to be of concern. The data show this. The only data evidencing correlation dependence are vertical velocity dependence on the head-on, vertical gust correlation in downwind flight, pitch dependence on ρ_{uw} at 20 ft/sec, roll dependence on ρ_{vw} at 120 ft/sec, and yaw dependence on ρ_{uv} at 43-ft/sec, 45-degree sideslip. In all cases correlation coefficient magnitudes less than 0.3 (estimated above to be the maximum) will not produce significant deviations of the response standard deviations from those produced assuming zero correlation.

In the 43-ft/sec, 45-degree sideslip case the side gust contribution to yaw is larger than the head-on gust contribution. In the data in Table XVII the side gust magnitude was reduced to make the two gusts' contributions to yaw about equal. The resulting yaw rate difference is as predicted by the above arguments.

The data in these four tables verify the theoretical result that, for correlations to be important, they must be large, and simultaneously the contributions of the correlated inputs to the response must be of approximately equal magnitude.

Table XIV. Nonlinear XV-5 Response Standard Deviations, Test of Gust Cross Correlations (20-ft/sec airspeed, downwind flight, zero average sideslip, 10-meter correlation length)

ρ_{uv}	0	1	-1	0	0	0	0
ρ_{uw}	0	0	0	1	-1	0	0
ρ_{vw}	0	0	0	0	0	1	-1
F_x	100	107	88	93	107	104	106
F_y	46	42	38	48	49	44	50
F_z	60	53	55	61	24	49	62
L	23	21	22	23	21	24	22
M	109	112	106	99	110	108	110
N	69	67	61	67	73	73	64
F_{xA}	73	79	65	71	77	79	81
F_{yA}	34	34	29	35	38	33	41
F_{zA}	49	41	48	13	66	46	49
L_A	36	36	30	36	39	34	44
M_A	286	316	258	227	382	330	318
N_A	89	88	73	90	96	83	111
u	0.85	1.16	1.27	1.46	1.18	1.18	1.30
v	0.40	0.51	0.61	0.41	0.49	0.39	0.68
w	0.90	0.77	0.59	0.75	0.41	0.39	0.72
p	0.055	0.056	0.053	0.053	0.055	0.062	0.047
q	0.13	0.12	0.11	0.10	0.14	0.12	0.13
r	0.16	0.14	0.13	0.16	0.16	0.15	0.15
θ	0.00034	0.00035	0.00035	0.00035	0.00034	0.00033	0.00035
ϕ	0.00061	0.00058	0.00058	0.00056	0.00061	0.00062	0.00058
α	0.071	0.059	0.070	0.051	0.072	0.058	0.069
β	0.095	0.099	0.088	0.099	0.105	0.087	0.107
Q	0.119	0.126	0.106	0.109	0.127	0.126	0.128
u_g	2.51	2.78	2.49	2.64	2.81	2.78	2.88
v_g	1.97	1.99	1.78	2.03	2.15	1.82	2.32
w_g	1.28	1.20	1.40	1.22	1.31	1.19	1.51
u_T	= u_g						
v_T	= v_g						
w_T	= w_g						
u_y	0	0	0	0	0	0	0
w_y	0	0	0	0	0	0	0
β_{sL}	0.089	0.084	0.080	0.086	0.090	0.091	0.083
β_{vL}	0.124	0.118	0.110	0.126	0.129	0.115	0.143
K_{Nf}	0.016	0.017	0.014	0.013	0.020	0.018	0.017

Table XV. Nonlinear XV-5 Response Standard Deviations, Test of Gust Cross Correlations (108-ft/sec airspeed, zero average sideslip, downwind flight, 54-meter correlation length)

ρ_{uv}	0	1	-1	0	0	0	0
ρ_{vw}	0	0	0	1	-1	0	0
ρ_{vw}	0	0	0	0	0	1	-1
F_x	158	199	173	198	145	201	169
F_y	511	494	471	527	573	510	511
F_z	346	366	349	207	409	340	328
L	212	191	190	214	209	222	204
M	341	324	328	413	192	329	309
N	637	589	570	636	640	613	635
F_{xA}	139	175	152	170	121	172	144
F_{yA}	144	137	129	148	146	139	138
F_{zA}	284	294	287	126	343	275	254
L_A	202	193	180	214	205	194	186
M_A	293	245	222	254	143	248	186
N_A	397	371	349	411	384	378	376
u	1.27	1.62	1.54	1.27	1.67	1.91	1.34
v	1.72	1.58	1.42	1.84	1.63	1.50	1.48
w	1.17	1.82	1.32	0.74	1.67	1.47	1.34
p	0.65	0.59	0.58	0.65	0.65	0.64	0.63
q	0.22	0.22	0.21	0.26	0.13	0.22	0.21
r	0.79	0.76	0.72	0.79	0.86	0.77	0.77
θ	0.00038	0.00037	0.00038	0.00036	0.00039	0.00036	0.00037
ϕ	0.0042	0.0041	0.038	0.0044	0.0044	0.0041	0.0040
α	0.013	0.015	0.014	0.014	0.011	0.015	0.011
β	0.015	0.014	0.013	0.015	0.015	0.014	0.014
Q	0.588	0.716	0.644	0.643	0.606	0.694	0.621
u_g	2.50	3.05	2.74	2.66	2.77	3.17	2.65
v_g	2.34	2.17	1.95	2.52	2.15	2.09	2.05
w_g	1.13	1.50	1.23	1.23	1.29	1.36	1.32
u_T	= u_g						
v_T	= v_g						
w_T	= w_g						
u_y	0	0	0	0	0	0	0
w_y	0	0	0	0	0	0	0
β_{sL}	0.99	0.92	0.38	0.99	1.00	0.97	0.96
β_{vL}	0.49	0.47	0.44	0.50	0.51	0.47	0.45
K_{Ni}	0.023	0.027	0.024	0.029	0.016	0.027	0.022

Table XVI. Nonlinear XV-5 Response Standard Deviations, Test of Gust Cross Correlations (43-ft/sec airspeed, 45-degree average sideslip, zero average heading, 21-meter correlation length)

ρ_{uv}	0	1	-1	0	0	0	0
ρ_{uw}	0	0	0	1	-1	0	0
ρ_{vw}	0	0	0	0	0	1	-1
F_x	133	144	121	144	135	163	135
F_y	226	156	266	257	217	243	246
F_z	140	124	144	159	142	136	153
L	309	303	285	354	341	315	291
M	157	167	130	149	176	144	164
N	350	239	459	415	383	402	420
F_{xA}	95	111	104	103	105	124	101
F_{yA}	129	82	156	149	125	141	139
F_{zA}	70	71	76	40	728	78	578
L_A	341	304	353	394	330	383	363
M_A	259	320	280	229	327	342	282
N_A	214	142	258	251	211	238	226
u	0.97	1.57	1.41	1.12	1.19	1.30	1.09
v	1.32	1.33	1.42	1.57	1.51	1.56	1.43
w	1.02	0.86	0.85	0.56	0.56	0.69	0.81
p	0.65	0.67	0.63	0.80	0.75	0.73	0.68
q	0.12	0.14	0.11	0.12	0.14	0.14	0.13
r	0.59	0.36	0.73	0.66	0.58	0.62	0.66
θ	0.00037	0.00036	0.00036	0.00035	0.00036	0.00037	0.00037
ϕ	0.0039	0.0051	0.0033	0.0047	0.0041	0.0050	0.0044
α	0.048	0.042	0.052	0.019	0.054	0.052	0.039
β	0.033	0.047	0.017	0.035	0.036	0.046	0.036
Q	0.211	0.080	0.299	0.248	0.203	0.235	0.231
u_g	2.35	2.97	2.75	2.54	2.67	3.10	2.54
v_g	2.05	2.12	1.96	2.43	2.14	2.23	2.22
w_g	1.25	1.31	1.35	1.18	1.24	1.45	1.44
u_T	$= u_g$						
v_T	$= v_g$						
w_T	$= w_g$						
u_y	0	0	0	0	0	0	0
w_y	0	0	0	0	0	0	0
β_{sL}	0.93	1.04	0.88	1.15	1.05	1.10	1.01
β_{vL}	0.40	0.25	0.48	0.46	0.38	0.43	0.43
K_{NI}	0.015	0.018	0.015	0.014	0.018	0.019	0.016

Table XVII. Nonlinear XV-5 Response Standard Deviations, Test of Cross Correlation with Reduced Side Gust (43-ft/sec airspeed, 45-degree average sideslip, zero average heading, 21-meter correlation length)

σ_{xy}	+1	-1
F_x	117	118
F_y	27	127
F_z	83	83
L	133	88
M	153	152
N	46	216
F_{xA}	107	115
F_{yA}	5	81
F_{zA}	76	75
L_A	87	145
M_A	303	323
N_A	24	136
u	1.49	1.40
v	0.36	0.64
w	0.81	0.68
p	0.28	0.21
q	0.14	0.13
r	0.04	0.36
θ	0.00034	0.00036
ϕ	0.0026	0.0017
α	0.048	0.048
β	0.036	0.027
Q	0.147	0.235
u_g	2.85	2.96
v_g	0.67	0.70
w_g	1.53	1.37
u_T	$= u_g$	$= u_g$
v_T	$= v_g$	$= v_g$
w_T	$= w_g$	$= w_g$
u_y	0	0
w_y	0	0
β_{sL}	0.45	0.31
β_{vL}	0.04	0.25
K_{NI}	0.017	0.018

5. Gust Penetration Tests

The gust penetration or transport delay effect is due to the fact that the gusts hitting the tail are those hitting the wing $t = d/u$ seconds before, where d is the wing-to-tail distance and u is the vehicle x velocity relative to the mean wind. (Actually the wing gusts change slightly by the time they get to the tail, but the correlation coefficients between the two will be nearly unity.) The effect of the delay is to first swing the vehicle nose, then swing the tail t seconds later in the same direction. If, in the meantime, the control system is trying to counteract the nose swing, the tail gusts will augment the control commands and produce an attitude overshoot.

The results of including the time delay on the responses at five flight conditions are presented in Tables XVIII and XIX. The differences between attitude rate responses with and without the delay are noticeable, and in the pitch response at 57 ft/sec they produce more than a 100 per cent change.

There is thus no question that gust penetration must be included in the gust model.

6. Intensity

Linear theory states that the ratios of response magnitudes to gust magnitudes should be independent of the gust magnitudes. Plotting one versus the other is then a convenient test as to whether nonlinearities are affecting responses.

Gust intensity tests were made at 112-ft/sec, 20-ft/sec, and zero-ft/sec (hover with respect to the wind) airspeeds. The raw data from these tests are presented in Tables XX, XXI and XXII. In the 112-ft/sec tests pitchups were seen at the 10-ft/sec gust level, and violent pitchups were seen at the two higher gust levels. The effects of these pitchups on lift, pitching moment, vertical velocity, and pitch rate are large. The data at the higher three gust amplitudes are not trustworthy as the pitch attitude contributions to the forces through gravity are missing, as mentioned above. The aircraft in these tests recovered from the violent pitchups, whereas in the earlier tests (with shear noise present) the head-on velocity decreases at pitchup were much larger and the aircraft occasionally plunged enough to be lost.

The 22-ft/sec data are much better behaved. The hover data are interesting in that linear theory predicts zero gust responses in hover, which clearly they are not.

Table XVIII. Nonlinear XV-5 Response Standard Deviations, Tests of Gust Penetration (All tests at zero average heading, 0.073-second sampling interval)

Average Airspeed (ft/sec) Correlation Length (meters) Average Time Delay (sec)	106 53 0.21		62 41 0.27		57 28 0.39	
w = with delay w/o = without delay	w	w/o	w	w/o	w	w/o
F_x	100	100	175	168	182	170
F_y	545	574	350	329	210	189
F_z	437	379	238	221	169	119
L	276	276	200	147	111	61
M	582	363	326	127	713	297
N	679	658	502	394	358	261
F_{zA}	150	150	146	146	151	141
F_{yA}	130	146	113	114	92	85
F_{xA}	337	307	239	216	141	155
L_A	208	205	137	151	103	95
M_A	237	221	230	172	350	298
N_A	304	391	326	305	291	222
u	1.02	1.05	1.42	1.22	1.55	1.55
v	1.01	1.57	1.15	1.45	1.01	1.01
w	1.56	1.50	1.15	1.08	0.64	0.99
p	0.78	0.06	0.55	0.41	0.31	0.22
q	0.32	0.22	0.18	0.075	0.38	0.14
r	0.22	0.05	0.04	0.58	0.50	0.43
σ	2.0026	0.0026	0.0026	0.0026	0.0026	0.0026
ϕ	0.0044	0.0044	0.0031	0.0028	0.0017	0.0013
ϵ	0.015	0.013	0.017	0.017	0.022	0.024
β	0.014	0.015	0.020	0.020	0.035	0.031
Q	0.08	0.08	0.50	0.50	0.36	0.34
u_g	2.06	2.06	2.82	2.72	2.96	2.87
v_g	2.31	2.13	1.95	2.20	2.18	2.05
w_g	1.38	1.44	1.29	1.32	1.23	1.54
u_T	$-u_g(t-0.21)$	$-u_g$	$-u_g(t-0.27)$	$-u_g$	$-u_g(t-0.39)$	$-u_g$
v_T	$-v_g(t-0.21)$	$-v_g$	$-v_g(t-0.27)$	$-v_g$	$-v_g(t-0.39)$	$-v_g$
w_T	$-w_g(t-0.21)$	$-w_g$	$-w_g(t-0.27)$	$-w_g$	$-w_g(t-0.39)$	$-w_g$
u_y	0	0	0	0	0	0
v_y	0	0	0	0	0	0
β_{vL}	1.15	1.06	0.80	0.63	0.45	0.33
β_{vL}	0.40	0.50	0.38	0.40	0.33	0.29
K_{M}	0.031	0.025	0.015	0.000	0.033	0.016

Table XIX. Nonlinear XV-5 Response Standard Deviations, Tests of Gust Penetration (All tests at zero average sideslip, zero average heading, 0.073-second sampling interval)

Average Airspeed (ft/sec) Correlation Length (meters) Average Time Delay (sec)	34 0.7 0.65		18 9 1.0	
w = with delay w/o = without delay	w	w/o	w	w/o
F_x	133	133	111	113
F_y	100	91	52	49
F_z	119	82	65	61
L	60	41	38	25
M	589	236	211	136
N	237	129	140	78
F_{xA}	113	115	88	69
F_{yA}	56	56	35	37
F_{zA}	97	86	51	51
L_A	62	61	38	30
M_A	439	385	384	364
N_A	206	151	137	98
u	1.10	0.92	1.19	1.24
v	0.89	0.75	0.53	0.46
w	6.96	0.75	0.58	0.46
p	0.20	0.14	0.09	0.04
q	0.35	0.20	0.17	0.13
r	0.33	0.25	0.25	0.17
θ	0.00026	0.00026	0.00026	0.00026
ϕ	0.0014	0.0000	0.00057	0.00034
α	0.046	0.041	0.062	0.005
β	0.064	0.058	0.100	0.105
Q	0.20	0.20	0.13	0.14
u_g	2.50	2.60	3.04	3.11
v_g	2.24	2.15	2.23	2.13
w_g	1.85	1.46	1.43	1.35
u_T	$= u_g(t-0.65)$	$= u_g$	$= u_g(t-1)$	$= u_g$
v_T	$= v_g(t-0.65)$	$= v_g$	$= v_g(t-1)$	$= v_g$
w_T	$= w_g(t-0.65)$	$= w_g$	$= w_g(t-1)$	$= w_g$
u_y	0	0	0	0
w_y	0	0	0	0
β_{sL}	0.33	0.33	0.15	0.005
β_{vL}	0.23	0.19	0.17	0.13
K_{Nf}	0.034	0.034	0.022	0.020

Table XX. Nonlinear XV-5 Response Standard Deviations, Tests of Gust Intensity (112-ft/sec airspeed, downwind flight, zero average sideslip, 56-meter correlation length)

Gust Magnification	x1	x2	x3	x4	x5
F _x	186	360	809	1210	1450
F _y	510	1130	1630	1840	2670
F _z	353	627	2730	3290	4250
L	213	448	731	900	1350
M	403	723	2950	3540	4390
N	615	1320	1880	2320	2980
F _{xA}	153	323	909	1160	1400
F _{yA}	145	308	443	530	709
F _{zA}	278	491	2330	2910	3850
L _A	305	425	661	757	1190
M _A	225	465	2290	2900	3750
N _A	395	819	1210	1500	1870
u	1.4	3.7	4.7	6.44	7.53
v	1.6	3.3	5.1	7.20	8.44
w	1.4	2.5	12.2	16.5	23.0
p	0.63	1.33	2.05	2.60	3.85
q	0.26	0.58	5.05	6.48	9.33
r	0.78	1.74	2.44	2.84	4.15
θ	0.00037	0.00038	0.00037	0.00038	0.00040
φ	0.0042	0.0089	0.014	0.17	0.027
α	0.014	0.028	0.122	0.157	0.216
β	0.015	0.031	0.044	0.055	0.072
Q	0.67	1.30	2.75	3.14	3.58
u _g	2.88	5.89	10.3	11.9	13.9
v _g	2.28	4.54	6.99	9.28	11.2
w _g	1.34	2.47	3.93	6.01	6.37
u _T	= u _g				
v _T	= v _g				
w _T	= w _g				
u _y	0	0	0	0	0
w _y	0	0	0	0	0
β _{sL}	0.26	2.04	3.17	3.94	5.2
β _{vL}	0.48	1.05	1.53	1.81	2.54
K _{Nf}	0.027	0.052	0.120	0.138	0.167

Table XXI. Nonlinear XV-5 Response Standard Deviations, Tests of Gust Intensity (22-ft/sec airspeed, downwind flight, zero average sideslip, 11-meter correlation length)

Gust Magnification	x1	x2	x3	x4	x5
F_x	109	208	345	425	484
F_y	46	96	193	290	456
F_z	61	122	217	266	326
L	23	70	237	343	589
M	108	399	802	1240	1320
N	69	122	257	320	468
F_{xA}	81	148	236	278	315
F_{yA}	34	73	132	183	247
F_{zA}	53	97	155	192	231
L_A	36	94	240	374	548
M_A	321	646	1040	1360	1530
N_A	88	166	260	344	453
u	1.04	2.94	4.20	3.43	6.15
v	0.36	1.29	2.25	2.08	4.46
w	0.64	1.43	2.30	2.53	4.03
p	0.07	0.16	0.45	0.69	1.17
q	0.13	0.29	0.51	0.78	0.82
r	0.16	0.25	0.48	0.62	0.83
θ	0.00037	0.00038	0.00038	0.00039	0.00039
ϕ	0.0008	0.0013	0.0029	0.0046	0.0069
α	0.078	0.154	0.277	0.409	0.487
β	0.095	0.21	0.349	0.450	0.547
Q	0.126	0.241	0.394	0.449	0.518
u_g	2.68	5.63	9.11	10.5	13.7
v_g	1.92	4.04	6.32	8.12	11.1
w_g	1.41	2.87	4.21	5.92	7.87
u_T	u_g	u_g	u_g	u_g	u_g
v_T	v_g	v_g	v_g	v_g	v_g
w_T	w_g	w_g	w_g	w_g	w_g
u_y	0	0	0	0	0
w_y	0	0	0	0	0
β_{sL}	0.09	0.24	0.64	1.02	1.66
β_{vL}	0.13	0.21	0.37	0.47	0.63
K_{Nf}	0.018	0.037	0.061	0.083	0.091

Table XXII. Nonlinear XV-5 Response Standard Deviations, Tests of Gust Intensity, (Zero average airspeed, zero average heading angle, zero average sideslip, gust filter time constant = 0.667 second)

Gust Magnification	x1	x2	x3	x4	x5
F_x	25	43	111	198	238
F_y	13	58	118	200	303
F_z	16	63	98	148	164
L	20	89	164	286	434
M	51	111	336	504	746
N	70	111	219	397	576
F_{xA}	16	40	106	174	199
F_{yA}	9	41	82	130	179
F_{zA}	9	39	65	150	137
L_A	21	101	200	312	432
M_A	51	126	352	749	890
N_A	17	71	143	223	290
u	0.76	0.83	2.40	2.00	3.36
v	0.51	0.74	1.10	1.30	2.28
w	1.15	2.54	2.05	2.57	3.58
p	0.05	0.21	0.37	0.61	0.90
q	0.04	0.07	0.20	0.37	0.45
r	0.04	0.16	0.36	0.78	1.06
θ	0.00034	0.00037	0.00038	0.00036	0.00037
ϕ	0.00076	0.0018	0.0031	0.0048	0.0057
α	0.30	0.52	0.58	0.57	0.61
β	0.59	0.65	0.64	0.58	0.64
Q	0.02	0.08	0.14	0.24	0.30
u_g	2.82	5.24	8.90	12.1	12.3
v_g	1.89	4.28	5.96	7.39	9.07
w_g	1.21	2.79	3.89	5.71	6.91
u_T	$= u_g$				
v_T	$= v_g$				
w_T	$= w_g$				
u_y	0	0	0	0	0
w_y	0	0	0	0	0
β_{sL}	0.08	0.32	0.59	0.95	1.32
β_{vL}	0.04	0.11	0.28	0.57	0.78
K_{Nf}	0.003	0.008	0.021	0.041	0.049

The force, moment, and attitude rate data from these tables are presented graphically in Figures 18 through 26. The linear attitude rates in Figures 20, 23 and 26 are those predicted by the linear analyses discussed in the previous section; they include gust shear effects, which the hybrid results do not.

It is evident in all of the force and moment graphs that the total forces and moments are in no cases small compared to the aerodynamic forces and moments. That is, the control system is not "bucking", or directly opposing gust forces with thrust changes, but is rather smoothing the ride.

The control system can produce x and z forces and L, M, N moments directly, but the only way it can produce y forces is by turning the aircraft. One would therefore expect the total y forces to be larger than the aerodynamic Y forces, and this is seen in every case. Because the control system senses attitudes and attitude rates, it is incapable as constituted of immediately opposing the instantaneous gust x, z forces and L, M, N moments, a situation that could be partially corrected by introducing feed-forward signals from wing tip angle-of-attack and sideslip-angle probes.

In the 112-ft/sec data the effects of pitchup on pitch plane forces, moments, and responses are large. The transition between the "linear" region below x2 magnification and the pitchup region may be sharper than the graphs indicate as the graphs were generated by drawing straight lines between data points. The lateral forces, moments, and responses appear to remain fairly linear in pitchup. Taking the slightly too-large side gusts in these tests into account, because the shear effects at this flight condition are fairly small, the yaw rate responses are almost exactly what the linear results predict and the roll rate responses are about 15 percent larger than the linear results predict. The pitch rate results in the linear region are almost 100 percent too large, as mentioned above.

The incidence of tail stall and pitchup is obviously gust-magnitude-dependent. It is also gust-spectra-dependent, as the number of pitchups in any time interval depends both on the angle-of-attack standard deviation and the standard deviation of angle-of-attack rate. [For a Gaussian process $\alpha(t)$, the expected number of occasions in T seconds that $\alpha(t)$ exceeds a limit α_S is, from the Rice formula,

$$E\{N(T)\} = \frac{\sigma_{\dot{\alpha}}}{\sigma_{\alpha}} e^{-1/2 \left(\frac{\alpha_S - \alpha_T}{\sigma_{\alpha}} \right)^2} \cdot \text{CONST} \cdot T$$

where α_T is the mean value of α . Increasing $\sigma_{\dot{\alpha}}$ or σ_{α} will increase the number of stalls.] The aircraft will fly through very slowly varying gusts

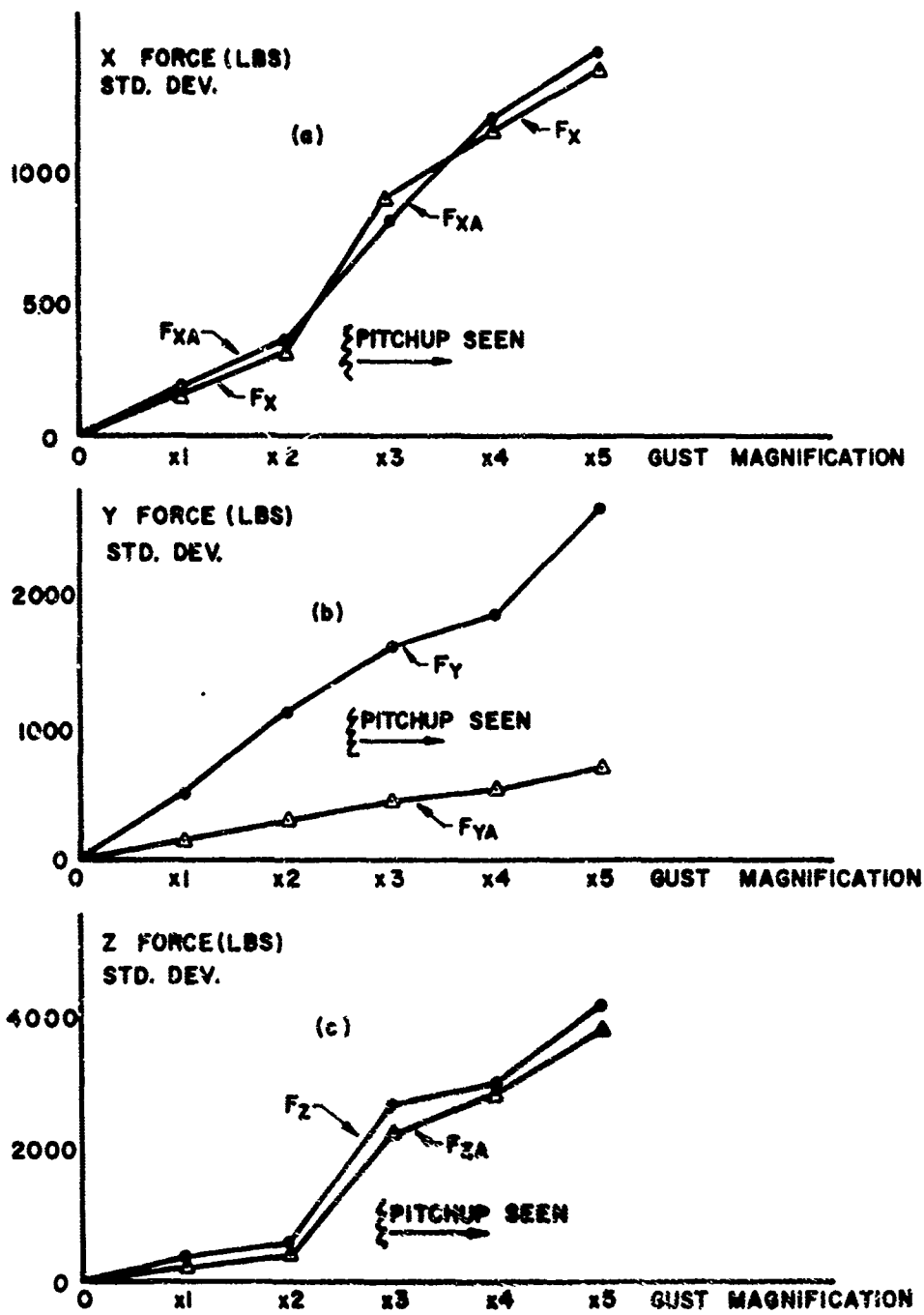


Figure 18. Total and Aerodynamic Forces versus Gust Intensity Hybrid Tests -- 112-ft/sec Airspeed

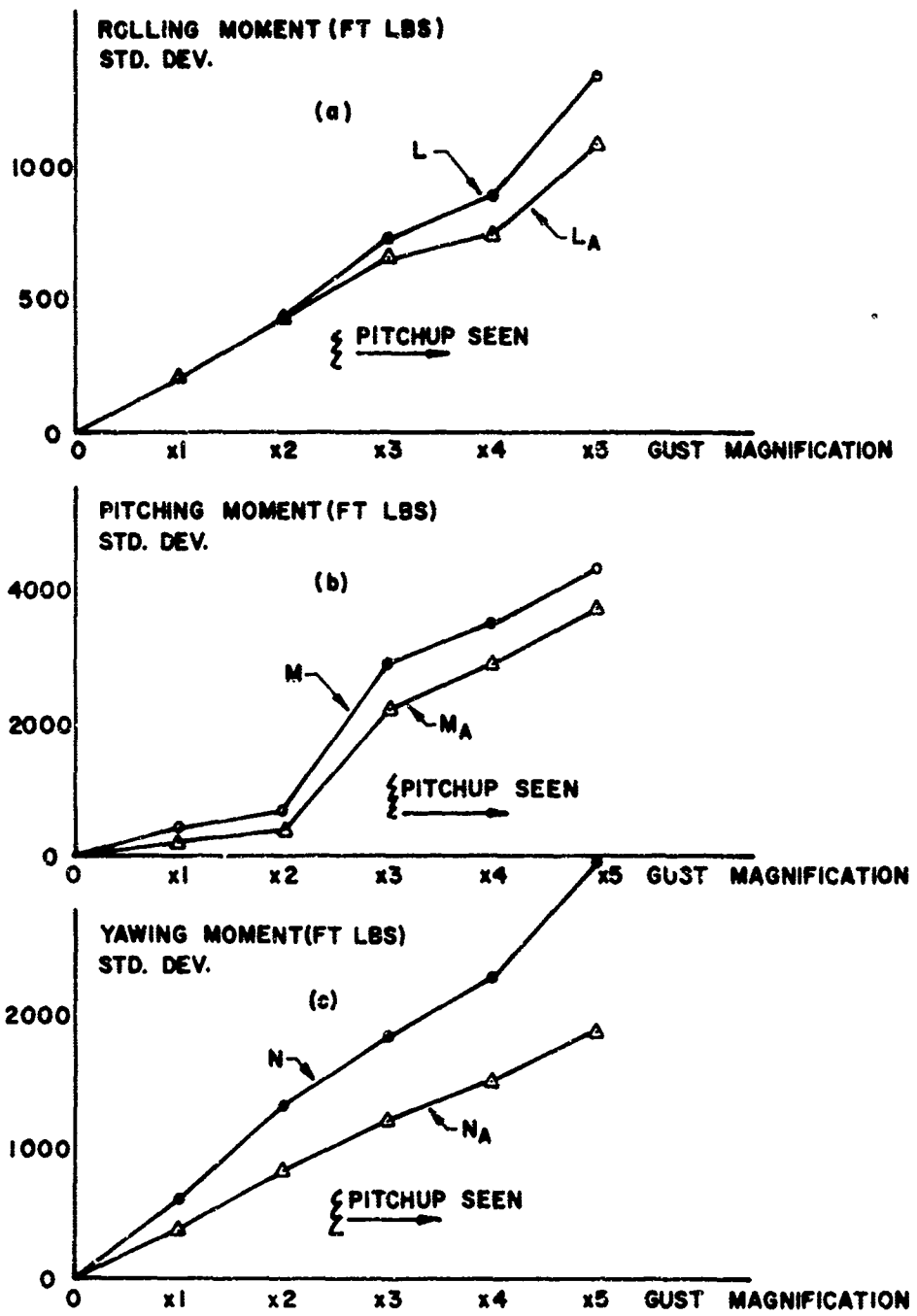


Figure 19. Total and Aerodynamic Moments versus Gust Intensity Hybrid Tests -- 112-ft/sec Airspeed

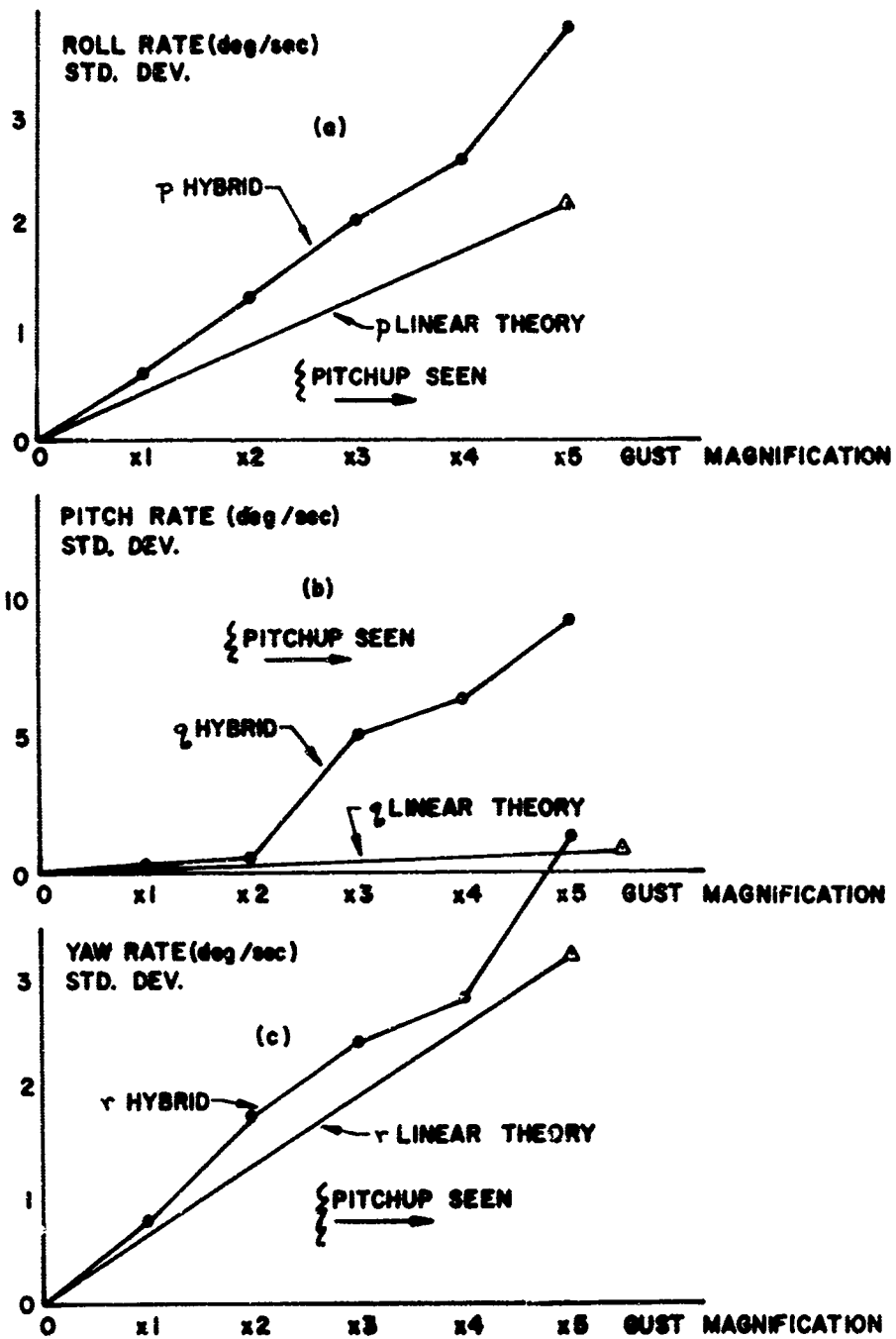


Figure 20. Hybrid and Linear Attitude Rates versus Gust Intensity -- 112-ft/sec Airspeed

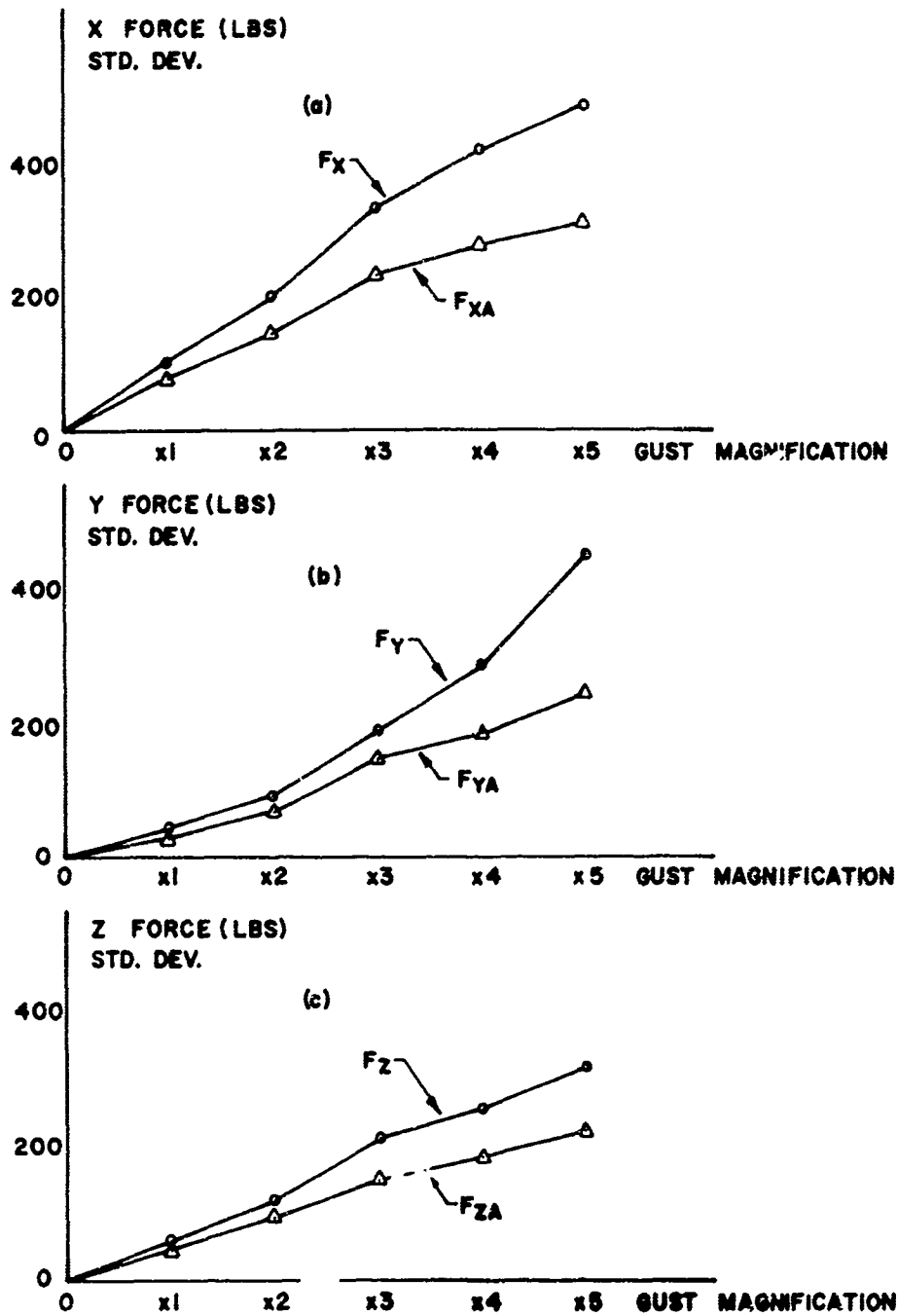


Figure 21. Total and Aerodynamic Forces versus Gust Intensity Hybrid Tests -- 22-ft/sec Airspeed

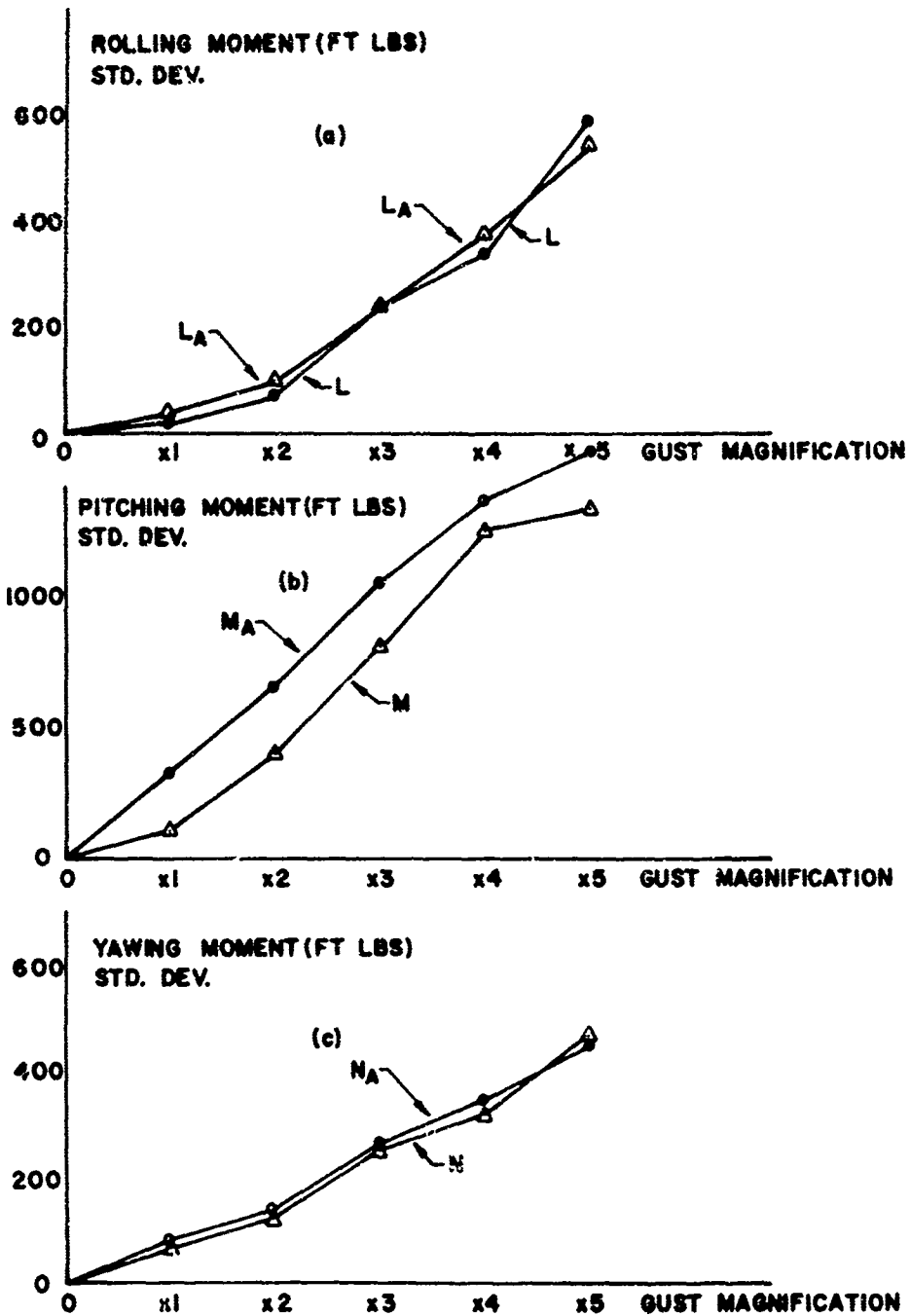


Figure 22. Total and Aerodynamic Moments versus Gust Intensity Hybrid Tests -- 22-ft/sec Airspeed

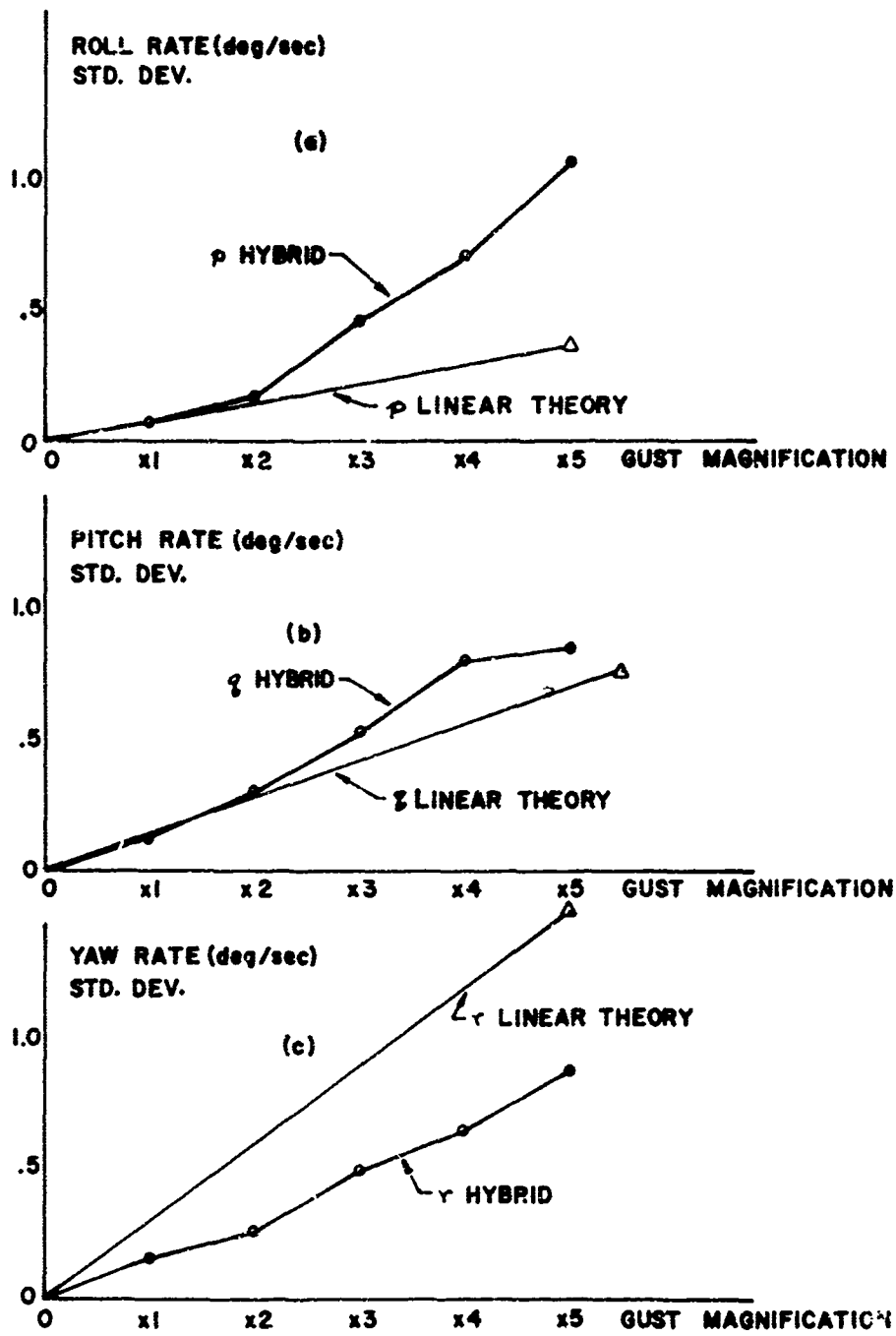


Figure 23. Hybrid and Linear Attitude Rates versus Gust Intensity -- 22-ft/sec Airspeed

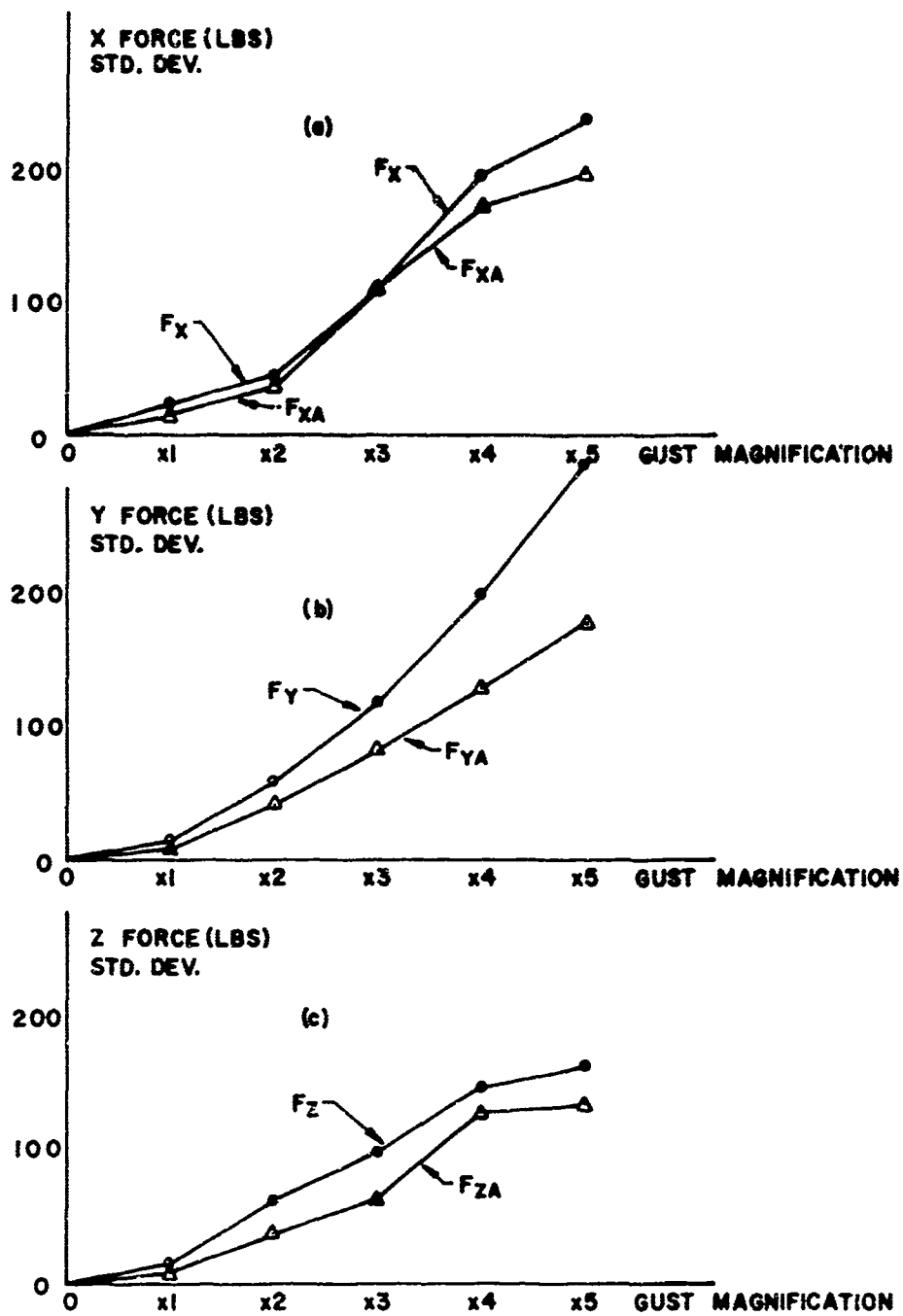


Figure 24. Total and Aerodynamic Forces versus Gust Intensity Hybrid Tests -- Hover

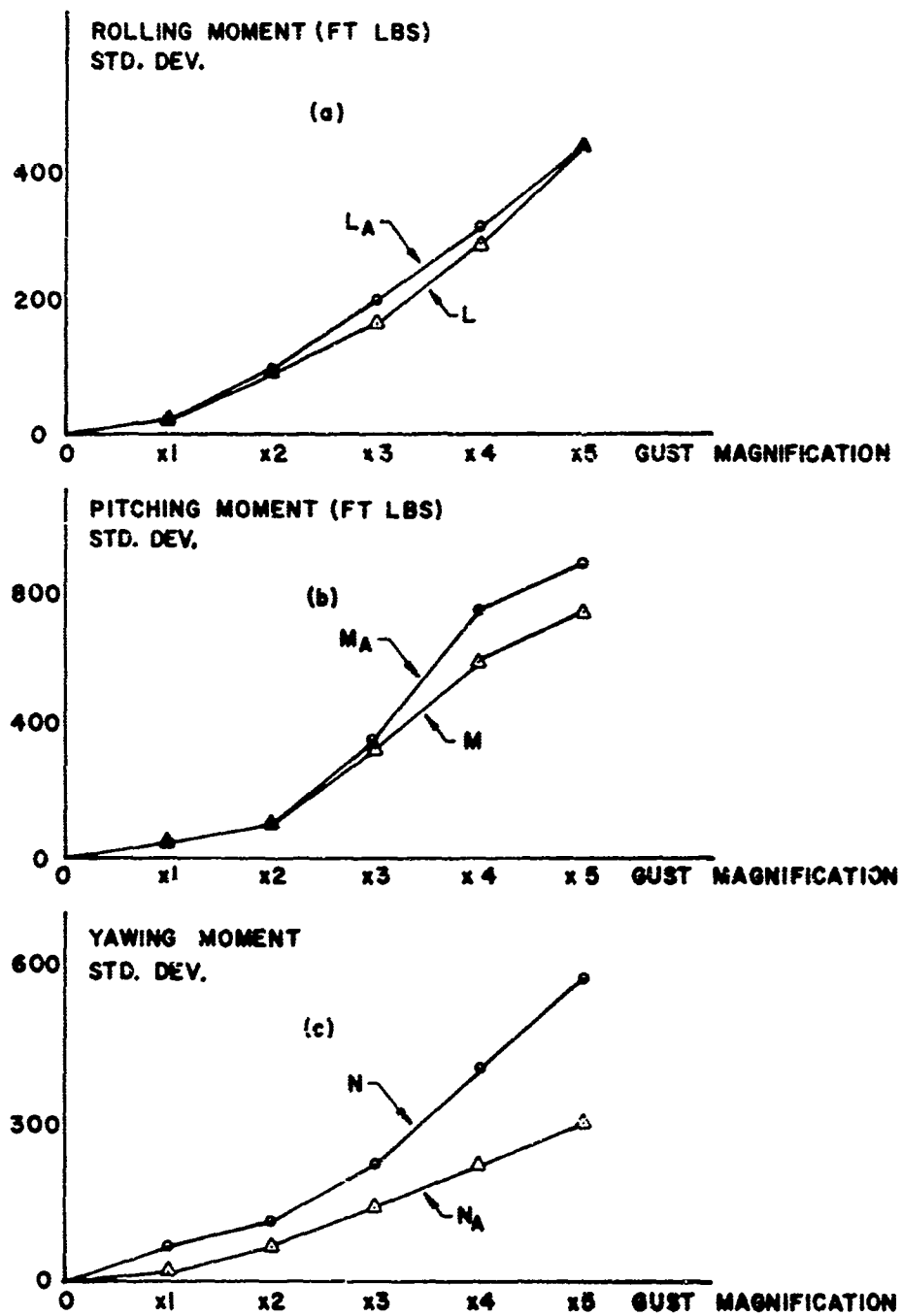


Figure 25. Total and Aerodynamic Moments versus Gust Intensity Hybrid Tests -- Hover

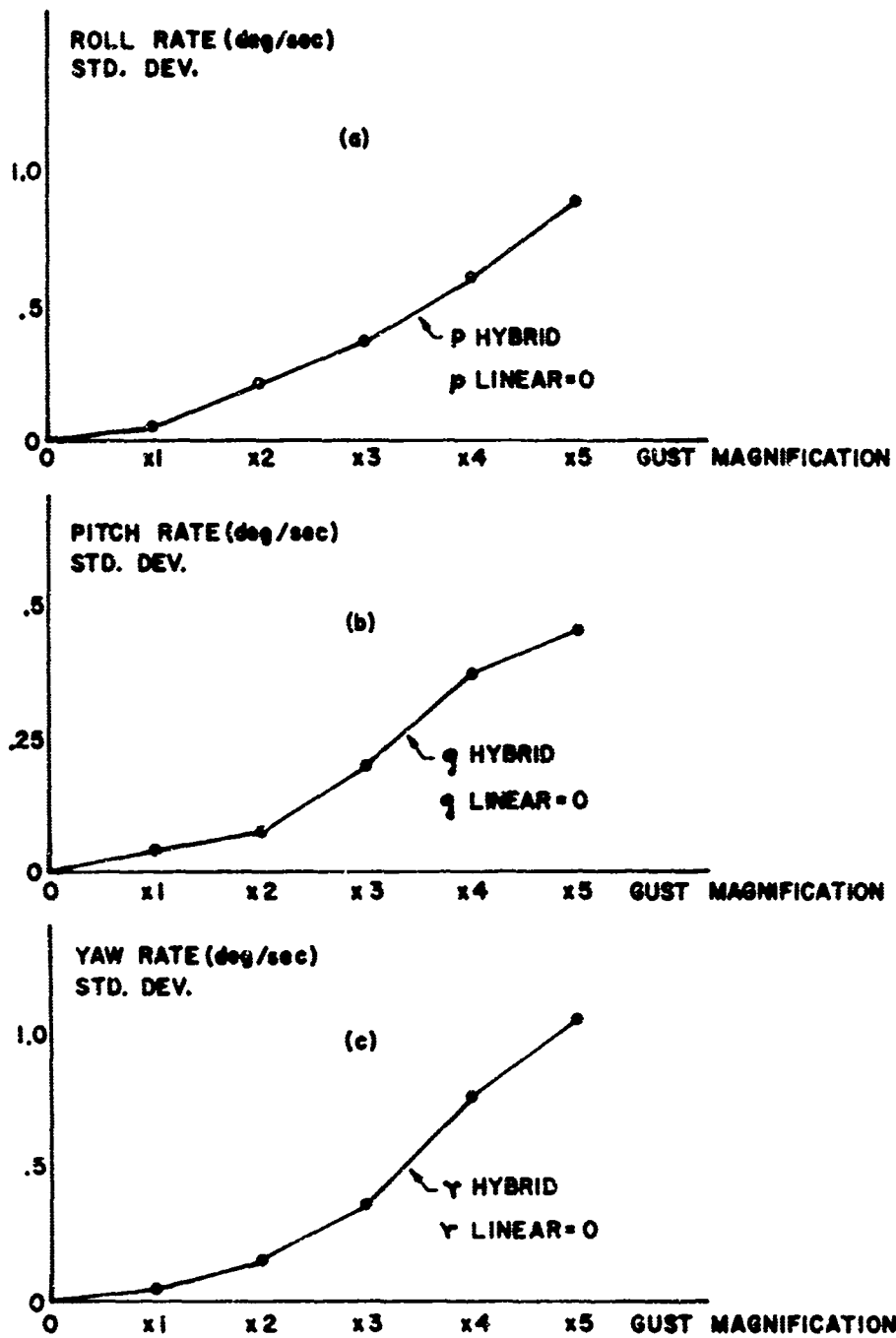


Figure 26. Hybrid Attitude Rates versus Gust Intensity -- Hover

and will average out very rapidly varying gusts. The magnitude of the gust spectra in the region of the controlled aircraft bandwidth determines the α and $\dot{\alpha}$ standard deviations, and increasing the magnitude will produce pitchup regardless of the gust energy at lower and higher frequencies.

The 22-ft/sec data in Figures 21, 22 and 23 are oddly behaved. The force standard deviations appear to be quite linear. The roll moments appear to be parabolic, and the yaw moments appear to be linear. The sharp takeoff of the total pitching moment at the x1 data point and the sharp increase in roll and pitch rates at the x2 data point are difficult to explain; the moment curves do not predict the p and q rate jumps at x2 magnification, and the q smoothness at x1 magnification does not predict the change in slope of the total pitching moment. The effect producing the p and q jumps cannot be simply a magnitude nonlinearity or it would appear in the total roll and pitch moments as well. It must therefore be a nonlinearity that produces a shift in the moments to higher frequencies to which p and q can respond and r can respond a little; at the same time, it cannot produce statistically larger forces and moments. The only mechanism that can produce this effect is dependence of the Wagner lag time constants on airspeed.¹⁴ Tail-to-nose head-on gusts will increase these time constants and nose-to-tail head-on gusts will decrease them; therefore the resulting forces and moments will have sharp spikes with the latter gust direction and broad, shallow valleys with the former. Since the roll axis has the least inertia and yaw has the most, this would explain the jumps seen. The spikes and valleys would not necessarily occur equally in wing lift, drag, and pitching moment as the former is more dependent on vertical gust velocity than the latter two, again concurring with what was observed.

This explanation was not checked by recording the lifts and drags on the two wings due to a lack of time. It is perhaps a bit far fetched, but it is the only explanation occurring to the writer that would explain an effect seen in roll rate and not in roll moment.

The parallelism of the total and aerodynamic pitching moments above x1 magnification and the absence of a slope change in pitch rate at x1 are even harder to explain. They could be due in part to data scatter, but it is felt that the effects are too pronounced for scatter to be plausible. The small vector and stagger angles at x1 magnitude more or less rule out assigning the cause to wing-fan nonlinearities, and the dynamic pressures are small enough to exclude dynamic pressure nonlinearities. It must be in the fans, however, as the aerodynamic pitching moment appears linear and the total pitching moment is the fan moments plus the aerodynamic moment. With a little imagination one can see the same effect in all three of the moment graphs, Figures 19(b), 22(b), and 25(b), further ruling out dynamic pressure

¹⁴As discussed in Appendix I, Kussner lags were approximated by running local, instantaneous airspeed on the wings and tail through Wagner lags.

dependence. The effect must then be due to nose fan door position and/or vector angles and/or stagger angles. It is not evident, however, how nonlinearities in one or more of these control inputs could affect total pitching moment and not pitch rate.

It is thought that the saturation seen in the pitching moments and pitch rate at x5 magnification are due to tail stall. The effect would not be as pronounced in lift and drag as the wings contribute the larger share of these forces.

The hover data in Figures 24, 25 and 26 are the best behaved of all of the data. The expected parabolic dependence on velocity products is seen in all responses, and evidence of wing and tail stall is seen in all of the pitch plane data at high amplitudes. The differences between these data and the linear theory predictions (of zero) are due entirely to the nonlinearities as all of the aerodynamic forces are proportional to velocity products which perturbation analyses linearize at zero.

It can safely be concluded from the intensity data that the XV-5 flies nonlinearly at moderate gust amplitudes at all airspeeds. Choosing a range of gust magnitudes where linearity is a valid approximation, the subject of the next subsection, is by no means a simple task.

A second conclusion that can be drawn from this data is that a V/STOL at low airspeeds can survive severe gusts. The XV-5 easily withstood head-on gusts of 14 ft/sec standard deviation. This corresponds to a friction velocity standard deviation of 5 ft/sec and a mean wind speed of about 60 ft/sec. The probability density curve for the mean wind assumed in the interim model in Section III gives the likelihood of a 20-meter/sec mean wind as 0.1 percent. While that assumed probability curve is undoubtedly off at low likelihoods, it is still fair to conclude that a reasonably configured V/STOL with reasonable excess thrust and a reasonable control system is going to be flyable in rough air. The ride may be rough, but one should be able to keep the airplane in the air.

C. LINEARITY

Linearity is probably the most convenient assumption that can be made in analysis. It permits the use of a very large body of mathematical theory, and it permits investigating responses without having to build a simulation. It is natural to ask, "For what range of gust magnitudes will linear analyses yield satisfactory approximations to actual responses?" This question is the subject of this subsection.

Eight kinds of nonlinearities are present in the XV-5 model, aerodynamic velocity products, sines and cosines, inertial velocity products, stalls, lift-buildup time-constant dependence on instantaneous airspeed, wing-to-tail

transport delay dependence on instantaneous airspeed, nonlinear fan dependence on dynamic pressure and vector angles, stagger angles, and nose fan door position, and fan and vector angle, stagger angle, and nose fan door saturations. The effects of these nonlinearities are different at different average airspeeds and sideslip angles, and the variations of gust spectral content and gust intensity with azimuth and heading angles will change the ordering of their importance.

Three dimensionless numbers which express measures of the magnitude and frequency dependence of the nonlinear effects are suggested,

- σ_g/V_{as} , the ratio of gust intensity to average airspeed, where

$$\sigma_g = \left(\sigma_{u_1}^2 + \sigma_{u_2}^2 + \sigma_{u_3}^2 \right)^{1/2}$$

- $\sigma_r/(r_l - r_t)$, the ratio of a response standard deviation to the difference between a response limit of interest and the trim value of that response
- $\sigma_r/\sigma_r \omega_n$, the ratio of the standard deviation of a response rate to the response standard deviation times the average radius ω_n of the dominant poles of the frequency response of that response

The first ratio measures the linearity of velocity products in force and moment calculations, the constancy of dynamic pressure in thrust calculations, and the constancy of lift-buildup time constants and wing-to-tail transport delays. The second ratio measures the percentage of time a response r exceeds a limit r_l of interest; stall angle-of-attack at the tail of the XV-5 at 120 ft/sec would be a good application.

The third ratio expresses a relation between the frequency distribution of the energy of the incident gusts and the frequency response characteristics of a vehicle. The first two ratios above are meaningless without it, as an airplane can fly linearly through very large gusts if $\sigma_r/\sigma_r \omega_n$ ratios are low (the "gusts" as seen by the moving aircraft will be of much smaller magnitude than those measured from a fixed flight path), and an airplane will average out the nonlinear effects when $\sigma_r/\sigma_r \omega_n$ ratios are large (in the same manner as linearization of a bang-bang nonlinearity by adding high-frequency dither to its input signal). When $\sigma_r/\sigma_r \omega_n$ is small the aircraft sees magnitude nonlinearities only occasionally and/or it has time to respond and keep σ_r and σ_r small. As $\sigma_r/\sigma_r \omega_n$ increases the incidence of large responses

increases and/or the airplane has less time to respond and keep σ_r and σ_r small. The former is clear from the Rice formula for the expected number of crossings per unit time of a level r_s by $r(t)$,

$$E\{N\} = \text{CONST.} \frac{\sigma_r}{\sigma_r} e^{-1/2 \left(\frac{r_s - r_t}{\sigma_r} \right)^2}$$

where r_t is the mean value of $r(t)$, and the latter follows from improving the match between gust spectra and frequency response. At some value of $\sigma_r / \sigma_r \omega_n$ (which may be different for different responses) the frequency of occurrence of a large response and the degradation of the ability of the vehicle to respond to them combine to produce maximum severity of the nonlinear effects. At larger $\sigma_r / \sigma_r \omega_n$ ratios the aircraft begins to see the average effects of more large responses, until eventually the dynamics of the aircraft almost completely smooth the nonlinearity effects.

Assigning numbers to these ratios based upon the XV-5 nonlinear intensity data is by no means an easy task. The only clear nonlinear demarcations in the data are pitchup at the 120-ft/sec airspeed flight condition and the pitch plane saturations at the 20-ft/sec airspeed flight condition. The parabolic velocity product effects are difficult to pick out, except for hover, and the nonlinearity producing the sharp change in the roll rate slope at the 20-ft/sec flight condition is not well understood. The $\sigma_r / \sigma_r \omega_n$ ratios are the most difficult of all to assign as Kussner and Wagner lag bandwidths vary linearly with average airspeed, the magnitudes of the aerodynamic force feedbacks due to aircraft velocity changes vary nonlinearly with average airspeed, and the controller and inertial response dynamics are invariant. The problem of picking significant slope changes out of the data is further complicated by the smoothing of the nonlinear effects produced by the dynamics of aircraft response and the fact that, except for upset, the nonlinear effects are introduced gradually and simultaneously as gust intensity increases. Last but not least of these problems is that there is inevitably scatter in the nonlinear XV-5 data as some gust records contain larger peaks than others, and basing incidence of nonlinearities on percentage deviation from linear results requires subjective judgments of the significance of the scatter.

It is probably a better course to assign numbers to the ratios based upon purely analytical methods, using the XV-5 intensity data only as guides. This course still requires subjective judgments, but at least one can look at the effects individually, and there are no data scatter and dynamic smoothing masking the nonlinearities. This course will be followed here.

1. Inconsequential Nonlinearities

The task of assigning numbers to the above ratios is simplified slightly by the fact that some nonlinear effects are seen before others, and the latter can thus be neglected.

Two nonlinearities that can be discarded at the start are the sine, cosine gravity nonlinearities and the inertial velocity products. The pitch and roll attitude responses are measured in degrees and tenths of degrees, and one can safely set

$$mg \sin \theta = mg \theta$$

$$mg \cos \theta \sin \phi = mg \phi$$

$$mg \cos \theta \cos \phi = mg$$

The angular rate responses are measured in tenths of degrees per second, and the moments they produce are therefore of the order of, for example

$$I_{qp} \approx \frac{17000 \times 0.1}{(57.3)^2}$$

$$\approx 0.5 \text{ ft-lbs}$$

certainly negligible. The only inertial velocity products that need be retained are those which include components of the vehicle airspeed relative to the mean wind, and these can safely be approximated by

$$m(vr-wq) = m(\bar{v}r-\bar{w}q)$$

$$m(wp-uq) = m(\bar{w}p-\bar{u}q)$$

$$m(uq-vp) = m(\bar{u}q-\bar{v}p)$$

where the overbar indicates the mean values of the aircraft linear velocities. (\bar{w} is not zero when the aircraft is pitched to fly forward or backward and \bar{v} is not zero when the airplane flies sideways, and the contributions of the \bar{w} and \bar{v} products are not always negligibly small.)

The change of the Kussner and Wagner lags time constants with instantaneous airspeed can probably be neglected. This effect is significant in stall and at very low airspeeds, but stall can be picked up with a $\sigma_{\alpha} / (\alpha_S - \alpha_T)$ ratio, and the low-airspeed effect can be lumped with the force magnitude dependence on velocity products. At higher airspeeds the bandwidths of the Kussner and Wagner lags will always be larger than the controlled aircraft bandwidth, and the distortion of the forces produced by time constant changes cannot be very large.

The percentage change of the wing-to-tail transport delay with airspeed is less than that of the time constant of the Kussner lag as the wing-to-tail distance is more than two wing chords (on the XV-5), but the effect of this delay is very noticeable at moderate airspeeds, and the nonlinearity there should probably be retained.

Nose fan door, vector, and stagger angle controller saturations can be completely neglected, as the only times they were observed in the nonlinear intensity tests were after upset. Fan response nonlinearities due to changes of nose fan door, vector angles, and stagger angles can also be neglected as these changes are very small.

2. σ_g/V_{as} Ratio

This ratio determines velocity product nonlinearities in aerodynamic forces and moments and in thruster dependence on dynamic pressure, it determines changes in the wing-to-tail transport delay, and it determines stall. The latter effect is more conveniently taken into account by the $\sigma_\alpha/(\alpha_s - \alpha_T)$ ratio, as the σ_g/V_{as} ratio alone does not take trim into account.

Thruster dynamic pressure nonlinearities are negligibly small in the XV-5 model employed in these studies, but the engine and fan models were based on static test data and do not include dynamics. The most violent dynamic effect that could occur would be to flame out the engine. As no engine data on this effect is available, it will be ignored here.

The velocity products in the aerodynamic forces are amenable to analysis. Neglecting the contributions of aircraft motion to these products, the gust-induced forces are proportional to $(V_{as} + u_g)V$ and Vw_g , where

$$V = [(V_{as} + u_g)^2 + w_g^2]^{1/2}$$

Letting $w_g = 0$ for the moment, the probability distribution of the $(V_{as} + u_g)|V_{as} + u_g|$ drag force is

$$\begin{aligned} \text{Prob}\{(V_{as} + u_g)|V_{as} + u_g| < \alpha\} &= \text{Prob}\{u_g < \sqrt{\alpha} - V_{as}\} \text{ for } \alpha > 0 \\ &= \text{Prob}\{u_g < -\sqrt{-\alpha} - V_{as}\} \text{ for } \alpha < 0 \end{aligned}$$

Assuming u_g is Gaussian and zero mean,

$$\text{Prob}\{u_g < \beta\} = \int_{-\infty}^{\beta} \frac{1}{\sqrt{2\pi}\sigma} e^{-1/2\left(\frac{y}{\sigma}\right)^2} dy$$

The force probability density $P(\alpha)$ is then

$$\begin{aligned} P(\alpha) &= \frac{\partial}{\partial \alpha} \text{Prob}\{(V_{as} + u_g) | V_{as} + u_g| < \alpha\} \\ &= \frac{1}{\sqrt{2\pi}\sigma} e^{-1/2\left(\frac{\sqrt{\alpha} - V_{as}}{\sigma}\right)^2} \cdot \frac{1}{2\sqrt{\alpha}} \text{ for } \alpha > 0 \\ &= \frac{1}{\sqrt{2\pi}\sigma} e^{-1/2\left(\frac{\sqrt{-\alpha} - V_{as}}{\sigma}\right)^2} \frac{1}{2\sqrt{-\alpha}} \text{ for } \alpha < 0 \\ &= \frac{1}{2\sqrt{2\pi}\sigma\sqrt{|\alpha|}} e^{-1/2\left(\frac{\sqrt{|\alpha|} - V_{as}\text{SGN}\alpha}{\sigma}\right)^2} \end{aligned}$$

In the neighborhood of the "steady-state" force V_{as}^2 ,

$$\alpha = V_{as}^2 + \Delta\alpha$$

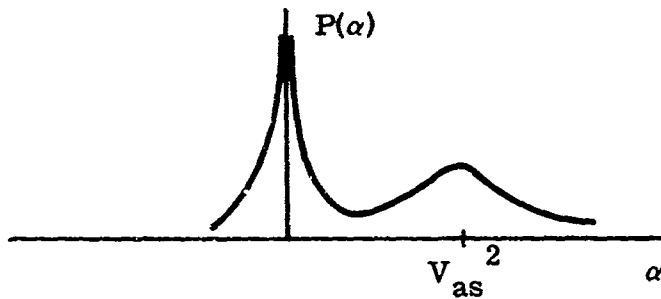
the above reduces to

$$\begin{aligned} \sqrt{|\alpha|} &\approx V_{as} \left(1 + \frac{1}{2} \frac{\Delta\alpha}{V_{as}^2}\right) \\ P(\alpha) &\approx \frac{1}{\sqrt{2\pi} 2\sigma V_{as}} e^{-1/2\left(\frac{\Delta\alpha}{2\sigma V_{as}}\right)^2} \end{aligned}$$

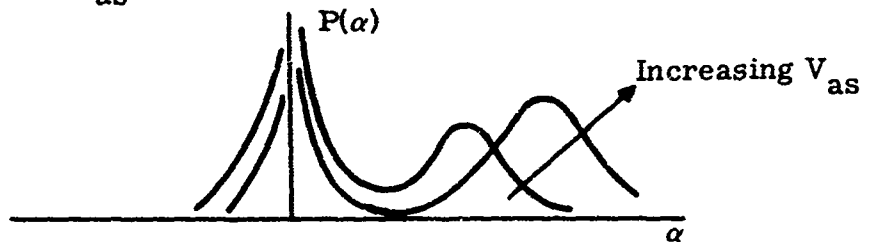
which is approximately Gaussian, as one would expect. In the neighborhood of the origin, however, it is dominated by the $1/\sqrt{|\alpha|}$ term, and $P(\alpha)$ hence has a removable singularity there. For hover with respect to the wind, $V_{as} = 0$ and $P(\alpha)$ reduces to

$$P(\alpha) = \frac{1}{2\sqrt{2\pi}\sigma\sqrt{|\alpha|}} e^{-\frac{|\alpha|}{2\sigma^2}}$$

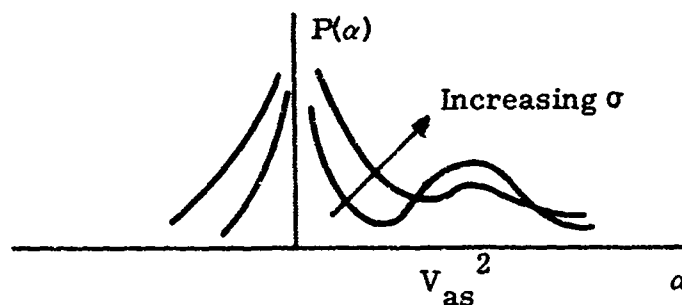
Sketching $P(\alpha)$ for a given V_{as} and σ , we then have the form:



The effect of increasing V_{as} , with σ fixed, is to narrow



the spike at $\alpha = 0$, move the Gaussian bump to the right, and enlarge it. The effect of increasing the gust standard deviation σ , with V_{as} fixed, is to widen the spike at $\alpha = 0$ and widen the Gaussian bump



It is clear that if the Gaussian bump is large enough and far enough from the spike at $\alpha = 0$, the gust-induced forces will be approximately proportional to the gust amplitudes, and linearity will be reasonable. That is, there is a number γ such that if $\sigma/V_{as} < \gamma$, linearity is reasonable, while for $\sigma/V_{as} > \gamma$, linearity is not. The choice of γ is subjective.

Looking at the lift forces due to vertical gusts, suppose the head-on gusts are zero, $u_g = 0$. The probability density of $w_g(V_{as}^2 + w_g^2)$ is after calculation,

$$P(\alpha) = \frac{1}{2\sqrt{2\pi}\sigma} \frac{1}{\sqrt{\alpha^2 + \frac{V_{as}^4}{4}}} \frac{\alpha}{\sqrt{\alpha^2 + \frac{V_{as}^4}{4} - \frac{V_{as}^2}{2}}} e^{-\frac{1}{2} \left(\frac{\sqrt{\alpha^2 + \frac{V_{as}^4}{4}} - \frac{V_{as}^2}{2}}{\sigma^2} \right)^2}$$

For α near zero

$$\sqrt{\alpha^2 + \frac{V_{as}^4}{4}} \approx \frac{V_{as}^2}{2} \left(1 + \frac{1}{2} \frac{4\alpha^2}{V_{as}^4} \right)$$

$$P(\alpha) \approx \frac{1}{2\pi\sigma V_{as}} e^{-\frac{1}{2} \left(\frac{\alpha}{\sigma V_{as}} \right)^2}$$

which is approximately Gaussian, as expected. For hover with respect to the wind, $V_{as} = 0$, however,

$$P(\alpha) = \frac{1}{2\sqrt{2\pi}\sigma\sqrt{|\alpha|}} e^{-\frac{|\alpha|}{2\sigma^2}}$$

which again introduces the 'spike' at $\sigma = 0$. As with the head-on gusts, increases in the ratio σ/V_{as} decrease the acceptability of linearity.

The above derivations are simple and do not take instantaneous vehicle velocities, mean vertical and side velocities, or lift-buildup dynamics into account. They should give some idea of what to expect in the wing and tail lift and drag force probability densities and the pitching moment probability densities. The probability densities of the roll and yaw moments due to side forces on the tail should possess these properties as well, but the roll and yaw moments due to differential lift and drag on the wings are more complex as one must take into account the conditional probabilities of the gusts on one wing given the gusts on the other.

Experimental probability densities of the V/STOL responses listed in the data tables were measured in most of the hybrid simulation tests. Thirteen typical densities are presented in Figures 27 through 39. The densities in general behaved much as predicted by the above formulae, but in some cases the densities were irregular and difficult to explain.

The notation for the plots is as follows: Run number, in the upper left hand corner of the graphs, can be ignored. It was used in the early tests as a log book number denoting the gust and vehicle models employed in a particular test, but it was found more convenient to keep the log by date rather than number. Response number is the number of the sampled response, response 28 in the first plot being the vertical gust. Number of sample points is self explanatory, run time is the number of sample points times the sampling interval, and mean and standard deviation are self explanatory.

The graphs ordinates are the probability densities. The abscissas are the deviation of the response magnitude from the mean, divided by the standard deviation. That is, for response r , the ordinate is

$$\frac{\partial}{\partial \alpha} \text{Prob}\{r(t) < \alpha\}$$

and the abscissa is

$$(\alpha - \bar{r})/\sigma$$

where

$$\bar{r} = \text{mean} = E\{r(t)\}$$

$$\sigma = \text{standard deviation}$$

$$= \left(E\{[r(t) - \bar{r}]^2\} \right)^{1/2}$$

The normalized abscissa scale was chosen for plotting convenience.

Each graph plots 25 points, each point being the number of samples within $\pm(1/8)\sigma$ of the abscissa value times 4 over the number of samples. The 4 is introduced to account for the $1/4\sigma$ width of the abscissa intervals. The end data points at $\pm 3\sigma$ include all points above and below $\pm 3\sigma$ respectively.

Figure 27 is a plot of the vertical gust component obtained during the intensity tests. The notch in the density near the peak and the large mean were typical of all of the gusts, both being attributable to noise source inadequacies. The gust densities as a whole were nearly Gaussian.

Figures 28 and 29 show the densities of total rolling moment and roll rate response at the 120-ft/sec airspeed. All of the 120-ft/sec densities were as nearly Gaussian and well behaved as these except for the pitch plane densities at gust amplitudes large enough to produce upset.

P L A N O : S A M P L E F O I N T S • 1 9 9 9 R F S P A S E N O . • 1 1 3 . 9 4 S E C 3 . 1 1
 M E A N • - 1 4 . 4 7 S T A N D A R D D E V I A T I O N • 3 . 1 1

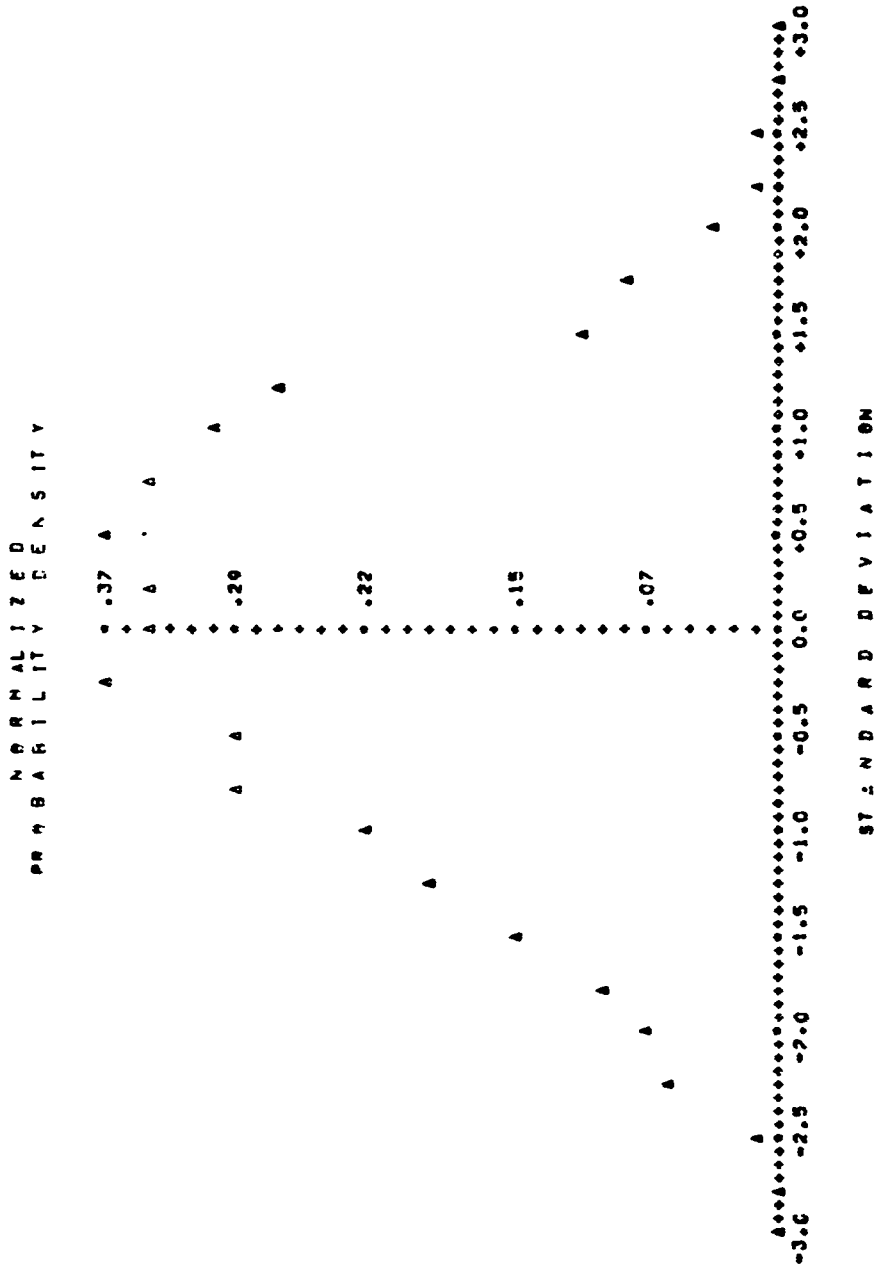


Figure 27. Vertical Gust Probability Density (ft/sec)

RUN NO: 0
 SAMPLE POINTS = 2000
 RESPONSE NO. = 114.00 SEC.
 STDEV = .57
 STANDARD DEVIATION = 429.05

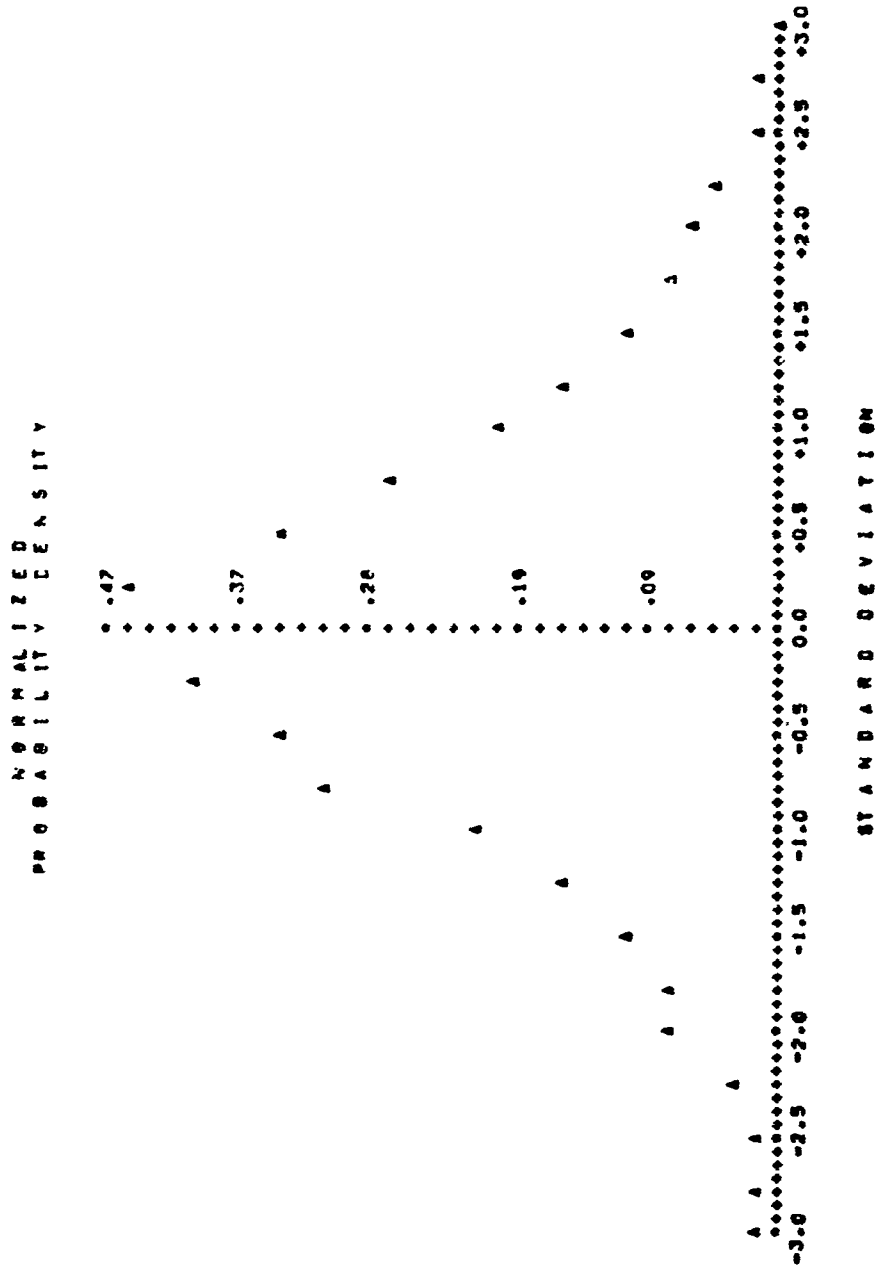


Figure 28. Total Rolling Moment Probability Density --
120-ft/sec Airspeed (ft-lbs)

RUN NO : 2000 RESPONSE NO : 16
 NO : SAMPLE POINTS : 2000 RUN TIME : 114.00 SEC.
 PEAK : STANDARD DEVIATION : 1.30

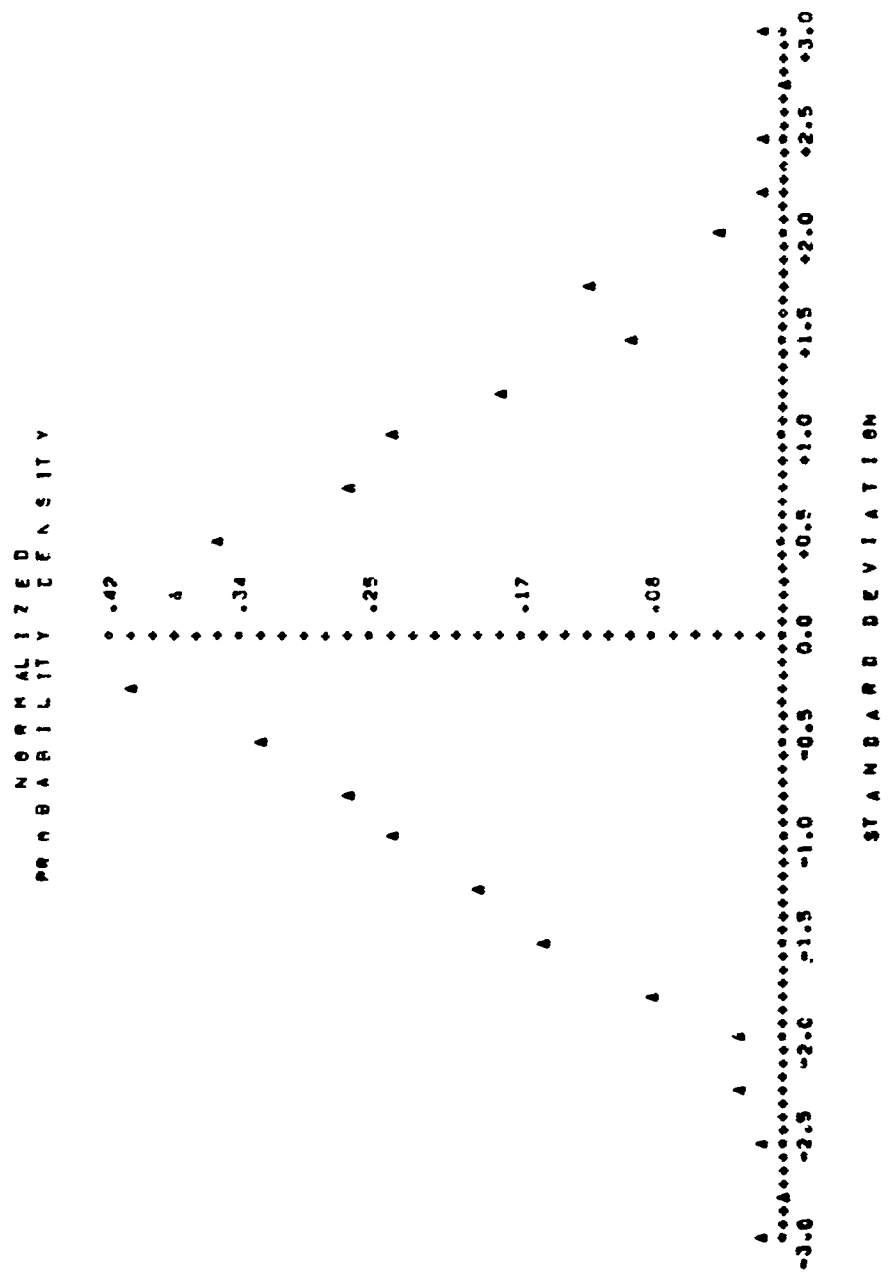


Figure 29. Roll Rate Probability Density -- 120-ft/sec

W L A N O . 0
 R E A . 0
 S A M P L E P O I N T S = 2000
 R U N T I M E = 114.00 S E C
 S T A N D A R D D E V I A T I O N = 150.04

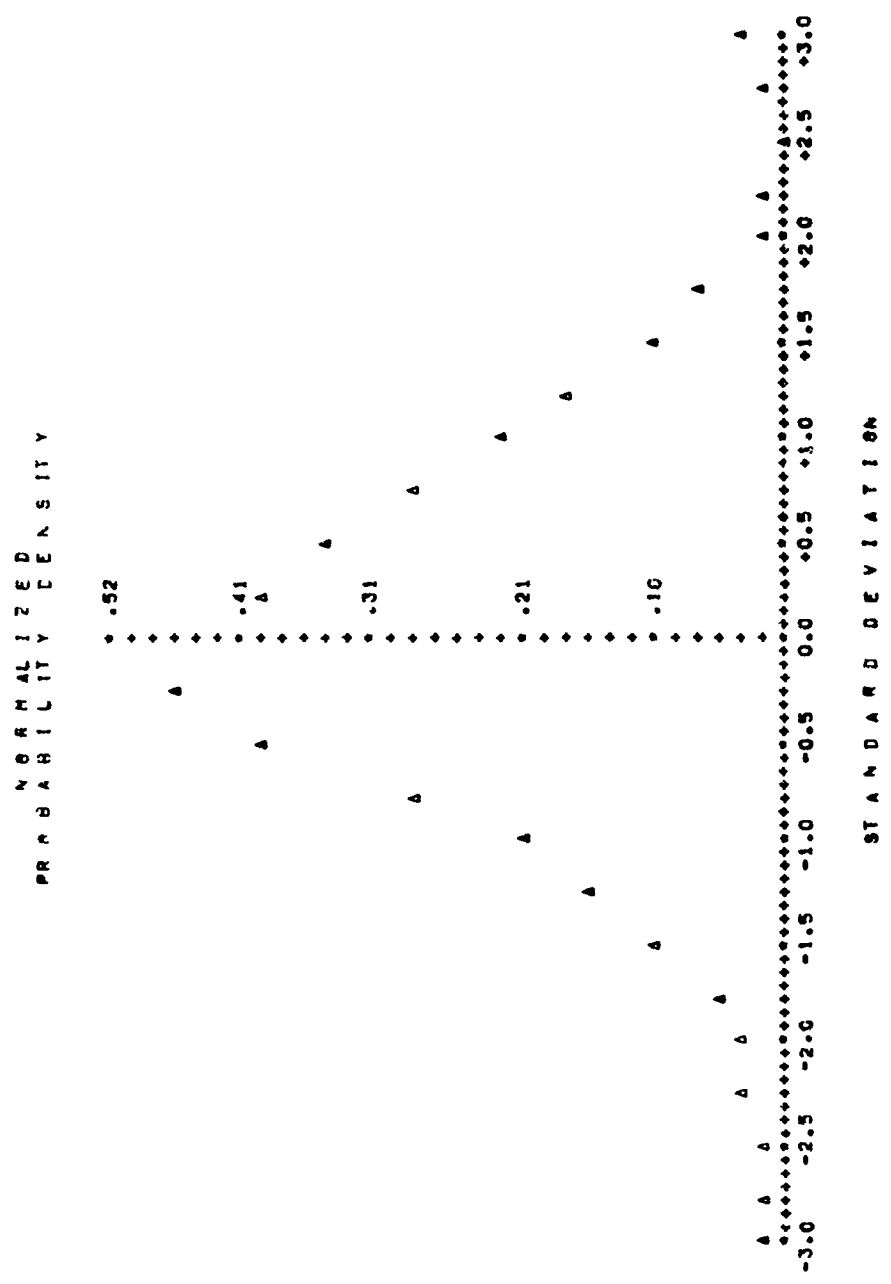


Figure 30. Aerodynamic Lift Force Probability Density -- 20-ft/sec
Airspeed, Low Gust Amplitude (lbs)

RUN NO. = 0
 NO. SAMPLE POINTS = 2000
 MEAN = -455.66
 RESPONSE NO. = 7
 RUN TIME = 114.00 SEC.
 STANDARD DEVIATION = 211.91

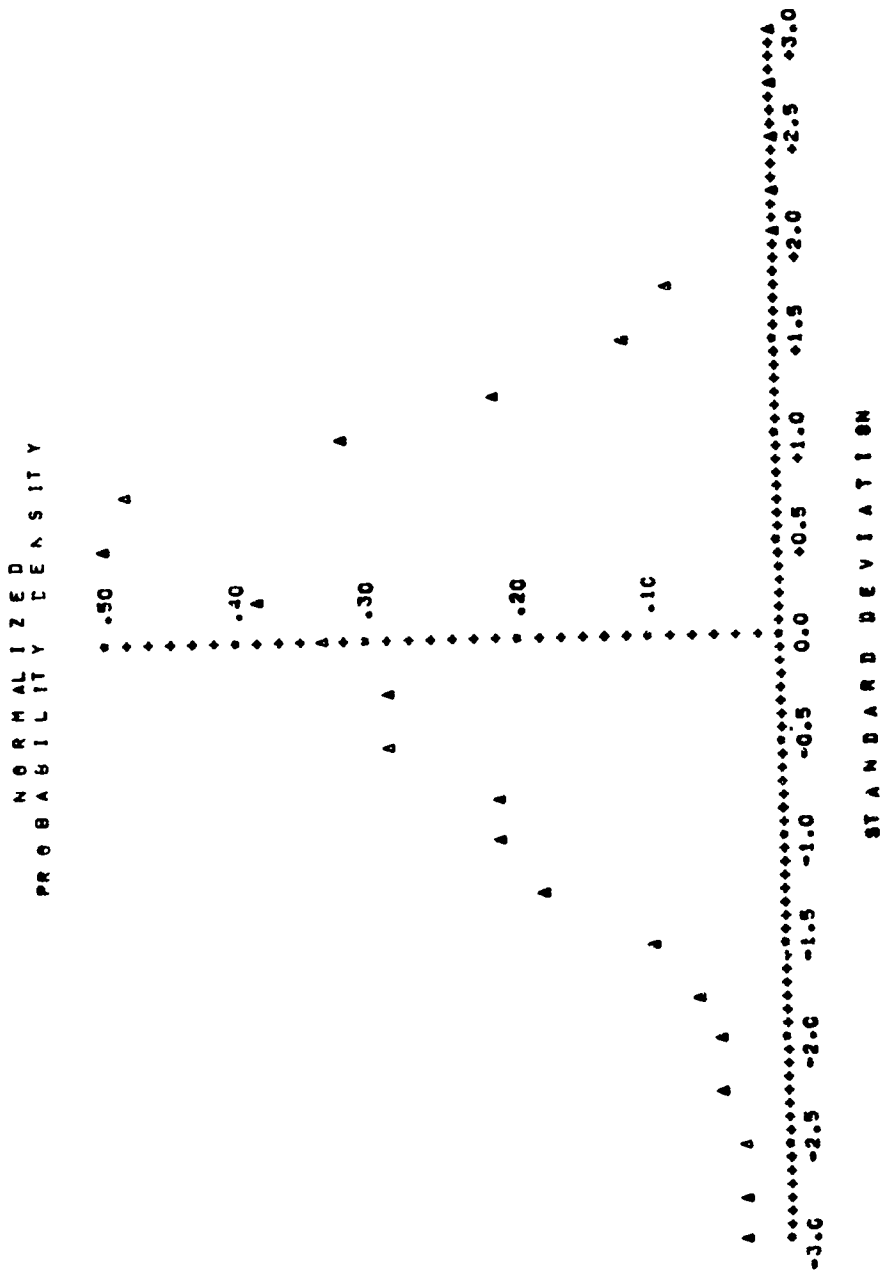


Figure 31. Aerodynamic Side Force Probability Density -- 20-ft/sec Airspeed, Low Gust Amplitude (lbs)

RUN NO = 0 RESPONSE NO. = 11
 SAMPLE POINTS = 2000 RUN TIME = 114.00 SFC:
 MEAN = 1763.76 STANDARD DEVIATION = 1260.65

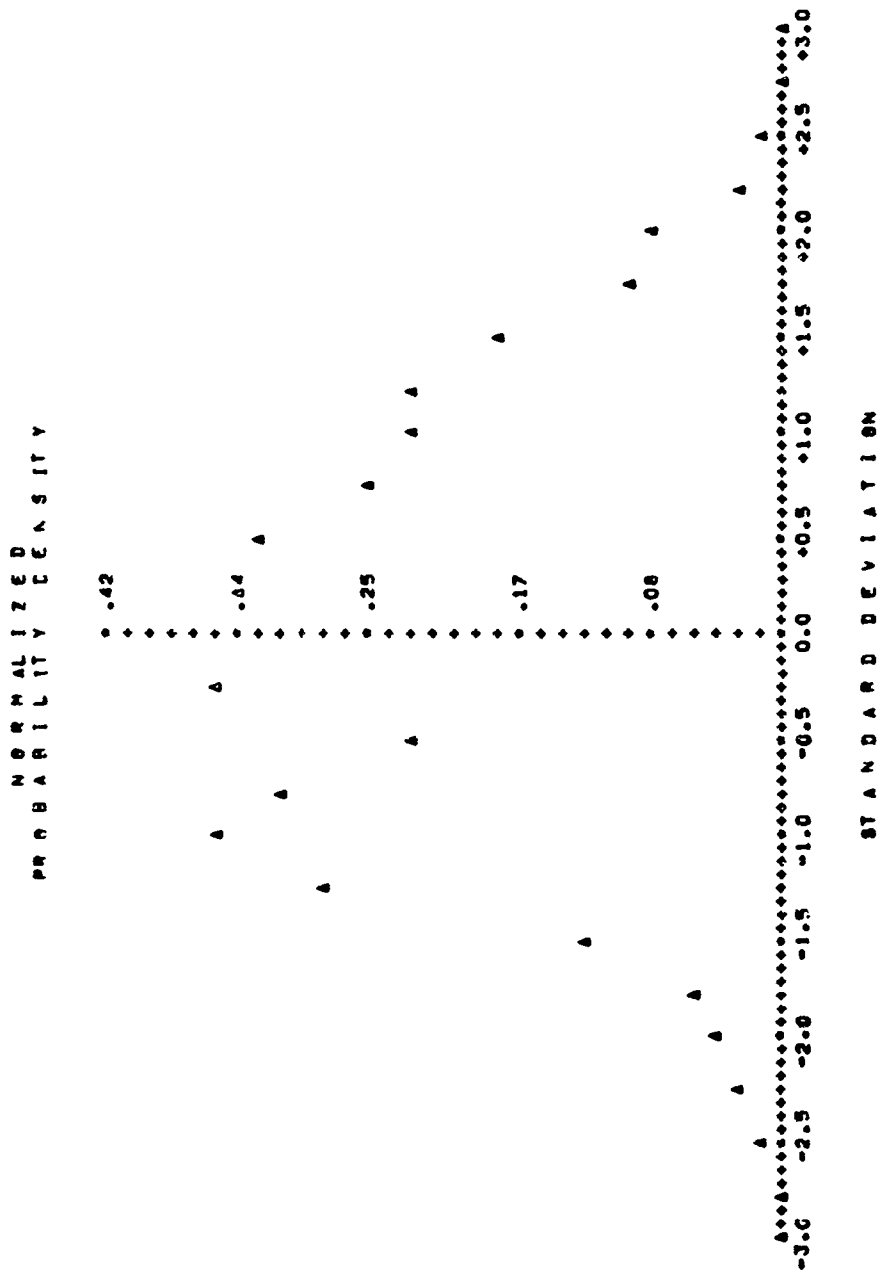


Figure 32. Aerodynamic Pitching Moment Probability Density --
20-ft/sec Airspeed, Large Gust Amplitude (ft-lbs)

NLA NO. = 0
 NR. SAMPLE POINTS = 2000
 RESPONSE AC. = 17
 MEAN = 0.01
 RUN TIME = 114.00 SEC.
 STANDARD DEVIATION = .02

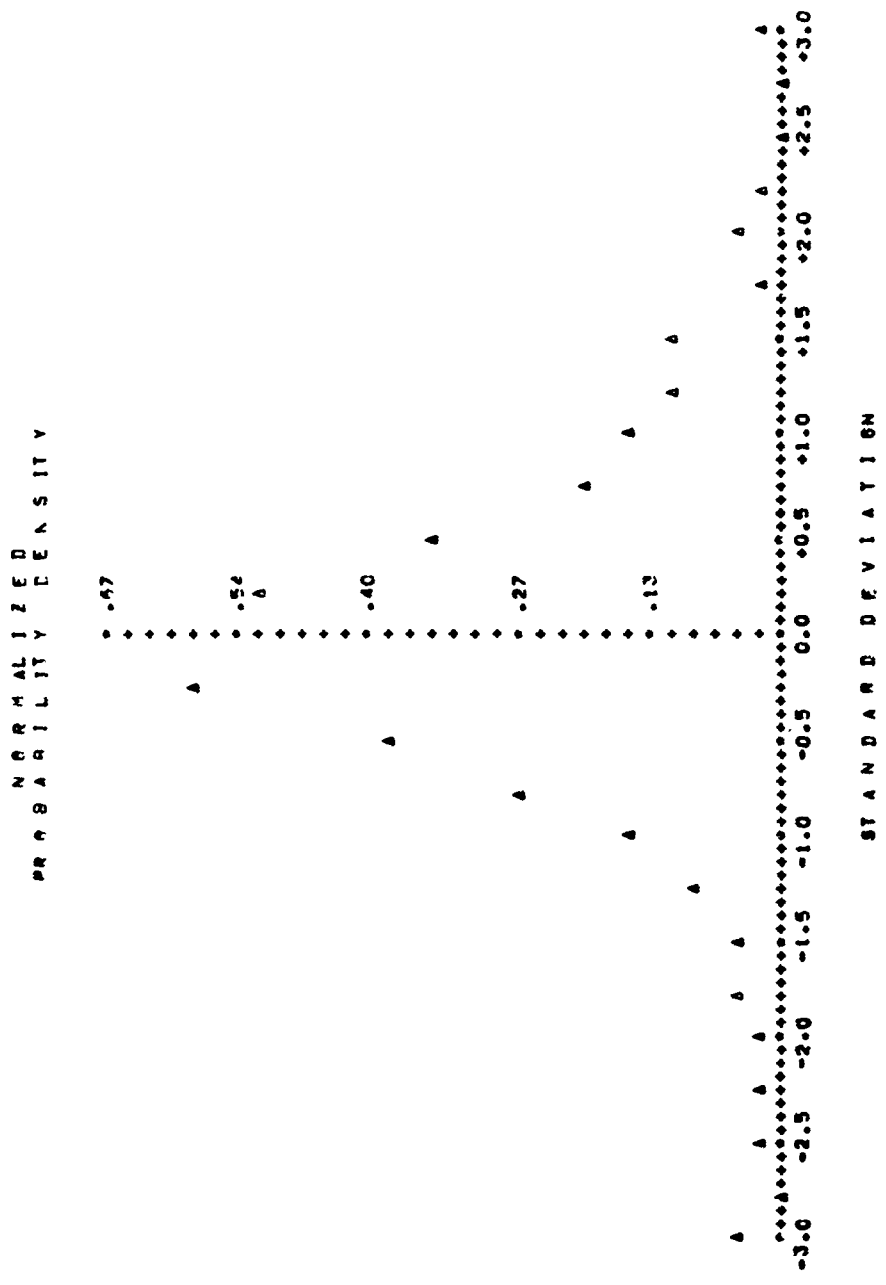


Figure 33. Pitch Rate Probability Density -- 20-ft/sec Airspeed, Moderate Gust Amplitude (deg/sec)

WLN NO: 17
 SAMPLE POINTS: 2000
 RESPONSE NO: 17
 RUN TIME: 114.00 SEC.
 STANDARD DEVIATION: .53

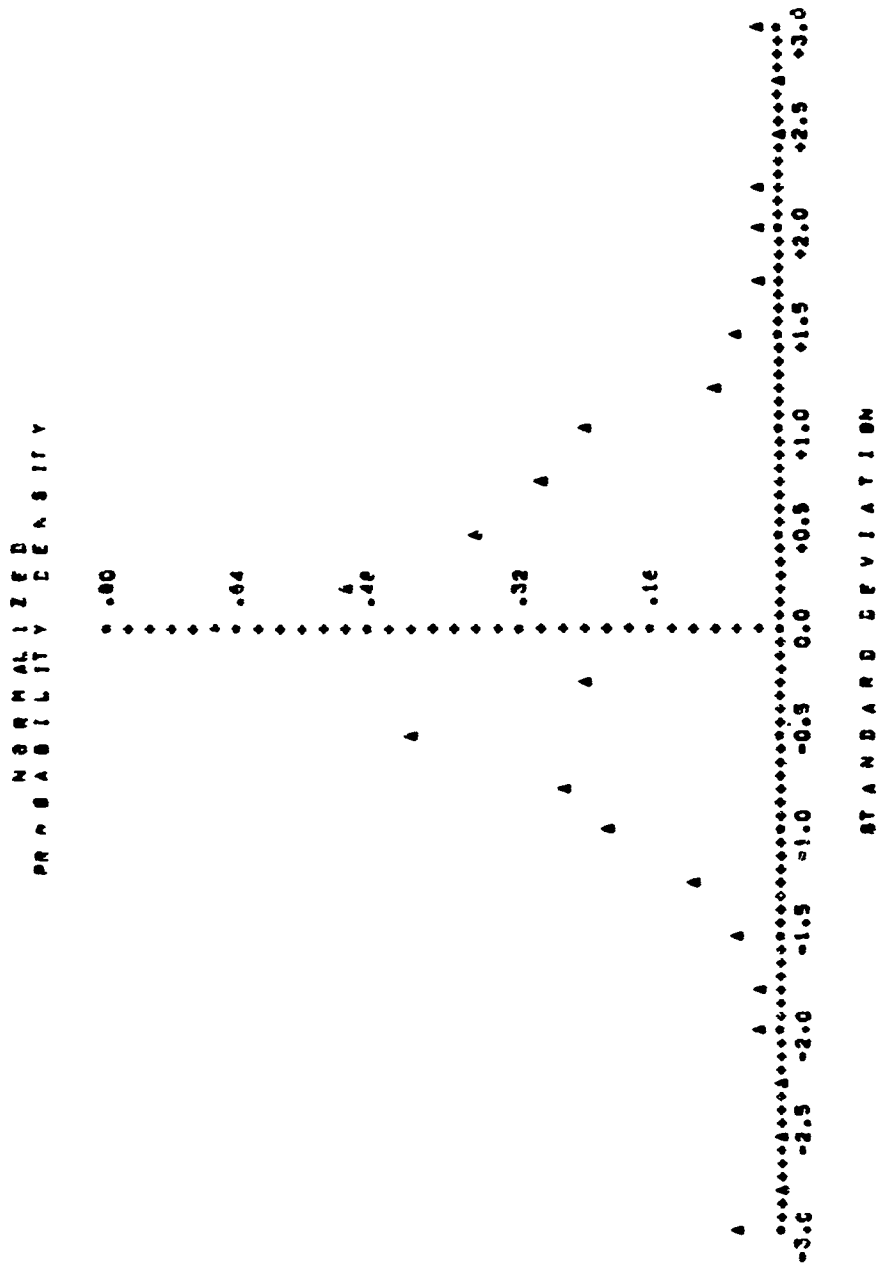


Figure 34. Pitch Rate Probability Density -- 20-ft/sec Airspeed, Large Gust Amplitude (deg/sec)

TEST SAMPLE POINTS = 2000
 TEST NUMBER = 114 CG SFC . 000
 TEST DATE = 17

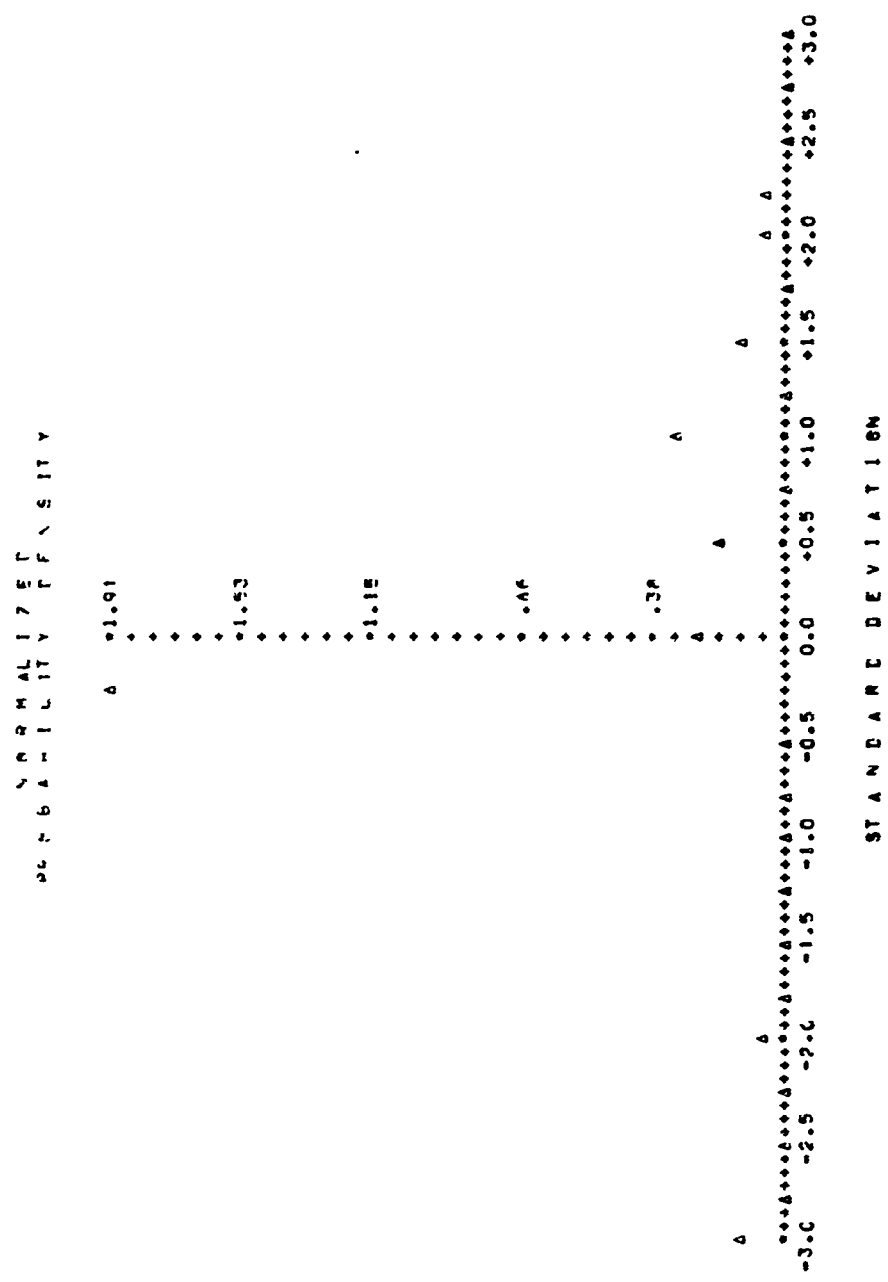


Figure 39. Pitch Rate Probability Density -- Hover (deg/sec)

Figures 30 through 35 show response probability densities at 20 ft/sec airspeed, downwind flight at zero average sideslip. Figures 30 and 31 show aerodynamic lift and side forces at low gust amplitudes; the latter is well behaved, as were all the side force densities, but the lift force is definitely skewed. The z axis was positive down, and the -455-pound mean is the average aerodynamic lift at this airspeed.

Figure 32 shows the density of the aerodynamic pitching moment at a large gust amplitude. It exhibits the double peak predicted above; these peaks were found in most of the forces and moments at this flight condition at large gust amplitudes. Figures 33 and 34 show pitch rate response densities at large and moderate amplitudes. The double peak exhibited by the pitching moment is very evident in the lower-amplitude plot, but the higher-amplitude density is more exponential than anything else. It is evident that force and response probability densities are different, even though force-to-response dynamics are nearly linear, and that one cannot safely predict the form of either density given the other.

Figure 35 shows the roll rate response density at large gust amplitudes. It is exponential, as one would predict.

Figures 36 through 39 show the probability densities of total side force, total yawing moment, aerodynamic yawing moment, and pitch rate response in hover. The side force and aerodynamic yawing moment densities are exponential, as expected. The total yawing moment shows two Gaussian peaks symmetric about an exponential peak at the origin. The side peaks must be due to the wing fans because, if they were aerodynamic, they would appear in the aerodynamic yaw moment as well. The pitch rate response density is one-sided and very irregular.

In general, the only densities which were ill behaved were pitch and yaw moments and pitch and yaw rate responses at gust amplitudes large enough to make the nonlinearities dominate the densities. The irregularities were due to the fans as they did not appear in the aerodynamic moments, and the response magnitudes were too small for them to be due to inertial velocity products.

One cannot pick a single σ_g/V_{as} ratio as separating linear and nonlinear response magnitudes for all responses, as the nonlinearities affect the various responses gradually and to different extents as gust amplitudes increase. The nonlinearities are, of course, more evident in the probability densities than in response standard deviations as the former contain more information than the latter.

Accepting this, for a rough figure it is reasonable to choose $\sigma_g/V_{as} = 0.4$ as a demarcation between linear and nonlinear responses. Below this figure all of the response standard deviations are reasonably close to linear theory predictions, while above it some responses are definitely larger than linearity predicts.

3. $\sigma_\alpha / (\alpha_S - \alpha_T)$ Ratios

Ratios of response standard deviations to the difference between trim response and the response magnitude at which a nonlinear effect becomes important are meaningful for all nonlinearities capable of linearization. For bang-bang or stiction type nonlinearities increases of these ratios indicate improvements in linearity, while for stall they indicate a degradation. As none of the former type, those more linear with larger amplitudes, are present in the XV-5 model, there are no data on which to base assignments of numbers to the ratios, and they will not be discussed further here.

Ratios of this type are meaningful for all nonlinearities which become more predominant as amplitudes increase, but they are especially significant where reaching the upper response magnitude triggers a violent response that does not occur at slightly smaller magnitudes. They are very meaningful where stall triggers upset, as in the XV-5 at a 100-ft/sec airspeed. At lower airspeeds where the aerodynamic forces and moments are but a small portion of the total forces and moments, the incidence of stall is not critical to performance and effects only gradual response saturations.

Concentrating then on upset, at the 100-ft/sec airspeed the trim angle-of-attack of the tail, taking wing downwash and tail incidence angle into account, is about 0.21 radian. The stall angle of attack is 0.35 radian, and upset occurred up to three times in 2-minute runs at vertical tail velocity standard deviations of about 6 ft/sec. With these figures

$$\sigma_\alpha \approx \sigma_{w_T} / V_{as} = 6/120 = 0.05$$

$$\begin{aligned} \sigma_\alpha / (\alpha_S - \alpha_T) &= 0.05 / (0.35 - 0.21) \\ &\approx 0.36 \end{aligned}$$

This corresponds to being in stall 0.3 percent of the time, providing the vehicle can recover immediately. However, in upset it cannot.

To estimate the number of occasions per minute that stall will occur, the Rice formula gives the expected number of stalls per minute as

$$E\{N\} = \frac{60}{\sqrt{2\pi}} \frac{\sigma_{\dot{\alpha}}}{\sigma_\alpha} e^{-\frac{1}{2} \left(\frac{\alpha_S - \alpha_T}{\sigma_\alpha} \right)^2}$$

$\sigma_{\dot{\alpha}}$ is theoretically infinity with the gust model employed as the gust shears contain white noise, and infinitely many infinitesimal stalls should occur per

minute. This is, of course, meaningless as it depends solely on the high-frequency gust spectra, to which the vehicle cannot respond because of Kussner lags.

A better estimate of the frequency stall occurrence can be obtained by using the tail lift force at stall as this includes the Kussner lag. For this force

$$\frac{\sigma_f'}{\sigma_f} \approx \frac{V_{as}}{\sqrt{L\bar{c}}}$$

where L is the correlation length and \bar{c} is the tail chord. Using a 150-foot correlation length and a 7-foot chord produces

$$E\{N\} \approx 60 \frac{100}{\sqrt{150 \times 7}} \times \frac{1}{\sqrt{2\pi}} e^{-\frac{1}{2} \left(\frac{\alpha_s - \alpha_T}{\sigma_\alpha} \right)^2}$$

$$\approx 1.5 \text{ stalls/minute}$$

which is about what was observed.

It is evident that fairly small ratios of standard deviations to the response magnitude changes were nonlinearities become visible can be important. For these ratios to be of interest, however, the frequency of occurrence of reaching the response magnitude of concern must be large enough to be a problem, but not so rapid that the aircraft cannot respond to the individual events of reaching that magnitude. That is, one must examine $\sigma_f'/\sigma_\alpha \omega_n$ ratios at the same time.

4. $\sigma_f'/\sigma_r \omega_n$ Ratios

Very large values for ratios of this type imply that the aircraft does not respond to the individual nonlinearities but only to time averages of many nonlinear effects. Very small values imply that the nonlinear effects occur slowly, and the airplane will probably be able to fly with the gusts rather than through them. Presumably there is a critical point between where the nonlinear effects are most visible.

In spite of a considerable effort, no critical $\sigma_f'/\sigma_r \omega_n$ ratios were found that were valid at all flight conditions for any response or any particular nonlinearity. Two-to-one changes in critical values were found between flight conditions, and the ratios were so insensitive to some parameters and sensitive to others that they were useless for choosing critical correlation lengths and airspeeds. An examination of the combination of total and gust forces and moments showed why.

As shown in Figure 40, the gust frequencies seen by the aircraft (the gust spectral bandwidth) depend linearly upon V_{as}/L , airspeed over correlation length. The bandwidth of both Kussner and Wagner lags is proportional to V_{as}/\bar{c} , where \bar{c} is chord length. The magnitude of the forces depends on both airspeed and the gust and vehicle velocities (through dynamic pressure), and the aircraft inertial dynamics are independent of airspeed, chord length, and correlation length. The magnitude of the aircraft responses to gusts then depends on two bandwidth ratios, the ratio of the gust bandwidth seen by the aircraft to the Kussner bandwidth, and the ratio of the Kussner bandwidth to dominant feedback pole radii. The latter depend both on the Wagner lags (and thus V_{as}/\bar{c}) and the particular control system employed.

The difficulties these interactions produced were twofold. No single $\sigma_r^*/\sigma_r\omega_n$ ratio could be isolated that was dependent only on one of the bandwidth ratios, and the aerodynamic force rates (σ_f^*) were overly dependent on the high frequency portions of the gust spectra. No matter what forces or responses were chosen, either σ_r^*/ω_n would be invariant or σ_r^*/ω_n would vary almost linearly with V_{as} .

After many attempts at sorting out the force interactions, it was concluded that the difficulty lay in unrealistic σ_f^* and σ_r^* standard deviations. It is felt that very good models for the high-frequency gust spectra and for the high-frequency cutoff of the Kussner lags would produce realistic force and response rate standard deviations, and that with these one would have a good chance to define meaningful $\sigma_r^*/\sigma_r\omega_n$ ratios.

In summary, the data validates employment of σ_g/V_{as} and $\sigma_\alpha/(\alpha_S - \alpha_T)$ ratios as measures of the importance of nonlinearities. Both, however, need be modified by $\sigma_r^*/\sigma_r\omega_n$ ratios to determine whether the aircraft is flying with the gusts, or is flying through them and responding to them, or is flying so fast as to average out individual nonlinear effects. The inability to find meaningful $\sigma_r^*/\sigma_r\omega_n$ in this study is not thought to invalidate their importance, but is rather held to be due to poor gust and Kussner models and to a lack of cleverness on the part of the investigators.¹⁵

¹⁵Sorting out force interactions and frequency dependence is not easy, and as this was not a major issue of this study, little time could be devoted to it. However, there surely are clear insights which would greatly reduce the difficulty of the interactions, and the writer accuses himself of a lack of perceptiveness in not finding what surely exists.

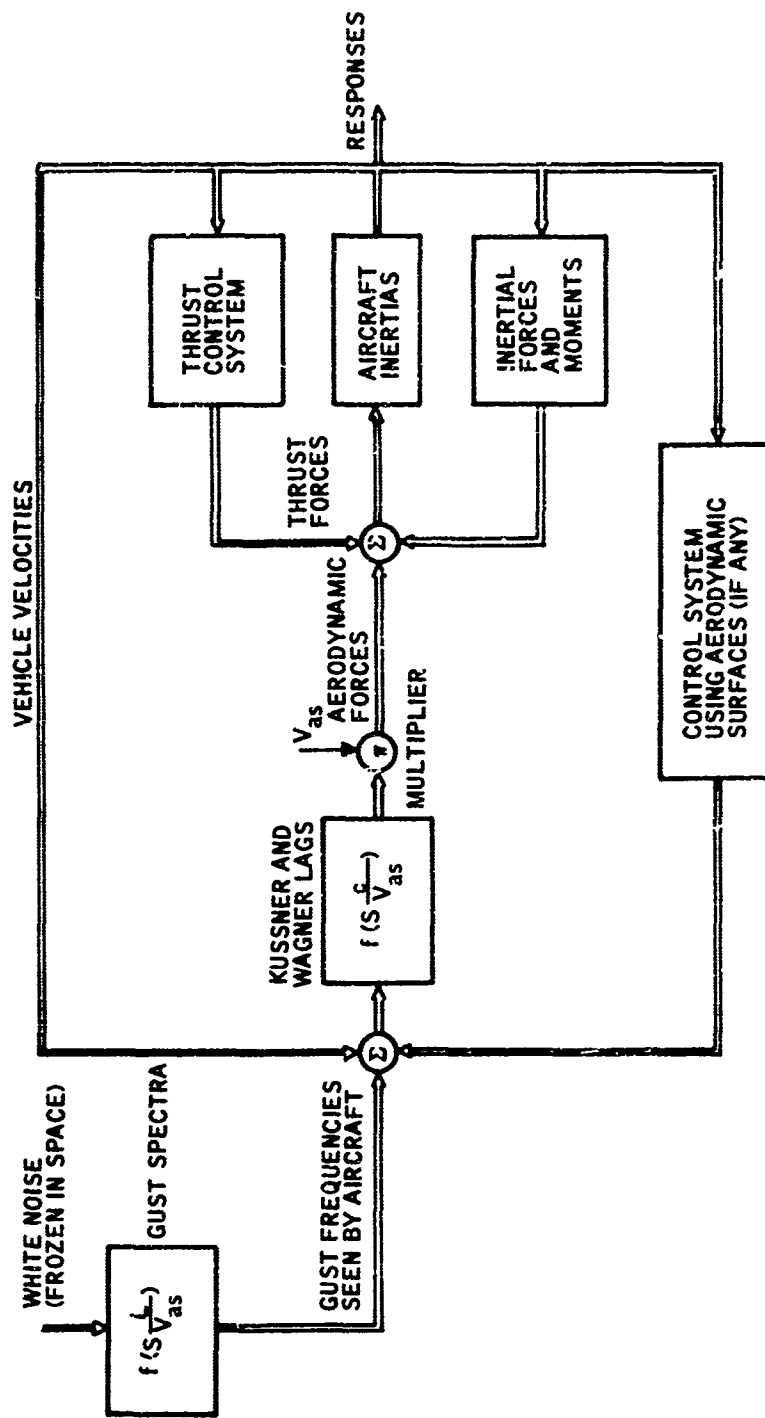


Figure 40. Force Schematic

D. OTHER SIMULATION TOPICS

In this final subsection a number of minor topics deserving mention but not the attention of a full subsection are discussed. All of these topics arose in connection with the nonlinear XV-5 analyses, though several carried over to the linear analyses. The topics are design of the three-axis controller employed, omission of consideration of reingestion, normalization of aerodynamic forces, and fan sensitivity to dynamic pressure.

1. Controller Design

The controller employed in all of the analyses was a three-axis attitude controller. Body-axis pitch rate and its integral were fed back to the nose fan door, body-axis roll rate and its integral were fed back as differential stagger commands to the wing fans, and body-axis yaw rate and its integral were fed back as differential vector commands to the wing fans. The integrals of body-axis rates were fed back rather than actual Euler attitudes as the former could be obtained from body-mounted rate gyros, while the latter would have required assumption of a platform or a vertical gyro.

Body or inertial axes translation velocities were not controlled, as doing so would have required integrating the outputs of body or platform-mounted accelerometers. This was regarded as an unneeded luxury; with the attitude loops operating, the velocity transfer functions were stable (except at hover), and velocities could easily be controlled via pitch and roll attitudes and net fan vector and stagger angles. This is not meant to imply that attitude loops alone eliminated the handling qualities problems produced by having to simultaneously control six degrees of freedom. No stick command or handling qualities tests were made in the study. Rather, attitude loops alone held trim sufficiently well for gust analyses purposes.

Elevator, ailerons, and rudder control surfaces were not employed in the controller as they were ineffectual at low airspeeds and, by test, the XV-5 simulation could successfully be controlled up to 120 ft/sec airspeed with fan control alone.

The controller was designed in one evening on the XV-5 simulation. At low airspeeds the XV-5 attitude and translation responses can be approximated by simple second-order pole pairs with simple cross coupling. Given the inertias, mass, and fan louver and nose fan door effects on thrust vectors, a pencil and paper trial design of the three-axis controller required less than an hour. The attitude rate loops, which in a sense constitute a stability augmentation system (SAS), were designed first. Then the attitude loops were closed with low enough gains to not increase the closed-loop bandwidths above the SAS bandwidths. The controller was then simulated and tested at low and high airspeeds. It was found that higher than trial design gains could be used at the low airspeeds, but lower gains were needed at 120 ft/sec. The system was tuned at the 120-ft/sec condition by starting with very low

gains, increasing the rate gains to instability, backing off on these gains to one-third or less the marginal values, then increasing the attitude gains until satisfactory responses were obtained. No stability problems were encountered with the attitude outer loops. This controller was then tested at the lower-air-speed flight conditions, retuned slightly, retested at high air-speed, retuned, etc., until satisfactory gains were found. Designing the controller for these small airspeeds was not envisioned as being as easy as it turned out to be.

The gains finally selected were:

$$\frac{\partial K_{Nf}}{\partial q} = -1/10 \text{ deg}^{-1}$$

$$\frac{\partial(\beta_{sR} - \beta_{sL})}{\partial p} = -1.5 \text{ deg}/(\text{deg}/\text{sec})$$

$$\frac{\partial(\beta_{vR} - \beta_{vL})}{\partial r} = 1/2 \text{ deg}/(\text{deg}/\text{sec})$$

$$\frac{\partial K_{Nf}}{\partial \dot{q}} = -1/10 (\text{deg}/\text{sec})^{-1}$$

$$\frac{\partial(\beta_{sR} - \beta_{sL})}{\partial \phi} = -2 \text{ deg}/\text{deg}$$

$$\frac{\partial(\beta_{vR} - \beta_{vL})}{\partial \dot{r}} = 1/2 \text{ deg}/\text{deg}$$

2. Reingestion

On the XV-5 the nose fan and the two wing fans are tip driven by the exhaust of a large jet engine mounted in the fuselage. The jet engine is used as a conventional thruster in normal flight. Reingestion is the ingestion of the engine exhaust from the fans after reflection of the exhaust off the ground. Reingestion affects an increase in the inlet temperature of the main jet, a loss in thrust, a decrease in fan power, and a divergent tendency towards rapid sink in hover. Since gusts can blow the reflected fan exhaust into or away from the jet inlet, the severity of reingestion depends upon the gust environment.

Reingestion was not considered in the present study for the following reasons:

- (1) Covariance analyses cannot be run on an unstable airplane, and uncontrolled reingestion is destabilizing (the rise of temperature causes a loss of thrust, a loss of altitude, and a further rise in temperature). To fly in the reingestion region then requires altitude control of thrust or direct thrust-maintenance control.
- (2) The static reingestion model (steady-state temperature rise versus altitude and forward speed) is based on very little data (reference 16), and the reingestion curves are largely a result of engineering common sense and imagination. Further, there is no data for sideways flight and little basis for extrapolating those curves to sideways flight.

- (3) The only data on the dynamics of reingestion are General Electric's engine dynamics and pilot comments that the reingestion time constant seemed to be about 4 seconds, and that decreasing stagger did not lift the airplane. Reingestion is in part a direct reflection of exhaust air off the ground into the engine inlet, with essentially zero transport delay, and in part a gradual heating of the inlet air by mixing the oncoming air with the turbulent fan exhaust. The time constant of the latter effect could be almost anything. Mr. C. R. Stone and Dr. G. Skelton of Honeywell were able to generate reasonable stagger-input commands for both zero- and 4-second fan-to-inlet lags that would produce the cited time constant and apparent stagger hangup.
- (4) The effects of wind gusts on the turbulent fan exhausts are not modeled at all.
- (5) The sum of (2), (3), and (4) is that the model for the airflow causing reingestion is very weak. Therefore, any control system maintaining altitude in reingestion would have to be very fast, fast enough to maintain thrust no matter how small the fan-to-inlet transport lag. This control system cannot be commanded by altitude errors, as the resulting loop through the vehicle mass ($1/\text{ms}^2$) would have a dominant time constant of the order of seconds. Therefore, a direct engine control is required, for example fuel scheduling by inlet or internal engine temperatures.
- (6) If a V/STOL is going to be flown in reingestion, its engine will have to have the excess capacity to quickly lift the airplane no matter what the reingestion temperatures and dynamics are. This implies non-optimum engine performance in hover, but the increased size and fuel requirements must be accepted for safe operation. Therefore, the control authority and response times demanded for successful reingestion engine control can be assumed available. (This does not say they are now available, but rather that they should be if it is intended that the V/STOL be flown in reingestion.)
- (7) Whether or not the fast thrust controller required is within the capabilities of engineering practice today is not known to the writer. However, the rapid response characteristics of modern fluidic sensors are good reason to believe that development of such controllers is reasonable.
- (8) Therefore, reingestion should not be a dynamics problem for a V/STOL designed to hover close to the ground, or, if it is a problem, the dynamics of the problem will depend upon the

capability of the presently-undesigned engine control system and the presently unknown exhaust flow dynamics.

- (S) The purpose of the present study was investigation of gust models, and reingestion was to be considered only in how it might affect specification of gust models. Given comments (4) and (8), there are no reingestion model bases on which to base valid gust model conclusions, and this desire therefore could not be fulfilled.

In summary, any conclusions reached about reingestion would have had to be based on too many arbitrary assumptions to be meaningful.

3. Normalization.

The Ryan XV-5 lift, drag, and wing moment equations used in the analyses employed dimensionless coefficients expressed as functions of the dimensionless ratio of thrust per unit area over slipstream dynamic pressure, where the latter is the sum of ordinary dynamic pressure and thrust per unit area. This normalization was convenient for static data as the wing lift, drag, and moment due to airflow into and out of the wing fans did not have to be separated from the conventional wing lift, drag, and moment, and it was an adequate dynamic approximation for the normal maneuvering purposes for which Ryan derived the model.

This normalization introduces minor anomalies, however, when gusts are introduced. Dynamic pressures vary over the aircraft, and thrust is dependent on dynamic pressure and fan vector and stagger angles. Aerodynamic forces and moments are written as products of (dynamic pressure) x (surface area) x (function of angle of attack) x (dimensionless coefficient),

$$\text{Force} = Q \cdot S \cdot f(\alpha) \cdot g \left(\frac{T/A}{Q+T/A} \right)$$

As the dimensionless coefficients $g(\)$ depend on thrust (T), through thrust aerodynamic forces depend on vector and stagger angles and on dynamic pressure. The aerodynamic forces are thus velocity dependent in four ways, in Q, in the velocity ratio dependence in angle of attack, on the Q used in the $g(\)$ computation, and on the Q used in the thrust calculation.

In the XV-5 equations used in the analyses the dependence of wing aerodynamic terms on vector and stagger angle and on velocity in four ways caused no problems, as the dynamic pressures on each wing were computed individually and the same dynamic pressures were employed individually in the thrust and $g(\)$ calculations (i. e., the fans and wings were treated individually). The anomalies come in through the tail lift and drag forces.

The tail lift and drag forces were also written as functions of the form

$$\text{Force} = Q_T \cdot S \cdot f(\alpha_T) \cdot g \left(\frac{T_W/A}{Q_W + T_W/A} \right)$$

The tail velocities were used in the Q_T and $f(\alpha_T)$ computations, but the aerodynamic coefficients $g(\)$ depended upon average wing dynamic pressure and the average thrust of the two wing fans. The tail forces were thus dependent on wing fan thrusts and on the gusts at the wing (as opposed to those on the tail), neither of which dependencies exist in nature. The aerodynamic force equations were thus over normalized.

These dependencies produced insignificant errors at low airspeeds, as thrust and the $g(\)$ coefficients were insensitive to dynamic pressure changes at low dynamic pressure. (This is not apparent in Ryan's equations, but the strong dependence indicated there can be eliminated by appropriate algebraic manipulations.) At 120 ft/sec airspeed, however, there resulted the dependences on differential vector and stagger

$$\frac{\partial(\text{tail lift})}{\partial(\beta_{vL} - \beta_{vR})} = 2.4 \text{ lbs/deg} \qquad \frac{\partial(\text{tail lift})}{\partial(\beta_{sL} - \beta_{sR})} = 0.4 \text{ lbs/deg}$$

$$\frac{\partial(\text{tail drag})}{\partial(\beta_{vL} - \beta_{vR})} = 0.4 \text{ lbs/deg} \qquad \frac{\partial(\text{tail drag})}{\partial(\beta_{sL} - \beta_{sR})} = 0.06 \text{ lbs/deg}$$

all of which are insignificant, but all of which should be exactly zero.

The only anomalies of any consequence were the differences in the dependence of tail lift and drag on aircraft vertical velocity w and on the tail gust velocity w_T ,

$$\frac{\partial(\text{tail lift})}{\partial w} = -186 \text{ lbs/ft/sec} \qquad \frac{\partial(\text{tail lift})}{\partial w_T} = -360 \text{ lbs/ft/sec}$$

$$\frac{\partial(\text{tail drag})}{\partial w} = -25 \text{ lbs/ft/sec} \qquad \frac{\partial(\text{tail drag})}{\partial w_T} = -56 \text{ lbs/ft/sec}$$

The left- and right-hand figures should be equal. Neither figures are correct, as the $g(\)$ coefficients in the tail lift and drag forces should depend on the dynamic pressure at the tail, and neither of the above derivatives expresses this dependence.

Rederiving Ryan's expressions to correctly represent the tail coefficients dependencies on dynamic pressure was impossible without knowledge of the trim-thrust-dynamic pressure interrelation they had used in generating the coefficients (trim and thrust are not unique functions of airspeed). Further, the anomaly was not discovered until the final month of the study, in the course of determining the cause of the too-large simulator responses, and there was no money left to pursue the issue and repeat the linear analyses. Finally, correcting the anomalies would not change the trends in the XV-5 response dependencies on gust model parameters, so the conclusions reached would not change. The issue therefore was dropped.

4. Fan Dependence on Dynamic Pressure Changes

Intuitively one would expect that the dependence of fan thrust on dynamic pressure changes would be so small as to be ignorable. This hypothesis was tested in the nonlinear simulation by holding the fan dynamic pressures at their trim values while all other dynamic pressures and other variables were allowed to vary normally. The tests were run with head-on and vertical gusts and the shears of those gusts present (side gust velocity was zero). The tests produced pitch rate standard deviations at the 120-ft/sec airspeed flight condition of 0.24 deg/sec with dynamic pressure changes, and 0.16 deg/sec with constant dynamic pressure.

Thrust dependence on dynamic pressure changes is, therefore, not ignorable. This partly accounts for the differences in the tail force derivatives above, and it suggests that the resulting nonlinear thrust dependence on gust velocity at moderate gust amplitudes may not be an ignorable nonlinearity.

REFERENCES

1. Batchelor, G.K., Homogenous Turbulence, Cambridge University Press, Cambridge, 1953.
2. Lumley, J. L. and Panofsky, H. A., The Structure of Atmospheric Turbulence, Wiley, New York, 1964.
3. Chandrasekhar, Hydrodynamic and Hydromagnetic Instability, Oxford University Press, 1961, p. 491.
4. Elderkin, C. E., "Experimental Investigation of the Turbulence Structure in the Lower Atmosphere", Battelle-Northwest Report 329, December, 1966.
5. Haltiner, G. J. and Martin, F. L., Dynamical and Physical Meteorology, McGraw Hill, New York, 1957.
6. Scoggins, et al, "Terrestrial Environment (Climatic) Criteria Guidelines for Use in Space Vehicle Development, 1966 Revision", Marshall Space Flight Center, Huntsville, Ala., May 1, 1966. (NASA TMX-53328).
7. Shiotani, M., "Local Structures of Gusts in High Winds", Physical Science Lab., Nippon Univ. at Namashino, Funabashi, Chiba, Japan, March, 1967.
8. Etkin, B., "Theory of the Flight Airplanes in Isotropic Turbulence; Review and Extension", University of Toronto Report No. 72, February 1961.
9. Parks, W. C., Schattschneider, D. G., and Davis, W. B., "Wind Tunnel Test Report One-Sixth Scale Powered Lift-Fan Model U. S. Army Lift-Fan Research Aircraft", Ryan Aeronautical Company, Report No. 63B092 (AD 647 386), 11 Sept. 1963.
10. "Estimated Static Stability and Control Characteristics", Ryan Aeronautical Company, (AD 639 236).
11. Shear, Jr., H. J., Starkey, H. E., and Utgoff, V. A., "Final Systems Analysis and Flight Simulation Report U. S. Army XV-5A Lift Fan Research Aircraft", Vol. 1, Ryan Aeronautical Company, Report No. 64B129 (AD639 229), 11 Sept. 1964.

12. LaPlant, II, Porter and Baldwin, Robert L., "Flight Evaluation of the XV-5A V/STOL Aircraft", Technical Report No. 66-30, (AD 810 922) Air Force Flight Test Center, March, 1967
13. Shapiro, Jacob, Principles of Helicopter Engineering, McGraw Hill Book Co., 1956.
14. Strand, T., Levinsky, E. S., and Wei, M. H. Y., "Unified Performance Theory for V/STOL in Equilibrium Flight. Part I", Journal of Aircraft, March-April, 1967.
15. Etkin, B., "A Theory of the Response of Airplanes to Random Atmospheric Turbulence", Journal of Aerospace Sciences, July, 1959.
16. "Some Comments on Reingestion - Ames Wind Tunnel Test Results", XV-5A Datum - No. 4, 1 September 1963.
17. "XV-5A Lift Fan Flight Research Aircraft Program; Calculated Installed Power Plant Performance", General Electric Company, Report No. 150 (AD 647 387), September, 1964.
18. Berkhoff, "Hydrodynamics: A Study of Fact, Logic, and Similtude!"

BIBLIOGRAPHY

Appelby, J. F. and Ohmstede, W. D., "Numerical Solution of the Distribution of Wind and Turbulence in the Planetary Boundary Layer", September, 1964, DDC No. 66-424.

Bernstein, A. B., "Dimensional Analysis Applied to the Wind Distribution in the Planetary Boundary Layer", Monthly Weather Review, Vol. 93, October 1965.

Blackador, et al, "Structure of Turbulence and Mean Wind Profiles Within the Atmospheric Boundary Layer", Dept. of Meterology, Penn. St. Univ., University Park, Penn., October, 1960, Astia No. AD259 571.

Blackador, A.K. and Chaplin, A.S., "Wind Profiles, Spectra, and Cross-Spectra Over Homogeneous Terrain", TRECOM 01388-1, U.S. Army Electronics Command, Fort Monmouth, N.J., Feb., 1967.

Busch, N. E. and Panofsky, H. A., "Recent Spectra of Atmospheric Turbulence". To appear in Qtr. Jour. of Royal Meteorological Soc.

Byzova, N. L. (editor), "Investigation of the Bottom 300 Meter Layer of the Atmosphere". Translation from Russian, NASA Scientific & Tech. Info. Facility, No. N66-18972.

Calder, K. L., "Concerning the Similarity Theory of A. S. Monin and A. M. Obukov for the Turbulent Structure of the Thermally Stratified Surface Layer of the Atmosphere". Qtr. Jour., Royal Meteorological Soc., Vol. 92, No. 391, January, 1966.

Cashmore, R. A., "Severe Turbulence at Low Levels Over the United Kingdom", Meteorological Mag., Vol. 95, January, 1966.

Cermack, J. E. and Horn, J. D., "The Tower Shadow Effect", Atm. Sci. Lab., U.S. Army Electronics Command, White Sands, N. M., August, 1966.

Danard, M. B., "On the Dependence of Wind Variability on Surface Wind Speed; Richardson No., and Height Above Terrain", Jour. of Applied Meteorology, Vol. 4, No. 3, June, 1965.

Davidson, et al, "Local Wind Circulations - Final Report, Volume II: Studies of the Field of Turbulence in the Lee of Mountain Ridges and Tree Lines", N. Y. U., September, 1961, AD 275 611.

Derrickson, Jr., R. J., "Structure of Atmospheric Turbulence in the Surface Layer", Ph. D. Thesis, Dept. of Meteorology, MIT, May, 1964.

Dwyer, J. and Tucker, F. L., "Summary of One Year of Data from the Cape Kennedy WIND System", Air Force Cambridge Research Laboratories, Bedford, Mass., August, 1965, AFCRL-65-637.

Gazzola, A., "The Effects of Mountains on Air Currents", Rivista di Meteorologia Aeronautica, No. 1, 1963.

Hanson, F. V., and Hanson, P. S., "The Formation of an Interval Boundary Over Heterogeneous Terrain", U. S. Army Electronics Command, Fort Monmouth, N. J., November, 1965. 66. 348.

Hanson, F. V., "Turbulence Characteristics of the First 62 Meters of the Atmosphere", White Sands Missile Range, December, 1963, AD 426 681.

Hasseltine, C., "Cape Kennedy Low Level Wind Study for September 23-25, 1963". George C. Marshall Space Flight Center, Huntsville, Ala., April, 1964, NASA TM X-53027.

Hsi, G. and Cermak, J. E., "Meteorological-Tower Induced Wind-Field Perturbations" College of Engrg., Colorado St. Univ., Fort Collins, Colo., Oct., 1959, AD 623 946.

Kravchenko, I. M., "On the Wind Profile in the Mean-Ground Layer of the Atmosphere" Bulletin, Geophysics Series, Acad. of Sci. (USSR), March, 1963.

Lemon, et al, "The Energy Budget at the Earth's Surface, Part II", U.S. Dept. of Agriculture, Sept., 1962, AD 505 527.

Lettan, et al, "Studies of the Three-Dimensional Structure of the Planetary Boundary Layer", Dept. of Meteorology, Univ. of Wisc., August, 1961.

Mitchell, L. W., "Wind Shear and Turbulence Over Selected Stations of the Air Force Western Test Range", Air Weather Service (MAC), USAF, Dec., 1966, TR 189.

Monin, A. S., "The Structure of the Wind-Velocity and Temperature Fields in the Atmospheric Surface Boundary Layer". Translated from Trudy, Institut Fiziki Atmosfery, No. 4-5-20, 1962, Akademiia Nauk SSSR.

Monin, A. S., "Empirical Data on Turbulence in the Surface Layer of the Atmosphere", J. of Geophysical Research, Vol. 67, No. 8, July, 1962.

O'Brien, J. J., "Investigation of the Diabatic Wind Profile of the Atmospheric Boundary Layer", J. of Geophysical Research, Vol. 70, No. 10, May, 1965.

Obukov, A. M., "Some Specific Features of Atmospheric Turbulence", J. of Fluid Mech., Vol. 13, 1962.

Panofsky, et al, "The Relation Between Eulerian Time and Space Spectra", Qtr. J., Royal Meteorological Soc., Vol. 79, 1958.

Panofsky, H. A. and McCormick, R. A., "The Spectrum of Vertical Velocity Near the Surface". Presented at JAS 27th Annual Meeting, New York, IAS Report No. 59-6.

Panofsky, H. A., "Scale Analysis of Atmospheric Turbulence at 2 Meters", Qtr. J., Royal Meteorological Soc., Vol. 88, No. 375, January 1962.

Panofsky, H. A. and Townsend, A. A., "Change of Terrain Roughness and the Wind Profile", Royal Meteorological Soc., Qtr. J., Vol. 90, April, 1964, pp. 147-155.

Panofsky, H. A. and Prasad, B. . "Similarity Theories and Diffusion",
Int. J. Air Wat. Poll. Pergamon Press, 1965, Vol. 9, pp. 419-430.

Pond, et al, "Turbulence Spectra in the Wind Over Waves", J. of
Atmospheric Sciences, Vol. 20, July, 1963.

Pond, et al, "Spectra of Velocity and Temperature Fluctuations in the
Atmospheric Boundary Layer Over the Sea", J. of Atmospheric Sciences,
Vol. 23, No. 4, July, 1966.

Potter, T. D. , "Wind Structure in the Lowest 1500 Feet in Convective
Conditions" PhD Thesis, Dept. of Meteorology, Penn. St. Univ. ,
University Park, Penn. , 1962.

Pritchard, F. E. , "The Turbulence and Terrain Environments Affecting
Low-Altitude, High Speed Flight", Cornell Aeronautical Laboratory,
Buffalo, N. Y. , July, 1966.

Singer, I. A. , "A Study of the Wind Profile in the Lowest 400 Feet of the
Atmosphere" Brookhaven National Laboratory, Prog. Report No. 2, Jan. ,
1959, Prog. Report No. 3, October, 1959, Prog. Report No. 4, Jan. , 1960.

Tsvang, et al, "Measurement of Some Properties of Turbulence in the
Lowest 300 Meters of the Atmosphere", Bulletin, Geophysics Series, Acad.
of Sci. (USSR), 1963.

Zilitinkevich, S. S. , "Non-stationary Turbulent Regime in the Surface Layer
of the Atmosphere". Translation from Russian, Sept. , 1965, DDC No. AD
628 972.

APPENDIX I
A DYNAMIC MODEL OF THE RYAN XV-5A AIRCRAFT

ABSTRACT

A dynamic representation of the Ryan XV-5A V/STOL was developed for use in the V/STOL gust investigation. The model differs from Ryan's model in the re-expression of continuous angle-of-attack dynamics, in re-expression of aerodynamic derivatives in a simpler form, and in one fan power equation.

INTRODUCTION

The objective of developing a dynamic model of the XV-5A was to provide a test vehicle for evaluating the relative importance of various gust model descriptors. This objective implies that the wind loads must be distributed over the vehicle with reasonable accuracy, and that full circles of angle-of-attack and sideslip must be taken into account. These implications follow from the importance of gust shears across the wing and the importance of wing-to-tail transport delays, and also from likelihood calculations which show occasional local airspeed reversals at gust amplitudes and airspeeds where the ratio of r. m. s. gust amplitude to mean airspeed is large.

The XV-5 model must therefore contain nonlinear aerodynamics, and this dictates that wind tunnel and flight test data be employed to obtain reasonably accurate force estimates. Present aerodynamic theory is inadequate for representing fan-in-wing vehicles of the XV-5A type.

Once forced to the wind tunnel data, there are still problems in trying to separate the cause and effect relations in the various force terms to permit adding terms not accounted for in the static tunnel data. The effects are total aerodynamic forces and moments, while the causes are mixtures of fan and ordinary aerodynamic effects.

The principal assumptions made in treating the total aerodynamic loads are, first, that they can be separated into fan loads, ordinary aerodynamic loads, and loads due to interferences between the fans and ordinary aerodynamics. It is next assumed that the fan loads can be estimated, so that they can be removed or added as necessary. The ordinary aerodynamic effects and the interference effects are then lumped together, and it is further assumed that unsteady effects (Kussner and Wagner delays) operate on the combined effects in the same manner as for ordinary aerodynamic forces alone.

Insofar as separating the fan and aerodynamic forces, there are no errors introduced by their separation as far as steady-state (static) forces and moments. Dynamic derivatives such as the wings contribution to C_{M_q} will generally be in error as the unsteady dynamics assigned may distribute these contributions inaccurately.

Wind tunnel data are generally available in the linear range (small angles-of-attack) and at ± 90 -degree extremes, and it is necessary to assume the load characteristics at intermediate angles of attack. The procedure used to connect the data was to fit the linear and extreme data separately and to rely on continuity for the transition between. The assumed transitions may well be inaccurate for rapid changes in local airspeed angles, but there are no data against which the validity of the assumed transitions may be tested.

Regarding the simplification of the expressions for the aerodynamic coefficients, at low airspeeds lift is a much stronger function of thrust than of ordinary dynamic pressure effects. Ryan chose to emphasize this dependence by expressing the coefficients as functions of the ratio of thrust per unit fan area to slip stream dynamic pressure, where slipstream dynamic pressure is the sum of ordinary dynamic pressure and thrust per unit fan area. In the present study the emphasis was on gusts and therefore on the dynamic pressure term, and it was therefore convenient to manipulate Ryan's expressions to be functions of dynamic pressure over slipstream dynamic pressure. Ryan's graphical representations of the aerodynamic derivatives were then replaced by ratios of polynomials in this new variable. This does not constitute a change in Ryan's model, and it permitted cancellation of thrusts and dynamic pressures appearing in both the numerators and denominators of the load expressions and thereby lead to simpler expressions.

As discussed in Section VI of the main body of this report, Ryan's writing of tail derivatives in terms of thrust lead to some minor anomalies in force expressions. These anomalies were not known early in the study, at the time this model was generated.

The change in the fan power equation was an error. The nose fan efficiency equation was used for both wing fans to convert zero-speed thrust to actual thrust. The zero-speed thrusts were computed correctly. This error was not detected until the writing of this final report. The effect of the error is to make the wing fans less sensitive to dynamic pressure variations at high airspeeds than they actually are. It will not change any of the gust model conclusions reached nor change the data in Section V to any extent. The non-linear data in Section VI would show slightly stronger roll and yaw responses at the 120-ft/sec airspeed flight condition.

DETAILS OF MODEL GENERATION

Sign Conventions

The sign conventions chosen for the equations obey the right-hand rule. They are:

x, y, z body axes	positive forward, out the right wing, and down.
u, v, w	vehicle velocities in the x, y, z body axes, positive forward, out the right wing, and down respectively, referenced to a coordinate system moving downwind with the mean wind.
F_x, F_y, F_z	forces in the x, y, z body axes, positive forward, out the right wing, and down respectively.
p, q, r	angular velocities about the body axes, in body coordinates, all obeying the right-hand rule. p = roll rate positive right wing down, q = pitch rate, positive nose up, r = yaw rate, positive nose right.
L, M, N	moments about x, y, z body axes, with same signs as p, q, r respectively.
ϕ, θ, ψ	Euler angles between body axes and earth-fixed axes. Beginning with the vehicle aligned in the earth-fixed axes, the order of rotation is first, ψ radians about the aircraft z axis, then θ radians about the y axis, then ϕ radians about the x axis, positive being the directions of positive p, q, r respectively.
h	altitude, positive up
u_g, v_g, w_g	gusts at a point in body axes, positive forward, out right wing, and up respectively (in conformance with meteorological convention).
u_y, w_y	shear of head-on and vertical gusts across wing, positive with gust on left wing larger than that on right.
δ_e	elevator angle, positive down
δ_a	differential aileron angle, positive left wing down.

δ_r	rudder angle, positive left
β_v	vector angle on either wing fan, positive to rear
β_s	stagger angle on either wing fan, positive to choke thrust
δ_{N_f}	nose fan door angle, positive to produce nose up moment.

Inertial and Geometric Terms

With these definitions the equations of motion for the vehicle are written

$$m\dot{u} = \Sigma F_x + m(vr-wq)$$

$$m\dot{v} = \Sigma F_y + m(wp-ur)$$

$$m\dot{w} = \Sigma F_z + m(uq-vp)$$

$$\dot{p}I_x - \dot{r}J_{xz} = \Sigma L + (I_y - I_z)qr + J_{xz}pq$$

$$\dot{q}I_y = \Sigma M + (I_z - I_x)pr + (r^2 - p^2)J_{xz}$$

$$\dot{r}I_z - \dot{p}J_{xz} = \Sigma N + (I_x - I_y)pq - J_{xz}qr$$

where

$$m = \text{mass} = 286 \text{ slugs}$$

$$I_x = \text{moment of inertia about x axis} = 4,252 \text{ slug ft}^2$$

$$I_y = \text{moment of inertia about y axis} = 15,139 \text{ slug ft}^2$$

$$I_z = \text{moment of inertia about z axis} = 17,418 \text{ slug ft}^2$$

$$J_{xz} = \text{xz product of inertia} = 919 \text{ slug ft}^2$$

The Euler angular rates in terms of the body axes are:

$$\dot{\phi} = p$$

$$\dot{\theta} = q \cos \phi - r \sin \phi$$

$$\dot{\psi} = (r \cos \phi + q \sin \phi) \cos \theta - p \sin \theta$$

The components of the gravity force in the body axes are

$$x \text{ axis: } -mg \sin \theta$$

$$y \text{ axis: } mg \cos \theta \sin \phi$$

$$z \text{ axis: } mg \cos \theta \cos \phi$$

and the altitude rate of the vehicle is

$$\frac{dh}{dt} = u \sin \theta - (w \cos \phi + v \sin \phi) \cos \theta$$

positive up.

Aerodynamic Forces and Moments

Dimensionless Systems -- Ryan found it convenient to express the various aerodynamic terms as functions of two sets of dimensionless numbers. Both can be derived with the π theorem of dimensional analysis.

Assume (for constant angles-of-attack α and sideslip β) that

$$L = f[\rho, V, A, T_{000}]$$

where

$$L = \text{lift} \sim \left\{ \frac{ML}{T^2} \right\}$$

$$\rho = \text{air density} \sim \left\{ \frac{M}{L^3} \right\}$$

$$A = \text{reference area} \sim \{L^2\}$$

$$T_{000} = \text{fan thrust (at zero speed, vector, and stagger - a known function of fan speed)} \sim \left\{ \frac{ML}{T^2} \right\}$$

{ } ~ indicates dimensions

M ~ mass

L ~ length

T ~ time

f is a continuous, single-valued function of positive arguments ρ, V, A, T_{000} .

For later use define

$$Q = \frac{1}{2} \rho V^2 \Delta \quad \text{dynamic pressure}$$

$$A_F = \text{fan area}$$

$$Q^S = Q + \frac{T_{000}}{A_F} \Delta \quad \text{slipstream dynamic pressure}$$

$$T_c^S = \frac{T_{000}}{Q^S A_F} \Delta \quad \text{slipstream thrust coefficient}$$

$$T_c = \frac{T_{000}}{QA} \Delta \quad \text{thrust coefficient}$$

The π theorem yields (using ρ, V, A as basis vectors)

$$L = \rho V^2 A g \frac{T_{000}}{\rho V^2 A} \Delta = QA g \frac{T_{000}}{QA} = QA g [T_c]$$

One could now let α and β vary to get

$$L = QAC_L [T_c, \alpha, \beta]$$

which shows now that the ordinary aerodynamic coefficients are dependent on the thrust coefficient T_c .

For forces such as lift, the above two formulae place undue emphasis on ordinary dynamic pressure at low speeds. Under these conditions the lift is a much stronger function of fan thrust. Ryan chose to emphasize this dependence. To do this they used the definitions and the fan area as a reference to get

$$Q = Q^S (1 - T_c^S)$$

$$T_c = \frac{T_c^S}{1 - T_c^S}$$

$$L = Q^S A_F (1 - T_c^S) g \left[\frac{T_c^S}{1 - T_c^S} \right] \triangleq Q^S A_F h [T_c^S]$$

The function h is continuous for $T_c^S < 1$ ($Q \neq 0$). At zero dynamic pressure the lift force is due solely to the fans and can be calculated. Hence, by special definition the latter formula can be generally used.

Letting the angles of attack and sideslip again vary, one obtains

$$L = Q^S A_F C_L^S [T_c^S, \alpha, \beta]$$

Identical arguments can be used to get

$$\begin{aligned} M &= QA \bar{c} C_M [T_c^S, \alpha, \beta] = QA \bar{c} C_M^S [T_c^S, \alpha, \beta] \\ &= Q^S A_F D_F C_M^S [T_c^S, \alpha, \beta] \end{aligned}$$

where

M = pitching moment

\bar{c} = mean aerodynamic chord

D_F = fan diameter

Where forces or moments are primarily Q dependent, the common system was used. For strongly fan dependent forces or moments the latter was used.

It was found convenient in the present study to write the aerodynamic coefficients in terms of $1 - T_c^S$, rather than T_c^S . The former is simply

$$\begin{aligned} 1 - T_c^S &= 1 - \frac{T_{000}/A_F}{Q + T_{000}/AF} \\ &= \frac{Q}{Q_S} \end{aligned}$$

The conveniences this purchased were more accurate table lookups of fan data at low dynamic pressures ($1 - T_c^S$ contains the same information as T_c^S , but in fewer significant figures), and simplification of the aerodynamic force terms themselves. $C_{m_\alpha}^S$, for example, could be approximated by

$$C_{m_\alpha}^s = \frac{1.46(1-T_c^s)}{0.0923+(1-T_c^s)} \text{ rad}^{-1}$$

which produced the moment coefficient

$$Q^s A_F D_F C_{m_\alpha}^s = Q A_F D_F 1.46 / (0.0923 + (1 - T_c^s))$$

The aerodynamic coefficient graphs fitted in this manner with ratios of polynomials in $1 - T_c^s$ were:

$$C_{L_\alpha}^s = 14.3(1 - T_c^s) \text{ rad}^{-1} = \text{lift curve slope}$$

$$\alpha_{L_0}^s = -0.265 - 0.35(1 - T_c^s) \text{ rad} = \text{angle-of-attack for zero lift}$$

$$C_D^s = \frac{0.825(1 - T_c^s)}{0.045 + 1 - T_c^s} = \text{drag coefficient}$$

$$C_{m_\alpha}^s = \frac{1.46(1 - T_c^s)}{0.923 + 1 - T_c^s} \text{ rad}^{-1} = \text{pitch derivative, forward flight}$$

$$C_{m_0}^s = \frac{0.313(1 - T_c^s)}{0.0161 + 1 - T_c^s} = \text{forward flight pitching bias}$$

$$C_{m_\alpha}^s = 22.9(1 - T_c^s) \text{ rad}^{-1} = \text{pitch derivative, rearward flight}$$

$$C_{m_{180\text{Aero}}}^s = -9(1 - T_c^s) = \text{rearward flight pitching bias}$$

Other Changes -- The only other changes made in Ryan's data were to treat the two wings separately. The forces on each wing and each wing fan were calculated individually using the local velocity on the wing. This is (c. g. velocity less gust velocity) plus (angular rate less gust shear) times a 6-foot moment arm. The forces on the tail were calculated with pitch rate times an 18.22-foot moment arm added to the vertical velocity, and roll rate

times a 4-foot arm and yaw rate times an 18.22-foot arm added to the tail side velocity. These additions permitted dropping C_{N_p} , C_{L_p} , etc., from the simulated equations.

x and z Wing Forces -- The wing lift and drag forces were calculated as follows. The wing velocities were:

$$\text{Right wing velocities: } u_R = u - u_{cg} - 6(r - u_y)$$

$$v_R = v - v_{cg}$$

$$w_R = w + w_{cg} + 6(p - w_y)$$

where the subscript cg denotes the cg gusts, and

$$\text{Left wing velocities: } u_L = u - u_{cg} + 6(r - u_y)$$

$$v_L = v - v_{cg}$$

$$w_L = w - w_{cg} - 6(p - w_y)$$

$$\text{Either wing: } v_1 = u^2 + w^2, Q = \frac{1}{2} \rho v_1^2$$

$$\alpha = w/v_1$$

$$\alpha_{LIM} = \begin{cases} \alpha & \text{for } |\alpha| < 0.35 \text{ rad} \\ 0.35 \text{ sgn } w & \text{for } |\alpha| > 0.35 \text{ rad} \end{cases}$$

where $\text{sgn } x = 1$ if $x > 0$ and -1 if $x < 0$.

$$\text{LIFT} = Q \frac{A_F}{2} 14.3 (\alpha_{LIM} - \alpha_{L_0}^S) \left(1 + \left(0.0148 + \frac{0.0134(1 - T_c^S)}{0.057 + (1 - T_c^S)} \right) \beta_v \text{sgn } u \right)$$

where β_v is the vector angle in degrees,

$$\text{DRAG} = Q \frac{A_F}{2} \frac{0.825}{0.045 + (1 - T_c^S)}$$

$$F_x = \frac{w}{v_1} \text{LIFT} \operatorname{sgn}(u) - \frac{u}{v_1} \text{DRAG}$$

$$F_z = \frac{|u|}{v_1} \text{LIFT} - \frac{w}{v_1} \text{DRAG}$$

Both of these forces are multiplied by phasing functions and passed through Wagner lags below (the phasing functions are introduced to take angle-of-attack nonlinearities into account).

For vertical ascent or descent, the non-Wagner-lagged z force is

$$F_{zNL} = -\frac{(Q_L + Q_R)}{2} A_F 0.14 \operatorname{sgn} \frac{(\alpha_L + \alpha_R)}{2}$$

where the R, L subscripts denote values for the right and left wing, respectively. This term is multiplied by a phasing function below.

Pitch Due to Wings and Fuselage -- Both wings were treated together in calculating the pitching moments. Letting the subscripts R, L denote the left and right wing,

$$\text{Forward Flight: } Q_1 = \frac{1}{2}(Q_L + Q_R) \quad \alpha_w = \frac{1}{2}(\alpha_{LLIM} + \alpha_{RLIM})$$

$$M_A = Q_1 A_F D_F \left(\frac{1.46 \alpha_w}{0.0923 + (1 - T_c^S)} + \frac{0.313}{0.0161 + (1 - T_c^S)} \right)$$

This term is multiplied by a phasing function and passed through a Wagner lag below

$$\text{Airplane sinking vertically} = M_1 = Q_1 A_F D_F 6.5$$

$$\text{Airplane rising vertically} = M_2 = -Q_1 A_F D_F 10$$

$$\text{Rearward Flight} = M_3 = -Q_1 A_F D_F (9 + 22.9 \alpha_w)$$

These terms are multiplied by phasing functions below, but are not Wagner lagged.

Side Force on Fuselage --

$$v_2 = \sqrt{\frac{(u_L + u_R)^2}{2} + \frac{(v_L + v_R)^2}{2}} \quad Q_2 = \frac{1}{2} \rho v_2^2$$

$$\beta = \frac{v_L + v_R}{2v_2}$$

$$\begin{aligned} \beta_{L1M} &= \beta \text{ for } |\beta| < 0.35 \text{ rad} \\ &= 0.35 \operatorname{sgn} \beta \text{ for } |\beta| > 0.35 \text{ rad} \end{aligned}$$

$$\begin{aligned} f_{15} &= 0 \text{ for } |\beta| < 0.35 \\ &= 0.8 \text{ for } |\beta| > 0.9 \\ &= 1.455 |\beta| - 0.508 \text{ for } 0.35 < |\beta| < 0.9 \end{aligned}$$

$$F_{Y_{FUS}} = -Q_2 S_w [2.07\beta + 0.006 \delta_A - 2.64 f_{15} \operatorname{sgn} \beta]$$

where δ_A is the differential aileron deflection in degrees and S_w is the wing area, 260 ft².

Longitudinal and Normal Forces on Tail -- The tail velocities are

$$u_T = u - u_{TG}$$

$$v_T = v - v_{TG} + 4p - 18.22r$$

$$w_T = w + w_{TG} + 18.22q$$

where the subscript TG denotes a tail gust.

$$v_{1T} = u_T^2 + w_T^2 \quad Q_{1T} = \frac{1}{2} \rho v_{1T}^2$$

The tail downwash angle ϵ_T and the tail efficiency factor K_{η_T} are defined by the direction of flight and the wing angle of attack. Define

$$\begin{aligned} f_{17} &= 1 \text{ for } |\alpha_w| < 0.35 \\ &= 0 \text{ for } |\alpha_w| > 0.52 \\ &= 3.06 - 5.88 |\alpha_w| \text{ for } 0.35 < |\alpha_w| < 0.52 \end{aligned}$$

Then for $\frac{u_L + u_R}{2} > 0$,

$$\epsilon_w = (-0.35(1 - T_c^S) + 0.175 + 0.40 w) f_{17} \text{ rad}$$

$$K_{\eta_T} = 1 - (0.1 + 0.429 \alpha_w) f_{17}$$

while for $\frac{u_L + u_R}{2} < 0$

$$\epsilon_w = 0$$

$$K_{\eta_T} = 1$$

The angle of the on-rushing air at the tail with respect to the vehicle x fuselage axis is

$$\alpha_T = w_T / v_{1T} + \epsilon_w$$

while the angle between the on-rushing air and the tail surface is

$$\alpha_{T_S} = \alpha_T + (I_t + 0.435 \delta e) / 57.3$$

where I_t is the tail incidence angle and δe is the elevator angle, both in degrees. Taking into account the effect of elevator position on the region of tail effectiveness, for

$$u_T > 0, \text{ define } \alpha_{T_{L1M}} = \alpha_{T_S} \text{ for } |\alpha_{T_S}| < 0.35 \text{ rad}$$

$$\alpha_{T_{L1M}} = 0.35 \text{ sgn } |\alpha_{T_S}| \text{ for } |\alpha_{T_S}| > 0.35 \text{ rad}$$

and for

$$\begin{aligned}
 u_T < 0 \text{ define } \alpha_{T_{L1M}} &= \alpha_{T_S} \text{ for } -0.175 + \frac{\delta e}{57.3} < \alpha_{T_S} < 0.175 + \frac{\delta e}{57.3} \\
 &= 0.35 + \frac{1 + \alpha_{T_S} (0.175 - \delta e / 57.3)}{0.825 + \frac{\delta e}{57.3}} \text{ for } \alpha_{T_S} < -0.175 + \frac{\delta e}{57.3} \\
 &= 0.35 - \frac{1 - \alpha_{T_S} (0.175 - \delta e / 57.3)}{0.825 - \frac{\delta e}{57.3}} \text{ for } 0.175 + \frac{\delta e}{57.3} < \alpha_{T_S}
 \end{aligned}$$

The lift on the tail is then

$$LIFT = Q_{1T} S_T K_{\eta_T} 3.04 \alpha_{T_{L1M}}$$

and the drag is

$$DRAG = Q_{1T} S_T K_{\eta_T} (0.015 + 1(3.04 \alpha_{T_{L1M}}))$$

The x and z force components are

$$F_{xT} = (LIFT \sin \alpha_T - DRAG \cos \alpha_T) \sin u_T$$

$$F_{zT} = -LIFT \cos \alpha_T - DRAG \sin \alpha_T$$

Both of these terms are Wagner Lagged below.

Tail Side Force --

$$v_{2T} = \sqrt{u_T \cdot u_T + v_T \cdot v_T} \quad Q_{qT} = \frac{1}{2} \rho v_{2T}^2$$

$$\beta_T = v_T / v_{2T} \text{ for } u_T < 0$$

$$= v_T / v_{2t} - 0.00247 \delta r \text{ for } u_T > 0$$

where δr is the rudder angle in degrees. The saturation β_T , taking into account the effect of rudder angle in rearward flight, is for $u_T > 0$,

$$\begin{aligned}\beta_{T_{L1M}} &= \beta_T \text{ for } |\beta_T| > 0.265 \text{ rad} \\ &= 0.265 \operatorname{sgn} \beta_T \text{ for } |\beta_T| > 0.265 \text{ rad}\end{aligned}$$

and for $u_T < 0$,

$$\begin{aligned}\beta_{T_{L1M}} &= \beta_T \text{ for } -0.175 - \frac{\delta r}{57.3} < \beta_T < 0.175 - \frac{\delta r}{57.3} \\ &= -0.265 + \frac{(1+\beta_T)(0.09-\delta r/57.3)}{0.825-\delta r/57.3} \text{ for } \beta_T < -0.175 - \delta r/57.3 \\ &= 0.265 - \frac{(1-\beta_T)(0.09+\delta r/57.3)}{0.825+\delta r/57.3} \text{ for } 0.175 - \delta r/57.3 < \beta_T\end{aligned}$$

The side force on the tail is

$$Y_{vT} = -Q_{2T} S_w 0.79 \beta_{T_{L1M}}$$

which is Wagner lagged. To account for the additional side force at $\beta_T = 90^\circ$, to Y_{vT} is added

$$Y_{vTNL} = -Q_{2T} S_w 0.302 f_{28}$$

where

$$\begin{aligned}f_{28} &= 0 \text{ for } |\beta_T| < 0.35 \\ &= 0.8 \text{ for } |\beta_T| < 0.9 \\ &= 1.455 |\beta_T| - 0.508 \text{ for } 0.35 < |\beta_T| < 0.9\end{aligned}$$

This term will not be Wagner lagged.

Yawing Moments -- The yawing moments, in addition to those due to the side force on the tail and the differential x wing forces, are simply

$$\begin{aligned}N_3 &= -Q_2 S_w 5.9 \beta_{L1M} - Q_1 S_w b C_{n\delta_A} \delta_A \\ &= -Q_2 S_w 5.9 \beta_{L1M} - Q_1 (2.4(1-T_c^S) - 3.18) \delta_A\end{aligned}$$

This term is not Wagner lagged.

Rolling Moments -- The rolling moments, in addition to those due to the side force on the tail and the differential z wing forces, are

$$\begin{aligned} L_1 &= -Q_1 S_w b C_{l\beta} \beta_{L1M} \\ &= -Q_1 16.7 \beta_{L1M} \end{aligned}$$

which term is lagged, plus

$$L_2 = Q_1 6.83 \delta a + Q_2 S_w 8.75 f_{15} \operatorname{sgn} \beta$$

where f_{15} is as defined for the side force on the fuselage, plus a component L_3 for the shear across the wing when the vehicle is falling or rising.

$$L_3 = - \left[\int_{-b/2}^{b/2} \frac{1}{2} \rho \left(\frac{w_L + w_R}{2} + y(p - w_y) \right)^2 \bar{c} y dy \right] \operatorname{sgn} (p - w_y)$$

For no zero-vertical velocity point on the wing.

$$\left| \frac{w_L + w_R}{2} \right| > \frac{b}{2} |p - w_y|$$

$$L_3 = - \left| \frac{\rho \bar{c} b^3}{12} \frac{(w_L + w_R)}{2} \right| (p - w_y) \operatorname{sgn} (p - w_y)$$

while for

$$\left| \frac{w_L + w_R}{2} \right| < \frac{b}{2} |p - w_y|$$

$$L_3 = - \left| \frac{\rho \bar{c}}{4} - \frac{w_1^4}{3p_1^2} + \frac{w_1^2 b^2}{2} + \frac{p_1^2 b^4}{16} \right| \operatorname{sgn} p$$

where $w_1 = \frac{w_L + w_R}{2}$, $p_1 = p - w_y$. This term will be multiplied by a phasing function below so that it comes in only around 90 degrees angle of attack.

Wagner Lags -- Nine of the above aerodynamic forces and moments are passed through aerodynamic lags. Since the gusts have been lumped with the local vehicle velocities in computing local air velocities, the Kussner and Wagner lags are in effect identical.

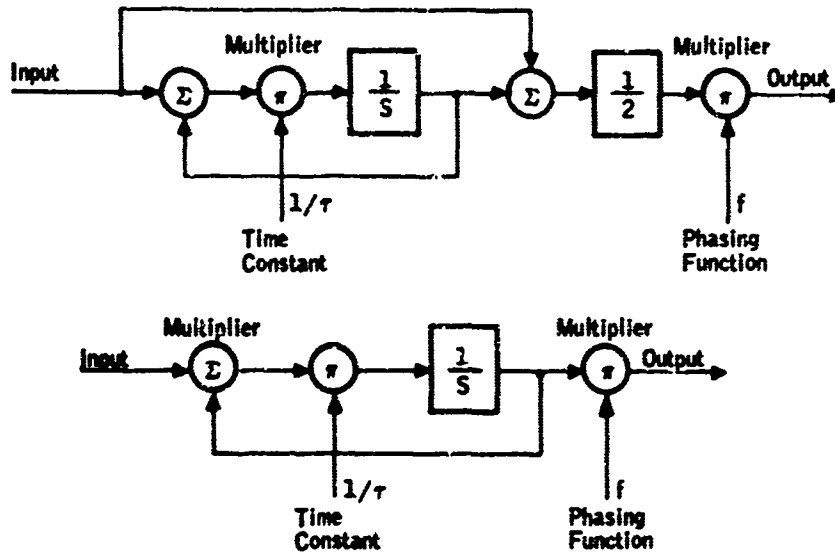
Eight of the Wagner lags are of the form

$$\frac{1+0.5\tau S}{1+\tau S} \cdot f,$$

while the ninth, M_A , is run through

$$\frac{1}{1+\tau S} \cdot f$$

The actual schematics for these filters are:



The time constants, phasing functions, and output notations used are

<u>Input</u>	<u>Output</u>	<u>1/τ</u>	<u>f</u>
F _{xR}	F _{xRL}	f _{1R}	f _{4R}
F _{zR}	F _{zRL}	f _{1R}	f _{4R}
F _{xL}	F _{xLL}	f _{1L}	f _{4L}
F _{zL}	F _{zLL}	f _{1L}	f _{4L}
F _{xT}	F _{xTL}	f _{1T}	f ₁₇
F _{zT}	F _{zTL}	f _{1T}	f ₁₇
Y _{vT}	Y _{vTL}	f _y	1
L ₁	L _{1L}	f _{1M}	1
M _A	M _{AL}	f _{1M}	f ₁₇

where, for either wing,

$$\begin{aligned}
 f_4 &= 1 \text{ for } |w/v_1| < 0.35 \\
 &= 0 \text{ for } |w/v_1| > 0.9 \\
 &= 1.464 - 1.11 |w/v_1| \text{ for } 0.35 < |w/v_1| < 0.9
 \end{aligned}$$

$$f_1 = \frac{v_1}{c} / (f_4 + 0.001)$$

The pitch and roll 1/τ function f_{1M} is the average of that for the wings

$$f_{1M} = \frac{1}{2} (f_{1R} + f_{1L})$$

f₁₇ was described in the tail x and z force discussion. f_{1T} is

$$\begin{aligned}
f_{1T} &= \frac{v_{1T}}{\bar{c}_{TAIL}} \quad \text{for } \left| \frac{w_T}{v_{1T}} \right| < 0.35 \\
&= 10^4 \frac{v_{1T}}{\bar{c}_{TAIL}} \quad \text{for } \left| \frac{w_T}{v_{1T}} \right| > 0.9 \\
&= \frac{v_{1T}}{\bar{c}_{TAIL}} \quad 18200 \left| \frac{w_T}{c_{1T}} \right| - 0.35 \quad \text{for } 0.35 < \frac{w_T}{v_{1T}} < 0.9
\end{aligned}$$

f_y is

$$f_y = f_{1T} / (1 - 1.24 f_{28})$$

f_{28} was described in the tail side force discussion.

Note that for all but the side force and roll terms, these phasing functions a) kill the lagged responses at 90-degree angle-of-attack and b) force the integrators to store the 90-degree angle-of-attack input magnitudes. The roll phasing function does only b), and the side force phasing function does b) for 90-degree sideslip angles. When angle-of-attack or sideslip angle is reduced to less than 0.35 radian from $\pi/2$ radians, then, the integrators are carrying the 90-degree values plus what they pick up as the angles are reduced.

The representation is reasonably accurate provided transitions between linear and nonlinear regions are not made at frequencies larger than those corresponding to the Wagner-Kussner time constants. A representation avoiding the approximation would be considerably more complex.

Fan Forces and Moments

The fan force and moment expressions employed were generated by table lookups and iterative calculations in the manner indicated in Ryan's report, reference 11. The only changes made in Ryan's expressions were reversal of the sign of the x force due stagger angle at negative vector angle, omission of Ryan's ram-drag terms, and the above mentioned fan power error. The ram-drag terms were dropped under the assumption that the fan force is normal to the actuator disk. This is the Glauert assumption of propeller theory (references 13 and 14), and it is corroborated in the XV-5A case by the data in Figures 4.64 and 4.65 of reference 9 which show no yaw moment or side force due to lateral translation of the nose fan. This is also implied by Ryan's main fan equation (reference 11, pg. 80).

Ryan's data on the correction of longitudinal and normal forces and pitching moment due to vector and stagger angle are applicable only to forward flight. Considering the physics of the airflow, that the fan efflux is rearward for positive vector, but the incoming air direction depends upon the direction of travel, there is no way to extend their data to zero or negative x velocities. Since the x velocities are small in rearward flight and the corrections are small for small velocities, using the forward velocity corrections in rearward flight introduces little error, with the exception of one term, the drag correction due to increased stagger. This term chokes the inflow and efflux. Assuming the magnitude of the x velocity is small, the principal effect of increased stagger is to decrease the rearward efflux for positive vector, or forward efflux for negative vector. This term was therefore multiplied by $\text{sgn}(\beta_v)$.

$$\text{DRAG}(\beta_s) = -Q^s \frac{A_F}{2} \Delta C_x(\beta_s) \cdot \text{sgn}(\beta_v)$$

where

$$\text{sgn}(\beta_v) = 1 \text{ for } \beta_v > 0$$

$$0 \text{ for } \beta_v = 0$$

$$-1 \text{ for } \beta_v < 0$$

This appears reasonable for small velocities, and for large forward velocities β_v is positive, so the correction does not change anything in forward flight.

The error in the term was detected while flying the simulated vehicle backwards. With $\beta_v = 0$ and the nose up, decreasing the stagger increased the x velocity (decreased its magnitude), when it should have done the opposite or nothing at all.

Fan Thrust -- The nose and two wing fans were treated individually. Each of the wing fans required iterative calculation as each thrust is a function of T_c^s for that fan, and T_c^s is in turn a function of that thrust.

Let the subscript R denote the right wing fan and L the left. Taking the right fan first, the fan thrust is

$$E_{zR} = -\frac{A_F}{2} \cdot \frac{T_{\text{oo}R}}{A_F} \cdot g[T_c^s R]$$

where

$$g[T_c^s] = 1 + (1 - T_c^s)^2 (15(1 - T_c^s) - 4.8)$$

is a polynomial fit to the fan coefficient ratio, Figure 38, page 40, reference 11. This expression is the nose fan efficiency. The wing fan efficiencies

$$g = C_p^s / C_{p_o} \Big|_{\beta_v = 0}$$

should have been used instead of the expression above for the wing fans. E_{zR} is then defined by Q_R , the right fan dynamic pressure, and T_{ooR} , as

$$T_{cR}^s = T_{ooR} / (A_F \cdot Q_R + T_{ooR})$$

From equation 1F, page 80, reference 11, T_{ooR} is

$$\frac{T_{ooR}}{A_F} = (P_F)^{2/3} \frac{\rho^{1/3}}{A_F^{2/3}} \cdot \left[\frac{C_{pR}^s}{C_{p_o}^s} + \frac{\Delta C_{p\beta_{sR}}^s}{C_{p_o}^s} \right]^{-2/3}$$

where P_F is fan power (a controllable input), $C_{p_o}^s = 1$, C_{pR}^s is a table lookup function of T_{cR}^s and the vector angle β_{vR} , and $\Delta C_{p\beta_{sR}}^s$ is a function of stagger angle. C_{pR}^s is given by Figure 35 and $\Delta C_{p\beta_{sR}}^s$ by Figure 36, both page 39, reference 11. The latter curve was fit by

$$\Delta C_{p\beta_{sR}}^s = -0.00075(\beta_{sR})^2$$

To solve these equations a starting value of

$$T_{cR}^s = \frac{250}{Q+250}$$

was assumed and $\Delta C_{p\beta_{sR}}^s$ was calculated. C_{pR}^s was then found by table lookup, T_{ooR}/A_F was then calculated, and

$$T_{cR}^s = \frac{T_{000R} / A_F}{Q_R + T_{000R} / A_F}$$

was then calculated. This process was iterated until $1 - T_{cR}^s$ converged to within 0.0001 of its previous value. It was found experimentally that this iteration converged rapidly even if $T_{cR}^s = 1$ was assumed as a starting value.

The left fan thrust calculations were the same as the above with the subscript R replaced by L.

The nose fan calculations were only slightly different. The nose fan thrust was

$$E_{FzNF} = - T_o \cdot K_{NF} \cdot g [T_c^s A]$$

where K_{NF} was the nose fan efficiency, a unique function of nose fan door position (Figure 39, page 40, reference 11), and $T_c^s A$ was the wing fan average

$$T_c^s A = A_{NF} \cdot (P_{NF})^{2/3} \cdot \left(\frac{\rho^{1/3}}{A_{NF}^{2/3}} \right) \cdot \frac{C_{p_o NF}^s}{C_{p NF}^s}$$

where A_{NF} is the nose fan area, ρ is the density,

$$C_{p_o NF}^s = g [T_c^s A]$$

and the nose fan power P_{NF} is

$$P_{NF}^{2/3} = 0.2855 \cdot (P_F^{2/3} - 2250)$$

The latter function was derived by comparing the dependencies of P_F and P_{NF} on rpm, Figures 34 and 37, page 38 and 40, reference 11. These equations were solved once, without iteration.

Fan Corrections -- The above thrusts act in the aircraft z direction, and they do not take the effects of vector and stagger angle on lift, drag, and pitching moment into account. These effects are taken into account by adding the terms:

$$\begin{aligned} E_{FzR} &= \text{lift correction, right fan} \\ &= -Q_R^s \frac{A_F}{2} (\Delta C_N(\beta_{sR}) + \Delta C_N(\beta_{vR})) \end{aligned}$$

$$\begin{aligned} E_{FxR} &= \text{drag correction, right fan} \\ &= Q_R^s \frac{A_F}{2} (\Delta C_x(\beta_{sR}) \cdot \text{sgn}(\beta_{vR}) + \Delta C_x(\beta_{vR})) \end{aligned}$$

$$\begin{aligned} E_{MR} &= \text{pitch correction, right fan} \\ &= -Q_R^s \frac{A_F}{2} (\Delta C_m(\beta_{sR}) + \Delta C_m(\beta_{vR})) \end{aligned}$$

with similar notation for the left fan (R replaced by L). The functions $\Delta C_N(\beta_s)$, $\Delta C_N(\beta_v)$, $\Delta C_x(\beta_s)$, $\Delta C_x(\beta_v)$, $\Delta C_m(\beta_s)$, $\Delta C_m(\beta_v)$ were obtained by table lookup. The data for these curves are given in Figures 2, 3, 4, page 11, 12, reference 11.

Sum of Forces and Moments

The total forces and moments in each axis are the aerodynamic terms plus the fan terms plus the inertial coupling terms plus the gravity terms.

$$\begin{aligned} F_{xTOTAL} &= F_{xLL} + F_{xRL} + F_{xTL} && \text{aerodynamic} \\ &+ E_{FxR} + E_{FxL} && \text{fan correction} \\ &+ m(vr - wg) && \text{inertial} \\ &- mg \sin \theta && \text{gravity} \\ \\ F_{yTOTAL} &= Y_{vTL} + Y_{FUS} + Y_{vTNL} && \text{aerodynamic} \\ &+ m(wp - ur) && \text{inertial} \\ &+ mg \cos \theta \sin \phi && \text{gravity} \end{aligned}$$

$$\begin{aligned}
F_{zTOTAL} &= F_{zRL} + F_{xLL} + F_{zTL} + F_{zRL} \\
&+ F_{zNL} \cdot (2-f_{4R} - f_{4L})/2 && \text{aerodynamic} \\
&+ E_{zR} + E_{zL} + E_{FzR} + E_{FzL} && \text{fan + fan correction} \\
&+ E_{FzNF} && \text{nose fan} \\
&+ m(uq - vp) && \text{inertial} \\
&+ mg \cos \theta \cos \phi && \text{gravity}
\end{aligned}$$

$$\begin{aligned}
L_{TOTAL} &= L_{1L} + L_2 + L_3(2-f_{4R} - f_{4L})/2 && \text{aerodynamic} \\
&+ 4(Y_{vTL} + Y_{vTNL}) + 6(F_{zRL} - F_{zLL}) && \text{aerodynamic} \\
&+ 5.07(E_{zR} + E_{FzR} - E_{zL} - E_{FzL}) && \text{wing fans} \\
&+ I_{xz} qp - (I_z - I_y) qr && \text{inertial}
\end{aligned}$$

Letting $u_{-1}(x)$ be the step function

$$u_{-1}(x) = 0 \text{ for } x \leq 0$$

$$1 \text{ for } x > 0$$

$$\begin{aligned}
M_{\text{TOTAL}} = & M_{\text{AL}} u_{-1} \left(\frac{u_L + u_R}{2} \right) + M_3 u_{-1} \left(\frac{-u_L - u_R}{2} \right) f_{17} \\
& + \left[M_2 u_{-1} \left(\frac{w_L + w_R}{2} \right) + M_1 u_{-1} \left(\frac{-w_L - w_R}{2} \right) (1-f_{17}) \right] \left. \vphantom{M_{\text{TOTAL}}} \right\} \text{aero-dynamic} \\
& + 0.8333(E_{zR} + E_{zL}) + E_{MR} + E_{ML} \quad \text{wing fans} \\
& - 15.6 E_{FzNF} \quad \text{nose fan} \\
& + (I_z - I_x) pq + (r^2 - p^2) I_{xz} \quad \text{inertial}
\end{aligned}$$

$$\begin{aligned}
N_{\text{TOTAL}} = & N_3 - 18.22 (Y_{vTL} + Y_{vTNL}) + 6(F_{xL} - F_{xRL}) \quad \text{aero-dynamic} \\
& + 5.07 (E_{xL} - E_{xR}) \quad \text{fan correction} \\
& + (I_x - I_y) pq - I_{xz} qr \quad \text{inertial}
\end{aligned}$$

$$\frac{d\theta}{dt} = q \cos \phi - r \sin \phi$$

$$\frac{dh}{dt} = u \sin \theta - w \cos \theta \cos \phi - v \cos \theta \sin \phi$$

Actuator Dynamics

The wing fan louver actuators and nose fan door actuators are considered by Ryan to be so fast as to be ignorable. Feeling uncomfortable without actuator dynamics, all of the actuators were assigned first-order transfer functions with a 1/10-second lag.

$$\frac{1}{0.1s + 1}$$

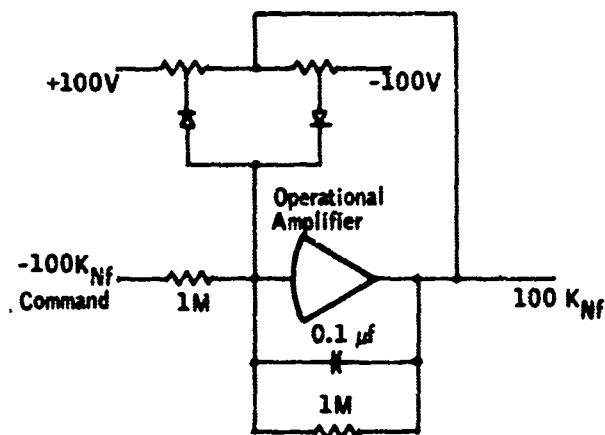
The nose fan door position uniquely defines K_{Nf} , the nose fan door efficiency. Below transition the vehicle is flown with the nose fan door open, in which case K_{Nf} is approximately

$$K_{Nf} \approx \frac{1.2}{75} (\delta_{NF} - 57) \text{ for } 40 < \delta_{NF} < 115$$

where δ_{NF} is the nose fan door position in degrees (figure 39, page 41, reference 11). For convenience it was decided to use K_{Nf} as the control input rather than δ_{NF} as in this region one is a unique function of the other. The K_{Nf} limits are

$$-0.2 < K_{Nf} < 1$$

which was simulated by limiting the travel of the lag output. The circuit used was:



where the limiter potentiometers were set for +100v, -20v limits.

The vector and stagger angles for each wing fan correspond to the sum and differences of the angles of adjacent louvers. The angles through which each louver can travel depend nonlinearly upon the current angles of the adjacent louvers. Ryan gives fan data in reference 11 for stagger and vector angles in the ranges

$$0 < \beta_s < 40 \text{ deg}$$

$$-10 < \beta_v < 50 \text{ deg}$$

To simplify the simulation vector and stagger angles actuators were simulated directly with the above limits, with circuits of the above type.

The vector and stagger limits were not hit in any of the gust tests, so the limits could be ignored. The nose fan door limit was hit only in pitchup at high airspeed.

APPENDIX II HYBRID SIMULATION

This appendix contains a brief discussion of the hybrid simulation employed in the nonlinear analyses described in Section VI of the main body of the report. The simulation described was constructed on the SDS 9300 digital computer and a connected PACE analog computer at Honeywell Aeronautical Division's simulation facility in Minneapolis.

ANALOG COMPUTATION

The PACE analog computer was used to simulate the gust models, the vehicle inertial dynamics, and the three-axis controller.

The gust model simulated consisted of three white noise sources plus three first-order lag networks with appropriate cross feeds for the correlation coefficients. The equations simulated were, in transform notation,

$$r_1(s) = \frac{1}{Cs+1} K_{11} \cdot \eta_1(s)$$

$$r_2(s) = \frac{1}{Cs+1} [K_{21} \cdot \eta_1(s) + K_{22} \cdot \eta_2(s)]$$

$$r_3(s) = \frac{1}{Cs+1} [K_{31} \cdot \eta_1(s) + K_{32} \cdot \eta_2(s) \cdot \eta_3(s)]$$

where $\eta_i(s)$ were the outputs of the white noise sources and the $r_i(s)$ simulated the various gust triplets employed in the analyses described in Section VI. C is the reciprocal of the bandwidth of the gust spectra as seen by the V/STOL, and the coefficients K_{ij} were chosen to produce the intensities and cross correlations desired in the individual tests.

The vehicle translation dynamics simulated were

$$u = \frac{1}{m} \int F_{x \text{ TOTAL}} dt$$

$$v = \frac{1}{m} \int F_{y \text{ TOTAL}} dt$$

$$z = \frac{1}{m} \int F_{z \text{ TOTAL}} dt$$

With

$$\dot{p}I_x - \dot{r}I_{xz} = L_{TOTAL}$$

$$gI_y = M_{TOTAL}$$

$$\dot{r}I_z - \dot{p}I_{xz} = N_{TOTAL}$$

$$\begin{bmatrix} I_x & -I_{xz} \\ -I_{xz} & I_z \end{bmatrix}^{-1} \approx \begin{bmatrix} \frac{1}{I_x} & \frac{I_{xz}}{I_x I_z} \\ \frac{I_{xz}}{I_x I_z} & \frac{1}{I_z} \end{bmatrix}$$

$$p = \int \frac{L_{TOTAL}}{I_x} + \frac{N_{TOTAL} I_{xz}}{I_x I_z} dt$$

$$q = \int \frac{M_{TOTAL}}{I_y} dt$$

$$r = \int \frac{L_{TOTAL} I_{xz}}{I_x I_z} + \frac{N_{TOTAL}}{I_z} dt$$

$$\phi = \int p dt$$

$$\theta = \int \frac{d\theta}{dt} dt$$

$$h = \int \frac{dh}{dt} dt$$

The controller consisted of three attitude controllers (pitch, roll and yaw) as shown in Figure 41.

The trim settings employed are given in Section V and the control gains in Section VI.

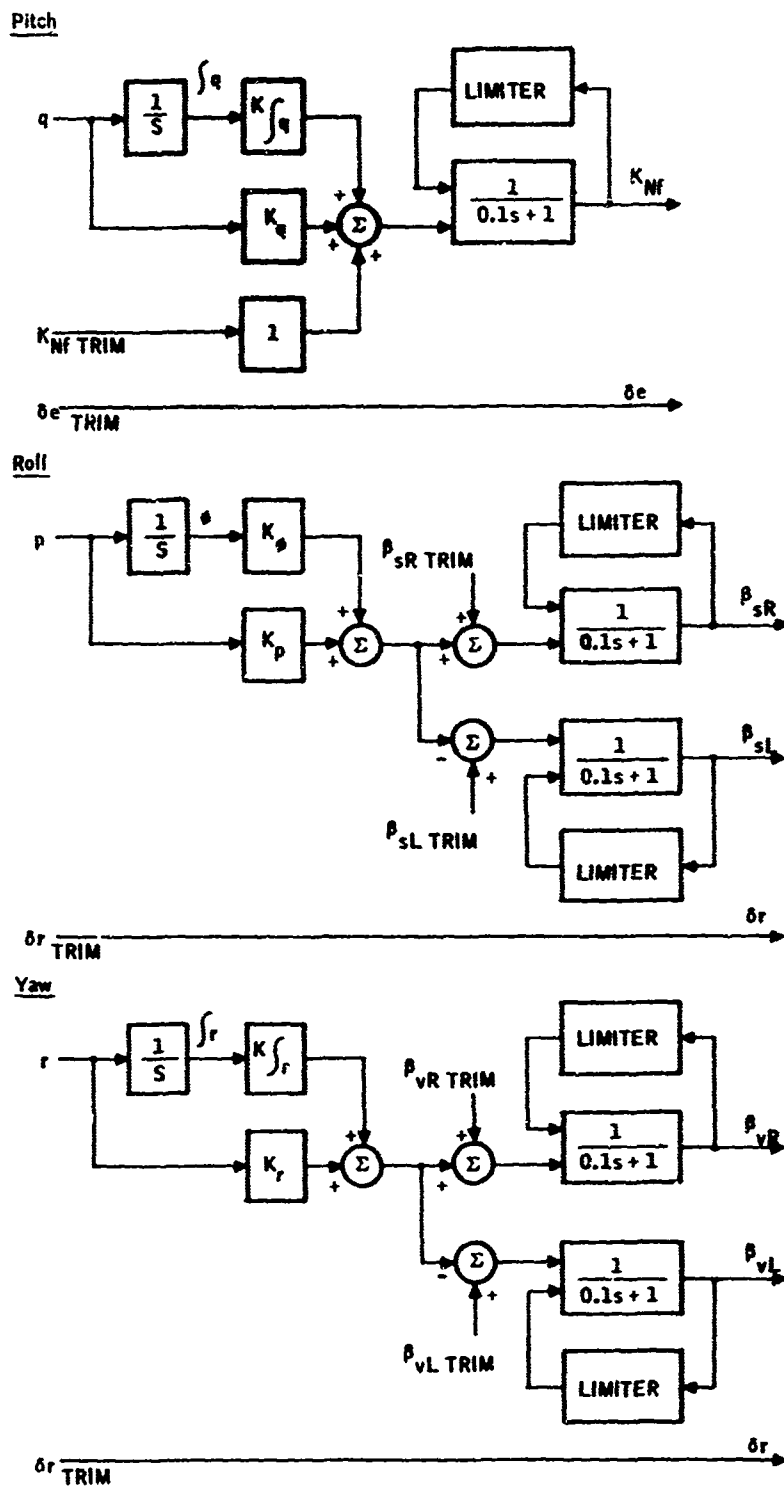


Figure 41. Pitch, Roll and Yaw Attitude Controllers

The only other functions assigned to the analog computer were generation with potentiometers of the tail incidence angle I_t and the fan power $P_F^{2/3}$.

The digital-to-analog (D/A) inputs to the analog computer were then F_{xTOTAL} , F_{yTOTAL} , F_{zTOTAL} , L_{TOTAL} , M_{TOTAL} , N_{TOTAL} , θ , and h .

The analog-to-digital (A/D) inputs to the digital computer were u , v , w , p , q , r , θ , ϕ , $P_F^{2/3}$, β_{SR} , β_{SL} , β_{VR} , β_{VL} , K_{NF} , δe , δa , δr , I_t , and the gusts u_{cg} , v_{cg} , w_{cg} , u_y , w_y , u_T , v_T , w_T , where cg indicates the average wing gusts, y indicates a gust shear, and T indicates tail gusts.

DIGITAL COMPUTATION

The SDS 9300 digital computer computed all of the forces and moments, and the means, standard deviations, and probability densities of up to 35 variables.

The force and moment calculations simulated were those described in Appendix I of this report. The Wagner lags described there were simulated on the SDS 9300 with difference equations.

The gust delay lines employed in the penetration tests were also simulated on the digital computer. The three average wing gusts were each delayed by d/u seconds before reaching the tail ($d = 22$ ft = wing-to-tail distance, $u = x$ component of instantaneous vehicle velocity relative to the mean wind). The delay lines were programmed as an option that could be switched in by pressing a sense switch on the computer control panel.

Sampling intervals of between 42 and 72 milliseconds were used for the various tests, the lower interval for low airspeeds without penetration effects and without statistical computation, the higher interval for high airspeeds with penetration and statistical computations. (The fan iterations converge faster at lower airspeeds.) The sampling interval desired was typed on the computer typewriter at the beginning of each data-collection run. If the selected interval proved too short, the computer would return control to the typewriter and ask for a longer interval.

Two statistical subroutines were employed, one that computed the means and standard deviations of 35 variables simultaneously, and one that computed the means, standard deviations, and probability densities of up to six variables. As explained in Section VI, the latter routine was memory-limited, and its use greatly increased the total simulation time for testing a particular vehicle-gust combination. The variables which could be sampled were the eight D/A outputs, all of the A/D inputs except δe , δa , I_t , $P_F^{2/3}$, and the internally-generated average dynamic pressure, angle of attack, and the six aerodynamic forces and moments.

The digital simulation had two interesting features. At the end of each test the final A/D inputs and D/A outputs were printed on the attached line printer, thereby providing a convenient record of flight condition. In addition, by pressing a sense switch the left-hand sides of more than 50 key equations in the force and moment computations were printed on the line printer. These two printouts greatly simplified the task of debugging the digital simulation, locating A/D interconnect problems, and locating burned out analog potentiometers. The use of such printouts is strongly recommended to other investigators.

The second interesting feature was the format chosen for the probability densities computed. These densities were calculated at the end of each test, and probability density graphs were then displayed on a connected TV screen and printed out on the line printer. The printed graphs made hand plotting unnecessary, and the TV display gave the simulation operator a better picture of the densities than could be obtained by watching the paper move through the line printer.

Unclassified
Security Classification

DOCUMENT CONTROL DATA - R&D		
<i>(Security classification of title, body of abstract and indexing annotation must be entered when the overall report is classified)</i>		
1. ORIGINATING ACTIVITY (Corporate author) Honeywell Inc. Systems and Research Division, Research Dept. St. Paul, Minnesota 55113		2a. REPORT SECURITY CLASSIFICATION Unclassified
		2b. GROUP NA
3. REPORT TITLE INVESTIGATION OF THE EFFECTS OF GUSTS ON V/STOL CRAFT IN TRANSITION AND HOVER		
4. DESCRIPTIVE NOTES (Type of report and inclusive dates) Final Technical Report, April 1967-March 1968		
5. AUTHOR(S) (Last name, first name, initial) Skelton, Grant B.		
6. REPORT DATE October 1968	7a. TOTAL NO. OF PAGES 248	7b. NO. OF REFS 18
8a. CONTRACT OR GRANT NO. F33615-67-C-1563	9a. ORIGINATOR'S REPORT NUMBER(S) 12060-FR1	
a. PROJECT NO.	9b. OTHER REPORT NO(S) (Any other numbers that may be assigned this report) AFFDL-TR-68-85	
c.		
d.		
10. AVAILABILITY/LIMITATION NOTICES This document has been approved for public release and sale; its distribution is unlimited.		
11. SUPPLEMENTARY NOTES	12. SPONSORING MILITARY ACTIVITY Air Force Flight Dynamics Laboratory Air Force Systems Command Wright-Patterson Air Force Base, Ohio	
13. ABSTRACT The concern in the work reported is the development of statistical models for the gust environment in the earth's boundary layer for use in determining the gust response characteristics of V/STOL aircraft. A general gust model based upon published gust data was developed, and analyses of V/STOL responses with that model were conducted to determine the gust descriptors significant to V/STOL performance. An interim gust model embodying the significant descriptors was then developed for use in V/STOL gust analyses. Suggestions for meteorological experiments to measure the significant descriptors are made. The significant gust descriptors determined from the analyses are the diagonal terms of the gust covariance tensor, gust probability distributions, mean wind probability distributions, and the dependencies of these statistics on thermal stability, surface roughness, and altitude. Less critical descriptors include the off-diagonal components in the gust covariance tensor and the space-time interplay in that tensor. The significant gusts seen by the aircraft are head-on and vertical gusts on the wings; head-on and vertical gust shears across the wings; head-on, side, and vertical gusts on the tail; and head-on and side gusts on the fuselage. Mean air-speed and sideslip angle are important parameters in V/STOL gust responses. The wing-to-tail transport delay of the gusts in forward flight also has a significant effect. V/STOL gust responses at low airspeeds are generally small due to the low dynamic pressures, and the responses are decidedly nonlinear except at low gust amplitudes.		

DD FORM 1473 0101-807-8200
1 JAN 64

Unclassified
Security Classification

14. KEY WORDS	LINK A		LINK B		LINK C	
	ROLE	WT	ROLE	WT	ROLE	WT
V/STOL						
XV-5						
Gusts						
Low Altitude						
Statistics						
Models						

INSTRUCTIONS

1. ORIGINATING ACTIVITY: Enter the name and address of the contractor, subcontractor, grantee, Department of Defense activity or other organization (*corporate author*) issuing the report.

2a. REPORT SECURITY CLASSIFICATION: Enter the overall security classification of the report. Indicate whether "Restricted Data" is included. Marking is to be in accordance with appropriate security regulations.

2b. GROUP: Automatic downgrading is specified in DoD Directive 5200.10 and Armed Forces Industrial Manual. Enter the group number. Also, when applicable, show that optional markings have been used for Group 3 and Group 4 as authorized.

3. REPORT TITLE: Enter the complete report title in all capital letters. Titles in all cases should be unclassified. If a meaningful title cannot be selected without classification, show title classification in all capitals in parentheses immediately following the title.

4. DESCRIPTIVE NOTES: If appropriate, enter the type of report, e.g., interim, progress, summary, annual, or final. Give the inclusive dates when a specific reporting period is covered.

5. AUTHOR(S): Enter the name(s) of author(s) as shown on or in the report. Enter last name, first name, middle initial. If military, show rank and branch of service. The name of the principal author is an absolute minimum requirement.

6. REPORT DATE: Enter the date of the report as day, month, year, or month, year. If more than one date appears on the report, use date of publication.

7a. TOTAL NUMBER OF PAGES: The total page count should follow normal pagination procedures, i.e., enter the number of pages containing information.

7b. NUMBER OF REFERENCES: Enter the total number of references cited in the report.

8a. CONTRACT OR GRANT NUMBER: If appropriate, enter the applicable number of the contract or grant under which the report was written.

8b, 8c, & 8d. PROJECT NUMBER: Enter the appropriate military department identification, such as project number, subproject number, system numbers, task number, etc.

9a. ORIGINATOR'S REPORT NUMBER(S): Enter the official report number by which the document will be identified and controlled by the originating activity. This number must be unique to this report.

9b. OTHER REPORT NUMBER(S): If the report has been assigned any other report numbers (*either by the originator or by the sponsor*), also enter this number(s).

10. AVAILABILITY/LIMITATION NOTICES: Enter any limitations on further dissemination of the report, other than those

imposed by security classification, using standard statements such as:

- (1) "Qualified requesters may obtain copies of this report from DDC."
- (2) "Foreign announcement and dissemination of this report by DDC is not authorized."
- (3) "U. S. Government agencies may obtain copies of this report directly from DDC. Other qualified DDC users shall request through _____."
- (4) "U. S. military agencies may obtain copies of this report directly from DDC. Other qualified users shall request through _____."
- (5) "All distribution of this report is controlled. Qualified DDC users shall request through _____."

If the report has been furnished to the Office of Technical Services, Department of Commerce, for sale to the public, indicate this fact and enter the price, if known.

11. SUPPLEMENTARY NOTES: Use for additional explanatory notes.

12. SPONSORING MILITARY ACTIVITY: Enter the name of the departmental project office or laboratory sponsoring (*paying for*) the research and development. Include address.

13. ABSTRACT: Enter an abstract giving a brief and factual summary of the document indicative of the report, even though it may also appear elsewhere in the body of the technical report. If additional space is required, a continuation sheet shall be attached.

It is highly desirable that the abstract of classified reports be unclassified. Each paragraph of the abstract shall end with an indication of the military security classification of the information in the paragraph, represented as (TS), (S), (C), or (U).

There is no limitation on the length of the abstract. However, the suggested length is from 150 to 225 words.

14. KEY WORDS: Key words are technically meaningful terms or short phrases that characterize a report and may be used as index entries for cataloging the report. Key words must be selected so that no security classification is required. Identifiers, such as equipment model designation, trade name, military project code name, geographic location, may be used as key words but will be followed by an indication of technical context. The assignment of links, roles, and weights is optional.